DYNAMIC SUBSTRUCTURAL CONDITION ASSESSMENT

JUN LI

Ph.D

The Hong Kong Polytechnic University

2012

THE HONG KONG POLYTECHNIC UNIVERISTY

DEPARMENT OF CIVIL AND STRUCTURAL ENGINEERING

DYNAMIC SUBSTRUCTURAL CONDITION ASSESSMENT

Jun Li

B.Sc, M.Sc.

A thesis submitted in partial fulfillment of the requirements for the

Degree of **Doctor of Philosophy**

June 2011

To my parents and sister

for their love and support

CERTIFICATE OF ORIGINALITY

I hereby declare that this thesis is my own work and that, to the best of my knowledge and belief, it reproduces no material previously published or written, nor material that has been accepted for the award of any other degree or diploma, except where due acknowledgement has been made in the text.

____________ ____________ (Signed)

_________Jun Li____________ (Name of student)

ABSTRACT

Vibration measurements, such as dynamic acceleration response data from civil infrastructures, are usually used for structural condition assessment with system identification techniques. Substructural condition assessment approaches are receiving increasing attentions in recent years since they have the advantages of reducing the number of unknown system parameters to be identified and system degrees-of-freedom (DOFs) involved in the computation. Measurements at the interface DOFs are normally required and treated as input excitations to the target substructure in many existing substructural identification approaches. However, it may not be possible to measure all the responses at the interface DOFs. On the other hand, the interface forces may be identified as well as the system stiffness parameters in the substructural condition assessment. This dissertation proposes a dynamic substructural condition assessment approach without information of responses and forces at the interface DOFs. Dynamic response reconstruction techniques in both the frequency and wavelet domains are developed. The relationship between two sets of time-domain response vectors is formulated based on the frequency response function in the frequency domain or unit impulse response function in the wavelet domain. Only the finite element model of the intact target substructure and measured acceleration data from the target substructure in the damaged state are required in the identification. A dynamic response sensitivity-based method is used for the damage identification and the adaptive Tikhonov regularization technique is adopted to improve the identification results when large noise effect is included in the measurements. Local damage is identified as a change in the elemental stiffness factor. Numerical and experimental studies are conducted to validate the effectiveness and accuracy of the proposed substructural damage identification approach. The local damage in the target substructure can be identified efficiently with the measurement noise and initial model errors in the finite element model.

Another development in this thesis is to detect the local damage using measured acceleration responses from the target structure subject to moving vehicular loads which serve as excitations to the structure. The dynamic response reconstruction in wavelet domain is developed for the scenario when a structure or a target substructure is subject to moving vehicular loads. The transmissibility matrix between two sets of time-domain response vectors is formulated using the unit impulse response functions when the moving loads are at different locations. Measured acceleration responses from the structure or the target substructure in the damaged state are used for the damage identification. A three-dimensional box-section girder subject to a two-axle three-dimensional moving vehicle is taken as an example to validate the proposed approach for damage identification. The simulated damage can be effectively identified with noise effect included in the measurements.

PUBLICATIONS

Refereed Journal Papers:

Law, S. S., Li, J., and Ding, Y., 2011. "Structural response reconstruction with transmissibility concept in frequency domain", *Mechanical Systems and Signal Processing*, 25(3): 952-968.

Li, J., and Law, S. S., 2011, "Substructural response reconstruction in wavelet domain", *Journal of Applied Mechanics ASME*, 78(4), 041010.

Li, J., and Law, S. S., (in press), "Substructural damage detection with incomplete information of the structure", *Journal of Applied Mechanics ASME*.

Li, J., and Law, S. S., (under review), "Damage identification of a target substructure with moving load excitation", *Mechanical Systems and Signal Processing*.

Li, J., and Law, S. S., (under review), "Damage identification in a bridge structure subject to moving vehicular loads", *International Journal of Mechanical Sciences*.

Li, J., Law, S. S., and Ding, Y., "Damage assessment based on structural response reconstruction in frequency domain: numerical and experimental studies", *Mechanical Systems and Signal processing*. (under preparation)

Refereed Conference Papers:

Li, J., Law, S. S., and Ding, Y., (accepted), "Damage assessment based on structural response reconstruction in frequency domain", *14th Asia Pacific Vibration Conference*, Hong Kong, 2011.

Law, S. S., and Li, J., (accepted), "Damage detection in a bridge structure under traffic loads", 14th *Asia Pacific Vibration Conference*, Hong Kong, 2011.

Li, J., and Law, S. S., (accepted), "Damage identification in a substructure of a box-section girder", *8th International Conference on Structural Dynamics*, Leuven, Belgium, 2011.

Law, S. S., and Li, J., 2011, “Damage identification of a segment of a box-section girder subject to a moving load”, *International Operational Modal Analysis Conference 2011*, Istanbul, Turkey.

Li, J., and Law, S. S., 2010, “Identification of interface forces in a substructure in the frequency-time domain”, *Proceedings of the Second International Postgraduate Conference on Infrastructure and Environment*, Hong Kong, V2, 315-322.

Li. J., and Law, S. S., 2008, “Reliability analysis for a bridge structure based on condition assessment results”, *Proceedings of the Eleventh East Asia-Pacific Conference on Structural Engineering and Construction (EASEC-11)*, Taipei, Taiwan, paper ID 605.

Law, S. S., and Li. J., 2008, “Condition assessment of a bridge structure under moving vehicle load including uncertainties”, *Proceedings of the Eleventh East Asia-Pacific Conference on Structural Engineering and Construction (EASEC-11)*, Taipei, Taiwan, paper ID 603.

ACKNOWLEDGEMENTS

First of all and most importantly, I would like to send my sincere thanks to my supervisor, Prof. S. S. Law, for accepting me as his PhD student in 2007 and for his knowledge, expert guidance, valuable discussions, patience and continuous support throughout the whole period of my PhD study. The working and research experiences with Prof. Law and the PhD training he gave me in the past four years will definitely benefit me a lot in the future academic and engineering work. I have also learned a lot from Prof. Law on the research attitude, research methodology, academic writing, passion for research, critical thinking and dedication to excellence with a high standard.

I am truly grateful to the financial support from grants of Hong Kong Research Grants Council projects and a grant at The Hong Kong Polytechnic University to make the completion of my PhD study possible. I also wish to thank our university and department for providing the excellent research facilities and library resources.

I wish to particularly thank the committee members, Dr. Y. L. Wong in our department, Prof. C. G. Koh at the National University of Singapore and Prof. Francis. T. K. Au at The University of Hong Kong, for taking their time to comment, advice and examine my dissertation.

I want to express my special thanks to Prof. H. P. Zhu in the School of Civil Engineering and Mechanics at the Huazhong University of Science and Technology (HUST), who is the supervisor of my master study. He recommended and encouraged me to pursue the PhD degree and gave me many helpful advices. I especially thank Dr. Y. Xia and Dr. G. M. Chen for their great supports, beneficial discussions and nice communications when I face difficulties in my study and personal life.

My thanks also go to the past and current members of Prof. Law's research group, Dr. X. Q. Zhu, Dr. Z. R. Lu, Dr. X. Y. Li, Dr. S. Q. Wu, Mr. Y. Ding, Miss. Q. You, Miss. J. Wang, Dr. K. Zhang, Miss. K. Liu, etc, for their discussions and constructive comments. I appreciate Mr. Y. Ding for his help and discussions in the laboratory work. I am also truly grateful to colleagues from HUST, Dr. S. Weng, Dr. T. Yin, Mr. S. S. Zhang, Ms. Y. N. Shi, Dr. L. Hu, Mr. P. Zhang and Dr. J. B. Zhang. We worked in Hong Kong and I would like to thank for their support and good care.

I would like to express my gratitude to those wonderful fellow graduate students in our department, Dr. W. Lin, Ms. X. H. Zhang, Dr. Z. H. Chen, Miss. S. Q. Ye, Dr. Z. W. Chen, Mr. W. A. Shen, Mr. H. W. Xia and Mr. W. Y. Liao, some of whom have lunch and supper together everyday. We discussed many issues in our work and lives, and they let me know how important our friendship is. I also wish to thank my friends, Mr. Hong-Bin. Luo, Mr. Y. X. Wang, Mr. Hou-Bing. Luo, Mr. D. X. Yang, Dr. C. S. Zhou and Mr. L. Xu. We have been good friends since I was taking the undergraduate and master studies at HUST. All the fellow students and friends are so important to me and I cannot achieve anything without their support and understanding.

I wish to thank the research fellow, Mr. S. Zhan and senior technical staffs, Mr. T. T. Wai, Mr. C. F. Cheung, Mr. M. C. Ng and Mr. Eric. Ho in the Light Structures Laboratory at The Hong Kong Polytechnic University for their very professional, useful suggestions and help in my experimental work. I also want to thank the staffs in the departmental general office and university research office for their kind assistances in my study affairs, such as visa extension, conference attendance and expense reimbursement, etc.

Finally, I would like to take this chance to thank my parents and older sister, without whom I could not stand, for their ultimate love, consistent support and tolerance. They tried so hard and actually their best to provide a good and peaceful living environment for me to learn and grow up since I am a kid. I appreciate that they instructed me how to be a kind, honest and brave man of integrity, which I am in pursuit of. I attribute what I have got and what I have experienced to their great efforts.

CONTENT

LIST OF FIGURES

LIST OF TABLES

LIST OF NOTATIONS

A^C	continuous state matrix
A^D	discrete state matrix
a_1, a_2	Rayleigh damping coefficients
B^C	continuous input matrix
B^D	discrete input matrix
C	damping matrix
D	mapping vector
C^D	discrete output matrix
D^C	continuous feedthrough matrix
D^D	discrete feedthrough matrix
F	applied excitation
$F(\omega)$	applied excitation in frequency domain
$f(t)$	applied excitation in time domain
F_e^{DWT}	discrete wavelet transform of external excitation
$F_e(\omega)$	applied external excitation on the substructure in frequency domain
F_I^{DWT}	discrete wavelet transform of interface force
$F_I(\omega)$	interface force on the substructure in frequency domain
$H_a(\omega)$	acceleration frequency response function
$H_d(\omega)$	displacement frequency response function
h	unit impulse displacement vector
$\dot{h}$	unit impulse velocity vector

$\ddot{h}$	unit impulse acceleration vector
h_S	unit impulse displacement vector under support excitation
$\dot{h}_S$	unit impulse velocity vector under support excitation
$\ddot{h}_S$	unit impulse acceleration vector under support excitation
$\ddot{h}^{DWT}$	discrete wavelet transform of impulse response function matrix
$h_{2^j+k}^{DWT}$	expansion coefficients of discrete wavelet transform
L	mapping vector
M	mass matrix
K	stiffness matrix
K_d	damaged stiffness matrix
K_i	i th elemental stiffness matrix in the intact state
$P_{\text{int}}(t)$	bridge-vehicle interaction force vector
R	output matrix
R_a	output influence matrix for acceleration response vector
R_v	output influence matrix for velocity response vector
R_d	output influence matrix for displacement response vector
S	sensitivity matrix
T	transmissibility matrix
$T(\omega)$	transmissibility matrix in frequency domain
$u(t)$	input signals
$X(\omega)$	displacement vector in frequency domain
$\ddot{X}(\omega)$	acceleration vector in frequency domain
x	displacement vector
$\dot{x}$	velocity vector

$\ddot{x}$	acceleration vector
$\ddot{x}_s(t)$	support excitation acceleration record
y	output vector
z	state vector
$\Phi_l^p(t)$	mapping vector of moving interaction force
α	elemental stiffness vector
α_i	i th elemental stiffness factor
$\Delta\alpha_i$	stiffness reduction in the i th elemental stiffness factor
j	imaginary unit
ω	radius frequency
$\delta(t)$	Dirac delta function

LIST OF ABBREVIATIONS

COV	coefficient of variation
DOF	degree-of-freedom
DWT	discrete wavelet transform
FFT	fast Fourier transform
FOH	First-Order-Hold
FRF	frequency response function
IDFT	inverse discrete Fourier transform
IIRS	Iterative Improved Reduction System
SP	sensor placement
SVD	singular value decomposition
TSVD	truncated singular value decomposition
UIR	unit impulse response
ZOH	Zero-Order-Hold

CHAPTER 1

INTRODUCTION

1.1 Background

Civil infrastructures deteriorate with time and will continuously accumulate damage during their services due to material deterioration, natural hazard and harsh environment such as earthquakes, storms, fires, long-term fatigues and corrosions. Such unnoticed and uncorrected anomalies could potentially produce more damage and finally lead to catastrophic structural failures with a huge loss of properties and human lives. Therefore the interest to monitor a structure for detecting local damage at an early stage is prevailing throughout the civil engineering community. Collected data from the structures and subsequent data analysis would indicate the existence of damage, detect the potential damage location and help management authorities to make quick and timely decisions on whether the repair, partial replacement or demolition activities are necessary or not.

Non-destructive examination methods have been becoming popular and a hotspot in recent years to assess the damage status of engineering structures. They are widely applied in aerospace, mechanical and civil engineering community. Generally, structural damage detection can be classified as local damage detection and global damage detection (Yan *et al*. 2007). Local damage detection normally refers to non-destructive testing techniques, such as visual inspection, ultrasonic, X-ray, acoustic emission and thermal field methods (Doherty 1993), etc. These techniques are mainly used to detect the existence and location of local anomalies of materials in structures. These investigations usually require that the structure is out of service for inspection. For those large and complicated structures that are not easy to access or to close for inspection, it is very difficult to inspect the damage using local damage detection methods. Therefore, local damage detection techniques have some limitations and can only be used for the detection of some special components in a structure. The global vibration-based structural damage detection has been proposed to detect the damage in the whole structure. A structure can be considered as a dynamic system with stiffness, mass and damping components. The structural damage may be introduced by various reasons, such as operating loads, impact, fracture, fatigue, corrosion, manufacturing fault, etc. Once some damages occur in the structure, the structural physical properties (i.e., stiffness, mass and damping matrices) will change, and modal parameters of the structure will also change. Therefore, the changes in the structural vibration characteristics, such as natural frequencies, mode shapes, frequency response function, flexibility matrix and dynamic responses etc. can be used to indicate the existence of damage and to identify the location and severity of damages (Doebling *et al*. 1998). Damage may be defined as a change introduced into a system that adversely affects the current or future performance of the system. The definition of damage will be confined to the changes of the material and/or geometric properties of these systems, including changes to the boundary conditions and system connectivity (Farrar *et al*. 2001). In many existing research literatures, damage is mainly in the form of a loss in the stiffness of a specific element of the structure.

The effect of damage on a structure can be classified as linear or nonlinear. A linear damage situation is defined as the case when the initially linear-elastic structure remains linear-elastic after damage. The changes in modal properties are a function of changes in the geometry and/or the material properties of the structure, but the structural response can still be modeled using linear equations of motion. Nonlinear damage is defined as the case when the initially linear-elastic structure behaves in a nonlinear manner after the damage has been introduced. One example of nonlinear damage is the formation of a fatigue crack that subsequently opens and closes under the normal operating vibration environment. The majority of the studies reported in the technical literature address only the problem of linear damage detection.

1.2 Research Objectives

It is interesting and desirable for practical engineering applications that the condition assessment for a large-scale or a complex structure may be conducted by dividing the full structure into several smaller substructures for independent studies one at a time in the inverse analysis. This study aims to propose a dynamic substructural condition assessment approach by using the measured acceleration response data directly. The integration and derivation of vibration signals will not be required to avoid any additional errors. Normally the measurements and interface forces at the interface degrees-of-freedom (DOFs) of the substructure of interest may be required or the interface forces be treated as unknowns which are needed to be identified as well as the system stiffness parameters in the substructural condition assessment. This dissertation attempts to eliminate this restraint based on the proposed dynamic response reconstruction techniques. The relationship between two sets of time-domain response vectors from the substructure could be formulated by using the transmissibility matrix based on the frequency response function (FRF) and unit impulse response (UIR) function from the finite element model of the substructure. The damage identification can be conducted in the target substructure and a limited number of measured response data, such as accelerations, from the substructure in the damaged state and the initial finite element model of the substructure will be used for the identification. The information, such as the finite element model of and measurements from the rest of the structure other than the target substructure are not required in the identification, and the condition assessment is purely based on the target substructure and only the elemental stiffness factors of the target substructure are formulated in the identification algorithm resulting in a much reduced dimension in the inverse problem. More specifically, the main objectives of this research are to:

(1) Propose the dynamic response reconstruction technique based on the generalized transmissibility concept in frequency domain. The accuracy of structural response reconstruction in a full structure or in a substructure is

numerically investigated.

(2) Extend the dynamic response reconstruction technique in the wavelet domain by using the unit impulse response function. The response reconstruction is explored to make use of the features of wavelet analysis, such as completeness and exactness in the forward and inverse wavelet transform. A comparison on the accuracy between the response reconstruction approaches in the frequency and wavelet domains is made.

(3) Focus on the substructural condition assessment problem and conduct the damage identification in a target substructure based on the response reconstruction techniques in both the frequency and wavelet domains. The effect with considerations of system uncertainties in the identification is investigated.

(4) Develop the response reconstruction for a bridge structure subject to moving vehicular loads. The damage identification problem will be examined in the full bridge structure and in a target substructure. The advantages of condition assessment of bridge structures based on the response reconstruction techniques are clarified.

(5) Verify the proposed substructural damage identification approach with experimental studies.

1.3 Outline of the Thesis

This dissertation consists of seven chapters. Chapter 1 introduces the background, motivations of the research and the organization of this dissertation. Chapter 2 presents the literature review on the vibration-based condition assessment approaches for structures with the emphasis on the research work of condition assessment in a substructure and in a bridge structure subject to moving vehicular excitations. Chapter 3 proposes the structural response reconstruction techniques both in the frequency and wavelet domains. The frequency response function and unit impulse response function are used to form the transmissibility matrix to formulate the relationship between two sets of time-domain response vectors.

Chapter 4 conducts the substructural damage identification based on the above response reconstruction techniques in frequency and wavelet domains. The acceleration measurements from the damaged structure and the finite element model of the intact substructure are used for damage identification. Information of the responses and forces at the interface DOFs will not be required in the identification algorithm. The accuracy and efficiency of the proposed substructural damage identification approach will be numerically investigated. The effect of measurement noise and model errors in the initial finite element model will be examined. The condition assessment work is then extended into the scenario where a bridge structure or a substructure is subject to moving vehicular excitations in Chapter 5. The performance of damage identification in a full structure and in a target substructure is numerically investigated. Chapter 6 delivers the experimental studies to verify the proposed structural response reconstruction techniques and the substructural damage identification approach. A seven-storey frame structure is manufactured in the laboratory and two damage scenarios are introduced in the structure. Acceleration measurements from hammer tests are used to identify the damage locations and severities in the target substructure, and the identified results are compared with the theoretical values to evaluate the effectiveness of the proposed substructural damage identification approach. Chapter 7 summarizes the main conclusions derived in this dissertation and discusses on the future research directions.

CHAPTER 2

LITERATURE REVIEW

2.1 Vibration-based Condition Assessment

Vibration measurements are generally used with the system identification techniques to determine the location and extent of structural local damage. The early approaches were based on correlating numerical models with measured modal properties from undamaged and damaged structures. Salawu (1997) and Doebling *et al*. (1998) have presented comprehensive reviews on damage detection from structural vibration characteristics. The basic idea is that the measured modal parameters (frequencies, mode shapes, and modal damping, etc) are functions of the physical properties of the structure (mass, damping and stiffness). Therefore, changes in the physical properties, such as reductions in stiffness resulting from the onset of cracks or loosening of a connection, will cause detectable changes in these modal properties. Since changes in modal properties or properties derived from these quantities are being used as indicators of damage, the process of vibration-based damage detection eventually reduces to some form of a pattern recognition problem.

Significant work has been done in the detection of local damage in structures using changes in structural dynamic properties, such as frequency changes (Cawley and Adams 1979; Stubbs and Osegueda 1990; Koh *et al*. 1995), mode shape changes (Fox 1992; Ratcliffe 1997; Shi *et al*. 2000a), mode shape curvature/strain mode shape changes (Pandey *et al*. 1991; Wahab and De Roeck 1999; Shi *et al*. 2000b), measured flexibility matrix (Pandey *et al*. 1994; Peterson *et al*. 1995), and residual force vector method (Liu 1995; Kosmatka and Ricles 1999), etc.

Farrar and Jauregui (1998a; 1998b) compared five methods for damage assessment using experimental modal data from an undamaged and damaged bridge.

The damage identification methods included damage index method, mode shape curvature method, change in flexibility method, change in uniform load surface curvature and change in stiffness method. It reported that standard modal properties such as resonant frequencies and mode shapes were not good indicators of damage. Ndambi *et al.* (2002) presented a comparative study of damage detection methods based on laboratory tests of two cracked RC beams. The damage detection methods based on eigenfrequencies, MAC, COMAC, flexibility matrices and strain energy were evaluated. The results showed that: (1) The eigenfrequency evolutions can follow the damage severity but were not influenced by the crack damage locations; (2) The MAC factors were, in contrast, less sensitive to crack damage compared with eigenfrequencies; (3) With the COMAC factor evolution, it was possible to detect and localize damage in the tested RC beams but difficult to follow severity and spreading; (4) The change in flexibility matrices allowed also detection of the crack damage in RC beams, but the damage localization was difficult; and (5) Damage indices method based on the strain energy appeared to be more precise than the others in damage localization, but the difficulty remained when the damage was spread out over a certain length of the RC beam. Huth *et al.* (2005) compared several identification techniques based on modal parameters data on a progressively damaged prestressed concrete bridge. Although the bridge was severely cracked, natural frequencies as well as mode shapes displayed only minor changes. However, the relative changes of mode shapes were larger than those observed for natural frequencies. Damage detection or localization via changes of the flexibility matrix performed better than natural frequencies or mode shapes alone.

The natural frequency and mode shape data are easy to measure with a high level of accuracy, and are the most common modal parameters for damage detection. Frequency and mode shape changes caused by damage are usually very small, and may be disappeared in the changes caused by environmental and operational conditions. Changes in natural frequencies due to damage result in phase shifts between the vibration responses of the healthy structure and the damaged structure. There are also studies on damage detection using time domain responses directly (Li and Mau 1991; Ghanem and Shinozuka 1995), such as accelerations, velocities and displacement of structures. The incompleteness exists when structural responses are not measured at all DOFs corresponding to its numerical model. Some system identification algorithms circumvented this difficulty by including the unmeasured DOFs as system parameters to be estimated (Hjelmstad *et al.* 1995). The incompleteness in state also occurs in most dynamic measurements because only one state of acceleration, velocity, or displacement time history is usually measured. Numerical schemes for integrating or differentiating the measured state vector were applied to compute the unmeasured state vectors (Banan *et al.* 1995). Since the numerical schemes naturally develop computational error and amplify noise in measured responses, the most desirable way may be to avoid computing the unmeasured responses using measured data in formulating a system identification algorithm. Cattarius and Inman (1997) used the time histories of vibration response of the structure to identify damage in smart structures. Choi and Stubbs (2004) formed the damage index directly from the time responses to locate and quantify damage in a structure. Kang *et al*. (2005) presented a system identification scheme in time domain to estimate stiffness and damping parameters of a structure using measured acceleration data. An error function was defined as the time integral of the least-squared errors between the measured and calculated accelerations from a numerical model of a structure. A sequential non-linear least-square estimation approach was proposed to identify the structural parameters as well as the unmeasured excitations. The accuracy and effectiveness of the proposed approach have been demonstrated using the Phase I ASCE structural health monitoring benchmark building, which is a non-linear elastic structure or a non-linear hysteretic structure (Yang *et al*. 2006a; Yang *et al*. 2007a). An adaptive tracking technique based on the extended Kalman filter approach was proposed to identify the structural parameters and their changes where the location and severity of structural damage may be detected on-line (Yang *et al*. 2006b; Yang *et al*. 2007b). Perry and Koh (2008) proposed an out-put only structural identification strategy to identify unknown stiffness and damping parameters. Numerical and experimental results demonstrated the power of the strategy in accurate and efficient identification of structural parameters and damage using only incomplete acceleration measurements. Link and Weiland (2009) reported about experiences with damage identification using two different model updating techniques. The first one was based on classical modal information residuals, such as natural frequencies and mode shapes. The second technique used residuals composing of measured and analytical time histories. It was found that simultaneous occurrence of many different types of damage made it even more difficult to derive a unique mathematical physical model since it depended on the large variety of possible assumptions introduced in the finite element modeling. The model must have the ability to reflect the physical reality as close as possible because otherwise the identified parameters may indicate a damage symptom but will lose their prediction capability. Depending on the size of the damage, high spatial resolution of the test data is necessary (natural frequencies alone are not sufficient for localizing small damage). Time domain response data have the advantage of carrying high-frequency information which is beneficial for the detection of local damage and which usually is lost when modal residuals are used.

Numerous studies were conducted to investigate the damage detection problems of structures based on Genetic Algorithm (GA) and Artificial Neural Network (NN). A detailed review on system identification with GA and NN methods can be referred in (Carden and Fanning 2004; Yan *et al*. 2007).

2.2 Damage Identification Based on Model Updating

The finite element model updating method can be used to identify unknown structural parameters of civil structures and to determine structural damage. The method aims to minimizing the discrepancies between the numerical and experimental modal data or time-domain dynamic responses by adjusting the unknown parameters of the finite element model. The structural damage is represented as a decrease in the stiffness of individual elements. The initial analytical finite element model is tuned to the undamaged structure, which is used as a reference model. Then this reference model is updated to obtain a model that can reproduce the experimental modal data or measured dynamic responses in the damaged state.

2.2.1 Optimal Matrix Update Methods

Methods that use a closed-form direct solution to compute the damaged model matrices or the perturbation matrices are commonly referred to as optimal matrix update methods. McGowan *et al*. (1990) examined stiffness matrix adjustment algorithms for application to damage identification using measured mode shape information from sensor locations. Mode shape expansion was employed to extrapolate the measured mode shapes such that they can be compared with analytical model results. Smith (1992) presented an iterative approach to the optimal update problem that enforces the sparsity of the matrix in each iteration cycle. Kim and Bartkowicz (1993) investigated damage detection capabilities with respect to various matrix update methods, model reduction methods, mode shape expansion methods, numbers of damaged elements, number of sensors, number of modes, and levels of noise. Liu (1995) presented an optimal update technique for computing the elemental stiffness and mass parameters of a truss structure from measured modal frequencies and mode shapes. Another class of optimal matrix update problem involves the minimization of the rank of the perturbation matrix rather than the norm of the perturbation matrix. The solution for the perturbation matrices is based on the assumption that a unique minimum rank matrix solution of the underdetermined system exists. This approach has been studied extensively (Zimmerman and Kaouk 1994; Kaouk and Zimmerman 1994; Doebling 1996; Zimmerman 2006).

The optimal matrix update methods do not require the parametric analytical models and the system matrices are reconstructed arbitrarily, which may not have clear physical meanings and have disadvantages in damage detection and parameter estimation.

2.2.2 Sensitivity-based Model Updating

Sensitivity-based model updating is usually based on a first- or second-order Taylor series that minimizes an error function of the matrix perturbations. An excellent review on model updating techniques with modal sensitivities has been made (Mottershead and Friswell 1993; Friswell and Mottershead 1995). Analytical sensitivity methods usually require the evaluation of the stiffness and mass matrix derivatives, which are less sensitive than experimental sensitivity matrices to noise in the data and to large perturbations of the parameters. Ricles (1991) presented a methodology for the sensitivity-based matrix update, which takes into account variations in system mass and stiffness, center of mass locations, changes in natural frequency and mode shapes, and statistical confidence factors for the structural parameters and experimental instrumentation. Farhat and Hemez (1993) presented a sensitivity-based matrix update procedure that formulated the sensitivities at the element level. This had the advantage of being computationally more efficient than forming the sensitivities at the global matrix level. The objective function in the model updating procedure is normally built up by the residuals between the measurement results and the numerical predictions. Hassiotis and Jeong (1995) presented a method for the identification of localized reductions in the stiffness of a structure using natural frequency measurements and optimization techniques. Mottershead *et al*. (1996) used the eigenvalue sensitivities to update finite element models of welded joints and the boundary condition of a cantilever plate. Zhao and Dewolf (1999) conducted a sensitivity study comparing the use of natural frequencies, mode shapes, and modal flexibilities for damage detection. Wahab *et al*. (1999) presented a finite element model updating technique to detect and quantify damage in reinforced concrete beams by minimizing the difference between the measured and calculated modal parameters. Brownjohn *et al*. (2001) presented the sensitivity-based finite element model updating method based on modal information, such as frequencies and mode shapes, and it was applied to conduct structural condition assessment with particular reference to bridge structures. Maeck *et al*.

(2000) used a sensitivity-based model updating procedure to conduct the damage identification in reinforce concrete structures by achieving a good agreement between experimental and calculated numerical modal parameters. The sensitivity-based finite element model updating method using experimental modal data for damage assessment was improved by using the damage functions (Teughels *et al*. 2002) and coupled local minimizers (Teughels *et al*. 2003; Bakir *et al.* 2008) and by introducing some constraints in the updating process (Zhang *et al*. 2000; Bakir *et al*. 2007). The application of this model updating method with damage functions in the condition assessment of a highway bridge Z24 was presented (Teughels and Roeck 2004). The modal flexibility information (Jaishi and Ren 2006), strain energy residuals (Jaishi and Ren 2007) and optical fiber strain data (Reynders *et al*. 2007) were also introduced in the sensitivity-based model updating to conduct the damage assessment. Perera and Ruiz (2008) developed a multistage scheme for damage detection of large-scale structures based on modal data and finite element model updating techniques with multi-objective evolutionary optimization. In the first stage, occurrence and approximate location of damage were estimated by using damage functions in order to decrease the number of parameters to be updated. The goal in the second stage was to identify the specific damaged members and damage extent by considering only the members belonging to the regions detected as damage in the first stage. Regularization techniques were introduced in the model updating process to obtain more stable and reliable results (Tikhonov 1995; Ahmadian *et al*. 1998; Gorl and Link 2003; Weber *et al*. 2009). Moaveni *et al*. (2009) investigated systematically the performance of finite element model updating for damage identification. The uncertainty of the identified damage (location and extent) due to variability of five input factors was quantified through analysis-of-variance and meta-modeling. Results demonstrated that the level of confidence in the damage identification results obtained through finite element model updating was a function of not only the level of uncertainty in the identified modal information, but also choices made in the design of experiments, such as the spatial density of measurements and modeling errors.

The dynamic response sensitivity-based model updating method in time domain was proposed to identify the prestress force (Lu and Law 2006a), to conduct the force identification (Lu and Law 2006b) and damage detection (Lu and Law 2007a) from vibration measured response data. Later, this method was developed for identifying both the system parameters and input excitation forces of a structure (Lu and Law 2007b). It was found that the dynamic response sensitivity-based update can provide more identification equations and only a few sensors were required. This work was further studied with the sensitivity of the wavelet coefficients from the structural responses (Law *et al*. 2006). To reduce the effect of uncertainty in the excitation, the unit impulse response was directly considered instead of the time response in the damage identification process (Law and Li 2007). A statistical method for damage identification based on the response sensitivity with considerations of uncertainties in the analytical model, the excitation and measured dynamic response data was proposed (Li and Law 2008). Mean value and standard deviations of the identification results were obtained. Later, the dynamic response sensitivity-based was further applied to identify the moving loads and local damage in a three-span bridge deck and the condition assessment results were included in the reliability analysis of the bridge system (Law and Li 2010). An adaptive regularization approach for solving the model updating problem was presented and it was shown that the adaptive Tikhonov regularization was superior to the traditional Tikhonov regularization when the damage identification problem included the noise effect and significant improved results were obtained without divergence (Li and Law 2010).

2.3 Substructural Condition Assessment Methods

Koh *et al.* (1991) proposed a substructure approach to estimate the stiffness and damping coefficients of structures from measured dynamic responses using the extended Kalman filter with a weighted global iteration algorithm. Other substructural identification methods for the estimation of local damages were developed using the ARMAX model with the sequential prediction error method (Yun and Lee 1997) and using a backpropagation neural network (Yun and Bahng 2000). Recently, Koh *et al.* (2003) adopted the GA approach to conduct the substructural system identification in which the response measurements at the interface DOFs were assumed known and the calculated inertia forces from these responses were taken as the input to the substructure of interest. Tee *et al.* (2005) presented two system identification methods at the substructural level on identifying the first-order and second-order models. A strategy that used model condensation and recovery in identifying substructural parameters was proposed (Tee *et al.* 2009).

In the above-mentioned substructural identification work, measurements at the interface DOFs between substructures are required and they are treated as input excitations to the substructure of interest. However, it may always not be possible to measure all the responses at the interface DOFs, particularly for those rotational DOFs. Therefore, a substructural method in the frequency domain without using interface measurements was proposed by employing the GA approach for identification (Koh and Shankar 2003). On the other hand, other researchers (Law *et al.* 2010, Huang and Yang 2008) explored the simultaneous identification of both the input and system parameters in substructural condition assessment. The number of measurements was found to have significant influences on identifying the interface forces and system parameters simultaneously because a sufficient number of identification equations should be provided. The computation load may also be increased with this approach.

2.4 Condition Assessment Subject to Moving Loads

An important issue in this research area is to detect the local damage using measured responses from the structure under moving vehicular loads which serve as excitations to the structure. Studies on this issue first attempted to conduct the modal testing and analysis of structures from the dynamic responses under operational loads. Mazurek and Dewolf (1990) conducted the experimental studies on simple two-span girders with structural deterioration under moving loads by vibration analysis. Structural damage was artificially introduced by the release of supports and insertion of cracks. Piombo *et al.* (2000) modeled the vehicle-bridge interaction system as a three-span supported orthotropic plate subject to a seven DOFs multibody system with linear suspensions and tires flexibility. The wavelet technique was used to extract the modal parameters. Lee *et al.* (2002) presented a method for damage estimation of a simple bridge structure using vibration data caused by the traffic loadings. The operational modal properties were identified and the damage assessment was conducted based on these estimated modal parameters using the neural network technique. In the above studies, the bridge-vehicle structure interaction effect was not considered in the modal parameters identification. In fact, the vehicle-bridge interaction system constitutes a time-varying system. The modal parameters of this system are changing when the vehicle is moving on the bridge. Li *et al.* (2003) presented the eigenvalue analysis on the natural frequencies of the bridge deck with the moving vehicle on top. Farrar and James (1999) identified the modal properties by curve-fitting the cross-correlation functions between two response measurements using the traffic excitation as the vibration source. A comparison between the identified results with those from standard forced vibration methods showed that a maximum discrepancy of 3.63% in the natural frequency existed. This phenomenon was also found in field measurements with vehicles moving on top of the bridge deck where heavy vehicles would reduce the system stiffness while light vehicles increase the stiffness (Kim *et al.* 2003). When these identified modal parameters are used to detect local damage in the structure directly, errors would be introduced due to the ignoring of the bridge-vehicle system interaction.

Traffic excitations are usually mixed with other ambient excitation sources, such as ground motions, wind loading and temperature effect for bridge structures in real situations. The response due to the moving vehicular loads is generally far larger than that under ambient vibrations especially for short- and medium-span concrete bridge decks under normal conditions. Therefore the deterministic damage identification could also be conducted in the time domain using measured dynamic responses directly instead of the modal information in the frequency domain. Majumder and Manohar (2003; 2004) developed a time-domain approach to detect damages in a beam using vibration data under the passage of a moving oscillator. The study combined finite element modeling for the vehicle-bridge system with a time-domain formulation to detect changes in structural parameters. The structural properties and motion characteristics of the moving vehicle were assumed to be known, and the different damage scenarios were defined in terms of the elemental stiffness loss. Park *et al*. (2009) proposed a method to identify the distribution of stiffness reductions in a damaged reinforced concrete slab bridge under moving loads by using a modified bivariate Gaussian distribution function. The information of moving loads was assumed available in this study. A method for simultaneous identification of moving masses and structural local damage from measured responses has been presented (Zhang *et al*. 2010). The masses and damage extents were used as the optimization variables with a decreased number of unknowns, and the number of required sensors was reduced. The mass model may not accurately represent the moving vehicle and the bridge-vehicle interaction effect. In practical applications, the properties of the moving vehicle and the road surface roughness are not easy to obtain and thus they are usually assumed as unknown. Then the interaction forces on the bridge structure induced by the moving vehicle should be treated as unknown moving loads time-histories.

It is desirable to conduct the system identification based only on the system output (vibration responses of the bridge) because the system input (traffic excitations) is difficult to measure. With the aid of high computation capacity of digital computers, it is possible to analyze the bridge-vehicle interaction problem with more sophisticated bridge configurations and vehicle models. Zhu and Law (2007) proposed a method for simultaneous identification of the time-histories of interaction forces and structural damage iteratively using a two-step identification procedure. Later, structural condition assessment problem was studied in a three-span box-section concrete bridge deck subject to a three-dimensional moving vehicle by identifying the time-histories of the interaction forces and system parameters simultaneously in an iterative manner (Law and Li 2010). The effect of bridge-vehicle system interaction and road surface roughness profile was implicitly taken into account by identifying the moving interaction forces using measurements from the bridge structure. It was found that sufficient number of sensors may be required to make sure that the identification equation is over-determined. It was noted that the accuracy of the identified moving loads may have a large influence on the identification accuracy of the structural damage.

2.5 Structural Response Reconstruction Methods

Many studies have been conducted to investigate the problem of estimating the responses with limited measurements in a structural system. Kammer (1997) proposed a method for estimating the response of a structure during its operation at locations that were inaccessible for measurement using sensors. The prediction was based on measuring response at other locations on the structure and transforming it into the response at the desired locations using a transformation matrix, which was computed using the system Markov parameters determined from a vibration test. The predicted responses were good even with noise in the measurements. The time domain response, response quantity (including internal forces, moments or shears), and intensity in beams can also be reconstructed using a wave decomposition technique (Mace and Halkyard 2000). The wave decomposition approach enabled sensors to be optimally spaced, reducing sensitivity to noise and incorrect calibration. Ma *et al*. (2001) reconstructed the transient system responses using Karhunen-Loeve modes because the K-L based low order models were found to be able to capture the transient dynamics satisfactory. A method based on the interpolation of available responses through a spline shape function was developed to reconstruct unknown responses (Limongelli 2003). Reconstruction of unknown responses is performed by modeling the evolution of the relative acceleration along the height of a multistory frame building with a spline shape function. The support vector machine based method was proposed to simulate and predict the nonlinear dynamic responses of structures. Before the nonlinear responses were predicted, the linear responses were simulated and predicted using the ARMAX model and SISO system. Then the SVM technique was used to predict the nonlinear responses (Dong *et al*. 2008).

The generalized transmissibility matrix for a multi-degrees-of-freedom system in the frequency domain has been proposed by Ribeiro *et al.* (2000). The transmissibility matrix formulated the relationship between two sets of response vectors in frequency domain, and the use of transmissibility functions for damage detection has also been explored (Johnson and Adams 2002). System zeros in the transfer function were used as indicators to detect the damage. This transmissibility concept in frequency domain can also be used to identify the structural modal parameters (Devriendt and Guillaume 2007; Devriendt and Guillaume 2008), to conduct finite element model updating (Steenackers *et al*. 2007) and to evaluate the frequency response functions (Urgueira *et al*. 2011).

2.6 Challenges in Substructural Approaches

Existing structural damage identification approaches suffer from disadvantages with a large full-scale structure in the following areas: (a) There will be a large number of system DOFs and unknown parameters in the identification which is in contrast to the small number of measurements obtained from the structure in practice; (b) Structural identification is inherently an ill-conditioned inverse problem. The numerical difficulty to achieve computation convergence increases dramatically with the large number of unknown parameters in a full-scale structure. The computation effort would also increase tremendously with the large system matrices in both the forward and backward analysis; and (c) The uncertainty with the boundary conditions, material and physical parameters increases with the scale of a structure. It is often difficult to have a close to accurate finite element model of a large-scale structure for the system identification. Inclusion of incorrect boundary conditions into the forward and inverse analysis will introduce errors in the identified results.

With considerations of the above deficiencies with existing approaches, it is desirable to have the damage identification conducted basing on a substructure only without the need of information of the rest of the structure. A large and complex structural system can then be divided into smaller substructures for independent studies one at a time in the inverse analysis.

Responses or forces at the interface DOFs were normally required in many existing studies for substructural damage identification. They were assumed to be known (Yun and Bahng 2000; Koh *et al*. 2003) or needed to be identified with the structural local damage simultaneously (Lei *et al*. 2010; Law and Yong 2011). A large number of unknown interface forces may be introduced in the identification process. It is interesting and important to develop a dynamic substructural condition assessment approach using measured acceleration responses in time domain directly. The velocity and displacement response data are not formulated in the identification equation, and the integration of acceleration signals to obtain velocity and displacement is not required. The relationship between two sets of time-domain responses may be formulated with the transmissibility matrix and it could be used for structural dynamic response reconstruction. Then the limitation of requirement of responses and forces at the interface DOFs for substructural condition assessment may be removed.

In the bridge-vehicle system analysis and identification, many studies were conducted to identify the moving loads (Zhu and Law 2000; Law *et al*. 2001; Zhu and Law 2006; Pinkaew 2006; Gonzalez *et al*. 2008; Deng and Cai 2010) or the parameters of the vehicle (Jiang *et al*. 2003, 2004; Au 2004; Deng and Cai 2009) from dynamic responses with an available finite element model of the bridge. Yang *et al*. (2004) proposed an approach to extract the fundamental bridge frequency from the dynamic response of a passing vehicle and an experimental verification was conducted (Lin and Yang 2005). The bridge frequency was contained in and can be extracted from the vehicle acceleration spectrum, but a correction must be made for the shifting effect. The bridge frequency will be blurred due to the involvement of high-frequency components resulting from the cart structure of the truck and the pavement roughness. Condition assessment for bridge structures under moving vehicular loads were investigated in recent years, and the parameters of the moving vehicle were assumed available (Majumder and Manohar 2003; 2004; Park *et al*. 2009; Nasrellah and Manohar 2010) or the moving load time histories and stiffness parameters of the bridge structure should be identified simultaneously (Zhu and Law 2007; Law and Li 2010; Nasrellah and Manohar 2010; Lu and Liu in press). These methods need to identify the vehicle-bridge interaction load from measured responses of the structure and the accuracy of damage identification results depends on the accuracy of the identified moving loads. Study on damage identification where knowledge of the moving vehicular loads is not required, may be conducted by using the response reconstruction technique and there is no need to identify these loads in the damage detection algorithm. Large-scale bridge structures may have a great number of elements and DOFs, and a lot of unknowns and system DOFs are involved in the structural identification. Substructural condition assessment approaches have the advantages of reducing the unknown parameters in the identification and the number of DOFs involved in the computation. However, study on substructural condition assessment with moving vehicle excitations is not reported yet and it is required to be investigated.

CHAPTER 3

DYNAMIC RESPONSE RECONSTRUCTION

3.1 Introduction

The dynamic response reconstruction techniques will be developed in a full structure and in a substructure in both the frequency and wavelet domains in this Chapter. They are named as frequency domain method and wavelet domain method in this dissertation, respectively. The response reconstruction process is based on transforming the measured responses into responses at other selected locations. The forces at the interface DOFs are taken as input excitations to the substructure. In the frequency domain method, the generalized transmissibility concept in frequency domain is used for the reconstruction. The unit impulse response function will be adopted to conduct the response reconstruction in the wavelet domain method.

3.2 Response Reconstruction in Frequency Domain

The generalized transmissibility concept formulated with the frequency response function is explored to conduct the structural response reconstruction in a full structure and it will be further applied in a substructure. Two cases are considered in the study, the first case is when the finite element model of the full structure is known while the second case has only the finite element model of the substructure available in the response reconstruction.

3.2.1 Response Reconstruction in a Full Structure

3.2.1.1 Frequency Response Function

The general equation of motion of a damped structure with N DOFs can be written as,

$$[M]\{\ddot{x}(t)\}+[C]\{\dot{x}(t)\}+[K]\{x(t)\}=\{F(t)\} \tag{3.1}$$

where M, C and K are the $N \times N$ mass, damping and stiffness matrices of the structure respectively; $\ddot{x}$, $\dot{x}$ and x are respectively the nodal acceleration, velocity and displacement vectors of the structure; $\{F(t)\}$ is a vector of applied forces on the associated DOFs of the structure. Rayleigh damping $[C]=a_1[M]+a_2[K]$ is assumed in this study, where a_1 and a_2 are the Rayleigh damping coefficients.

The Fourier transform of Equation (3.1) gives:

$$\left(-\omega^2 M + j\omega C + K\right)X(\omega)=F(\omega) \tag{3.2}$$

Therefore, the displacement response in frequency domain is given as,

$$X(\omega)=H_d(\omega)F(\omega)=\left(-\omega^2 M + j\omega C + K\right)^{-1}F(\omega) \tag{3.3}$$

in which, $H_d(\omega)=\left(-\omega^2 M + j\omega C + K\right)^{-1}$ is the displacement frequency response function matrix. The FRF matrix represents the inherent system frequency response characteristics and it can be measured experimentally, reconstructed from an experimental modal analysis, or obtained from the finite element analysis of the structure.

The acceleration response in frequency domain could be obtained from Equation (3.2) as,

$$\ddot{X}(\omega)=-\omega^2 X(\omega)=H_a(\omega)F(\omega)=-\omega^2 H_d(\omega)F(\omega) \tag{3.4}$$

where $H_a(\omega)=-\omega^2 H_d(\omega)$ is the acceleration frequency response function matrix.

3.2.1.2 Transmissibility Concept in a Full Structure

The generalized transmissibility concept in frequency domain for a multi-degrees-of-freedom system has been proposed by Ribeiro *et al.* (2000). The transmissibility matrix could be used to form the relationship between two sets of response vectors and the transmissibility concept will be reviewed briefly here with its application to a substructure in the next section.

Assuming that $F_a(\omega)$ is the vector of applied excitation forces on the structure in the frequency domain, $\ddot{X}_k(\omega)$ is the set of measured acceleration responses transformed in the frequency domain, denoted as the Known-set response vector, and $\ddot{X}_u(\omega)$ is the set of the predicted acceleration response, denoted as the Unknown-set response vector. The following equation can be obtained from Equation (3.4),

$$\begin{cases} \ddot{X}_k(\omega) = H_a^{ka}(\omega) F_a(\omega) \\ \ddot{X}_u(\omega) = H_a^{ua}(\omega) F_a(\omega) \end{cases} \tag{3.5}$$

where $H_a^{ka}(\omega)$, $H_a^{ua}(\omega)$ are the sub-matrices of the acceleration FRF matrix relating the applied forces to the Known-set and Unknown-set responses, respectively. From the first row of Equation (3.5), the applied force vector can be obtained as,

$$F_a(\omega) = \left(H_a^{ka}(\omega)\right)^+ \ddot{X}_k(\omega) \tag{3.6}$$

where, $\left(H_a^{ka}(\omega)\right)^+$ denotes the pseudo-inverse of matrix $H_a^{ka}(\omega)$.

Substituting Equation (3.6) into the second row of Equation (3.5), the following equation can be obtained as

$$\ddot{X}_u(\omega) = H_a^{ua}(\omega) F_a(\omega) = H_a^{ua}(\omega)\left(H_a^{ka}(\omega)\right)^+ \ddot{X}_k(\omega) \tag{3.7}$$

Equation (3.7) is the relationship between these two sets of responses. The transmissibility matrix is defined as,

$$T_{aku}(\omega) = H_a^{ua}(\omega)\left(H_a^{ka}(\omega)\right)^+ \tag{3.8}$$

Therefore, the Unknown-set response vector $\ddot{X}_u(\omega)$ can be obtained as,

$$\ddot{X}_u(\omega) = T_{aku}(\omega)\ddot{X}_k(\omega) \tag{3.9}$$

It should be noted that the number of coordinates in the Known-set response vector should be at least equal or greater than the number of applied force coordinates such that a pseudo-inverse $\left(H_a^{ka}(\omega)\right)^+$ may be obtained (Penrose 1955).

3.2.1.3 Computational Procedure

Step 1: Calculate the dynamic acceleration responses $\ddot{x}(t)$ of the structure from Equation (3.1) using the Newmark method. The analytical Known-set and Unknown-set response vectors of the structure are obtained as the simulated "measured" responses and Fast Fourier Transform (FFT) is used to transform the time domain response into frequency domain.

Step 2: The acceleration FRF matrices of the structure corresponding to the Known-set and Unknown-set DOFs in Equation (3.5) are obtained from Equation (3.4).

Step 3: Use Equation (3.9) for the response reconstruction in the full structure. Inverse discrete Fourier transform (IDFT) is performed to transform the reconstructed response in frequency domain into time domain response (Gupta *et al*. 1996).

Step 4: Compare the reconstructed Unknown-set response with the analytical one.

The finite element model of the full structure is assumed known to derive the FRF matrix and the information of time-histories of the applied force is not required in the above response reconstruction process. It should be noticed that the locations of the applied forces should be assumed to be known.

3.2.2 Response Reconstruction in a Substructure

3.2.2.1 When the Finite Element Model of the Full Structure is Available

Theoretical Background

When a substructure of the full structure is subject to both the applied external excitation forces and the interface forces from adjacent substructures, as shown in Figure 3.1, the dynamic acceleration response of the substructure in frequency domain can be written as,

$$\ddot{X}(\omega) = H_a^e(\omega)F_e(\omega) + H_a^I(\omega)F_I(\omega) \tag{3.10}$$

in which, $F_e(\omega)$ is the vector of applied external excitation forces in the frequency domain, $F_I(\omega)$ is the vector of interface forces in the frequency domain, and $H_a^e(\omega)$ and $H_a^I(\omega)$ are the acceleration FRF matrices associated with the external excitation forces and interface forces to the responses at the specific DOFs respectively.

The measured Known-set response vector $\ddot{X}_k(\omega)$ and Unknown-set response vector $\ddot{X}_u(\omega)$ which is required to be predicted are defined. They can be written in terms of Equation (3.10) in frequency domain as follows

$$\begin{cases} \ddot{X}_k(\omega) = H_a^{ke}(\omega)F_e(\omega) + H_a^{kI}(\omega)F_I(\omega) \\ \ddot{X}_u(\omega) = H_a^{ue}(\omega)F_e(\omega) + H_a^{uI}(\omega)F_I(\omega) \end{cases} \tag{3.11}$$

From the first row of the above equation, we have,

$$F_e(\omega) = H_a^{ke}(\omega)^+ (\ddot{X}_k(\omega) - H_a^{kI}(\omega)F_I(\omega)) \tag{3.12}$$

Substituting Equation (3.12) into the second row of Equation (3.11), we have,

$$\begin{aligned} \ddot{X}_u(\omega) &= H_a^{ue}(\omega)F_e(\omega) + H_a^{uI}(\omega)F_I(\omega) \\ &= H_a^{ue}(\omega)H_a^{ke}(\omega)^+ (\ddot{X}_k(\omega) - H_a^{kI}(\omega)F_I(\omega)) + H_a^{uI}(\omega)F_I(\omega) \\ &= H_a^{ue}(\omega)H_a^{ke}(\omega)^+ \ddot{X}_k(\omega) + \left(H_a^{uI}(\omega) - H_a^{ue}(\omega)H_a^{ke}(\omega)^+ H_a^{kI}(\omega)\right)F_I(\omega) \end{aligned} \tag{3.13}$$

With the definition of transmissibility matrix in Equation (3.8), we have,

$$T_{aku}(\omega) = H_a^{ue}(\omega)\left(H_a^{ke}(\omega)\right)^+ \tag{3.14}$$

Defining

$$H_{aku}^I(\omega) = H_a^{uI}(\omega) - T_{aku}H_a^{kI}(\omega) \tag{3.15}$$

Equation (3.13) can be expressed as,

$$\ddot{X}_u(\omega) = T_{aku}(\omega)\ddot{X}_k(\omega) + H_{aku}^I(\omega)F_I(\omega) \tag{3.16}$$

It can be noticed that Equation (3.16) relates the Known-set measured response vector $\ddot{X}_k(\omega)$ and the interface forces vector $F_I(\omega)$ to the Unknown-set predicted response vector $\ddot{X}_u(\omega)$ in a substructure.

Computational Procedure

Step 1: Calculate the dynamic acceleration responses $\ddot{x}(t)$ of the structure from Equation (3.1) using the Newmark method. Then obtain the analytical Known-set and Unknown-set response vectors of the substructure.

Step 2: Compute the interface forces on the substructure from the finite element analysis using the dynamic responses obtained in Step 1. They are assumed known from measurement or computation.

Step 3: The FRF sub-matrices of the substructure in Equation (3.11) are obtained from the finite element model of the substructure.

Step 4: Use Equation (3.16) for the response reconstruction in the substructure. IDFT is then performed to transform the reconstructed response in frequency domain into the structural response in time domain.

Step 5: Compare the reconstructed Unknown-set response with the analytical one.

In the above response reconstruction process, the interface forces are obtained from the finite element response analysis of the full structure model in Step 2. The finite element model of the full structure and the applied external excitation on the structure are assumed known for computation of the interface forces.

3.2.2.2 When only the Finite Element Model of the Target Substructure is Available

Theoretical Background

It is desirable to conduct the response reconstruction based on only the finite element model of the substructure of interest. When the number of measurements in the Known-set response vector is at least equal or larger than the number of interface forces on the substructure, the pseudo-inverse of matrix $\left(H_a^{kI}\right)^+$ exists and the following equation can be obtained from the first row of Equation (3.11),

$$F_I(\omega) = \left(H_a^{kI}\right)^+ \left(\ddot{X}_k(\omega) - H_a^{ke}(\omega)F_e(\omega)\right) \tag{3.17}$$

Substituting Equation (3.17) into the second row of Equation (3.11), we have,

$$\ddot{X}_u(\omega) = T_{ku}(\omega)\ddot{X}_k(\omega) + H_{ku}^e(\omega)F_e(\omega) \tag{3.18}$$

in which,

$$T_{ku}(\omega) = H_a^{uI}(\omega)\left(H_a^{kI}(\omega)\right)^+ \tag{3.19a}$$

$$H_{ku}^e(\omega) = H_a^{ue}(\omega) - T_{ku}H_a^{ke}(\omega) \tag{3.19b}$$

The external excitation forces on the substructure are assumed known in this study and its Fourier transform $F_e(\omega)$ is then obtained. Transformation matrix $T_{ku}(\omega)$ and matrix $H_{ku}^e(\omega)$ in Equation (3.19) are obtained from the FRF of the finite element model of the substructure. Therefore the Unknown-set response vector $\ddot{X}_u(\omega)$ can be reconstructed from the First-set response vector $\ddot{X}_k(\omega)$ in the substructure from Equation (3.18). It should be noted that only the finite element model of the target substructure and acceleration responses from the substructure are required in the above-mentioned response reconstruction.

Computational Procedure

Step 1: Calculate the dynamic acceleration responses $\ddot{x}(t)$ of the structure from Equation (3.1) using the Newmark method. Then obtain the analytical Known-set and Unknown-set response vectors of the substructure. FFT is used to transform the time domain signals into the frequency domain.

Step 2: The FRF sub-matrices of the substructure in Equation (3.11) are obtained from the finite element model of the substructure.

Step 3: Use Equation (3.18) for the response reconstruction in the substructure. IDFT is performed to transform the reconstructed response in frequency domain into the structural response in time domain

Step 4: Compare the reconstructed Unknown-set response with the analytical one.

It should be noticed that the interface forces are not required in the above response reconstruction process of the substructure. The interface forces are taken as the input excitations to the substructure and only the finite element model of the substructure is assumed known to derive the transmissibility matrix.

3.2.3 First-Order-Hold Force Approximation in Structural Response Analysis

3.2.3.1 State Space Equation of Motion

The equation of motion of the damped structural system shown in Equation (3.1) can also be expressed in the state space as follows,

$$\dot{z} = A^C z + B^C L \cdot F \tag{3.20}$$

where $z = \begin{bmatrix} x \\ \dot{x} \end{bmatrix}$, $A^C = \begin{bmatrix} 0 & I \\ -M^{-1}K & -M^{-1}C \end{bmatrix}$ and $B^C = \begin{bmatrix} 0 \\ M^{-1} \end{bmatrix}$. L is the mapping vector relating the applied forces to the corresponding DOFs of the structure.

The superscript ^{C} denotes that those matrices represent the continuous structural system. If the response of the structure is represented in the output vector $y(t)$ from sensors such as accelerometers, velocity transducers or displacement transducers, the output equation can be expressed as,

$$y = R_a \ddot{x} + R_v \dot{x} + R_d x \tag{3.21}$$

where R_a , R_v and $R_d \in \Re^{m \times nd}$ are output influence matrices for the measured acceleration, velocity and displacement, respectively. m is the dimension of the measured responses and nd is the number of DOFs of the structure. Equation (3.21) can also be rewritten as

$$y = Rz + D^C \cdot L \cdot F \tag{3.22}$$

where $R = [R_d - R_a M^{-1} K \quad R_v - R_a M^{-1} C]$ and $D^C = R_a M^{-1}$.

Equations (3.20) and (3.22) are converted into discrete equations using the exponential matrix, and the discrete model is,

$$\begin{cases} z(j+1) = A^D z(j) + B^D \times LF(j) \\ y(j) = Rz(j) + D \times LF(j) \qquad (j = 1,2,\cdots,N) \end{cases} \tag{3.23}$$

Superscript ^{D} denotes that these matrices represent the discrete structural system. N is the total number of sampling points, dt is the time step between the state variables $z(j)$ and $z(j+1)$ and $A^D = \exp(A^C \cdot dt)$, $B^D = A^C\left(A^D - I\right)B^C$.

3.2.3.2 Triangle First-Order-Hold Force Approximation

Traditionally, the dynamic response analysis is conducted by considering the input at each step as the value at the beginning of the time interval, noted as the Zero-Order-Hold (ZOH) discrete generally. The ZOH discrete generates a continuous input signal $u(t)$ by holding each sample value $u[i]$ constant over one sample interval which can be expressed as the following form,

$$u(t) = u[i], \qquad iT_s \le t \le (i+1)T_s \tag{3.24}$$

First-Order-Hold (FOH) discrete differs from ZOH by the underlying hold mechanism. FOH uses linear interpolation between adjacent input samples, as shown in Figure 3.2,

$$u(t) = u[i] + \frac{t - iT_s}{T_s}(u[i+1] - u[i]), \qquad iT_s \le t \le (i+1)T_s \tag{3.25}$$

where T_s is the sampling interval and $u = LF$ is the system input excitation in Equation (3.23). This discretization is generally more accurate than ZOH for system response analysis with the smooth and accurate input approximation. Other discretization methods such as the Tustin or Tustin with frequency wrapping may also be used for the response analysis. However a previous study (Darby *et al*. 2001) has shown that the First-Order-Hold discrete, that is Triangle-Hold equivalent, could produce the best approximation to the continuous system. Therefore the modified First-Order-Hold (triangle-hold) discrete method (Franklin *et al*. 1998) is finally adopted for the simulation studies.

The unit impulse function δ, i.e. the Dirac delta function, is,

$$\delta(t) = \begin{cases} +\infty & t = 0 \\ 0 & t \neq 0 \end{cases} \tag{3.26}$$

and $\int_{-\infty}^{+\infty} \delta(t)dt = 1$.

The triangle hold is adopted in this study with the input samples extrapolated by connecting adjacent samples with a straight line. The impulse response of the extrapolation filter for the triangle hold is shown in Figure A-1 of Appendix A. The block diagram of the triangle hold is shown in Figure A-2 of Appendix A. The Laplace transformation of the extrapolation filter that follows the impulse sampling is

$$H(s) = \frac{e^{Ts} - 2 + e^{-Ts}}{Ts^2} \tag{3.27}$$

Based on the block diagram, the state variable v and w are constructed,

$$\dot{v} = w/T \tag{3.28}$$

$$\dot{w} = u(t+T)\delta(t+T) - 2u(t)\delta(t) + u(t-T)\delta(t-T) \tag{3.29}$$

where $\delta(t)$ is the unit impulse function as shown in Equation (3.26). It can be shown from the integration of Equations (3.28) and (3.29) that $v(i) = u(i)$ and $w(i) = u(i+1) - u(i)$. A new state space equation can be derived as

$$\begin{bmatrix} \dot{\mathrm{x}} \\ \dot{v} \\ \dot{w} \end{bmatrix} = \begin{bmatrix} A^C & B^C & 0 \\ 0 & 0 & 1/T \\ 0 & 0 & 0 \end{bmatrix} \begin{bmatrix} \mathrm{x} \\ v \\ w \end{bmatrix} + \begin{bmatrix} 0 \\ 0 \\ 1 \end{bmatrix} \bar{u} \tag{3.30}$$

where $\bar{u}$ represents the input impulse functions, as shown in Appendix A. The first matrix on the right-hand-side of Equation (3.30) is defined as

$$F_T = \begin{bmatrix} A_C & B_C & 0 \\ 0 & 0 & 1/T \\ 0 & 0 & 0 \end{bmatrix} \tag{3.31}$$

with the one-step solution as

$$\zeta(iT+1) = e^{F_T T} \zeta(iT) \tag{3.32}$$

If we define

$$\exp(F_T T) = \begin{bmatrix} \Phi & \Gamma_1 & \Gamma_2 \\ 0 & 1 & 0 \\ 0 & 0 & 1 \end{bmatrix} \tag{3.33}$$

then the equation in variable x can be written as

$$x(i+1) = \Phi x(i) - \Gamma_1 v(i) + \Gamma_2 w(i) \tag{3.34}$$

If a new state is defined as $z(i) = x(i) - \Gamma_2 u(i)$, Equation (3.30) for the modified First-Order-Hold can be rewritten as

$$z(i+1) = A^D z(i) + B^D u(i) \tag{3.35}$$

The output equation becomes

$$y(i) = C^D z(i) + D^D u(i) \tag{3.36}$$

where the system parameters in the above state space Equations (3.35) and (3.36) can be represented as

$$\begin{aligned} A^D &= \Phi, \\ B^D &= \Gamma_1 + \Phi\Gamma_2 - \Gamma_2, \\ C^D &= H, \\ D^D &= J + H\Gamma_2 \end{aligned} \tag{3.37}$$

3.3 Response Reconstruction in Wavelet Domain

FFT has been a valuable tool for the analysis of vibration signals. However, leakage, end effects and aliasing occur in the forward FFT process. Filtering, windowing and ensemble-averaging techniques are often employed to alleviate these deficiencies with some success. Nevertheless, these errors in the FFT process still exist which may lead to a reduction in the accuracy of subsequent analysis. More importantly, the basis functions associated with each frequency component in the Fourier-transformed domain span the entire measured time interval, hence making different signals indistinguishable as long as their spectral density is the same. Another disadvantage of Fourier analysis is that the frequency information can only be extracted from the complete duration of a signal record. When there is a local oscillation representing a particular feature at some point in the time history of a signal, it will contribute to the calculated Fourier transform but its information on the time axis will be lost (Newland 1993). Such disadvantage can be overcome in the wavelet analysis which provides an alternative significant tool in signal analysis.

In the following sections, the response reconstruction in the full structure and in the substructure is conducted using the impulse response function in the wavelet domain to avoid the above-mentioned errors in the frequency domain method.

3.3.1 Unit Impulse Response Function in Wavelet Domain

The unit impulse response (UIR) is the response function of the system under the input of a unit pulse. It is an intrinsic function of the structural system. Traditionally, FFT is used to extract the impulse response data or Markov parameters by an inverse FFT of the frequency response curves obtained from the measured input and output (Juang and Pappa 1985). It has been reported that the impulse response data is extracted via the wavelet transform from known measured responses and input excitation information to avoid errors in the Fourier transformation process of both the input and output signals (Robertson *et al*. 1998). Recently, the impulse response function has been derived from the general equation of motion and it will be introduced briefly below (Law and Li 2007).

The equation of motion of a N -DOFs damped structural system under the unit impulse excitation is,

$$[M]\{\ddot{x}(t)\}+[C]\{\dot{x}(t)\}+[K]\{x(t)\}=D\delta(t) \tag{3.38}$$

where D is the mapping matrix relating the force excitation location to the corresponding DOF and $\delta(t)$ is the Dirac delta function. The impulse response function can be represented as a free vibration state with some specific initial conditions. Assuming that the system is in static equilibrium initially, the unit impulse response function can be computed from the equation of motion using the Newmark method:

$$\begin{cases} [M]\ddot{h}(t)+[C]\dot{h}(t)+[K]h(t)=0 \\ h(0)=0, \quad \dot{h}(0)=M^{-1}D \end{cases} \tag{3.39}$$

where h, $\dot{h}$ and $\ddot{h}$ are the unit impulse displacement, velocity and acceleration vectors, respectively.

When the structural system is under general excitation $f(t)$ with zero initial conditions, the acceleration response $\ddot{x}_l(t_n)$ from location l at time t_n is

$$\ddot{x}_l(t_n)=\int_0^{t_n}\ddot{h}_l(t_n-\tau)f(\tau)d\tau \tag{3.40}$$

in which, $\ddot{h}_l(t)$ is the unit impulse response function at location l. The vectors $\ddot{h}_l(t_n-\tau)$ and $f(\tau)$ can be expanded in terms of the discrete wavelet transform (DWT) as (Newland 1993),

$$\ddot{h}_l(t_n-\tau)=h_0^{DWT}+\sum_j\sum_k h_{2^j+k}^{DWT}\psi(2^j\tau-k) \tag{3.41}$$

$$f(\tau)=f_0^{DWT}+\sum_j\sum_k f_{2^j+k}^{DWT}\psi(2^j\tau-k) \tag{3.42}$$

where $\psi(2^j\tau-k)$ is the wavelet basis function, $h_{2^j+k}^{DWT}$ and $f_{2^j+k}^{DWT}$ are the expansion coefficients for the impulse response function and excitation force vectors respectively. Substituting Equations (3.41) and (3.42) into the convolution integral in Equation (3.40) for $\ddot{x}_l(t_n)$, and using the orthogonal conditions of the wavelet basis functions (Daubechies 1992), we have

$$\int_0^{t_n}\psi(2^j\tau-k)d\tau=0 \tag{3.43}$$

$$\int_0^{t_n}\psi(2^j\tau-k)\psi(2^r\tau-s)d\tau=\begin{cases} 1/2^j & \text{when } r=j \text{ and } s=k \\ 0 & \text{otherwise} \end{cases} \tag{3.44}$$

The following formula can then be derived as

$$\ddot{x}_l(t_n)=\ddot{h}_l^{DWT}(t_n)f^{DWT} \tag{3.45}$$

in which, $\ddot{h}_l^{DWT}(t_n)$ and f^{DWT} are the discrete wavelet transform of $\ddot{h}_l(t_n-\tau)$ and $f(\tau)$, respectively and they are given as,

$$f^{DWT}=\begin{bmatrix} f_0^{DWT} & f_1^{DWT} & \cdots & f_{2^j+k}^{DWT} \end{bmatrix}^T \tag{3.46}$$

$$\ddot{h}_l^{DWT}(t_n) = [\ddot{h}_{l,0}^{DWT}(t_n) \quad \ddot{h}_{l,1}^{DWT}(t_n) \quad \cdots \quad \ddot{h}_{l,2^j+k}^{DWT}(t_n)/2^j] \tag{3.47}$$

For the entire time history data, for example, $\ddot{x}_l = [\ddot{x}_l(t_1) \quad \ddot{x}_l(t_2) \quad \cdots \quad \ddot{x}_l(t_n)]^T$, the input and output relationship can be rearranged as,

$$\ddot{x}_{l(n\times 1)} = \ddot{h}_l^{DWT}{}_{(n\times rl)} f^{DWT}{}_{(rl\times 1)} \tag{3.48}$$

in which,

$$\ddot{h}_l^{DWT} = \begin{bmatrix} \ddot{h}_l^{DWT}(t_1) \\ \ddot{h}_l^{DWT}(t_2) \\ \vdots \\ \ddot{h}_l^{DWT}(t_n) \end{bmatrix} \tag{3.49}$$

and n, r and l are the number of sampled data, the number of input excitations and the number of wavelet coefficients in the wavelet transform, respectively.

3.3.2 Response Reconstruction in a Full Structure

3.3.2.1 Theoretical Background

The measured responses from the full structure are divided into two sets, noted as the Known-set response vector $\ddot{x}_k(t)$ and the Unknown-set response vector $\ddot{x}_u(t)$ respectively. They are represented in the wavelet domain from Equation (3.45) as follows,

$$\begin{cases} \ddot{x}_k(t)_{(mn\times 1)} = \ddot{h}_k^{DWT}{}_{(mn\times rl)} P_{\text{int}}^{DWT}{}_{(rl\times 1)} \\ \ddot{x}_u(t)_{(sn\times 1)} = \ddot{h}_u^{DWT}{}_{(sn\times rl)} P_{\text{int}}^{DWT}{}_{(rl\times 1)} \end{cases} \tag{3.50}$$

in which, m, s, n, r and l are the number of measurements in the Known-set response vector, the number of measurements in the Unknown-set response vector, the number of sampled data points in each measurement, the number of external forces, and the number of wavelet coefficients in the discrete wavelet transform, respectively.

When the number of measurements in the Known-set response vector is at least equal or larger than the number of external forces on the structure, the pseudo-inverse $\left(h_k^{DWT}\right)^+$ exists and the following equation can be obtained from the first row of Equation (3.50),

$$P_{\text{int}}^{DWT} = \left(\ddot{h}_k^{DWT}\right)^+ \ddot{x}_k(t) \tag{3.51}$$

Substituting Equation (3.51) into the second row of Equation (3.50), we have,

$$\ddot{x}_{ur}(t) = T_{ku}\ddot{x}_k(t) \tag{3.52}$$

where,

$$T_{ku} = \ddot{h}_u^{DWT}\left(\ddot{h}_k^{DWT}\right)^+ \tag{3.53}$$

The Unknown-set response vector $\ddot{x}_{ur}(t)$ can be reconstructed from the Known-set response vector $\ddot{x}_k(t)$ in the structure from Equation (3.52). Moreover, Equation (3.53) defines the transmissibility matrix in wavelet domain between two sets of time-domain response vectors from the structure.

3.3.2.2 Computational procedure

Step 1: Calculate the dynamic acceleration responses $\ddot{x}(t)$ of the structure from Equation (3.1) using the Newmark method. The analytical Known-set and Unknown-set response vectors of the structure are obtained in time domain.

Step 2: The impulse response function of the structure corresponding to Known-set and Unknown-set DOFs in Equation (3.50) are obtained from Equation (3.39) with the finite element model of the full structure.

Step 3: Use Equation (3.52) for the response reconstruction in the full structure.

Step 4: Compare the reconstructed Unknown-set response obtained in Step 3 with the analytical one in time domain in Step 1.

The finite element model of the full structure and the locations of the applied forces are assumed available and the time-histories of the applied excitation force is not required in the response reconstruction in the full structure.

3.3.3 Response Reconstruction in a Substructure

3.3.3.1 When the Finite Element Model of the Full Structure is Available

Theoretical Background

When a substructure of the structure is subject to both applied external excitation forces and interface forces from adjacent substructures, the dynamic acceleration response of the substructure can be represented in wavelet domain in terms of Equation (3.48),

$$\ddot{x}(t) = \ddot{h}_e^{DWT} F_e^{DWT} + \ddot{h}_I^{DWT} F_I^{DWT} \tag{3.54}$$

where, F_e^{DWT} and F_I^{DWT} are the discrete wavelet transforms of external excitation force and interface force vectors on the substructure, respectively. $\ddot{h}_e^{DWT}$ and $\ddot{h}_I^{DWT}$ are the impulse response function matrix of the substructure for the external excitation and interface forces, respectively.

Two sets of responses, noted as the Known-set response vector $\ddot{x}_k(t)$ which is measured and the Unknown-set response vector $\ddot{x}_u(t)$ which is required to be predicted, have been defined in the frequency domain earlier in this work. They are defined in the wavelet domain as:

$$\begin{cases} \ddot{x}_k(t)_{(mn\times 1)} = \ddot{h}_{ke}^{DWT}{}_{(mn\times rl)} F_e^{DWT}{}_{(rl\times 1)} + \ddot{h}_{kI}^{DWT}{}_{(mn\times ql)} F_I^{DWT}{}_{(ql\times 1)} \\ \ddot{x}_u(t)_{(sn\times 1)} = \ddot{h}_{ue}^{DWT}{}_{(sn\times rl)} F_e^{DWT}{}_{(rl\times 1)} + \ddot{h}_{uI}^{DWT}{}_{(sn\times ql)} F_I^{DWT}{}_{(ql\times 1)} \end{cases} \tag{3.55}$$

in which, m, s, n, r, q and l are the number of measurements in the Known-set response vector, the number of measurements in the Unknown-set response vector, the number of sampled data points in each measurement, the number of external excitation forces, the number of interface forces and the number of wavelet coefficients in the wavelet transform, respectively.

The number of measurements in the Known-set is at least equal or larger than the number of applied external excitation forces on the substructure, and the following Equation can be obtained from the first row of Equation (3.55),

$$F_e^{DWT} = \left(\ddot{h}_{ke}^{DWT}\right)^+ \left(\ddot{x}_k(t) - \ddot{h}_{kI}^{DWT} F_I^{DWT}\right) \tag{3.56}$$

Substituting Equation (3.56) into the second row of Equation (3.55), we have,

$$\ddot{x}_u(t) = T_{ku}^e \ddot{x}_k(t) + H_{ku}^I F_I^{DWT} \tag{3.57}$$

where,

$$T_{ku}^e = \ddot{h}_{ue}^{DWT} \left(\ddot{h}_{ke}^{DWT}\right)^+ \tag{3.58}$$

$$H_{ku}^I = \ddot{h}_{uI}^{DWT} - T_{ku}^e \ddot{h}_{kI}^{DWT} \tag{3.59}$$

Equation (3.57) formulates the relationship amongst the measured Known-set response vector $\ddot{x}_k(t)$, discrete wavelet transform of interface forces vector F_I^{DWT} and the Unknown-set response vector $\ddot{x}_u(t)$ for prediction in a substructure.

Computational Procedure

Step 1: Calculate the dynamic acceleration responses $\ddot{x}(t)$ of the structure from Equation (3.1) using the Newmark method. Then the analytical Known-set and Unknown-set response vectors of the substructure are obtained in time domain.

Step 2: Compute the interface forces on the substructure from the finite element analysis of the full structure using the dynamic responses obtained in Step 1.

Step 3: The impulse response function matrices in Equation (3.55) are obtained from Equation (3.39) with the finite element model of the substructure.

Step 4: Use Equation (3.57) for the response reconstruction in the substructure.

Step 5: Compare the reconstructed Unknown-set response with the analytical one.

It should be noticed that the finite element model of the full structure and the applied external excitations on the structure are assumed known for computation of the interface forces from the finite element analysis.

3.3.3.2 When only the Finite Element Model of the Target Substructure is Available

Theoretical Background

When the number of measurements in the Known-set is at least equal or larger than the number of interface forces on the substructure, the following equation can be obtained from the first row of Equation (3.55),

$$F_I^{DWT} = \left(\ddot{h}_{kI}^{DWT}\right)^+ \left(\ddot{x}_k(t) - \ddot{h}_{ke}^{DWT} F_e^{DWT}\right) \tag{3.60}$$

Substituting Equation (3.60) into the second row of Equation (3.55), we have,

$$\ddot{x}_{ur}(t) = T_{ku}^I \ddot{x}_1(t) + H_{ku}^e F_e^{DWT} \tag{3.61}$$

where,

$$T_{ku}^I = \ddot{h}_{2I}^{DWT} \left(\ddot{h}_{1I}^{DWT}\right)^+ \tag{3.62}$$

$$H_{ku}^e = \ddot{h}_{ue}^{DWT} - T_{ku}^I \ddot{h}_{ke}^{DWT} \tag{3.63}$$

Transformation matrix T_{ku}^I and matrix H_{ku}^e in Equations (3.58) and (3.59) are obtained from the unit impulse response function matrix from Equation (3.39) with the finite element model of the substructure. Therefore the Unknown-set response vector $\ddot{x}_{2r}(t)$ can be reconstructed from the Known-set response vector $\ddot{x}_1(t)$ in the substructure from Equation (3.61). The external excitations are assumed available from measurement.

Computational Procedure

Step 1: Calculate the dynamic acceleration responses $\ddot{x}(t)$ of the structure from Equation (3.1) using the Newmark method. Then the analytical Known-set and Unknown-set response vectors of the substructure are obtained in time domain.

Step 2: The impulse response function matrices corresponding to Known-set and

Unknown-set locations in Equation (3.55) are obtained from Equation (3.39) with the finite element model of the substructure.

Step 3: Use Equation (3.61) for the response reconstruction in the substructure.

Step 4: Compare the reconstructed Unknown-set response with the analytical one.

The interface forces are not required in the response reconstruction of the substructure and they are taken as the input excitations to the substructure. Only the finite element model of the substructure is assumed known to derive the transmissibility matrix.

3.4 Numerical Simulation

Numerical studies on a seven-storey plane frame structure, as shown in Figure 3.3(a) are used to illustrate the accuracy and efficiency of the presented approach for structural response reconstruction in a structure or in a substructure. The sixth and seventh stories are taken as a substructure in this study, as shown in Figure 3.3(b). The cross-sectional area and moment of inertia of the frame element are $0.32m^2$ and $0.017m^4$, respectively. The Young's modulus and mass density are respectively $3.5\times10^4 MPa$ and $2500kg/m^3$. Rayleigh damping is assumed and the damping ratios for the first two modes are taken as $\xi = 0.012$. The finite element model consists of 44 nodes and 49 planar frame elements. Each node has three DOFs. With fixed supports at Nodes 1 and 44, the system has 126 DOFs in total. The first ten system natural frequencies are 2.4263, 7.8119, 14.7194, 22.5572, 23.9374, 31.423, 33.9257, 41.5662, 49.6753 and 51.859Hz respectively.

The relative error of the response reconstruction result in the Frequency Fourier spectrum is defined as,

$$RE = \frac{\left\| \left|\ddot{X}_{ur}(\omega)\right| - \left|\ddot{X}_{true}(\omega)\right| \right\|_2}{\left\| \ddot{X}_{true}(\omega) \right\|_2} \times 100(\%) \tag{3.64}$$

where, $\left|\ddot{X}_{true}(\omega)\right|$ and $\left|\ddot{X}_{ur}(\omega)\right|$ are modulus of the Fourier spectrum of the analytical and reconstructed response vectors of the Unknown-set in the frequency domain.

The relative error between analytical and recovered response in the time domain can be defined as,

$$RE = \frac{\left\| \ddot{X}_{ur}(t) - \ddot{X}_{true}(t) \right\|_2}{\left\| \ddot{X}_{true}(t) \right\|_2} \times 100(\%) \tag{3.65}$$

in which, $\ddot{X}_{true}(t)$ and $\ddot{X}_{ur}(t)$ are the analytical and reconstructed response vectors in the time domain, respectively.

The analytical time domain responses $\ddot{X}_{true}(t)$ at the "measured" DOFs are obtained using Equation (3.23) for the ZOH or Equations (3.35) and (3.36) for the FOH in the forward structural dynamic analysis.

Two multi-sine wave external excitation forces along horizontal and vertical directions are applied on the structure for the case study, as shown in Figure 3.3(a). These two forces are:

$$F1 = \begin{cases} 200\left(\sin\left(30\pi t\right) + 0.5\sin\left(15\pi t\right) + 0.2\sin\left(60\pi t\right)\right), & t \le 1s \\ 0, & t > 1s \end{cases} \quad \text{and}$$

$$F2 = \begin{cases} 200\left(\sin\left(50\pi t\right) + 0.6\sin\left(75\pi t\right) + 0.2\sin\left(100\pi t\right)\right), & t \le 1s \\ 0, & t > 1s \end{cases}$$

In order to obtain the frequency domain analysis results under the excitation forces accurately, the following parameters are defined as shown in Figure 3.4: the duration of the excitation force is t_d, the duration of free vibration is t_f and the total sampling duration is T_0. Since the peak response of the system may be attained after the excitation has ended, the analysis is carried out over a time duration T_0 which is much longer than t_d. Furthermore, it has been reported (Chopra 2007) that the classical discrete Fourier transform solution will become increasingly accurate as the duration t_f of free vibration becomes longer because T_0 should be long enough for the free vibration of the system to damp out to small motion at the end of the period T_0. On the other hand, in order to obtain the frequency domain responses accurately, the sampling interval Δt should be short enough compared both to the periods of significant harmonics in the excitation and to the natural period of the system.

Therefore in this study the duration t_d of the excitation forces described above is limited to the first one second and the duration of measurement is taken as 16.384s to ensure that T_0 is long enough for the system responses to decay to close to zero and the number of sampling points is a power of two for the Fourier transform. The sampling rate is at 1000Hz to ensure a good accuracy of discrete Fast Fourier Transform for the frequency domain response analysis. It should be noted that multi-sine excitation is used in this simulation study to reduce the leakage effects and to produce responses that are of better quality compared with the random noise excitation, especially when only short time sequences can be recorded from the structure (Verboven *et al*. 2004).

3.4.1 Response Reconstruction in Frequency domain

3.4.1.1 Response Reconstruction in a Full Structure

Response Calculation with ZOH and FOH Force Discrete Approximation

Six sensors are placed arbitrarily on this structure and their locations are at Node 13(y), 15(x), 17(y), 18(x), 30(y) and 32(x) where "13(y)" denotes that the sensor is placed along the y direction at Node 13. This sensor placement configuration is noted as Sensor Placement set 1 (SP set 1) in this study. Note that input locations and interface DOFs are not necessarily associated with the sensors. The responses from these six DOFs are "recorded" and they are taken as the Known-set response vector $\ddot{X}_k(\omega)$. The responses from the remaining DOFs are considered as the Unknown-set $\ddot{X}_u(\omega)$ which will be predicted. In the following numerical studies, simulated “measured” Known-set responses from the finite element analysis are used.

The structural response analysis is conducted using ZOH and FOH force approximations, respectively. These simulated “measured” acceleration responses are transformed into the frequency domain and are taken as the Known-set response vector $\ddot{X}_k(\omega)$. The response reconstruction in the full structure is performed to obtain the response vector of Unknown-set $\ddot{X}_u(\omega)$ with Equation (3.9). All data in the FFT spectrum are selected to compute the relative errors between the analytical and reconstructed frequency domain response vectors with Equation (3.64). Figure 3.5 shows the time domain response at measured location Node 15(x) with ZOH and FOH approximations, noted as ZOH and FOH responses respectively. As seen from Figure 3.5, these two sets of response are of very small difference since a high sampling rate has been adopted in this study. The differences between the force vectors from ZOH and FOH discrete are not large. The sampling duration T_0 is long enough with the system responses getting close to zero at the end which is good for frequency domain analysis. Response reconstruction is performed with Equation (3.9) and Figure 3.6 shows the relative errors of the frequency Fourier spectrum of the response reconstruction results at all the DOFs in the Unknown-set. Though the ZOH and FOH time responses are close to each other, the response reconstruction errors from ZOH responses are larger than those from FOH responses as shown in Figure 3.6. The maximum relative error with ZOH responses is up to 6% while that with FOH responses is less than 1%. This is because FOH force approximation can provide more accurate response analysis results compared with the ZOH approximation with more accurate force representation, which is closer to the real continuous form of forces.

The obtained reconstructed responses from FOH approximation shown in Figure 3.6 are used to recover the time domain responses by using IDFT, and the relative errors between analytical and recovered time domain responses can be obtained with Equation (3.65) and they are shown in Figure 3.7. Note that all the relative error values are less than 1% and this indicates that the presented method has good accuracy in the response reconstruction.

It is noted from Figures 3.6 and 3.7 that the maximum error in response reconstruction with FOH response is at DOF 44, i.e. at Node 16(y). The analytical and reconstructed frequency and time domain responses at Node 16(y) are displayed in Figure 3.8. The two sets of responses are almost overlapping indicating very high reconstruction accuracy.

Effect of Sampling Duration and Sampling Rate

Several important factors associated with the frequency domain analysis are the sampling duration and sampling rate of measurements. In order to study how these two factors affect the response reconstruction accuracy and determine the acceptable values of these two factors with good reconstruction accuracy, the sampling duration is considered varying from 4.192s to 32.768s and the sampling rate varies from 250Hz to 2000Hz in this study. When the sampling duration varies, the sampling rate is kept constant at 1000Hz. When the sampling rate varies, the sampling duration is set equal to 16.384s. Table 3.1 lists the average relative errors of the reconstructed response results in the frequency spectrum with different sampling duration and sampling rate settings. Note that the average error in this section denotes the mean value of relative errors from all DOFs in the Unknown-set. It may be concluded from Table 3.1 that when a longer sampling duration or a higher sampling rate are used, more accurate response reconstruction results can be obtained since a long duration T_0 is used with a longer sampling duration and more number of sampling points are obtained in the FFT process for frequency domain analysis with a higher sampling rate.

Effect of Number of Measured Responses

Another sensor placement configuration with three sensors is considered and their locations are at Node 13(y), 15(x) and 32(x), noted as Sensor Placement set 2

(SP set 2). The relative errors of frequency spectrum in response reconstruction results with different sampling duration and sampling rate are listed in Table 3.2. It can be found by comparing the results in Tables 3.1 and 3.2 that the accuracy for response reconstruction with SP set 1 is slightly better than that with SP set 2. Thus it may be advantageous for response reconstruction with more measurements in the Known-set response vector. However, how to find the optimal sensor placement configuration is not examined in this study.

Effect of Noise in the Measured Responses

To simulate the effect of measurement noise, a normally distributed random noise with zero mean and unit standard deviation is added to the calculated dynamic response as,

$$\ddot{x}_n = \ddot{x}_{cal} + E_p N_{oise} std(\ddot{x}_{cal}) \tag{3.66}$$

where $\ddot{x}_n$ and $\ddot{x}_{cal}$ are simulated noisy response and original calculated response, respectively; E_p is the noise level; N_{oise} is a standard normal distribution vector with zero mean and unit standard deviation and $std(\ddot{x}_{cal})$ denotes the standard deviation of the original calculated response.

The acceleration responses of the structure from SP set 1 with 6 sensors are simulated as “measured” for a duration of 16.384s with a sampling rate of 1000Hz. Note that the response analysis under ZOH and FOH approximations is performed respectively and 10% noise effect is included in the measurements from Equation (3.66). The “polluted” response time histories at sensor location Node 15(x) from ZOH and FOH are displayed in Figures 3.9 and 3.10, respectively. It can be found that the time domain response after 4s has decayed close to zero and the frequency Fourier spectrum data after 100Hz is very small.

The “polluted” response time histories are then filtered using a low-pass filter with a cutoff frequency of 100Hz which is much higher than the frequency of significant vibrations in this study. These filtered data are then used for response reconstruction. Figures 3.11 and 3.12 show the relative errors obtained from Equations (3-64) and (3-65) in the response reconstruction results at all DOFs in the Unknown-set under ZOH and FOH respectively. Note that most relative errors with large values are located at the rotational DOFs probably because no measurements at any rotational DOFs are included in the Known-set response vector. It is also noticed that the response reconstruction under ZOH and FOH gives similar accuracy as shown in Figures 3.11 and 3.12 and the relatively large noise effect is noted to have large influence on the response reconstruction. The maximum relative error in Figure 3.12 is around 10% at DOF Number 60, i.e. at Node 21(θ). Thus the analytical and reconstructed responses under FOH at Node 21(θ) are shown in Figure 3.13. It can be found that both the reconstructed response in frequency domain and reconstructed time domain response are close to the analytical true values except at frequencies higher than 70 Hz while the time domain responses are almost overlapping. This indicates that the proposed method can give good response reconstruction results even with large noise level. The relative error computed for the first 1.5s in the time domain is 4.7% which is much smaller than that shown in Figure 3.12 indicating a much high accuracy with the reconstruction when there is significant vibration component in the response close to the beginning of excitation.

3.4.1.2 Response Reconstruction in a Substructure

Case 1: When the Finite Element Model of the Full Structure is Available

The sixth and seventh storeys are taken as a substructure in this study, as shown in Figure 3.3(b). There are 14 nodes and 42 DOFs in the substructure. When Equation (3.16) is used for reconstructing the Unknown-set response vector in a substructure, the simulated “measured” Known-set response vector of this substructure and analytical interface forces vector from finite element analysis are used.

The sampling duration and sampling rate are 16.384s and 1000Hz, respectively. Figure 3.14 shows the relative errors in the response reconstruction results obtained from Equation (3.64) in the frequency domain using ZOH and FOH force approximations. Figure 3.15 shows the relative errors obtained with Equation (3.65) in the time domain with FOH approximation when the inverse discrete Fourier transform is used to recover the time domain response from the reconstructed response in frequency domain. It can be noticed that most of the relative errors are about 1% and this indicates that the presented response reconstruction process is accurate. Similarly, most large relative errors are at the rotational DOFs. The analytical and reconstructed responses in frequency and time domain at the third DOF in the substructure, that is Node 11(θ), are displayed in Figure 3.16. It can be found that these two sets of responses are also almost overlapping which indicates that the reconstruction process is close to exact.

Effect of Sampling Duration and Sampling Rate

The sampling duration varies from 4.192s to 32.768s and the sampling rate varies from 250Hz to 2000Hz. Table 3.3 lists the average relative errors of the frequency spectrum in the reconstructed response results with different sampling duration and sampling rate settings in the substructure. The results show that when longer sampling duration or higher sampling rate are used, more accurate response reconstruction results would be obtained similar to the observations in Section 3.4.1.1.

Effect of Numbers of Measured Responses

The SP set 2 is used and Table 3.4 lists the average relative errors of the frequency spectrum in the reconstructed response results when different sampling duration and sampling rate settings are used. It can be noticed by comparing the errors in Tables 3.3 and 3.4 that the accuracy for response reconstruction with SP set 1 is better than that with SP set 2.

Effect of Noise in the Measured Responses

Measurements from SP set 1 with a duration of 16.384s and 1000Hz sampling rate are used in this study, and the simulated "measured" data with noise effect is low-pass filtered with a cutoff frequency of 100Hz. These filtered sensor data are used for response reconstruction in this substructure with Equation (3.16). The responses at the interface DOFs are also reconstructed. Figures 3.17 and 3.18 show the relative errors obtained with Equations (3.64) and (3.65) in the response reconstruction results under ZOH and FOH respectively at all the DOFs in the Unknown-set when 10% noise effect is included in the measurements. It can be seen from Figures 3.17 and 3.18 that most relative errors are less than 10%. Most large relative errors are also located at the rotational DOFs and the two largest ones are related to the rotational DOF of interface Nodes 11 and 34. Observations similar to Figures 3.11 and 3.12 are obtained since large noise effect has large influence on the response reconstruction. Analytical and reconstructed responses at Node 34(θ) in frequency and time domain under FOH are shown in Figure 3.19. It may be concluded that good response reconstruction result can be obtained using the presented approach even with large noise level.

Inspection of Figure 3.19(b) shows that the recovered time response after 3s is affected by the noise effect because of their small magnitude. Another computation on the relative error is performed for the first 3s of the recovered time response, which is 9.6% and is much smaller than that shown in Figure 3.18 indicating a much higher accuracy with the response reconstruction when there is significant vibration component.

Case 2: When only the Finite Element Model of the Target Structure is Available

The sampling duration and sampling rate are 16.384s and 1000Hz, respectively. The number of sensor measurements in the Known-set response vector should be equal or greater than the number of interface forces. Therefore eight sensors at Node 12(x), 13(x), 13(y), 14(x), 15(y), 30(y), 31(x) and 33(x), noted as SP set 3, are placed in the substructure to record the dynamic acceleration responses which are included in the Known-set response vector. The responses from the remaining DOFs of the substructure are included in the Unknown-set response vector. Responses under ZOH and FOH force approximations are recorded at the Known-set response locations, and Equation (3.18) is used to conduct the response reconstruction. IDFT is used to transform the reconstructed frequency domain responses into time domain. The relative errors between the analytical and recovered time domain responses are shown in Figure 3.20. The response reconstruction errors from ZOH responses are far larger than those from FOH responses. It can also be noted in Figure 3.20(a) that relative errors at the rotational DOFs of two interface nodes are much larger than those at other DOFs. Figure 3.20(b) shows the relative errors at DOFs of internal nodes of the substructure. The response reconstruction errors at translational x and y DOFs are less than 5% while the errors at rotational DOFs are large since no rotational measurement is included in the Known-set response vector. The relative errors from FOH responses are generally less than 5%.

Effect of Sampling Duration and Sampling Rate

The sampling duration varies from 4.192 to 32.768s and the sampling rate varies from 250 to 2000Hz. Table 3.5 lists the average relative errors between the analytical and reconstruction time domain responses. Note that the average relative error here is the mean value of relative errors from all DOFs of internal nodes of the substructure. More accurate response reconstruction results can be obtained when a longer sampling duration or a higher sampling rate is used. However, the accuracy in response reconstruction with a low sampling rate may not good.

Effect of Noise in the Measured Responses

The sampling duration and sampling rate are 16.384s and 1000Hz, respectively. The response analysis under ZOH and FOH force approximations is performed and 10% noise effect is included in the measurements. The noisy measured responses are low-pass filtered with a cutoff frequency of 100Hz. Then these filtered data are used for the response reconstruction. Figure 3.21 shows the relative errors at DOFs of the internal nodes of the substructure. The errors at translational DOFs are around 10% while several relative errors at those rotational DOFs are large even up to 50%. This is probably because rotational information is difficult to reconstruct when no any rotational responses are used in the Known-set response vector. The largest error in all translational DOFs is at Node 32(x) and it is 12.83% from ZOH responses and 12.13% from FOH responses. Figure 3.22 shows the analytical and reconstructed responses in the first 2 seconds at Node 32(x) with 10% noise included in the measurements. Good response reconstruction results can be obtained when there is significant vibration component close to the beginning of the excitation. When more measurements are included in the Measured-set response vector or a sensor placement configuration with optimal locations covering richer response information, a better accuracy on the reconstruction of responses at the rotational DOFs could be obtained.

3.4.2 Response Reconstruction in Wavelet Domain

3.4.2.1 Response Reconstruction in a Full Structure

Response Reconstruction in Wavelet Domain

SP set 1 in Section 3.4.1.1 is used and the responses from these six measurement locations are simulated as "measured" responses and included in the Known-set response vector $x_k(t)$. The responses from the remaining DOFs are taken as the Unknown-set response $x_u(t)$, which will be predicted using Equation (3.52) in the full structure. The accuracy in the response reconstruction results using approaches in the frequency and wavelet domains will be compared. They are named as "frequency domain method" and "wavelet domain method" respectively.

When the response reconstruction process is performed with Equation (3.52) in wavelet domain, the dimensions of each matrix and vector are indicated in Equation

(3.50) and the dimensions of matrices $\ddot{h}_k^{DWT}$ and $\ddot{h}_u^{DWT}$ are $mn \times rl$ and $sn \times rl$, respectively. Since six sensors are included in the Known-set response vector and there are one hundred and twenty DOFs in the Unknown-set, the numbers m, s (number of measurements in the Known-set and Unknown-set) are 6 and 120, respectively. The response data in the first one second is considered. With a sampling rate of 1000Hz, n equals to 1000. r is the number of external excitation forces on the structure and is equal to 2. In this study, Daubechies 8-coefficient wavelet is chosen as the basis functions in the DWT due to its orthogonality properties and fairly smooth interpolation nature (Robertson *et al.* 1998). l equals to 1029 when two-level discrete wavelet transform is conducted for the 1000-point signal record. Therefore, the dimensions of matrices $\ddot{h}_k^{DWT}$ and $\ddot{h}_u^{DWT}$ are 6000×2058 and 120000×2058, respectively. Due to the large size of these two matrices, the computation load for computing T_{ku} matrix in Equation (3.53) is high especially for the computation of the pseudo-inverse of matrix $\ddot{h}_k^{DWT}$. The computation load would become much more intensive if a longer sampling duration or a higher sampling rate is used due to the increasing size of matrix $\ddot{h}_{ke}^{DWT}$. With consideration of available computation capacity, the case with one second data in the Known-set measurements is considered appropriate for response reconstruction using the wavelet domain method.

Comparison of Reconstructed Responses from the Frequency and Wavelet Domain Methods

The relative errors calculated from the first one second response data at all the DOFs of the Unknown-set in the structure are obtained from Equation (3.65). The response reconstruction in the frequency domain is conducted with the FOH input approximation in the forward response computation while ZOH is used in the wavelet domain method. Figures 3.23(a) and 3.23(b) show the relative errors in response reconstruction results from frequency and wavelet domain methods, respectively. It can be seen that the relative errors from wavelet domain method are far less than those from the frequency domain method. The relative errors for all DOFs in Figure 3.23(b) are less than $1.5\times10^{-9}\,\%$ indicating that the proposed response reconstruction method in wavelet domain is very accurate.

Effect of Number of Sampled Data and the Sampling Rate

For the frequency domain method, the effect of total sampled data and sampling rate of the measurements are studied. The sampling duration is selected to vary from 4.096s to 16.384s with a constant sampling rate of 1000Hz. In another study, the sampling rate is allowed to vary from 250Hz to 1000Hz with a constant sampling duration of 16.384s.

However in the response reconstruction with wavelet domain method, an increase in the number of sampled data would significantly increase the size of matrix $\ddot{h}_k^{DWT}$ and the computation load would become extremely intensive. Therefore, the sampling duration is limited to the first one second. The sampling rate is changing from 250Hz to 1000Hz.

Table 3.6 lists the relative errors averaged over all the DOFs in the Unknown-set response vector from the frequency and wavelet domain methods. The frequency domain method is shown to give slightly better response reconstruction results when a longer sampling duration or a higher sampling rate is used. While for the wavelet domain method, the accuracy of response reconstruction is not obviously affected by the sampling rate, and it gives much accurate results than the frequency domain method.

Effect of Number of Measured Responses

SP set 2 sensor placement configuration defined earlier in this Chapter is used here. The relative errors in the response reconstruction from the frequency and wavelet domain methods with different sampling duration and sampling rate are listed in Table 3.7. It can be found by comparing the results in Tables 3.6 and 3.7

that the accuracy in response reconstruction with SP set 1 is slightly better than that with SP set 2.

Effect of Noise in the Measured Responses

Acceleration responses of the structure from SP set 1 are simulated "measured" with 10% noise effect added in the measurements. For frequency domain method, a sampling duration of 16.384s with a sampling rate 1000 Hz is used. The noisy data are low-pass filtered with a cutoff frequency of 100Hz and these filtered data are used for response reconstruction.

Figure 3.24(a) and 3.24(b) show the relative errors in the response reconstruction results at all the DOFs in the Unknown-set response vector from frequency and wavelet domain methods respectively when 10% noise effect is considered in the measurements. It can be seen that all relative errors are less than 5%. Most of the larger relative errors are located at the rotational DOFs, which may be due to the absence of rotational response in the Known-set response vector. The largest errors in the results from the frequency and wavelet domain method are respectively 4.44% and 4.72%. The analytical and reconstructed time domain responses at DOF 48, that is Node 16(θ) from the frequency and wavelet domains, are shown in Figures 3.25(a) and 3.25(b). It is noted that good response reconstruction results can still be obtained using the proposed approach with 10% noise effect.

3.4.2.2 Response Reconstruction in a Substructure

Case 1: When the Finite Element Model of the Full Structure is Available

Comparison of Reconstructed Responses from the Frequency and Wavelet Domain Methods

When the response reconstruction process is performed with Equation (3.57) in the wavelet domain, the dimensions of each matrix and vector are indicated in

Equation (3.55), and the dimensions of matrices T_{ku}^{e} and H_{ku}^{I} are $sn \times mn$ and $sn \times ql$, respectively. SP1 set 1 sensor placement is used here and response data in the first one second with a sampling rate of 1000Hz is considered. Therefore, the dimensions of matrices $\ddot{h}_{ue}^{DWT}$ and $\ddot{h}_{ke}^{DWT}$ are 36000×2058 and 6000×2058, respectively. Figures 3.26(a) and 3.26(b) show the relative errors in response reconstruction results from the frequency and wavelet domain methods, respectively. It can be seen that the relative errors from wavelet domain method are far less than those from frequency domain method. The relative errors for all DOFs in Figure 3.26(b) are less than 4×10^{-9} % indicating that the proposed response reconstruction method in wavelet domain is very accurate. The maximum relative error in both Figures 3.26(a) and 3.26(b) is at the last DOF of the substructure, which is Node 34(θ). Figure 3.27 shows the analytical and reconstructed time domain responses with the frequency and wavelet domain methods at Node 34(θ) and it is noted that the analytical and reconstructed responses are almost overlapping.

Effect of Number of Sampled Data and the Sampling Rate

Table 3.8 lists the relative errors averaged over all the DOFs in the Unknown-set response vector using the frequency and wavelet domain methods. The frequency domain method is shown to give slightly better response reconstruction results when a longer sampling duration or a higher sampling rate is used. While for wavelet domain method, the accuracy of response reconstruction is not obviously affected by the sampling rate, and it generally gives much accurate results than the frequency domain method.

Effect of Number of Measured Responses

SP set 2 sensor placement configuration with three sensors is considered. The relative errors in the response reconstruction from the frequency and wavelet domain methods with different sampling durations and sampling rate are listed in Table 3.9.

Comparisons of Tables 3.8 and 3.9 show that both SP sets 1 and 2 exhibit similar accuracy in the reconstructed responses. It is also noted that more measurements in the Known-set with SP1 contribute a higher accuracy of response reconstruction from wavelet domain method.

Effect of Noise in the Measured Responses

Acceleration responses of the substructure from SP set 1 are "measured" for a sampling duration of 16.384s with a sampling rate 1000Hz. Note that 10% noise effect is included in the "measured" sensor responses. The "measured" responses including the noise effect are then low-pass filtered with a cutoff frequency of 100Hz which is much higher than the frequency of interest in this study. These filtered data are then used for the response reconstruction.

Figure 3.28(a) and 3.28(b) show the relative errors in the response reconstruction results at all the DOFs in the Unknown-set response vector from the frequency and wavelet domain methods when 10% noise effect is considered in the measurements. It can be seen that all relative errors are less than 10%. Most of the larger relative errors are located at the rotational DOFs, which may be due to the absence of rotational response in the Known-set response vector. The largest errors in the results from the frequency and wavelet domain method are respectively 7.43% and 7.30% and they are at the rotational DOF of interface Node 34. The analytical and reconstructed time domain responses at this DOF are shown in Figures 3.29(a) and 3.29(b). It is noted that satisfactory response reconstruction results can still be obtained using the proposed approach with 10% noise effect.

Case 2: When only the Finite Element Model of the Target Structure is Available

Comparison of Reconstructed Responses from the Frequency and Wavelet Domain Methods

SP set 3 defined in Section 3.4.1.2 is used to record the dynamic acceleration responses which are included in the Known-set response vector. The responses from the remaining DOFs of the substructure are included in the Unknown-set response vector. Equation (3.61) is used to conduct the response reconstruction in the substructure. Figures 3.30(a) and 3.30(b) show the relative errors in response reconstruction results within the first second data from frequency and wavelet domain methods, respectively. The errors from frequency domain method at the rotational DOFs of two interface nodes are very large while errors at those DOFs of internal nodes are less than 5%. It is noted that relative errors from wavelet domain method at all the DOFs of the substructure are less than 8×10^{-7}.

Effect of Number of Sampled Data and the Sampling Rate

Table 3.10 lists the relative errors averaged over all the DOFs in the Unknown-set response vector using frequency and wavelet domain methods. The adaptation of a higher sampling rate will give a better accuracy of the response reconstruction from frequency domain method. While for wavelet domain method, the accuracy of response reconstruction is not obviously affected by the sampling rate, but it gives much accurate results than the frequency domain method.

Effect of Noise in the Measured Responses

10% noise effect is included in the measurements. The noisy measured responses are low-pass filtered with a cutoff frequency of 100Hz. Then these filtered data are used for the response reconstruction. Figure 3.31 shows the relative errors at DOFs of internal nodes of the substructure. The errors at translational DOFs are around 5% while several relative errors at rotational DOFs are large. The largest error in all translational DOFs is at Node 32(x) and it is 5.34% from the frequency domain method and 5.14% from the wavelet domain method. Figure 3.32 shows the analytical and reconstructed responses within the first one seconds at Node 32(x) when 10% noise effect is included in the measurements. Good response reconstruction results can be obtained.

3.5 Discussion and Summary

This Chapter presents the structural dynamic response reconstruction approaches in both the frequency and wavelet domains. They are called “frequency domain method” and “wavelet domain method”, respectively. The frequency response function in frequency domain or the unit impulse response function in wavelet domain is used to formulate the transmissibility matrix and conduct the response reconstruction in the full structure and in the substructure. A seven-storey plane frame structure is taken as an example to investigate the accuracy and efficiency of the proposed frequency and wavelet domain methods for structural response reconstruction. Numerical studies show that these two techniques were successfully used for response reconstruction in the full structure and in the substructure.

(1) Response reconstruction in the full structure treats the applied excitations as unknown force vectors on the structure and the transmissibility matrix is formulated with frequency response function in frequency domain or unit impulse response function in wavelet domain to form the relationship between two sets of response vectors. The time-histories of the applied excitations are not required and the locations of these excitations should be assumed known. The FOH discrete force approximation is used in the forward response computation to improve the accuracy of the dynamic response analysis. Simulation studies show that response reconstruction using the frequency domain method with FOH discrete gives better response reconstruction results than that with ZOH.

(2) Two cases for response reconstruction in a substructure are considered. The first case assumes that the interface forces are available either from measurement or from computation from the full finite element model of the structure. The external excitations on the structure are used in the dynamic response analysis and then the interface forces are obtained from the finite element analysis of the full structure. The second case eliminates this restraint with only the finite element model of the substructure available in the response reconstruction

process. The interface forces are treated as the input excitations to the substructure. The transmissibility matrix is formulated using the frequency response function or unit impulse response function from the finite element model of the substructure.

It is found that more accurate response reconstruction results can be obtained from the frequency domain method when a longer sampling duration or a higher sampling rate is used, while the accuracy of response reconstruction from wavelet domain method is not subject to the sampling duration and sampling rate. More measurements in the Known-set response vector would contribute to a higher accuracy of reconstruction. For the noise-free case, the relative errors in the response reconstruction results from wavelet domain method are far less than those from frequency domain method. For the case when the measurements are included the noise effect, similar accuracies of response reconstruction are obtained from both the frequency and wavelet domain methods. It is observed that good response reconstruction results are obtained when there is significant vibration component in the response close to the beginning of excitation. It should also be noted that the selection of sensor numbers and locations may affect the accuracy in the response reconstruction results and this issue will be examined in future work.

Table 3.1: Errors (%) in the response reconstruction with different sampling duration and rate in frequency spectrum in a full structure (SP set 1)

Sampling Duration (s) (Sampling rate=1kHz)		4.096	8.192	16.384	32.768
Average error (%)	ZOH	1.34	0.83	0.81	0.81
	FOH	0.84	0.15	0.1	0.1
Sampling Rate (Hz) (Sampling duration = 16.384s)		250	500	1000	2000
Average error (%)	ZOH	13.76	3.41	0.81	0.2
	FOH	1.17	0.33	0.1	0.04

Table 3.2: Errors (%) in the response reconstruction with different sampling duration and rate in frequency spectrum in a full structure (SP set 2)

Sampling Duration (s) (Sampling rate=1kHz)		4.096	8.192	16.384	32.768
Average error (%)	ZOH	1.94	1.45	1.43	1.43
	FOH	0.93	0.17	0.12	0.12
Sampling Rate (Hz) (Sampling duration = 16.384s)		250	500	1000	2000
Average error (%)	ZOH	16.54	5.52	1.43	0.36
	FOH	1.49	0.36	0.12	0.04

Table 3.3: Errors (%) in the response reconstruction with different sampling duration and rate in frequency spectrum in a substructure (SP set 1)

Sampling Duration (s) (Sampling rate=1kHz)		4.096	8.192	16.384	32.768
Average error (%)	ZOH	3.52	0.85	0.48	0.45
	FOH	3.65	0.69	0.23	0.17
Sampling Rate (Hz) (Sampling duration = 16.384s)		250	500	1000	2000
Average error (%)	ZOH	7.58	1.86	0.48	0.23
	FOH	3.18	0.62	0.23	0.21

Table 3.4: Errors (%) in the response reconstruction with different sampling duration and rate in frequency spectrum in a substructure (SP set 2)

Sampling Duration (s) (Sampling rate=1kHz)		4.096	8.192	16.384	32.768
Average error (%)	ZOH	4.38	1.62	1.38	1.37
	FOH	4.18	0.76	0.25	0.2
Sampling Rate (Hz) (Sampling duration = 16.384s)		250	500	1000	2000
Average error (%)	ZOH	14.9	5.75	1.38	0.42
	FOH	3.64	0.65	0.25	0.23

Table 3.5: Errors (%) in the response reconstruction with different sampling duration and rate in time domain in a substructure

Sampling Duration (s) (Sampling rate=1kHz)		4.096	8.192	16.384	32.768
Average error (%)	ZOH	3.44	3.34	3.33	3.33
	FOH	0.97	0.57	0.55	0.55
Sampling Rate (Hz) (Sampling duration = 16.384s)		**250**	**500**	**1000**	**2000**
Average error (%)	ZOH	38.36	13.59	3.33	0.85
	FOH	8.47	1.92	0.55	0.19

Table 3.6: Errors (%) in the response reconstruction in the first second from SP set 1

	Sampling Duration (s) (Sampling Rate = 1000 Hz)			Sampling Rate (Hz) (Sampling Duration = 16.384 s)		
	4.096	8.192	16.384	250	500	1000
Error (%) from Frequency Domain Method	0.84	0.15	0.1	1.17	0.33	0.1
				Sampling Rate (Hz) (Sampling Duration = 1.0 s)		
		1.0		250	500	1000
Error (%) from Wavelet Domain Method		1.87×10^{-10}		5.28×10^{-11}	9.04×10^{-11}	1.87×10^{-10}

Table 3.7: Errors (%) in the response reconstruction in the first second from SP set 2

	Sampling Duration (s) (Sampling Rate = 1000 Hz)			Sampling Rate (Hz) (Sampling Duration = 16.384 s)		
	4.096	8.192	16.384	250	500	1000
Error (%) from Frequency Domain Method	0.93	0.17	0.12	1.49	0.36	0.12
				Sampling Rate (Hz) (Sampling Duration = 1.0 s)		
		1.0		250	500	1000
Error (%) from Wavelet Domain Method		1.32×10^{-9}		1.02×10^{-8}	1.59×10^{-8}	1.32×10^{-9}

Table 3.8: Errors (%) in the response reconstruction in the first second from SP set 1

	Sampling Duration (s) (Sampling Rate = 1000 Hz)			Sampling Rate (Hz) (Sampling Duration = 16.384 s)		
	4.096	8.192	16.384	250	500	1000
Error (%) from Frequency Domain Method	3.45	0.74	0.31	4.66	0.86	0.31
				Sampling Rate (Hz) (Sampling Duration = 1.0 s)		
		1.0		250	500	1000
Error (%) from Wavelet Domain Method		7.82×10^{-8}		7.65×10^{-8}	7.27×10^{-8}	7.82×10^{-8}

Table 3.9: Errors (%) in the response reconstruction in the first second from SP set 2

	Sampling Duration (s) (Sampling Rate = 1000 Hz)			Sampling Rate (Hz) (Sampling Duration = 16.384 s)		
	4.096	8.192	16.384	250	500	1000
Error (%) from Frequency Domain Method	3.41	0.71	0.30	4.90	0.86	0.30
				Sampling Rate (Hz) (Sampling Duration = 1.0 s)		
		1.0		250	500	1000
Error (%) from Wavelet Domain Method		2.40×10^{-6}		6.95×10^{-6}	4.26×10^{-6}	2.40×10^{-6}

Table 3.10: Errors (%) in the response reconstruction in the first second

	Sampling Duration (s) (Sampling Rate = 1000 Hz)			Sampling Rate (Hz) (Sampling Duration = 16.384 s)		
	4.096	8.192	16.384	250	500	1000
Error (%) from Frequency Domain Method	4.80	3.45	3.31	37.76	10.21	3.31
				Sampling Rate (Hz) (Sampling Duration = 1.0 s)		
		1.0		250	500	1000
Error (%) from Wavelet Domain Method		3.1×10^{-8}		0.099	3.22×10^{-5}	3.1×10^{-8}

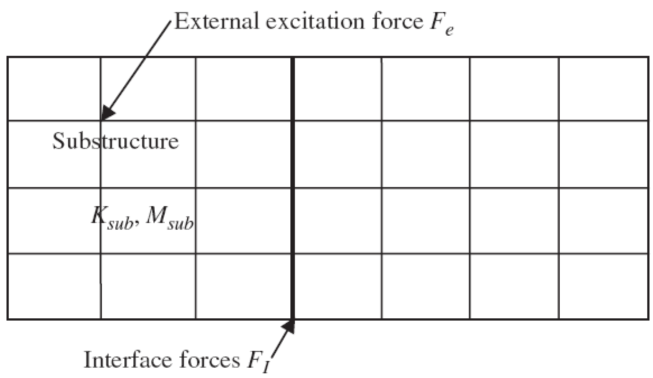

Figure 3.1: Example of a substructure

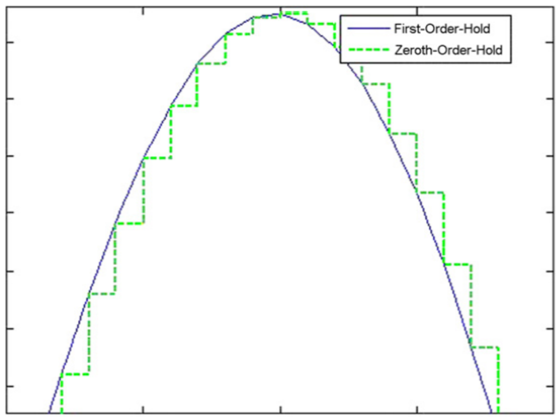

Figure 3.2: FOH and ZOH force approximations

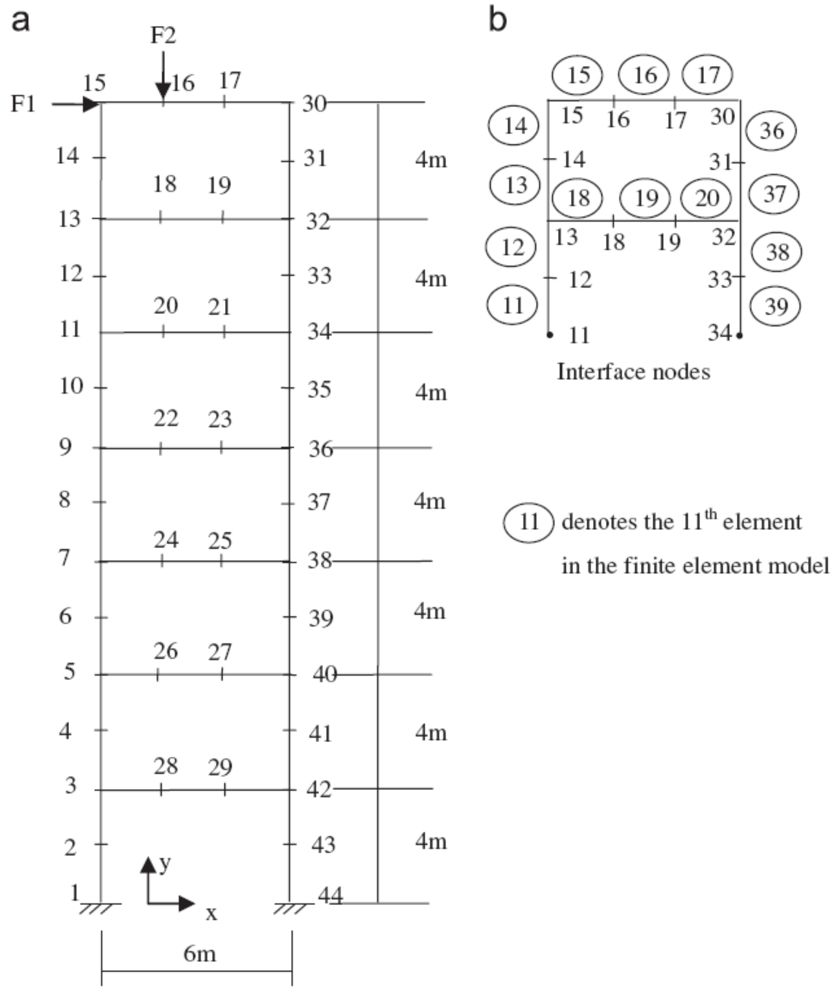

Figure 3.3: Finite element model of the frame structure

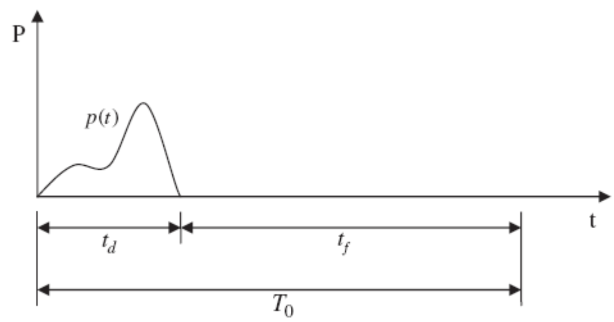

Figure 3.4: A schematic excitation force $p(t)$

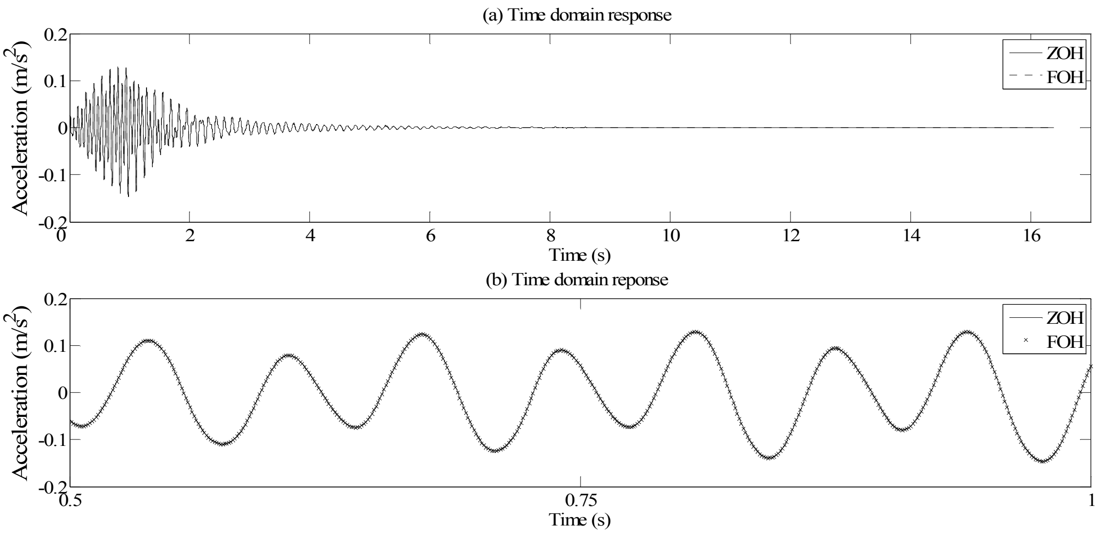

Figure 3.5: Time domain responses at sensor location Node 15(x) with ZOH and FOH force approximations

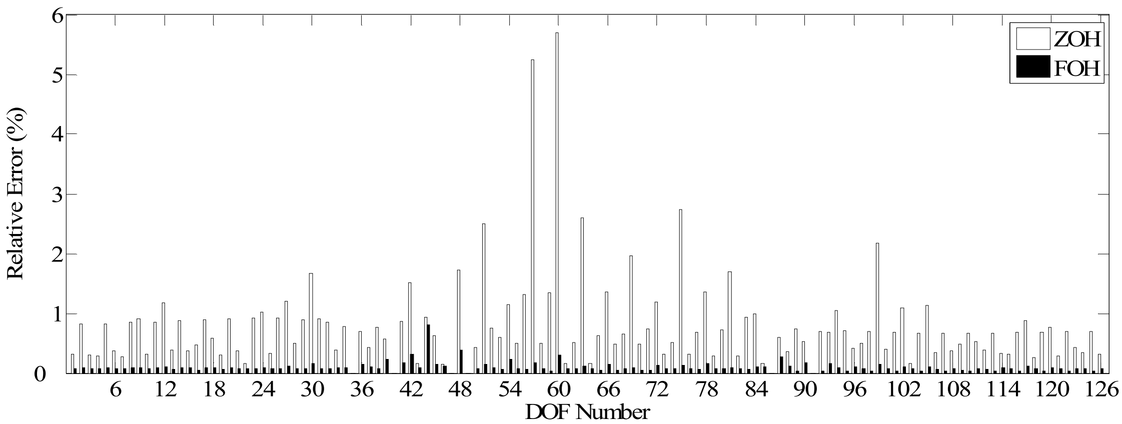

Figure 3.6: Relative errors of response reconstruction in frequency domain with "ZOH" and "FOH" responses

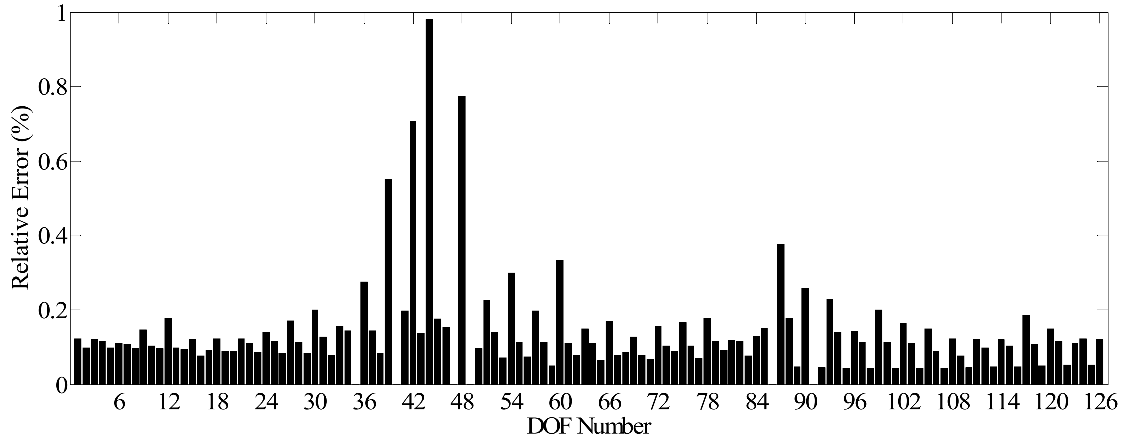

Figure 3.7: Relative errors of response reconstruction in time domain with FOH responses

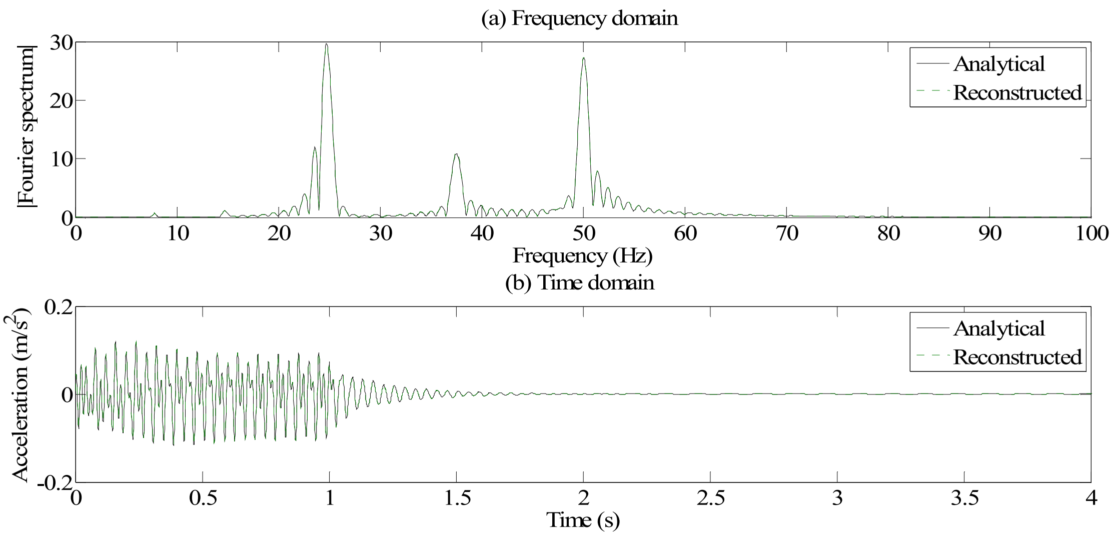

Figure 3.8: Analytical and reconstructed frequency and time domain responses at Node 16(y)

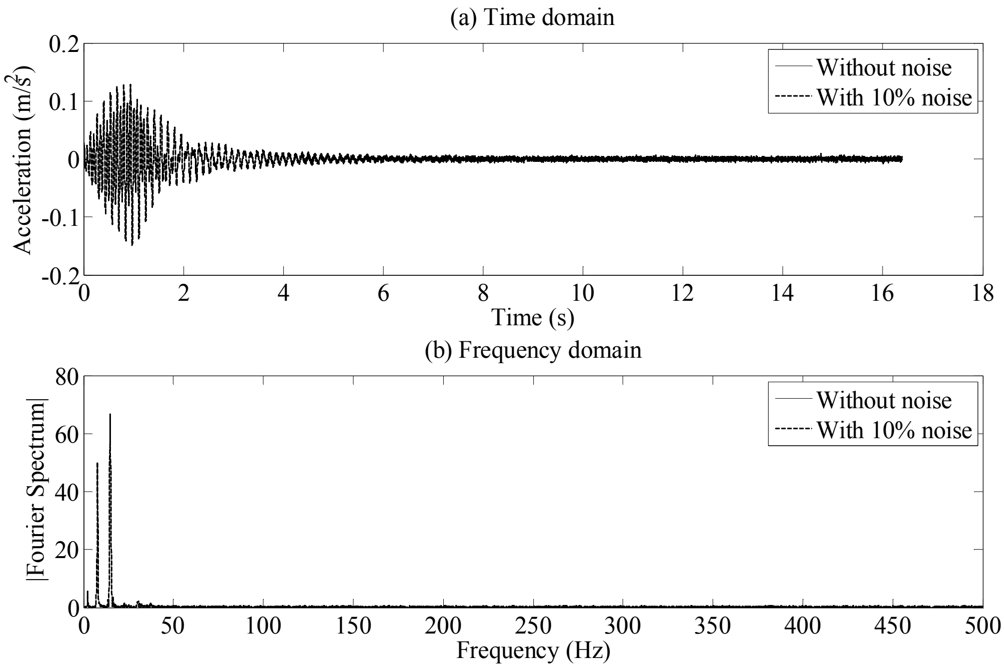

Figure 3.9: Simulated "measured" acceleration response at sensor location Node 15(x) under ZOH with 10% noise

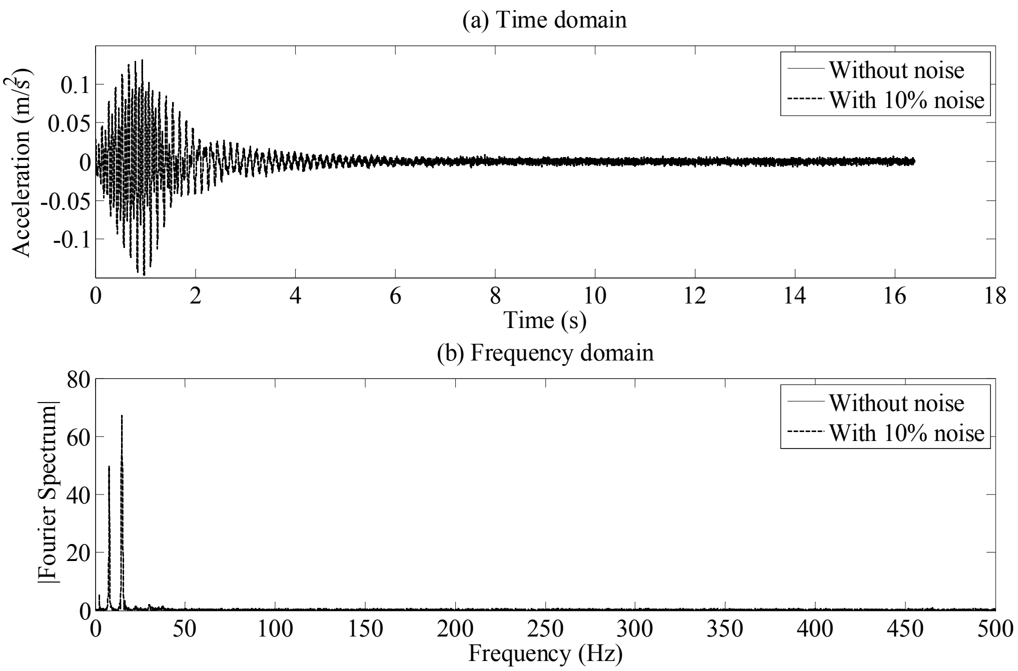

Figure 3.10: Simulated "measured" acceleration response at sensor location Node 15(x) under FOH with 10% noise

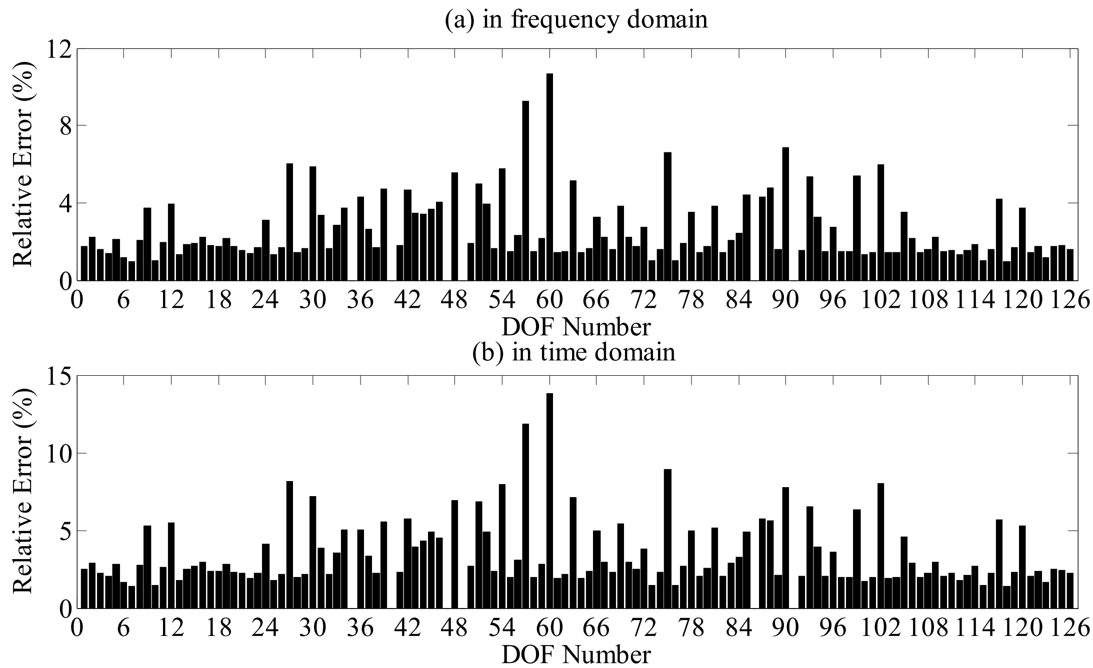

Figure 3.11: Relative errors in the response reconstruction results under ZOH with 10% noise in the measurements

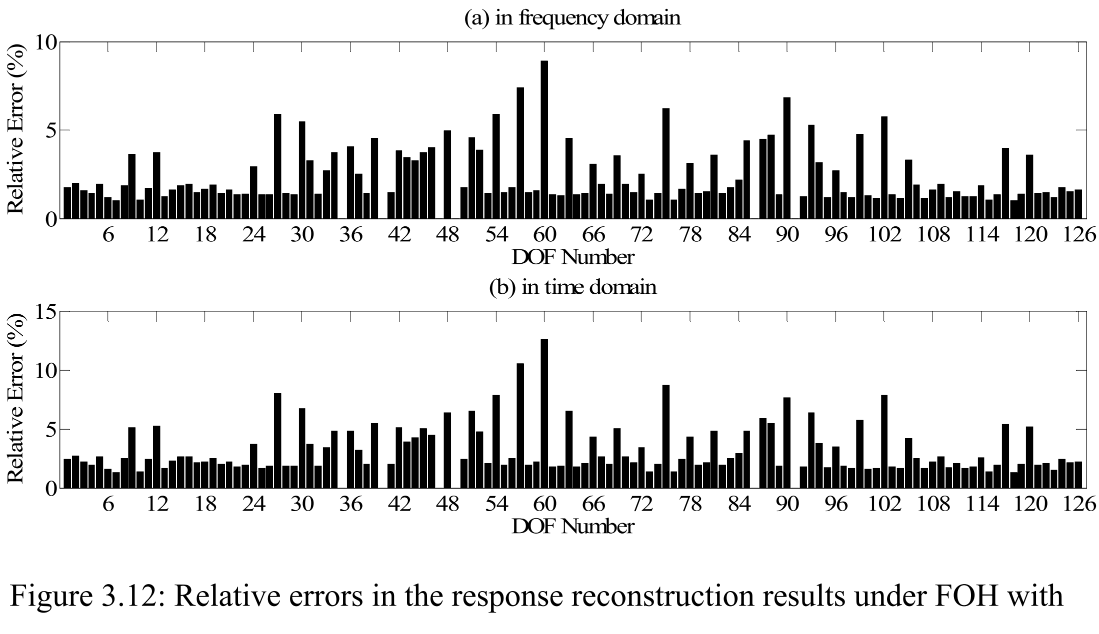

Figure 3.12: Relative errors in the response reconstruction results under FOH with 10% noise in the measurements

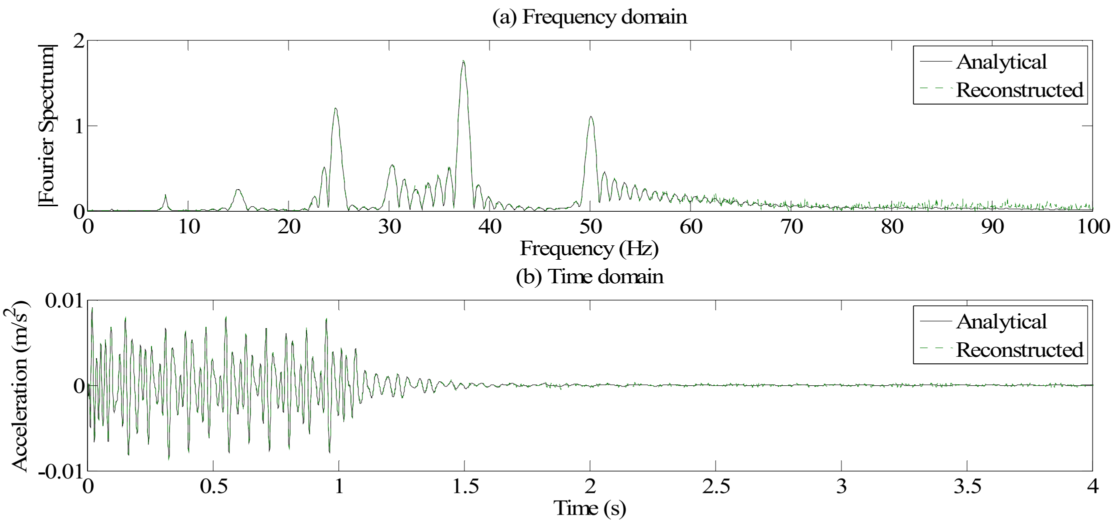

Figure 3.13: Analytical and reconstructed responses in frequency and time domain at Node 21(θ)

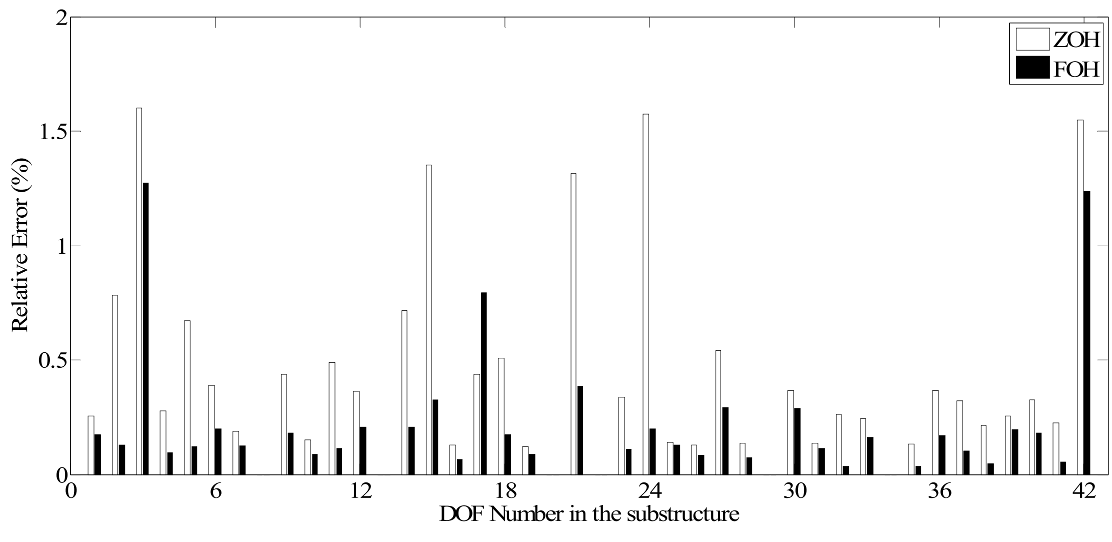

Figure 3.14: Relative errors of response reconstruction in the substructure in frequency domain with "ZOH" and "FOH" responses

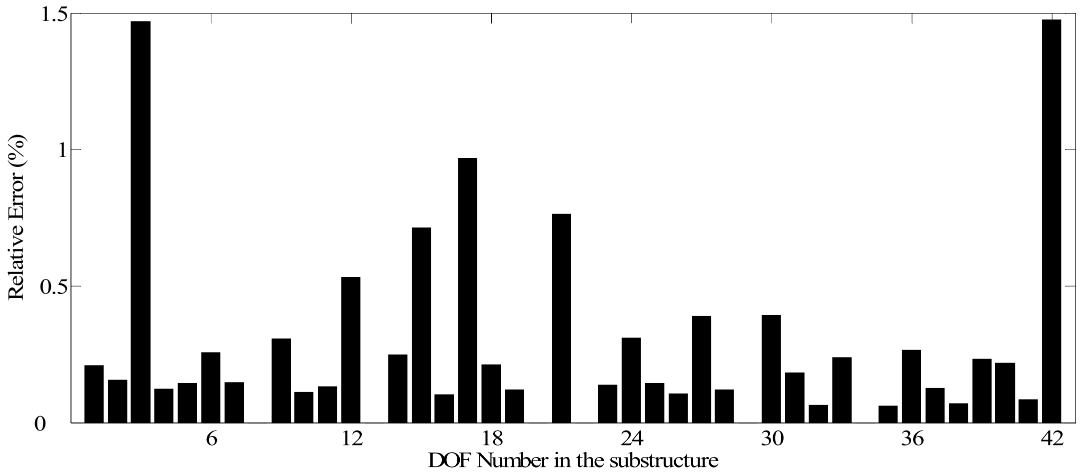

Figure 3.15: Relative errors of response reconstruction in the substructure in time domain with “FOH” responses

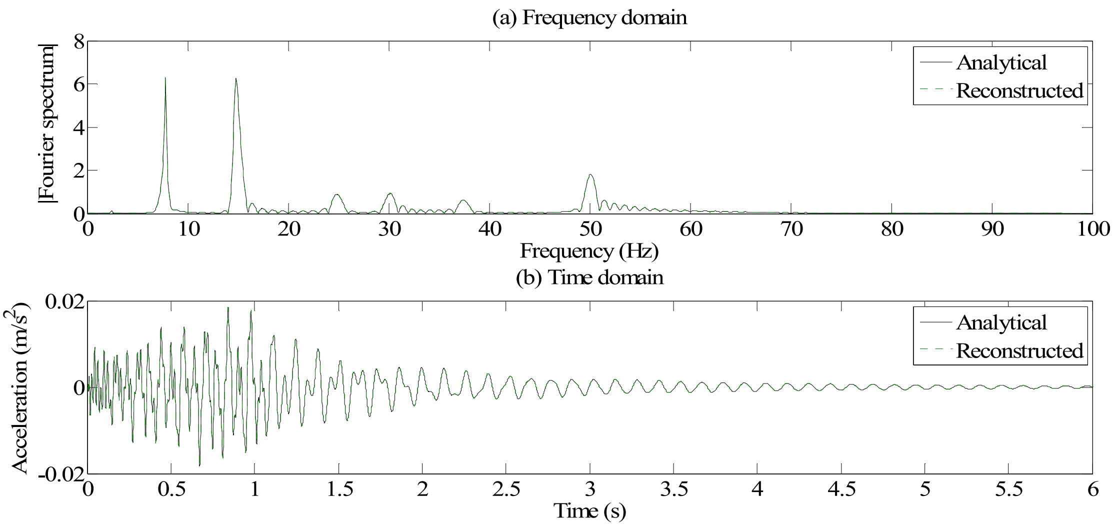

Figure 3.16: Analytical and reconstructed frequency and time domain responses in the substructure at Node 11(θ)

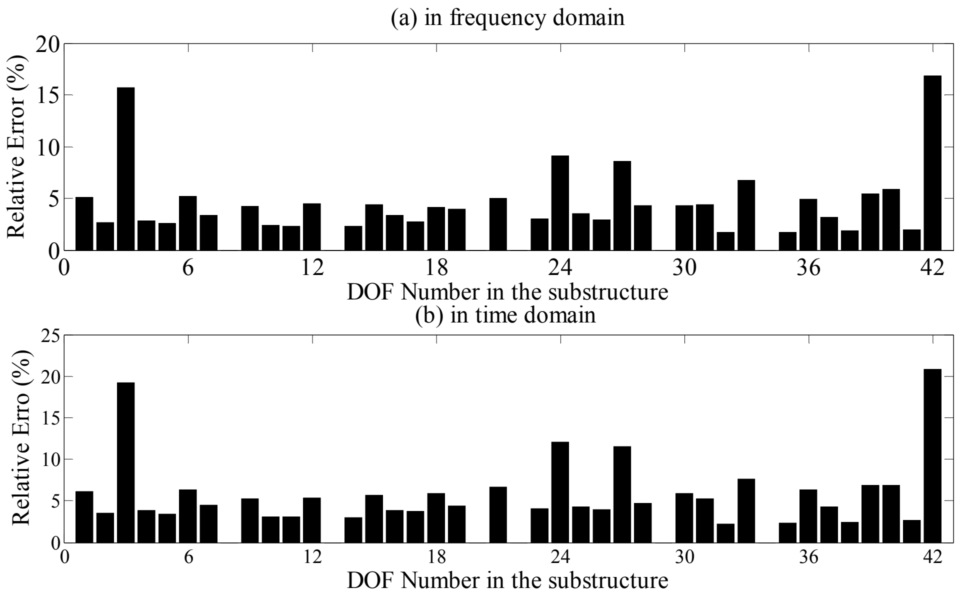

Figure 3.17: Relative errors in the response reconstruction results in the substructure under ZOH with 10% noise in the measurements

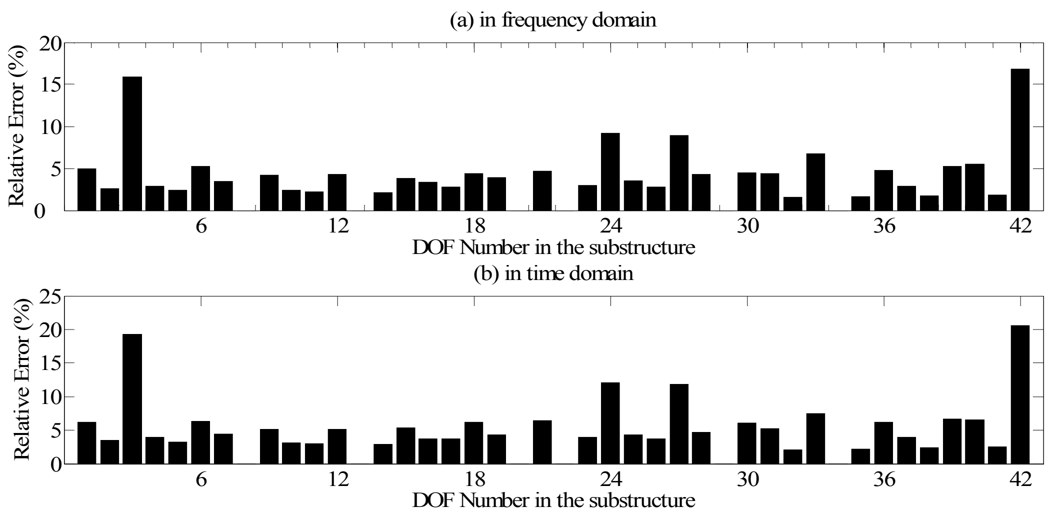

Figure 3.18: Relative errors in the response reconstruction results in the substructure under FOH with 10% noise in the measurements

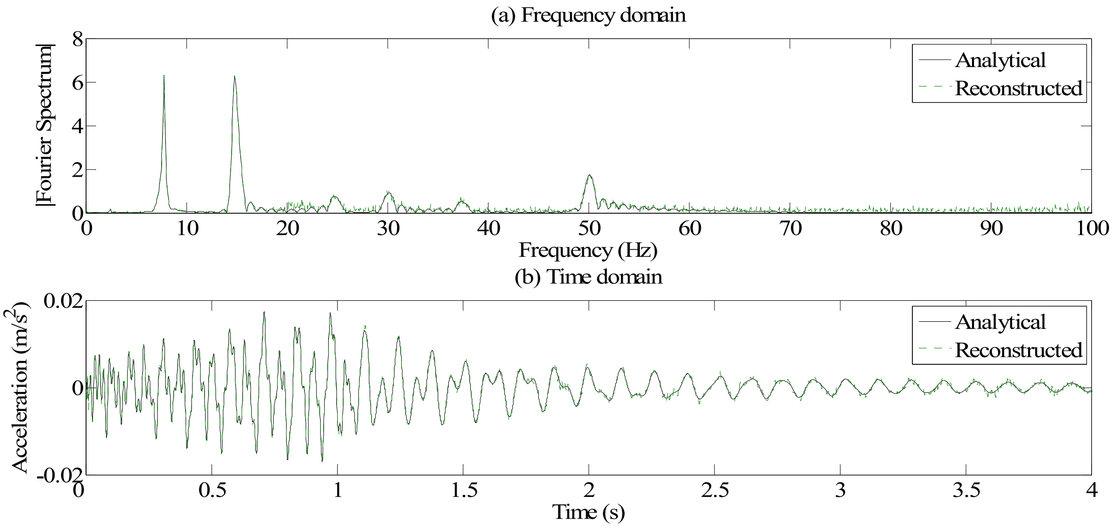

Figure 3.19: Analytical and reconstructed responses in frequency and time domain in the substructure at Node 34(θ)

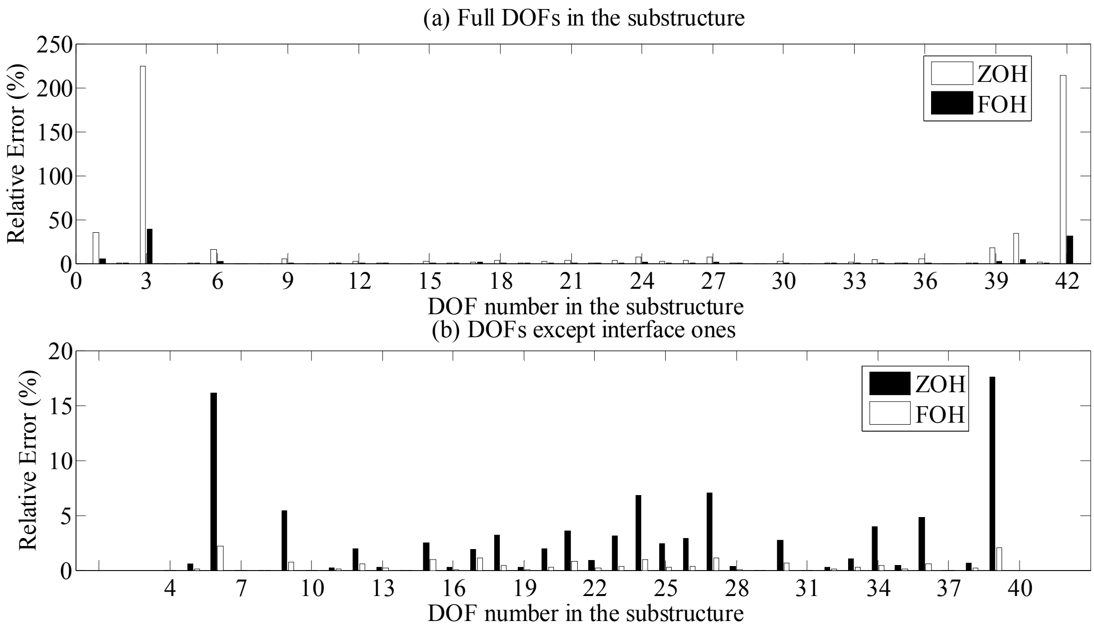

Figure 3.20: Relative errors of response reconstruction in the substructure in time domain with ZOH and FOH responses

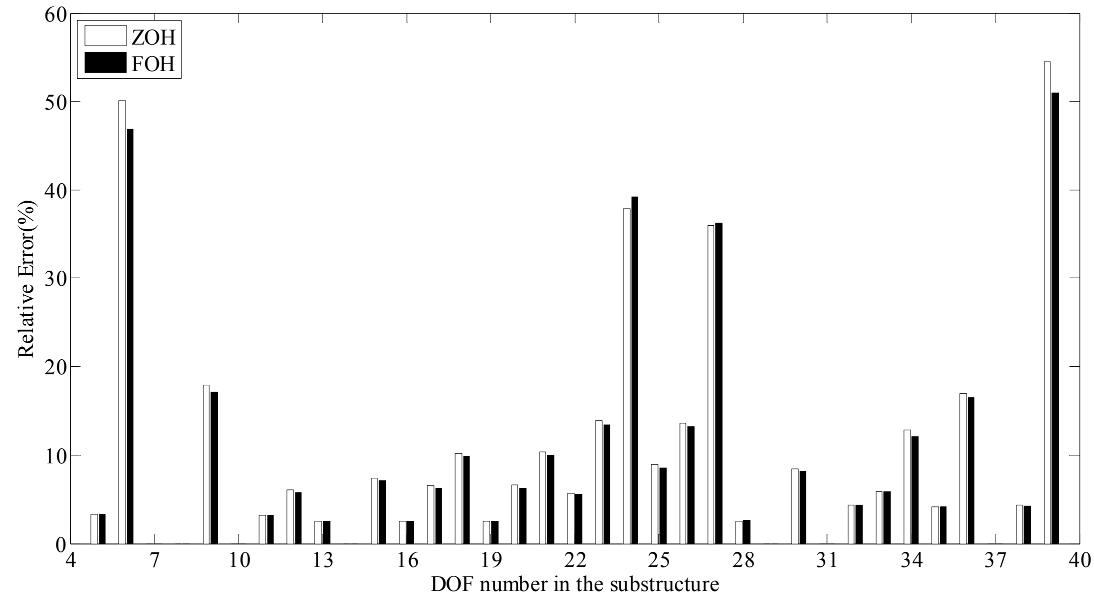

Figure 3.21: Relative errors of response reconstruction in the substructure in time domain with ZOH and FOH responses with 10% noise

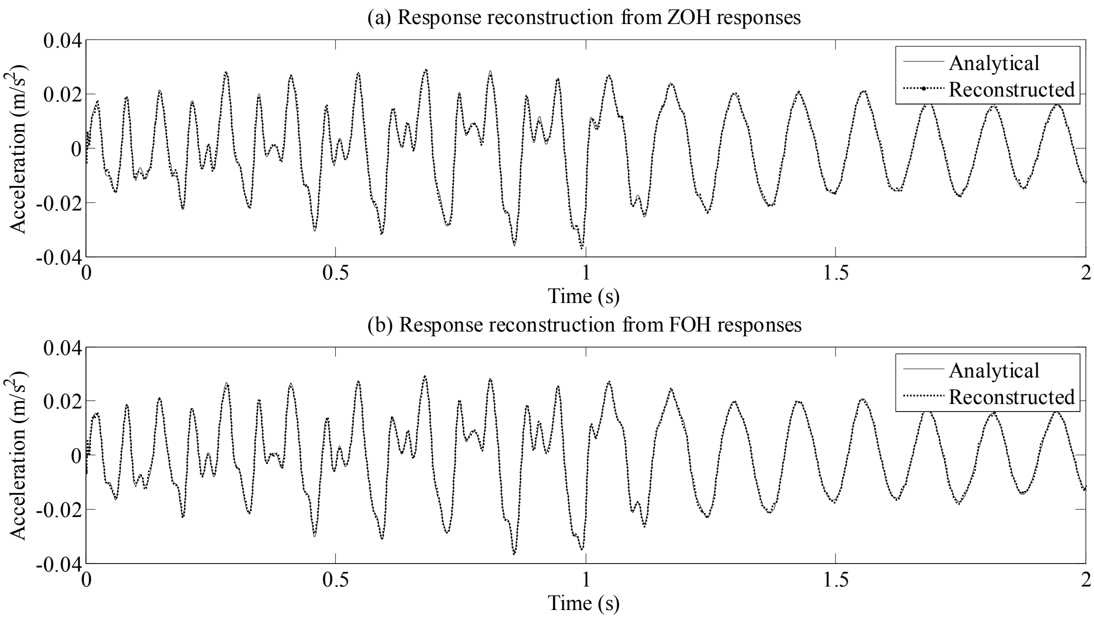

Figure 3.22: Analytical and reconstructed responses in time domain at Node 32(x) under 10% noise

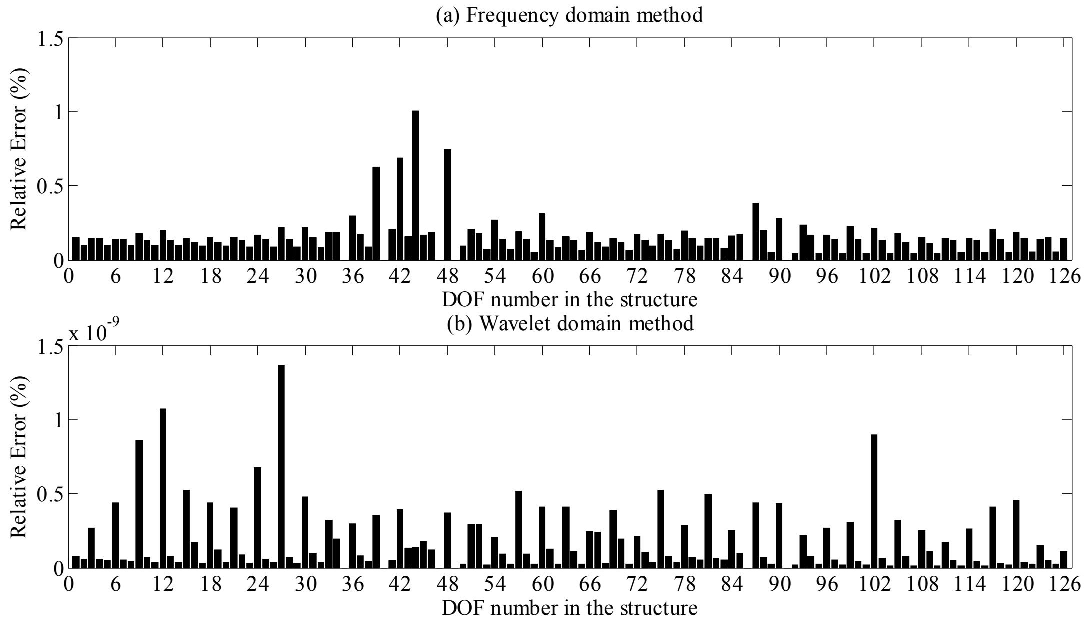

Figure 3.23: Relative errors of response reconstruction in the full structure in the time domain

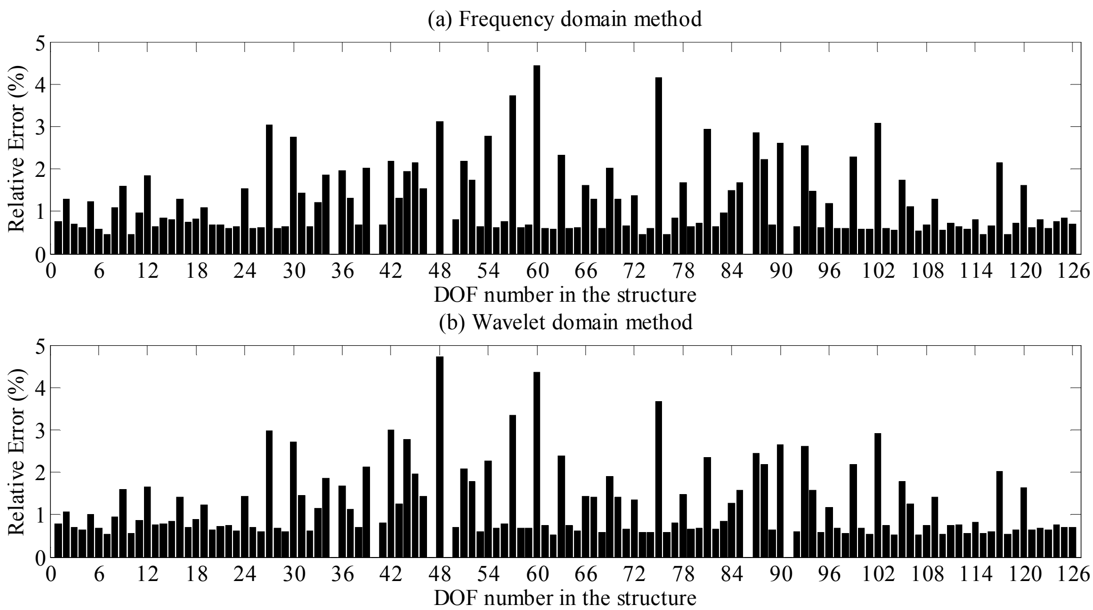

Figure 3.24: Relative errors in the response reconstruction results under 10% noise

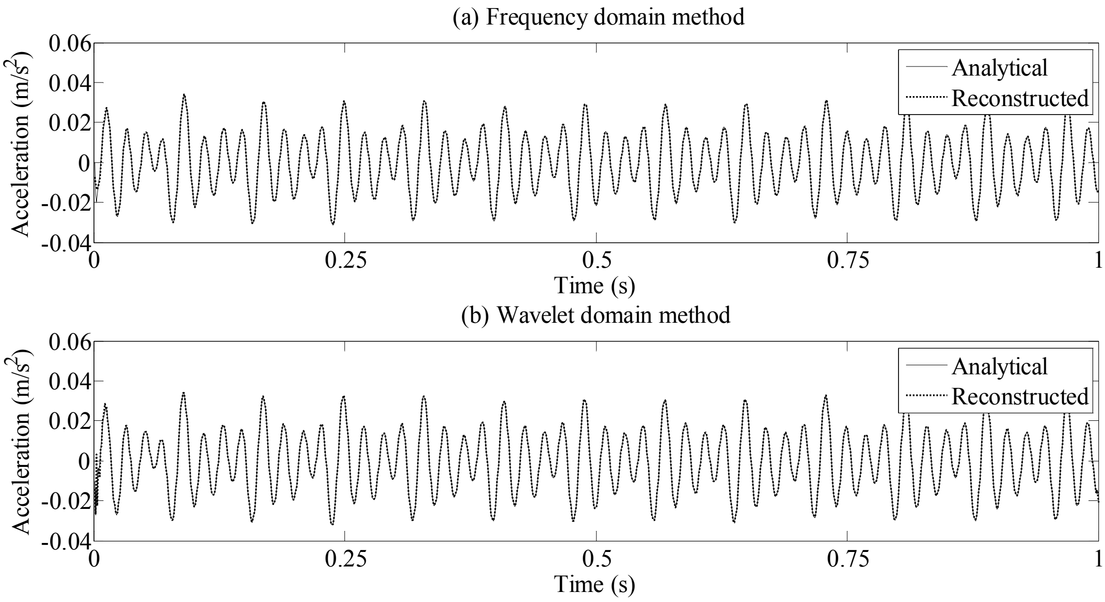

Figure 3.25: Analytical and reconstructed time domain responses at Node 16(θ) under 10% noise

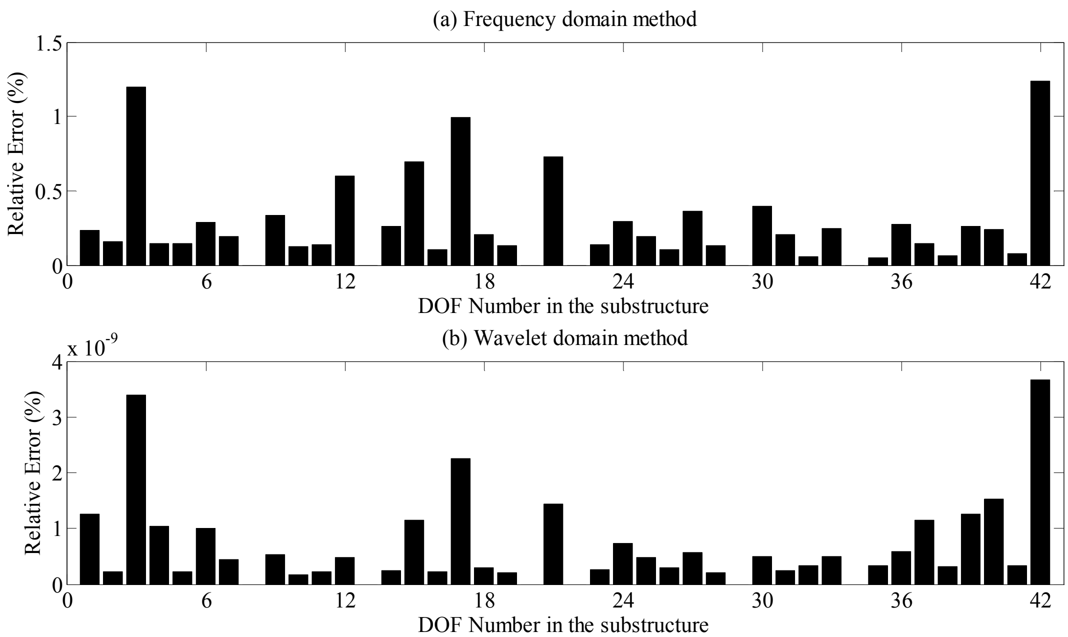

Figure 3.26: Relative errors of response reconstruction in time domain

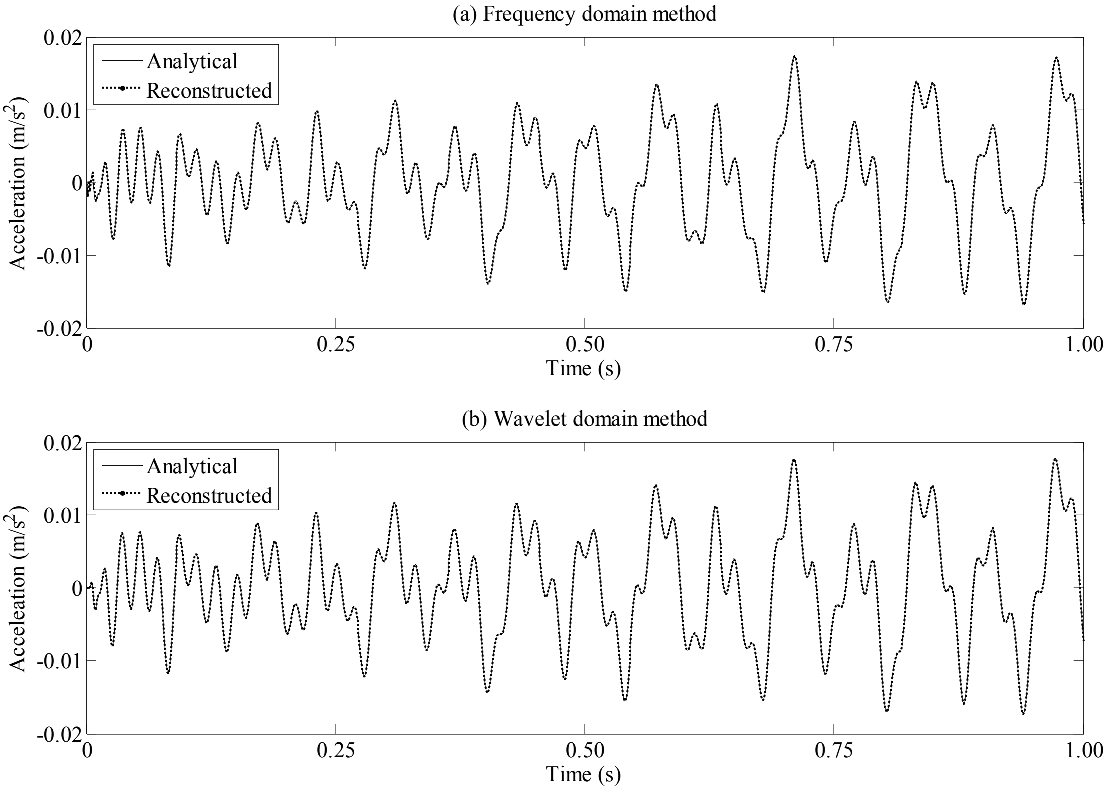

Figure 3.27: Time domain analytical and reconstructed responses at Node 34(θ)

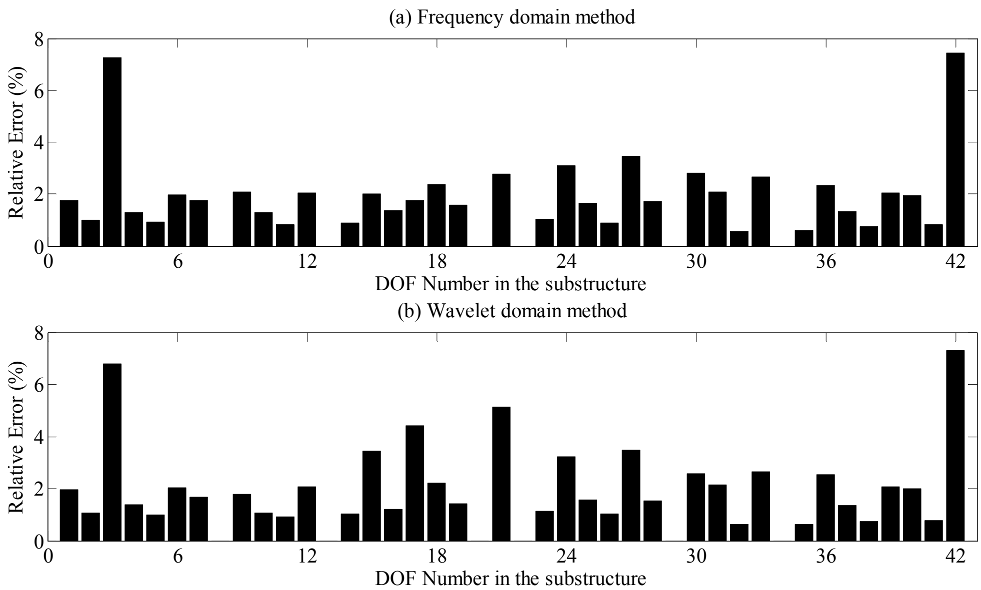

Figure 3.28: Relative errors of response reconstruction in time domain in the substructure under 10% noise

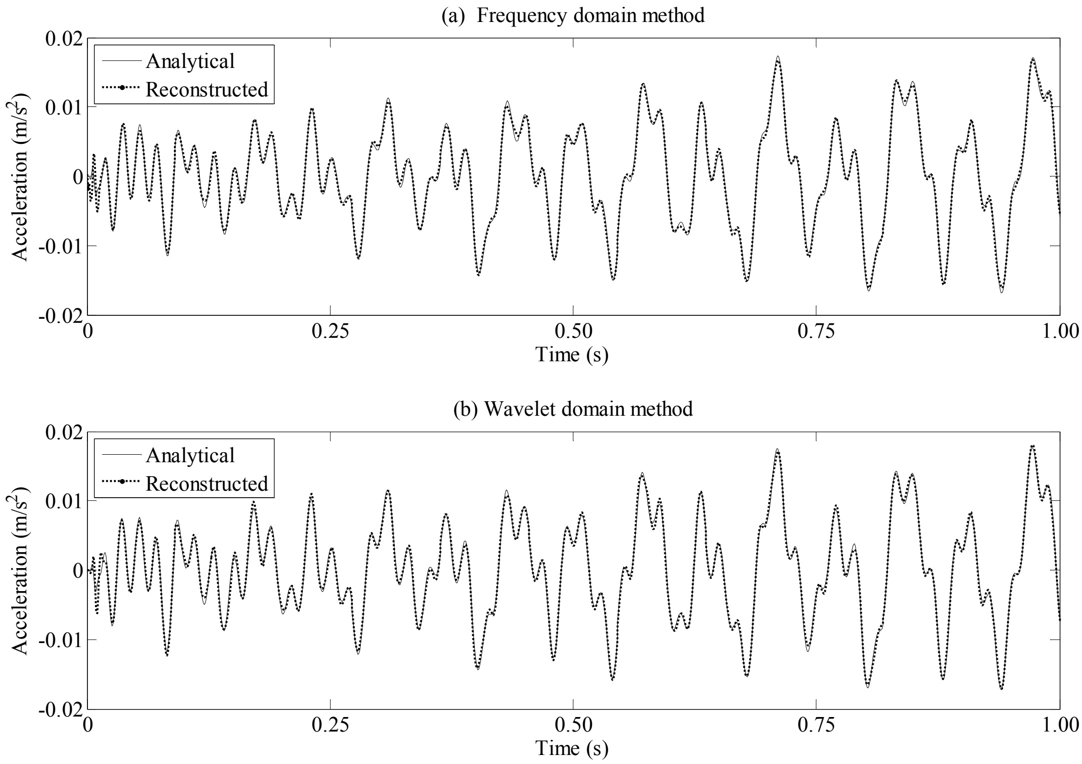

Figure 3.29: Analytical and reconstructed time domain responses at Node 34(θ) under 10% noise

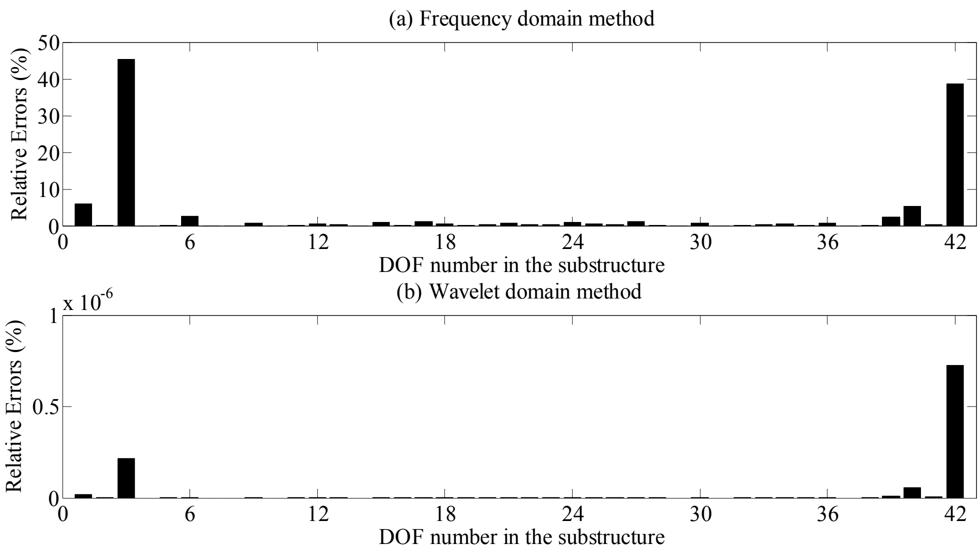

Figure 3.30: Relative errors in the response reconstruction results

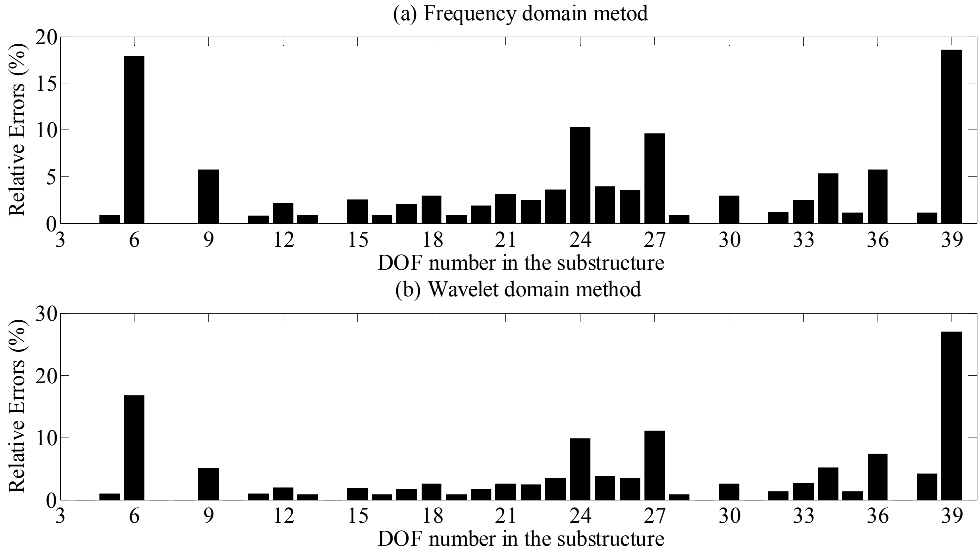

Figure 3.31: Relative errors in the response results in the substructure under 10% noise

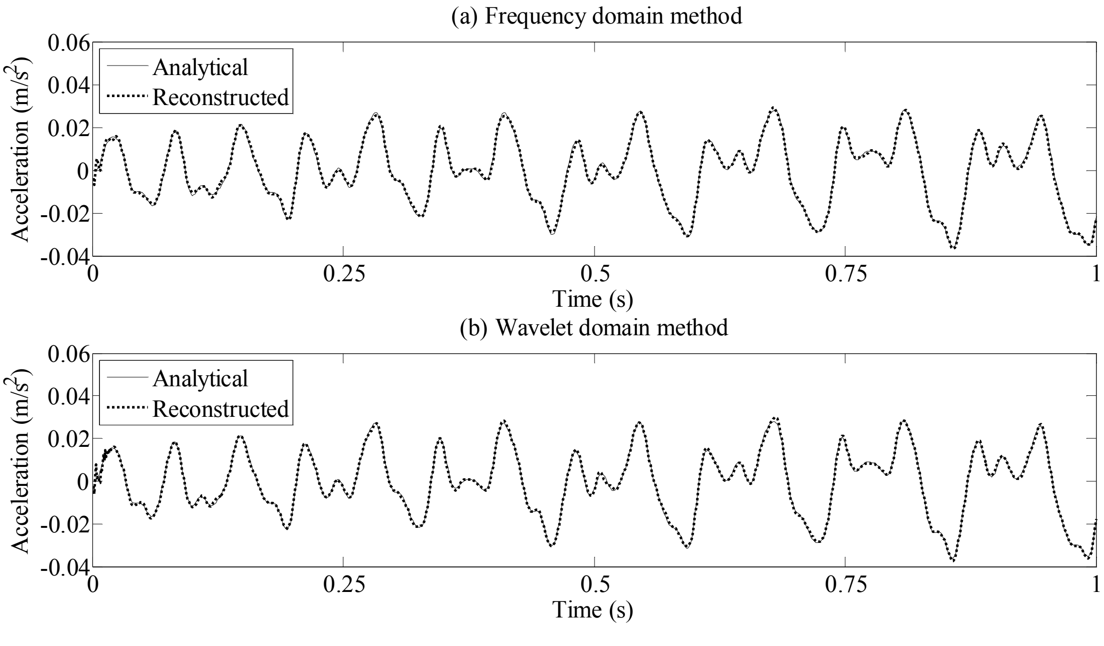

Figure 3.32: Analytical and reconstructed responses in time domain at Node 32(x) under 10% noise

CHAPTER 4

SUBSTRUCTURAL CONDITION ASSESSMENT

4.1 Introduction

It has been demonstrated in Chapter 3 that the transmissibility matrix between two sets of response vectors could be formulated and used to conduct the structural response reconstruction in a full structure and in a substructure by using frequency and wavelet domain methods. The response reconstruction in the wavelet domain is recommended to avoid the errors in the FFT process, such as leaking, end effect and aliasing.

The Fourier transform is advantageous in capturing frequency characteristics while the wavelet expansion preserves the temporal properties of a signal record during both the forward and inverse wavelet transforms. It has been reported (Alvin *et al.* 2003) that the deconvolution using the wavelet domain method for system identification show advantages over that using the frequency or time domain method since the wavelet domain method does not exhibit the rank-deficiency or ill-conditioning in the computation of pseudo-inverse of a matrix, and this is a key attribute of the wavelet analysis methods.

Existing structural damage identification approaches suffer from disadvantages with a large full-scale structure in the following areas: (a) There will be a large number of system DOFs and unknown parameters in the identification which is in contrast to the small number of measurements obtained from the structure in practice; (b) Structural identification is inherently an ill-conditioned inverse problem. The numerical difficulty to achieve computation convergence increases dramatically with the large number of unknown parameters in a full-scale structure. The computation effort would also increase tremendously with the large system matrices in both the forward and backward analysis; and (c) The uncertainty with the boundary conditions, material and physical parameters increases with the scale of a structure. It is often difficult to have a close to accurate finite element model of a large-scale structure for the system identification. Inclusion of incorrect boundary conditions into the inverse analysis will introduce errors in the identified results. With consideration of the above three deficiencies in existing approaches, it is desirable to have the damage identification conducted basing on a target substructure only without information of the rest of the structure. A large and complex structural system can then be divided into smaller substructures for independent studies one at a time in the inverse analysis.

In this Chapter, a substructural damage identification approach based on the response reconstruction techniques in frequency and wavelet domains is proposed. The responses and forces at the interface DOFs are not required. The dynamic response sensitivity-based method is used to formulate the damage identification algorithm in the target substructure, and local damage is identified as the change in the elemental stiffness factors. Numerical studies will be conducted to validate the correctness and effectiveness of the proposed substructural damage identification approach.

4.2 Substructural Damage Identification Based on the Response Reconstruction in Frequency Domain

4.2.1 Theoretical Formulation

4.2.1.1 Substructural Response Reconstruction

The response reconstruction procedure for the scenario with only the finite element model of the target substructure available described in Section 3.2.2.2, is used here and it will be briefly introduced. The measured responses from the damaged substructure are divided into two sets, noted as the First-set response vector $\ddot{x}_1(t)$ and the Second-set response vector $\ddot{x}_2(t)$ respectively in this Chapter.

The Second-set response vector is going to be reconstructed from the First-set response vector with the frequency domain method. The two sets of response vectors will be transformed in frequency domain and defined in terms of Equation (3.11) as follows,

$$\begin{cases} \ddot{X}_1(\omega) = H_{1a}^{e}(\omega)F_e(\omega) + H_{1a}^{I}(\omega)F_I(\omega) \\ \ddot{X}_2(\omega) = H_{2a}^{e}(\omega)F_e(\omega) + H_{2a}^{I}(\omega)F_I(\omega) \end{cases} \tag{4.1}$$

Equation (3.18) will be rewritten as,

$$\ddot{X}_{2r}(\omega) = T_{12}(\omega)\ddot{X}_1(\omega) + H_{12}^{e}(\omega)F_e(\omega) \tag{4.2}$$

in which,

$$T_{12}(\omega) = H_{2a}^{I}(\omega)\left(H_{1a}^{I}(\omega)\right)^{+} \tag{4.3a}$$

$$H_{12}^{e}(\omega) = H_{2a}^{e}(\omega) - T_{12}H_{1a}^{e}(\omega) \tag{4.3b}$$

The external excitation forces on the substructure are assumed known in this study and its Fourier transform $F_e(\omega)$ is then obtained. Transformation matrix $T_{12}(\omega)$ and matrix $H_{12}^{e}(\omega)$ in Equation (4.2) are obtained by using the FRF matrices obtained from the finite element model of the substructure with Equation (3.4) without knowledge of the rest of the structure. The number of measurements in the First-set response vector should at least equal or larger than the number of interface forces on the substructure to make sure that the pseudo-inverse $\left(H_{1a}^{I}(\omega)\right)^{+}$ in Equation (4.3a) exists. The reconstructed frequency domain response $\ddot{X}_{2r}(\omega)$ could be recovered into time domain $\ddot{x}_{2r}(t)$ by using the IDFT.

4.2.1.2 Substructural Damage Identification

For those condition assessment approaches which need an initial analytical finite element model, the parametric model updating methods for damage identification are popular because they keep the structural connectivity and the physical meaning of the stiffness matrix is clear. The initial finite element model is updated to match the predicted and measured vibration properties or vibration responses as closely as possible. In this study, a sensitivity-based finite element model updating method is used for substructural damage identification. The damage is assumed only related to a stiffness reduction such as a change in the elastic modulus. The mass matrix is assumed to be unchanged before and after the damage. The elemental stiffness factors in the initial intact substructural finite element model are iteratively updated to have the reconstructed responses matching with those measurements under the damaged state.

Damage Model

Linear damage assumption is adopted in this study, i.e., the initially linear-elastic structure is assumed remaining linear-elastic after the damage. The damaged substructural system stiffness matrix K_d can be expressed as,

$$K_d = \sum_{i=1}^{n} \alpha_i K_i = \sum_{i=1}^{n} (1 + \Delta\alpha_i) K_i \tag{4.4}$$

where, K_i, α_i are the ith elemental stiffness matrix in the intact state and the ith elemental stiffness factor in the damage state, respectively. Therefore, $\Delta\alpha_i$ represents the extent of stiffness reduction of the ith element.

Damage Identification Algorithm

The objective function of the damage identification algorithm is defined as the difference between two sets of response vectors

$$f_{obj} = \left\| \ddot{x}_{2m}(t) - \ddot{x}_{2r}(t) \right\|_2 \tag{4.5}$$

where, $\ddot{x}_{2m}(t)$ is the measured Second-set response vector from the substructure in the damaged state. $\ddot{x}_{2r}(t)$ is the reconstructed Second-set response vector from the measured First-set response vector. The wavelet transform coefficients of the measured and reconstruction responses can also be included in Equation (4.5) as the objective function. However, Equation (4.5) gives a clear physical meaning with matching of the measured and reconstruction responses as closely as possible in the optimized results. The vector α_i of substructural elemental stiffness factors is then iteratively updated by minimizing the objective function such that the reconstructed response vector $\ddot{x}_{2r}(t)$ can match the measured response vector $\ddot{x}_{2m}(t)$ well.

The dynamic response sensitivity-based model updating method (Lu and Law 2007) without considering the second- and higher-order effects is adopted here with

$$[S]\{\Delta\alpha\} = \{\Delta\ddot{x}\} = \{\ddot{x}_{2m}\} - \{\ddot{x}_{2r}\} \tag{4.6}$$

where, $\Delta\alpha$ is the perturbation of the vector of substructural elemental stiffness factors, $[S]$ is the sensitivity matrix of the response $\ddot{x}_{2r}(t)$ with respect to the substructural elemental stiffness factors. The objective function in Equation (4.5) is an implicit function with respect to the substructural elemental stiffness factors. It has been verified that the numerical sensitivity matrix can also be used for model updating effectively (Zivanovic et al. 2007), and thus the sensitivity matrix $[S]$ is obtained using numerical finite difference method (Morton and Mayers 2005). It is noted that the number of equations in Equation (4.6) should be larger than the number of unknown elemental stiffness parameters to make sure that the identification equation is over-determined.

Adaptive Tikhonov regularization

The adaptive Tikhonov regularization method has been proposed to improve the damage identification results by separating all the structural elements to be assessed into two categories of possible damaged elements and intact elements from results obtained in the previous iteration. The perturbations of elemental stiffness reduction factors of the possible damaged elements in each iteration are then limited to a small range and the reduction factors of other elements are restrained close to zeros. It has been shown that the adaptive Tikhonov regularization has obvious advantage over the traditional Tikhonov regularization with less false positives and false negatives especially when relatively high noise level exists in the measurements. On the other hand, the adaptive Tikhonov regularization can give results without divergence although with a slower convergence speed. The adaptive Tikhonov regularization technique is used in this study to obtain the solution vector $\Delta\alpha$ from Equation (4.6). The implementation of the adaptive Tikhonov regularization can be referred to (Li and Law 2010).

Iterative Damage Detection Procedure

Acceleration measurements from the substructure in the damaged state will be used to identify the substructural elemental stiffness factors α_i iteratively. Initially it is assumed that each elemental stiffness factor of the analytical substructural finite element model is equal to unity. An updated finite element model is assumed to be available as a reference model for the following iterative procedure of damage identification.

Step 1: Measure the dynamic acceleration responses at the First-set $\{\ddot{x}_{1m}(t)\}$ and Second-set $\{\ddot{x}_{2m}(t)\}$ measurement DOFs from the substructure in the damaged state. These responses are transformed in to frequency domain.

Step 2: Compute the acceleration FRF matrices $H^e(\omega)$ and $H^I(\omega)$ from Equation (3.4) with the finite element model of the substructure for the external excitation forces and interface forces, respectively.

Step 3: Calculate the matrices $T_{12}(\omega)$ and $H_{12}^I(\omega)$ from Equations (4.3a) and (4.3b). Then the reconstructed Second-set response vector $\{\ddot{X}_{2r}(\omega)\}$ is obtained from Equation (4.2) and then recovered in to time domain using IDFT.

Step 4: The response difference vector $\{\Delta\ddot{x}\}$ is computed between the Second-set measured response vector $\{\ddot{x}_{2m}(t)\}$ in Step 1 and the reconstructed Second-set response vector $\{\ddot{x}_{2r}(t)\}$ in Step 3. The sensitivity matrix $[S]$ of the response $\ddot{x}_2(t)$ with respect to substructural elemental stiffness factors is obtained using the numerical finite difference method.

Step 5: Obtain the perturbation vector of substructural elemental stiffness factors $\{\Delta\alpha\}$ from Equation (4.6) with the adaptive Tikhonov regularization technique.

Step 6: The vector of substructural elemental stiffness factors is iteratively updated with $\alpha_{i+1} = \alpha_i + \Delta\alpha$ for the next iteration. Repeat Steps 2 to 5 until the following convergence criterion is satisfied.

$$\frac{\|\alpha_{i+1} - \alpha_i\|_2}{\|\alpha_i\|_2} \le Tolerance \tag{4.7}$$

where i denotes the i th iteration.

In the above-mentioned iterative scheme for the proposed substructural damage identification approach, it should be noticed that: (a) The information of the responses and forces at the interface DOFs of the substructure are not necessarily required; (b) The finite element model of the intact target substructure and a limited set of acceleration measurements from the damaged substructure are needed in the damage identification; (c) Only the elemental stiffness factors of the target substructure are formulated in the identification algorithm resulting in a much reduced dimension in the inverse problem; (d) Information such as the finite element model and measurements from the rest of the structure other than the target substructure is not required in the identification.

4.2.2 Numerical Simulation

The same frame structure in Figure 3.3 is used in this study to demonstrate the proposed substructural damage identification approach based on the response reconstruction in frequency domain. The element numbers in the substructure are shown in Figure 4.1. The excitation locations are the same and the two multi-sine excitation forces are

$$F1 = \begin{cases} 16000\left(\sin(6\pi t) + 0.5\sin(3\pi t) + 0.2\sin(12\pi t)\right), & t \le 1s \\ 0, & t > 1s \end{cases} \quad \text{and}$$

$$F2 = \begin{cases} 16000\left(\sin(24\pi t) + 0.6\sin(36\pi t) + 0.2\sin(48\pi t)\right), & t \le 1s \\ 0, & t > 1s \end{cases}$$

Ten sensors are placed arbitrarily on the substructure, and they are divided into two sets, as listed in Table 4.1. The number of measurements in the First-set is eight and it is larger than the number of interface forces which is six. Two sensors are in the Second-set and they are placed along the x-direction because significant vibrations are observed in the horizontal direction of the frame structure. 15% damage and 10% damage are introduced in the 2nd and 4th elements of the substructure, respectively. The simulated "measured" responses from dynamic response analysis of the frame structure in the damaged state are used for identification. 10% noise effect is included in the acceleration measurements.

4.2.2.1 Forward Response Reconstruction

Damage is introduced in the structure as a reduction of elastic modulus in a specific element. FOH discrete is used in the response analysis and the analytical responses at the First- and Second-sets sensor locations are obtained from Equation (3.1). The sampling duration is 36.768s with a sampling rate of 1000Hz in order to have the responses damp out to close to zero and the sampled data is long enough to have a power of two for FFT. Figure 4.2 shows the dynamic acceleration response at sensor location Node 15(x). The reconstructed Second-set response vector is obtained from Equation (4.2) and IDFT is used to recover the time domain response from frequency domain. No measurement noise is added in the measurements for this study. Figures 4.3(a) and 4.3(c) shows the true and reconstructed responses at the two sensor locations in the Second-response vector, respectively. The difference vectors $\left(\ddot{x}_{true}(t) - \ddot{x}_{ur}(t)\right)$ between the true and reconstructed responses of these two sensors are shown in Figures 4.3(b) and 4.3(d). The two reconstructed responses match the true responses well and the relative errors in the first second response data of the sensors in the Second-set response vector are 0.05% and 0.14%, respectively.

4.2.2.2 Damage Identification Results

Measurements with noise effect are low-pass filtered with a cutoff of 100Hz. The response data from sensors in the Second-set within the first 0.5s are used for identification. The number of identification equation is $2 \times 500 = 1000$ and it is far larger than the unknown elemental stiffness parameters in the substructure which is 14. Measurements without and with 10% noise effect are used for damage identification. Table 4.2 lists the associated information on convergence of the iterative procedure. The damage identification results are shown in Figure 4.4. The tolerance is taken as 1.0×10^{-3} for both noise-free and noise cases in this study, respectively. For the noise-free case, the identified extents of local damage in 2^{nd} and 4^{th} elements are 14.70% and 9.63%, respectively. They are close to true values but are not exactly equal to those true assumed damage extents due to the error existing in the forward response reconstruction in the frequency domain, as indicated in Figure 4.3. For the case with 10% noise effect, the measurement noise has a large influence on the identification results. The identified extents in 2^{nd} and 4^{th} elements are 12.30% and 8.32%, respectively. It should be noticed that several false positives exist in the identification results in adjacent elements of damaged areas, such as the 3^{rd} element, due to the noise effect. An optimal selection of sensor number and placement in the First-set and Second-set response vector may exist and give better identification results.

It can be noticed from Figures 3. 20 and 3.21 that several large relative errors are observed at the rotational DOFs. However, the damage in the substructure can be identified effectively. The accuracy of damage identification depends on the accuracy of the response reconstruction process, and the accuracy of reconstruction at the translation DOFs is good. Since only responses at the translation DOFs in the x-direction are included for identification, then good damage identification results will be obtained.

4.2.2.3 Effect of Model Errors on the Identification Results

The influence of model errors in the stiffness parameters of the finite element model on the identification results is investigated. Other model error sources, such as uncertainties in the support stiffness, the mesh and element type in the finite element analysis and mass matrix, etc, are not considered in this study. It is assumed that the initial finite element model corresponds to a normal random distribution of the elastic modulus (Furukawa *et al.* 2006) with a mean of $3.5 \times 10^4 MPa$ and a coefficient of variation equal to 3%. 15% and 10% damage are introduced in the 2nd and 4th elements of the frame structure. The damage identification results with the initial mode errors in the stiffness of the finite element model of the structure are shown in Figure 4.5. The identified extents of local damage in the 2nd and 4th of the element in the substructure are identified as 11.17% and 10.02%, 12.99% and 8.94% from measurements without and with noise effect, respectively. It should be noticed that the identified damage in the substructure with measurements without noise effect are not exact to the simulated values as the initial mode errors may affect the identification results as well as the error in the response reconstruction from frequency domain method. Several large false positives and false negatives exist in the identification results due to both large measurement noise effect and the initial model errors in the finite element model when the 10% noise effect is included in the measurements.

4.2.2.4 Effect of Sampling Rate on the Identification Results

The effect of sampling rate on the identification results will be investigated. The sampling rate is changed to 500Hz and other settings are not changed. Figure 4.6 shows the identification results from measurements with 500Hz sampling rate. The identified extents in 2nd and 4th element are 13.74% and 8.44% for the noise-free case, and 13.09% and 12.20% for the case with the 10% noise effect. A comparison of Figures 4.4 and 4.6 shows that the identification results from measurements with

1000Hz sampling rate are better than those with 500Hz sampling rate since more identification equations are provided in the identification with a higher sampling rate. The sensitivity vectors of the interface elements are far smaller than those of other elements instead of interface ones. Then the identified stiffness changes in these interface elements would be very small and close to zero.

4.3 Substructural Damage Identification Based on the Response Reconstruction in Wavelet Domain

4.3.1 Theoretical Formulation

4.3.1.1 Unit Impulse Response Function under Support Excitation

The equation of motion of a damped N DOFs structural system under support excitation is given as:

$$[M]\{\ddot{x}(t)\}+[C]\{\dot{x}(t)\}+[K]\{x(t)\}=-[M][L]\ddot{x}_s(t) \tag{4.8}$$

where, $\ddot{x}_s(t)$ is the support excitation acceleration record; L is the mapping vector relating the support input to the corresponding DOFs of the structure.

When $\ddot{x}_s$ is an unit impulse acceleration, Equation (4.8) can be written as:

$$[M]\{\ddot{x}(t)\}+[C]\{\dot{x}(t)\}+[K]\{x(t)\}=-[M][L]\delta(t) \tag{4.9}$$

Assuming the system has zero initial conditions before the occurrence of the unit impulse acceleration excitation, the forced vibration state under the unit impulse support excitation can be represented by a free vibration state with the following initial conditions (Li and Law 2008b):

$$\begin{cases} [M]\ddot{h}_S(t)+[C]\dot{h}_S(t)+[K]h_S(t)=0 \\ h_S(0)=0, \quad \dot{h}_S(0)=L \end{cases} \tag{4.10}$$

in which, h_S , $\dot{h}_S$ and $\ddot{h}_S$ are the unit impulse displacement, velocity and acceleration vectors under the support excitation, respectively. Using the time-stepping integration method such as Newmark method, the unit impulse function can be obtained from the analytical finite element model.

When the structure is excited under the support excitation, the input-output relationship can also be built up in the wavelet domain in terms of the procedures from Equations (3.40) to (3.48) and it can be expressed as,

$$\ddot{x}_{l(n\times 1)} = \ddot{h}_{Sl}^{DWT}{}_{(n\times rl)} f_S^{DWT}{}_{(rl\times 1)} \tag{4.11}$$

where $\ddot{h}_{Sl}^{DWT}$ is the discrete wavelet transform of unit impulse acceleration matrix under the support excitation $\ddot{h}_{Sl}$. f_S^{DWT} is the discrete wavelet transform of the support excitation acceleration record $\ddot{x}_s$.

4.3.1.2 Response Reconstruction in a Substructure with the UIR function

The response reconstruction procedure in a substructure from the wavelet domain method for the scenario with only the finite element model of the target substructure available described in Section 3.3.3.2 is used here and it will be briefly introduced. The dynamic acceleration response of the substructure can be represented in the wavelet domain as,

$$\ddot{x}(t) = \ddot{h}_e^{DWT} F_e^{DWT} + \ddot{h}_I^{DWT} F_I^{DWT} \tag{4.12}$$

The measured responses from the substructure under the damaged state are divided into two sets, noted as the First-set response vector $\ddot{x}_1(t)$ and the Second-set response vector $\ddot{x}_2(t)$ respectively. They are defined in the wavelet domain as follows,

$$\begin{cases} \ddot{x}_1(t)_{(mn\times 1)} = \ddot{h}_{1e}^{DWT}{}_{(mn\times rl)} F_e^{DWT}{}_{(rl\times 1)} + \ddot{h}_{1I}^{DWT}{}_{(mn\times ql)} F_I^{DWT}{}_{(ql\times 1)} \\ \ddot{x}_2(t)_{(sn\times 1)} = \ddot{h}_{2e}^{DWT}{}_{(sn\times rl)} F_e^{DWT}{}_{(rl\times 1)} + \ddot{h}_{2I}^{DWT}{}_{(sn\times ql)} F_I^{DWT}{}_{(ql\times 1)} \end{cases} \tag{4.13}$$

in which, m, s, n, r, q and l are the number of measurements in the First-set response vector, the number of measurements in the Second-set response vector, the number of sampled data points in each measurement, the number of external excitation forces, the number of interface forces and the number of wavelet coefficients in the wavelet transform, respectively.

When the number of measurements in the First-set is at least equal or larger than the number of interface forces on the substructure, the following equation can be obtained from the first row of Equation (4.13),

$$F_I^{DWT} = \left(\ddot{h}_{1I}^{DWT}\right)^+ \left(\ddot{x}_1(t) - \ddot{h}_{1e}^{DWT} F_e^{DWT}\right) \tag{4.14}$$

Substituting Equation (4.14) into the second row of Equation (4.13), we have,

$$\ddot{x}_{2r}(t) = T_{12}^I \ddot{x}_1(t) + H_{12}^e F_e^{DWT} \tag{4.15}$$

where,

$$T_{12}^I = \ddot{h}_{2I}^{DWT} \left(\ddot{h}_{1I}^{DWT}\right)^+ \tag{4.16a}$$

$$H_{12}^e = \ddot{h}_{2e}^{DWT} - T_{12}^I \ddot{h}_{1e}^{DWT} \tag{4.16b}$$

The external excitation forces on the substructure are assumed known in this study and its discrete wavelet transform F_e^{DWT} is then obtained. Transformation matrix T_{12}^I and matrix H_{12}^e in Equation (4.16) are obtained from the unit impulse response function matrix from Equation (4.10) with the finite element model of the substructure. It should be noticed that the number of measurements in the First-set response vector should at least equal or larger than the number of interface forces on the substructure to make sure that the pseudo-inverse $\left(h_{1I}^{DWT}\right)^+$ in Equation (4.16a) exists. Therefore the Second-set response vector $\ddot{x}_{2r}(t)$ can be reconstructed from the First-set response vector $\ddot{x}_1(t)$ in the substructure from Equation (4.15). For the case with the structure subject to support motion excitation, F_e^{DWT} is the discrete wavelet transform of support excitation input record. The support excitations are assumed to be measured in this study.

4.3.1.3 Substructural Damage Identification

The same objective function and sensitivity-based damage identification method in Section 4.2.1.2 are used. The adaptive Tikhonov regularization is also used to improve the identification results when measurements are included with noise effect. The computation procedure for the substructural damage identification based on the response reconstruction in wavelet domain is,

Step 1: Measure the dynamic acceleration responses at the First-set $\{\ddot{x}_{1m}(t)\}$ and Second-set $\{\ddot{x}_{2m}(t)\}$ measurement DOFs from the substructure under the damaged state.

Step 2: Compute the unit impulse response function matrices $\ddot{h}_e$ and $\ddot{h}_I$ from Equation (4.10) for the external excitation forces and interface forces with the finite element model of the substructure, respectively when the substructure is subject to the support excitation.

Step 3: Calculate the matrices T_{12}^I and H_{12}^I from Equations (4.16a) and (4.16b). Then the reconstructed Second-set response vector $\{\ddot{x}_{2r}(t)\}$ is obtained from Equation (4.15).

Step 4: The response difference vector $\{\Delta\ddot{x}\}$ is computed between the Second-set measured response vector $\{\ddot{x}_{2m}(t)\}$ in Step 1 and the reconstructed Second-set response vector $\{\ddot{x}_{2r}(t)\}$ in Step 3. The sensitivity matrix $[S]$ of the response $\ddot{x}_2(t)$ with respect to substructural elemental stiffness factors is obtained using the numerical finite difference method.

Step 5: Obtain the perturbation vector of substructural elemental stiffness factors $\{\Delta\alpha\}$ from Equation (4.6) with the adaptive Tikhonov regularization technique.

Step 6: The vector of substructural elemental stiffness factors is iteratively updated with $\alpha_{i+1} = \alpha_i + \Delta\alpha$ for the next iteration. Repeat Steps 2 to 5 until the following convergence criterion is satisfied.

$$\frac{\left\|\alpha_{i+1} - \alpha_i\right\|_2}{\left\|\alpha_i\right\|_2} \le Tolerance \tag{4.17}$$

where i denotes the ith iteration. The tolerance is taken as 1.0×10^{-4} in this study.

In the above-mentioned iterative scheme for damage identification of the proposed method with incomplete information of the structure, the features are the same as those in the damage detection procedure based on the response reconstruction from frequency domain method in Section 4.2.1.2.

4.3.2 Numerical Simulation

Numerical studies on a simply-supported box-section girder structure are conducted to illustrate the accuracy and effectiveness of the proposed approach for substructural damage detection. The total length of the girder is 30m. The plan view and cross-section of the girder structure model are shown in Figures 4.7(a) and 4.7(b), respectively. The Young's modulus and mass density are respectively $2.6 \times 10^4 MPa$ and $2500 kg/m^3$.

The finite element model of the girder consists of 66 nodes and 60 flat shell elements (Kwon and Bang 2000) with six DOFs at each node. The structural system has 396 DOFs in total. The girder is simply-supported at nodes 5, 6, 65 and 66 at the two ends of the deck, and restraints at the supports are represented by a large stiffness of 3×10^9 N/m. The first ten intact undamped structural natural frequencies are from 4.44 to 21.61 Hz. Rayleigh damping is assumed in this study and the damping ratios for the first two modes are taken as $\xi = 0.012$. The target substructure to be investigated in this study is shown in Figure 4.7(a) with 36 nodes and 30 elements and the six interface nodes are from Nodes 31 to 36.

Forced excitation and ambient vibration excitation are commonly used for the damage detection of real structures. The latter is a low energy level excitation under which most small damages would not show up in the assessment. Forced vibration requires sufficiently large energy to mobilize all the local damages of the structure in the vibration and it could be too large if artificially generated. We could take advantage of the earthquake excitation in the structural damage detection. In practical earthquake situations, structures are generally subject to both the horizontal and vertical seismic support excitations simultaneously. Therefore in this study, the bridge deck is assumed to be subject to El-Centro seismic excitations acting along both the x- and z-axis of the structure at the supporting nodes without any phase difference. The El-Centro seismic acceleration records are taken from the "PEER Strong Motion Database" at the University of California (PEER Strong Motion Database). Figures 4.8(a) and 4.8(b) show the seismic acceleration records sampled at 50Hz along the x- and z-axis, respectively.

4.3.2.1 Model Condensation

There are 36 interface forces acting on the target substructure at the six interface nodes from Nodes 31 to 36, as shown in Figure 4.7(a). Thus at least 36 measured accelerations are required in the First-set response vector as noted from Equations (4.14) and (4.15). However, it is normally not easy to provide such a large number of measurements in practice due to the cost of data acquisition. Therefore, it is necessary to reduce the number of interface forces and the number of required sensors for a more practical application of the proposed method. The Iterative Improved Reduction System (IIRS) method (Friswell *et al.* 1995) is used for model condensation of the substructure to reduce the number of interface forces. Such treatment on reducing the number of interface forces is also referred in (Law *et al.* 2010). The slave DOFs should be those interface DOFs carrying smaller interface forces as the error of condensation would be smaller. In this study, the translational DOFs in the y-axis of all the six interface nodes are included in the master DOFs. Other interface DOFs, such as the translational DOFs along the x-, z-axis and rotational DOFs of the interface nodes are taken as the slave DOFs since their corresponding interface forces are much smaller than those in the translational DOFs along the y-axis of interface nodes. Therefore, the 36 interface forces become six reduced interface forces in the y-direction of the six interface nodes. Ten iterations are found sufficient to converge in the IIRS method in this case. After the condensation is conducted, the impulse response function matrices h_{1e}^{DWT}, h_{1I}^{DWT}, h_{2e}^{DWT} and h_{2I}^{DWT} in Equation (4.13) are also obtained from the condensed substructural finite element model of the target substructure.

4.3.2.2 Sensor Placement Configuration

Two sensor placement configurations listed in Table 4.3, denoted as SP1 and SP2 in this Chapter respectively, are used to investigate the accuracy and effectiveness of the proposed method for damage identification of the substructure. The number of measurements in the First-set response vector is kept at ten which is larger than the number of reduced interface forces. The x-direction response under horizontal seismic excitation is larger than that in z-direction. In addition, the responses in y-direction are measured and they would be useful for the condensation when the 36 interface forces are reduced to 6 forces in the y-direction of the six interface nodes. Therefore, sensors are placed in the x- and y-direction of nodes to measure the responses. The sensors in the Second-set response vector are located in the x-direction since their responses to the horizontal seismic excitation are larger than those in other directions. The choices of these two sensor placement configurations are also used to study how different sensor configurations in the First-set and Second-set response vectors affect the identification results.

Since ten sensors are included in the First-set response vector and there are two sensors in the Second-set, the numbers m, s (number of measurements in the First-set and Second-set) are 10 and 2, respectively. The response data within the first seven seconds are checked on its appropriateness for the identification. With a sampling rate of 50Hz, n equals to 350. r is the number of external excitation forces (support excitations in this study) on the substructure and is equal to 2 while q is the number of interface forces and it equals to 6. In this study, Daubechies 8-coefficient wavelet is chosen as the basis functions in the DWT due to its orthogonality properties and fairly smooth interpolation nature (Robertson *et al.* 1998). l equals to 378 when two-level discrete wavelet transform is conducted for the 350-point signal record. Therefore, the dimensions of matrices $\ddot{h}_{1e}^{DWT}$, $\ddot{h}_{1I}^{DWT}$, $\ddot{h}_{2e}^{DWT}$ and $\ddot{h}_{2I}^{DWT}$ in Equation (4.13) are 3500×756, 3500×2268, 700×756 and 700×2268, respectively. Due to the large sizes of the two matrices $\ddot{h}_{2I}^{DWT}$ and $\ddot{h}_{1I}^{DWT}$, the computation load for computing T_{12}^{I} matrix in Equation (4.16a) is high especially for the computation of the pseudo-inverse of matrix $\ddot{h}_{1I}^{DWT}$. The computation load would become much more intensive if a longer sampling duration or a higher sampling rate is adopted due to the increasing size of matrices. With consideration of available computation capacity and to include the maximum earthquake excitation in Figure 4.8, the acceleration response data within first 7 seconds are used except otherwise stated.

4.3.2.3 Forward Response Reconstruction

Damage is introduced in the structure as a reduction of elastic modulus in a specific element. In this study, 10% damage is simulated in both the 2nd and 8th elements of the substructure. The simulated local damages are introduced in the substructure and the responses are obtained at the First-set and Second-set sensor locations. The reconstructed Second-set response vector is obtained from Equation (4.15) and is compared with the true Second-set response. It is noted that no noise is added to the measurements here. Results of forward response reconstruction with SP1 sensor placement are shown in Figure 4.9. Figures 4.9(a) and 4.9(c) show the true and reconstructed responses at sensor locations Node 2(x) and 9(x) in the Second-set response vector of SP1, respectively. It can be found that these two responses are almost overlapping indicating that the response reconstruction process is accurate.

The relative error between the true and reconstructed responses in the time domain is defined as,

$$RE = \frac{\left\| \ddot{x}_{true}(t) - \ddot{x}_{ur}(t) \right\|_2}{\left\| \ddot{x}_{true}(t) \right\|_2} \times 100(\%) \tag{4.18}$$

in which, $\ddot{x}_{true}(t)$ and $\ddot{x}_{ur}(t)$ are the true and reconstructed response vectors in the time domain, respectively.

The difference vectors $\left(\ddot{x}_{true}(t) - \ddot{x}_{ur}(t)\right)$ between the true and reconstructed responses of these two sensors in the Second-set response vector are shown in Figures 4.9(b) and 4.9(d). The relative errors for these two sensors are 0.5% and 0.24%, respectively. These relative errors are not as small as the relative error in the simulation studies in Chapter 3 since additional error has been introduced with the IIRS model condensation method for reducing the number of interface forces acting on the substructure. It may be noted that different sensor placement configurations in the First-set and Second-set response vectors may give different accuracy in the response reconstruction process.

4.3.2.4 Damage Identification Results

Dynamic responses from the substructure in the damaged state are measured and they are divided as First- and Second-set response vectors. The iterative procedure described in Section 4.3.1.3 is followed to obtain an updated set of elemental stiffness factors.

The acceleration responses in the damaged state are calculated from Equation (4.8) and they are taken as the simulated “measured” responses. 10% noise effect is included in the measurements for this study.

Measurements without and with noise effect are used for damage identification.

Table 4.4 gives the associated information on convergence of the iterative procedure. The required iterations and error of convergence calculated from Equation (4.17) are listed. It should be noticed that approximately 1.5 hours are required for one iteration with a Intel Core 2 Quad 2.4G PC with 8G memory due to the large dimensions of matrices $\ddot{h}_{1e}^{DWT}$, $\ddot{h}_{1I}^{DWT}$, $\ddot{h}_{2e}^{DWT}$ and $\ddot{h}_{2I}^{DWT}$ in Equation (4.13).

Figures 4.10(a) and 4.10(b) show the damage identification results from SP1 and SP2 sensor placement configurations, respectively. The locations of the simulated damage can be identified accurately. For the noise-free case, the dynamic response data within the first 6 seconds are used for the damage identification. The identified extents of local damage without noise effect in Figures 4.10(a) and 4.10(b) are close to true values but they are not exactly equal to the true values due to the error involved with the model reduction for reducing the number of interface forces as shown in Figure 4.9. This error may affect the damage identification results.

For the case with 10% noise, the identification results are influenced by both the noise effect and error in response reconstruction process induced by IIRS condensation. It should be noticed that the dynamic response data within the first 4 to 6 seconds are used for the identification since the responses in this period are much larger and could be less sensitive to the noise effect. It can be seen from Figures 4.10(a) and 4.10(b) that the damage locations are identified correctly with 10% noise effect and the adaptive Tikhonov regularization technique improves the identification results on undamaged elements with very small false positives and false negatives.

As indicated in Table 4.3, the sensor locations in the Second-set response vector of SP1 configuration are much closer to the damaged elements than those of SP2. Therefore, it may be concluded from Table 4.4 that this is the reason why the identification with SP1 sensor placement configuration gives faster convergence speed than that with SP2. However, the simulated damage can be identified effectively under both sensor placement configurations with 10% noise effect in the measurements.

4.3.2.5 Effect of Sampling Rate on the Identification Results

The sampling rate is changed to 100Hz for identification in this section. Figure 4.11(a) and 4.11(b) show the damage identification results of SP1 sensor placement with 50Hz and 100Hz sampling rate without and with noise effect, respectively. Figure 4.11(a) shows that the identification with both 50Hz and 100Hz sampling rate can give similar accuracy in the damage detection results without noise effect. However, as shown in Figure 4.11(b) for the 10% noise case, the increase of sampling rate would slightly improve the identification results by providing more measured information in the identification.

4.3.2.6 Discussions

Why the IIRS Model Condensation is used to Reduce the Number of Interface Forces?

A requirement of Equation (4.14) is that the number of measurements in the First-set response vector is at least equal or larger than the number of interface forces acting on the substructure. If the substructure has fewer number of interface DOFs, e.g. in the substructure from a simply supported beam or a planar frame structure, the number of interface forces may not be large. Under this circumstance, the IIRS scheme is not required and only a small number of sensors may be provided in the First-set and Second-set response vectors to conduct the response reconstruction. However, in the study, the target substructure has 36 interface forces and this means that at least 36 measurements in the First-set response vector are required to reconstruct the Second-set response vector from Equation (4.15). In practical applications, measurements are usually obtained at a few locations due to the cost associated with data acquisition.

On the other hand, assuming that 36 measurements are included in the First-set response vector, the dimensions of matrices $\ddot{h}_{1e}^{DWT}$ and $\ddot{h}_{1I}^{DWT}$ in Equation (4.13) shall be 12600×756 and 12600×13608 respectively if response data within 7 seconds are considered. Then the computational load in Equation (4.16a) to obtain the pseudo-inverse of matrix $\ddot{h}_{1I}^{DWT}$ would be very intensive and the computation process could be time-consuming. Therefore, in the above studies, the IIRS model condensation is used to reduce the number of interface forces acting on the substructure to have a smaller number of measurements.

When the IIRS condensation is not used in the numerical studies, the identification accuracy of the proposed method for substructural damage detection will be verified here. A sensor placement configuration of 40 sensors in the First-set vector and two sensors in the Second-set vector is adopted for the identification. These 40 sensors in the First-set vector are taken from Node 13(x, y, z), 14(x, y, z), 16(x, y, z), 18(x, y, z), 19(x, y, z), 20(x, y, z), 21(x, y, z), 22(x, y, z), 25(x, y, z), 28(x, y, z), 29(x, y, z), 30(x, y, z), 7(y, z) and 10(y, z). The two sensors in the Second-set vector are from Node 7(x) and 10(x). In this verification exercise, only the response data within first two seconds are considered in the identification. The dimension of matrix $\ddot{h}_{1I}^{DWT}$ is 4000×4644 and m, n, r, q and l equal to 40, 2, 2, 36 and 129, respectively. The computation time per iteration is around six hours. The damage identification results are shown in Figure 4.12 and the identified damages also exactly match the true values. This indicates that the proposed approach can give exact damage values without the measurement noise effect.

Influence of Model Errors on the Identification Results

The influence of model errors in the stiffness parameters of the finite element model on the identification results is investigated. Other model error sources, such as uncertainties in the support stiffness, the mesh and element type in the finite element analysis and mass matrix etc., are not considered in this study. It is assumed that a finite element model corresponding to a normal random distribution of Young's modulus with a mean of $2.6 \times 10^4 MPa$ and with a coefficient of variation (COV) equal to 5% is used in this case. 20% damage is introduced in both the 2nd

and 8^{th} elements of the girder. The identification results with SP1 and SP2 sensor placement configurations are shown in Figure 4.13. For the noise-free case, the identification accuracy would be affected by the error induced by the IIRS condensation. The identified values in 2^{nd} and 8^{th} elements are 22.10% and 17.59%, 22.86% and 22.25% respectively with SP1 and SP2. For the case with 10% noise effect included in the acceleration measurements, the identification accuracy would be further affected by the model errors as well as the measurement noise. The locations of simulated damage can be detected accurately and the identified damage extents in 2^{nd} and 8^{th} elements are 18.70% and 23.45%, 13.24% and 9.97% with SP1 and SP2, respectively. It is found that SP1 gives better identification results than SP2 because sensors in the Second-set of SP1 are close to damage locations. Model errors may not be identified accurately in all elements with noisy measurements. It is observed that several large false positives and negatives also exist in the results.

Measurement Noise with Support Excitation on the Structure

In Equation (4.15), the external excitation forces are assumed known and its discrete wavelet transform vector F_e^{DWT} is then available. When the structure is subject to support excitation, F_e^{DWT} should be the discrete wavelet transform of the support acceleration input. However, in the present study, no measurement error is included in these support excitation measurements. This effect on the performance of the proposed method for damage identification will need to be studied in future.

Sensor Selections in the First-set and Second-set Response Vectors

The sensor locations in SP1 and SP2 are arbitrarily selected in this study and it may be noted that different sensor placement configuration in the First-set and Second-set response vectors would give different accuracy in the response reconstruction process. Therefore an optimal selection of sensor numbers and locations in the First- and Second-set response vectors may improve the identification.

4.4 Summary

A substructural damage identification approach is proposed based on the dynamic response reconstruction techniques in both the frequency and wavelet domains. The information of responses and forces at the interface DOFs is not required. The relationship between two-sets of time-domain response vectors is formulated with the transmissibility matrix. The finite element model of the intact target substructure and acceleration measurements from the damaged substructure are required in the damage identification algorithm. A dynamic response sensitivity-based method is used to formulate the substructural damage identification equation and the adaptive Tikhonov regularization technique is adopted to improve the identification results especially for the case with measurement noise effect. Numerical studies are conducted to illustrate the performance of the proposed substructural damage identification approach. Under the circumstance when a target substructure has a large number of interface DOFs, the IIRS model condensation may be used to reduce the number of interface forces as well as the required sensor measurements in the First-set response vector. The simulated damage in the substructure can be identified effectively with 10% noise effect in the measurements and initial model errors in the finite element model.

Table 4.1: Sensor Placement Configurations

Sensor Placement Configuration	Sensor locations
First-set	Node 12(x), 13(x, y), 14(x), 15(y), 30(y), 31(x), 33(x)
Second-set	Node 30(x), 32(x)

Note: "Node 12(x)" denotes that the sensor is placed along the x-direction at Node 12.

Table 4.2: Information on convergence

	No noise	10% noise
Required iterations	15	14
Error of convergence	9.9×10^{-4}	9.87×10^{-4}

Table 4.3: Sensor Placement Configurations

Sensor Placement Configuration		Sensor locations
SP1	First-set	Node 13(x, y) 16(x, y) 20(x, y) 21(x, y) 2(y) 9(y)
	Second-set	Node 2(x) 9(x)
SP2	First-set	Node 2(x, y) 13(x, y) 20(x, y) 21(x, y) 7(y) 16(y)
	Second-set	Node 7(x) 16(x)

Table 4.4: Information on convergence

	SP1		SP2	
	No noise	10% noise	No noise	10% noise
Required iterations	6	11	11	26
Error of convergence	2.6×10^{-5}	7.1×10^{-5}	7.4×10^{-5}	9.4×10^{-5}

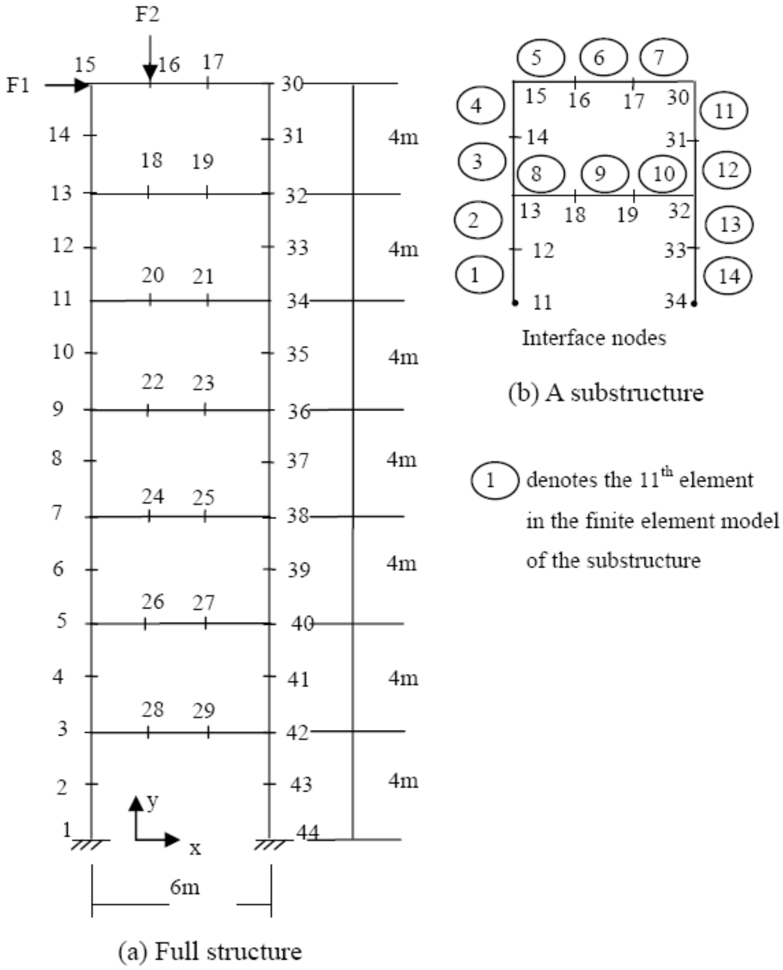

Figure 4.1: Finite element model of the frame structure

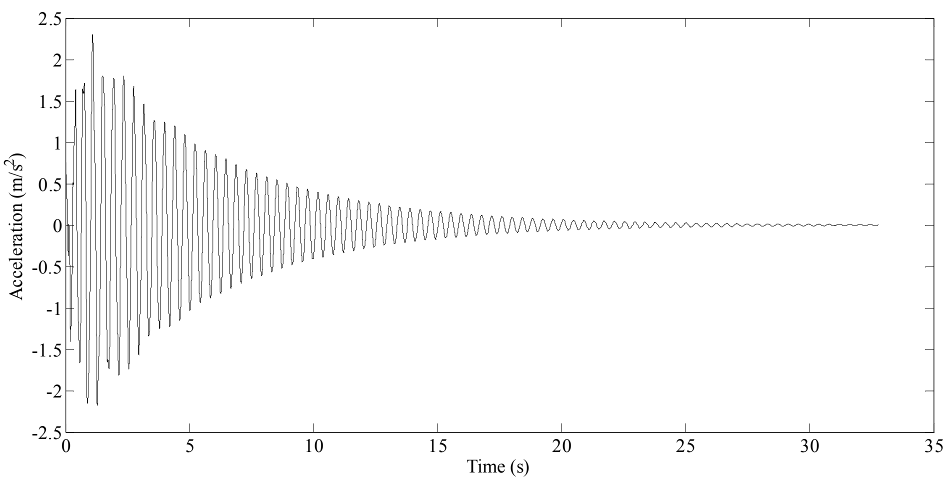

Figure 4.2: Dynamic acceleration response at sensor location Node 12(x)

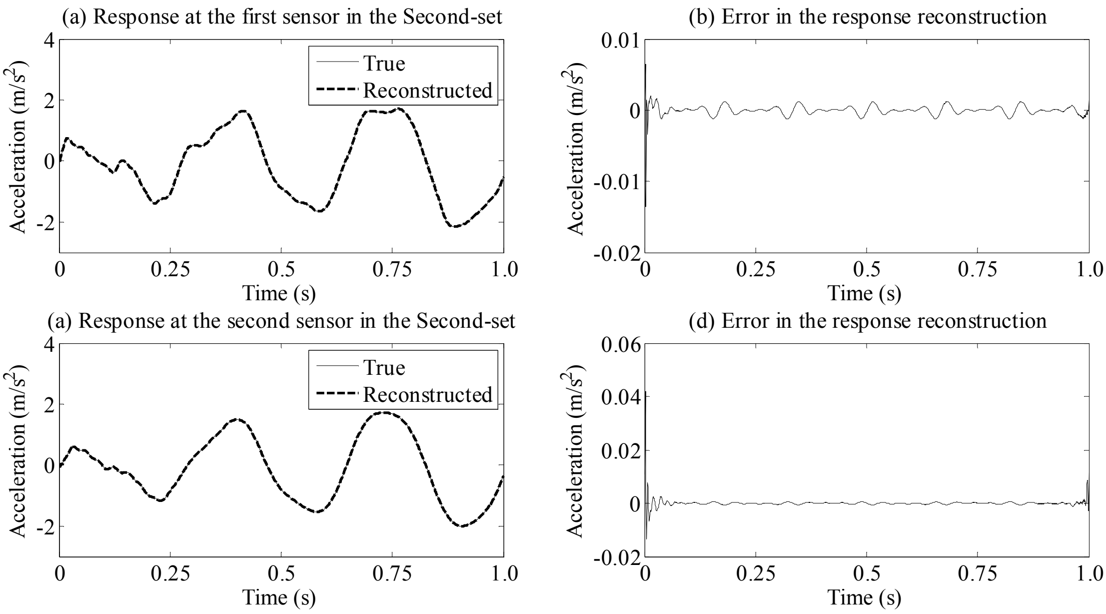

Figure 4.3: True and reconstructed responses in the Second-set response vector

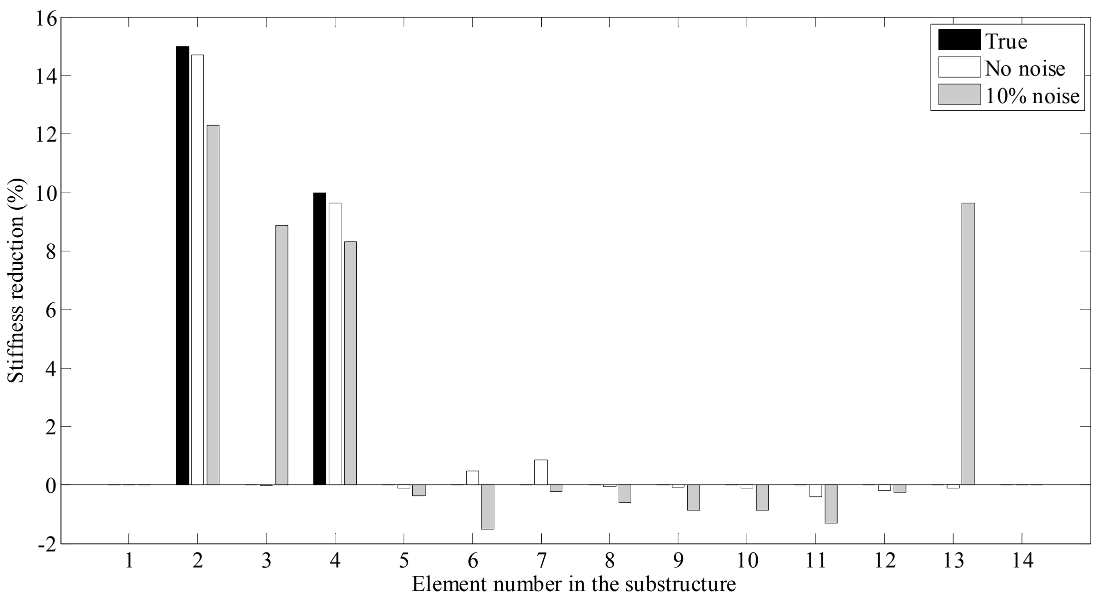

Figure 4.4: Damage identification results

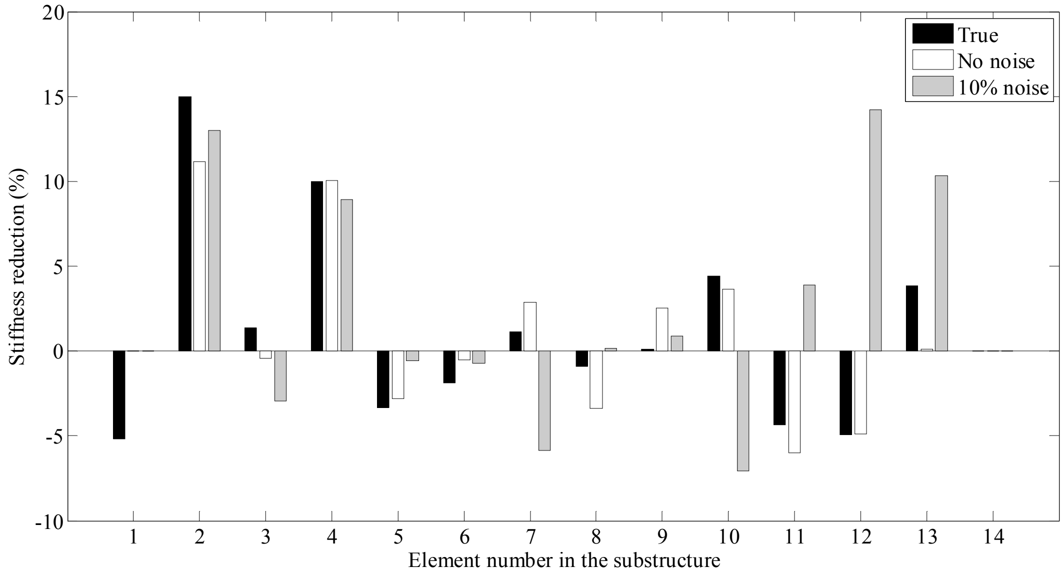

Figure 4.5: Damage identification results with initial model errors

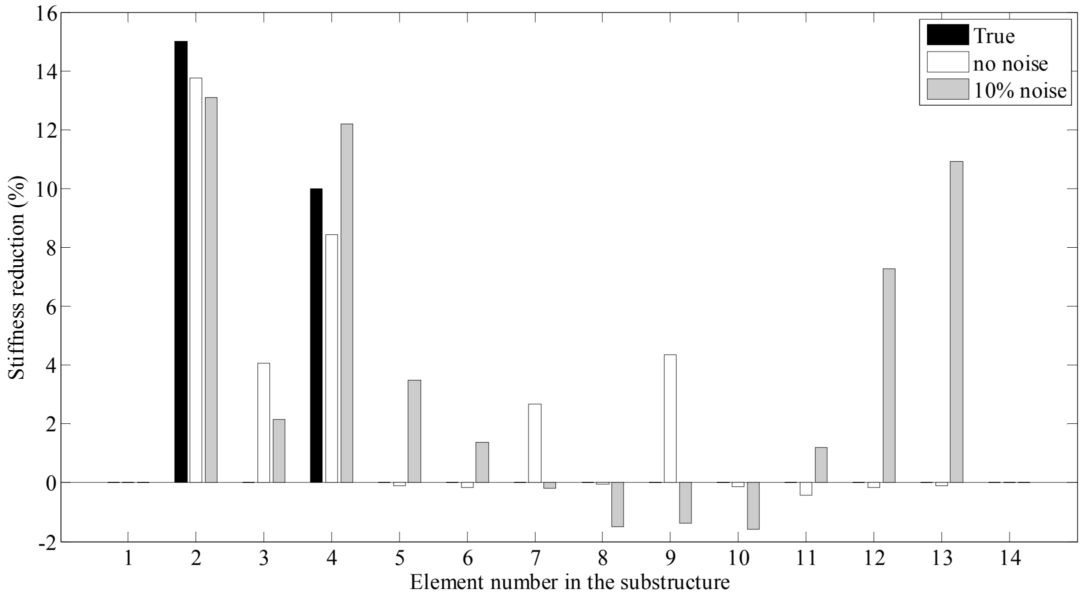

Figure 4.6: Damage identification results with 500Hz sampling rate

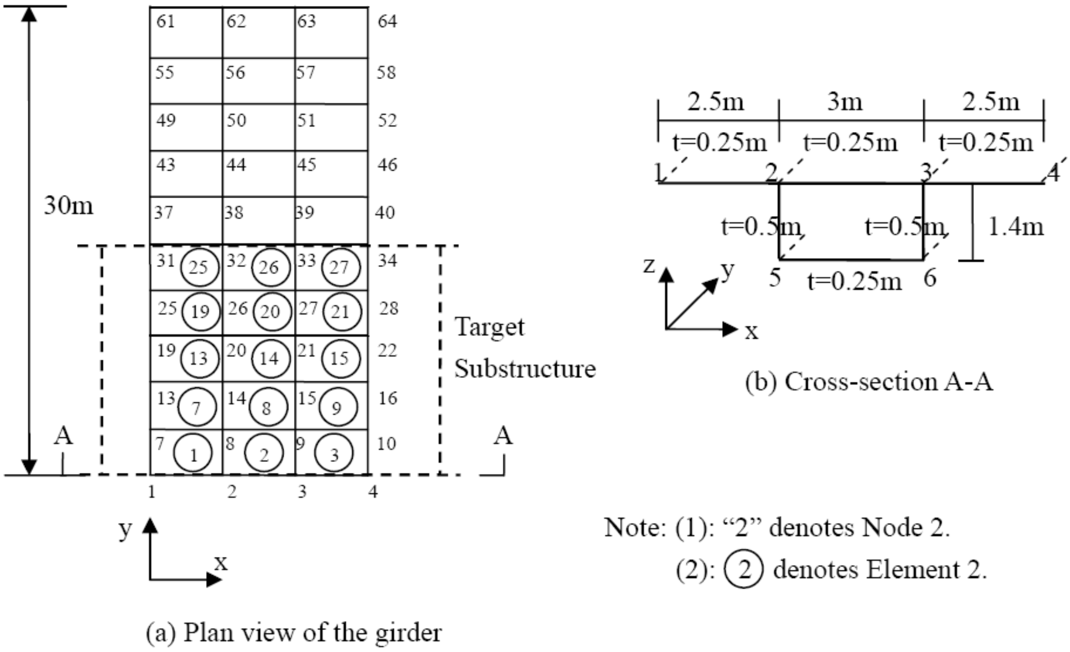

Figure 4.7: Finite element model of the box-section bridge girder

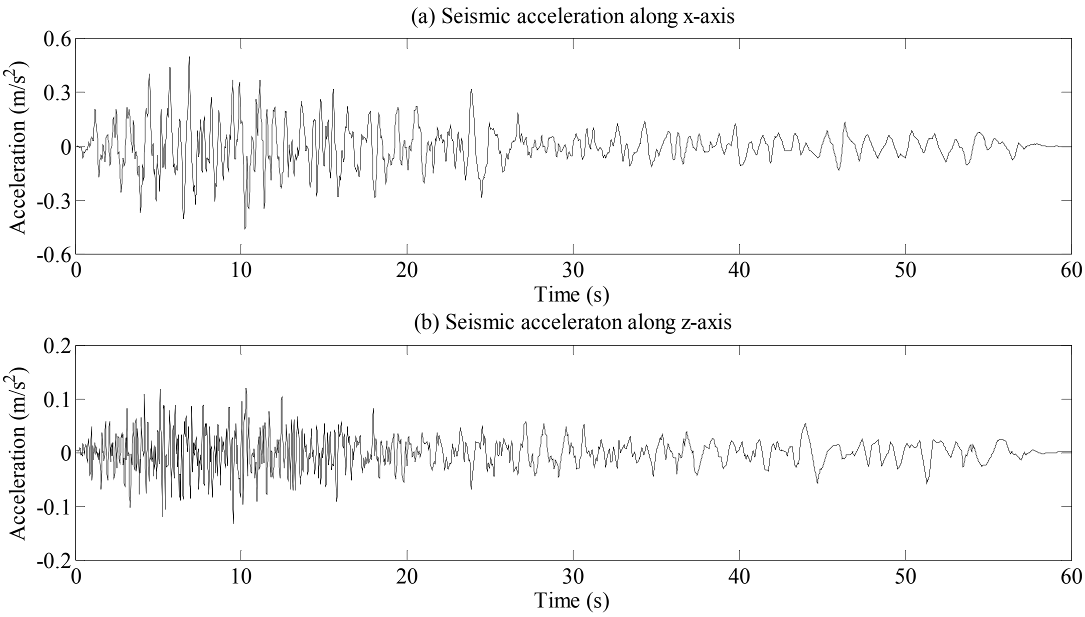

Figure 4.8: El-Centro seismic acceleration records acting along x-axis and z-axis

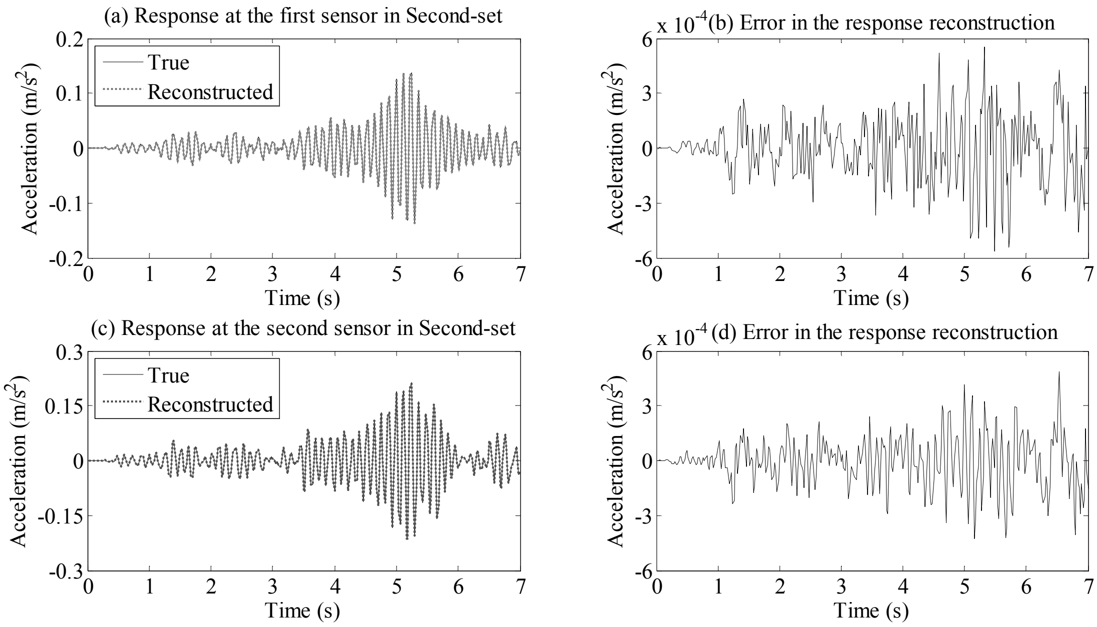

Figure 4.9: True and reconstructed responses in the Second-set response vector of SP1

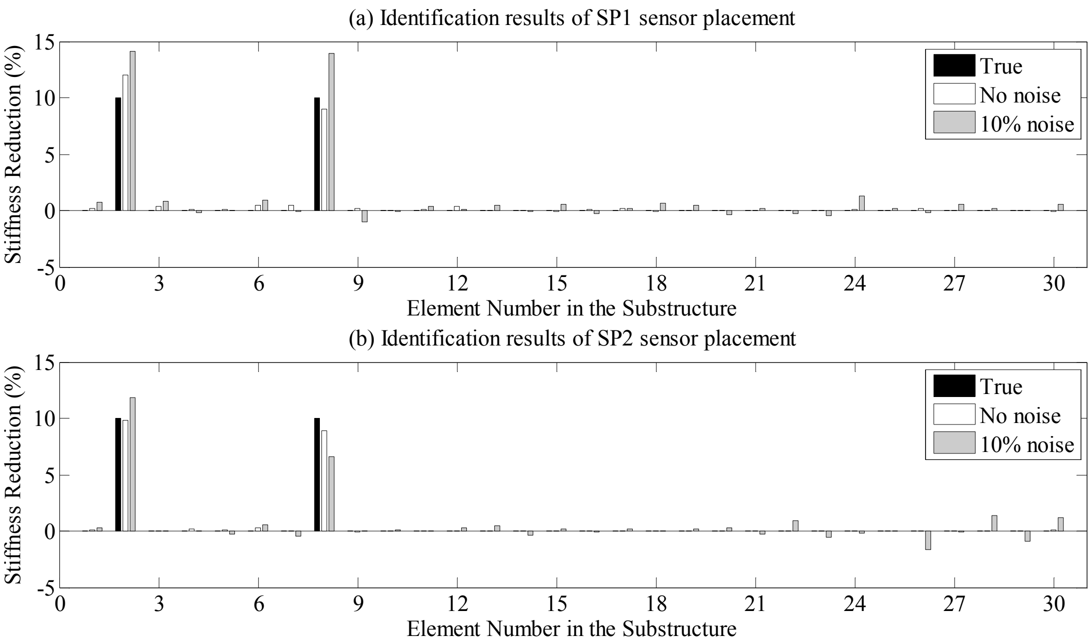

Figure 4.10: Damage identification results of SP1 and SP2 sensor placement configuration

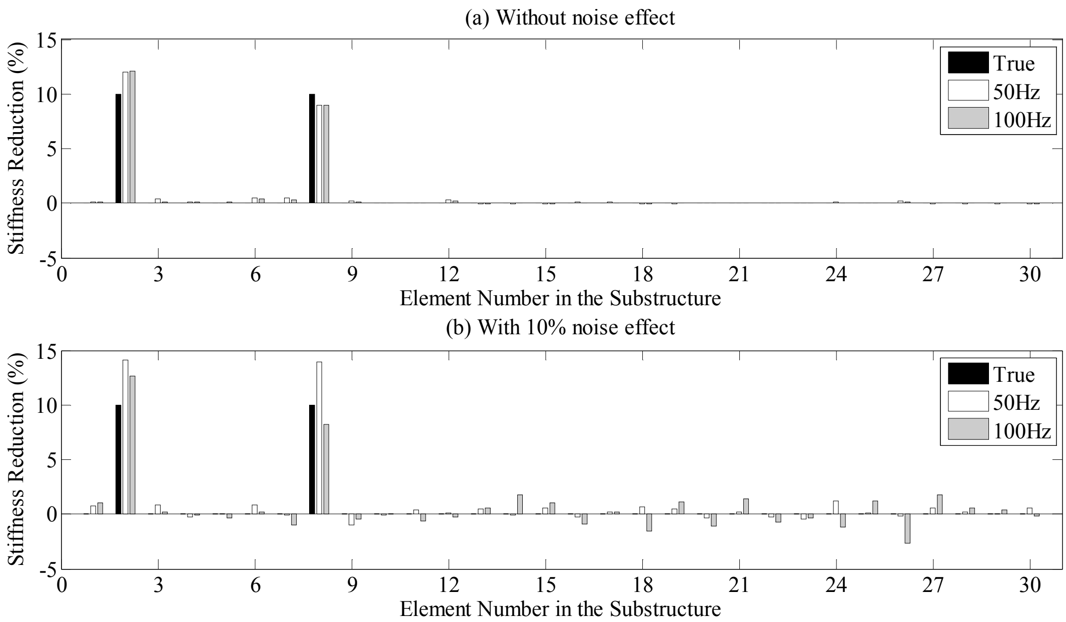

Figure 4.11: Damage identification results of SP1 with 50Hz and 100Hz sampling rate

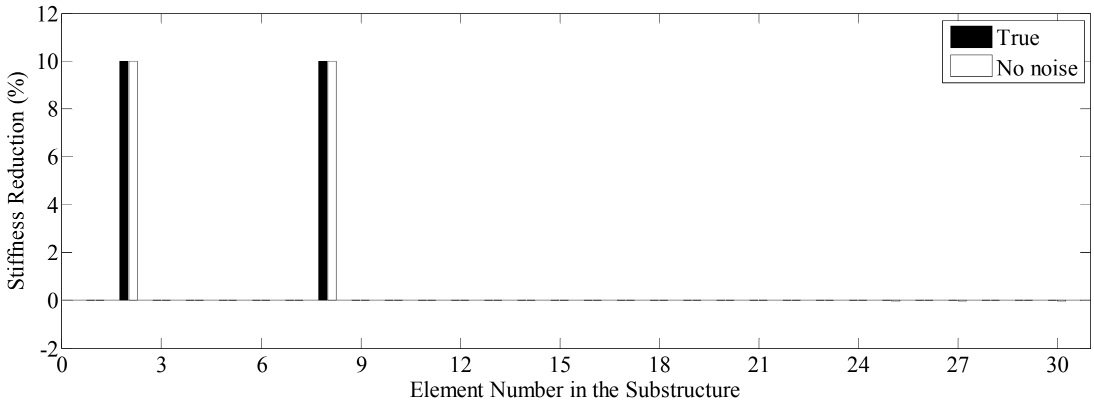

Figure 4.12: Damage identification results without use of IIRS condensation

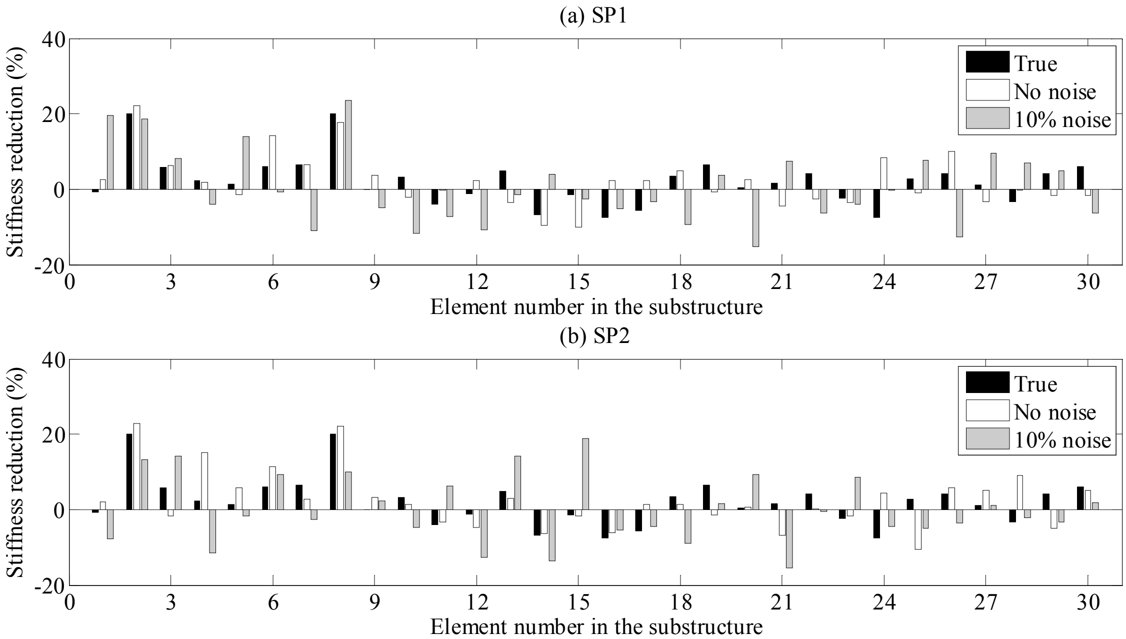

Figure 4.13: Damage identification results with model errors

CHAPTER 5

CONDITION ASSESSMENT FOR STRUCTURES SUBJECT TO MOVING VEHICULAR LOADS

5.1 Introduction

It has been reviewed in Chapter 2 that existing damage identification methods for bridge structures subject to moving vehicular loads need to assume that the information of the moving vehicular loads are available or to identify the vehicle-bridge interaction loads from measured responses of the structure, and the accuracy of damage identification results in bridge structures depends on the accuracy of the identified moving loads. This Chapter attempts to explore a damage identification approach for bridge structures subject to moving vehicular loads based on the dynamic response reconstruction technique in the wavelet domain. The knowledge of the moving vehicular loads is not required and there is no need to identify the moving loads in the identification algorithm. The dynamic response reconstruction technique in the wavelet domain is developed for the case of a bridge structure and a target substructure subject to moving vehicular loads. The transmissibility matrix between two sets of time-domain response vectors of the structure is formulated using the unit impulse response function in the wavelet domain with the moving loads at different locations. Measured acceleration responses from the structure or the substructure in the damaged state are used for the damage detection. A dynamic response sensitivity-based method is used for the structural damage identification, and local damage is modeled as a change in the elemental stiffness factors. Numerical studies on a three-dimensional box-section girder will be conducted to illustrate the effectiveness and performance of the proposed approach.

5.2 Damage Identification in a Full Structure Subject to Moving Vehicular Loads

5.2.1 Theoretical Formulation

5.2.1.1 Dynamic Response Analysis of a Structure Subject to Moving Vehicular Loads

The governing equation of motion of a damped structural system with N-DOFs subject to moving vehicular loads can be written as,

$$[M]\{\ddot{x}(t)\}+[C]\{\dot{x}(t)\}+[K]\{x(t)\}=\{\Phi_R^p(t)\}\{P_{\text{int}}(t)\} \tag{5.1}$$

where M, C and K are the $N \times N$ mass, damping and stiffness matrices of the structure respectively; $\ddot{x}$, $\dot{x}$ and x are respectively the acceleration, velocity and displacement response vectors of the structure; $\{P_{\text{int}}(t)\}$ is the bridge-vehicle interaction force vector acting on the bridge structure by the moving vehicle. $\{\Phi_R^p(t)\}\{P_{\text{int}}(t)\}$ is the equivalent nodal load vector applied on the structure at location R at time constant t with the mapping vector $\Phi_R^p(t)$. The vector $\Phi_R^p(t)$ is time-varying and it can be represented by the shape function to compute the equivalent nodal loads (Law *et al*. 2004). Rayleigh damping $[C]=a_1[M]+a_2[K]$ is assumed, where a_1 and a_2 are the Rayleigh damping coefficients. The dynamic responses of the structure can be obtained from Equation (5.1) using the Newmark-β method (Newmark 1959).

5.2.1.2 Unit Impulse Response Function in Wavelet Domain Subject to Moving Loads

It should be noticed that the mapping vector $\{\Phi_R^p(t)\}$ in Equation (5.1) is time-varying when the structure is subject to moving vehicular loads. The impulse response function under the moving load will be developed in this section and it will be used to formulate the input-output relationship for the structure when it is subject to the interaction forces $\{P_{\text{int}}(t)\}$ induced by the moving loads.

The equation of motion of the damped structural system under the unit impulse interaction force at location R at a specific time instant t is,

$$[M]\{\ddot{x}(t)\}+[C]\{\dot{x}(t)\}+[K]\{x(t)\}=\{\Phi_R^p(t)\}\delta(t) \tag{5.2}$$

where, $\Phi_R^p(t)$ denotes the shape function mapping the interaction force at location R at time instant t to the associated DOFs of the structure. Similar to the solution of Equation (3.38), the impulse response function under the moving load at location R can be obtained using the Newmark-β method by solving the following equation of motion with some specific initial conditions,

$$\begin{cases}[M]\ddot{h}_R(t)+[C]\dot{h}_R(t)+[K]h_R(t)=0\\ \quad h_R(0)=0, \quad \dot{h}_R(0)=M^{-1}\Phi_R^p(t)\end{cases} \tag{5.3}$$

where, h_R , $\dot{h}_R$ and $\ddot{h}_R$ are the unit impulse displacement, velocity and acceleration vectors under the moving load at location R, respectively.

When the structural system is subject to the moving load $P_{\text{int}}(t)$ with zero initial conditions, the acceleration response $\ddot{x}_s(t)$ from sensor location s at time instant t can be obtained as,

$$\ddot{x}_s(t)=\int_0^t \ddot{h}_{s,R_\tau}(t-\tau)P_{\text{int}}(\tau)d\tau \tag{5.4}$$

in which, $\ddot{h}_{s,R_\tau}(t)$ is the unit impulse response function under the moving load at location R_τ for sensor location s. It is noted that $\ddot{h}_{s,R_\tau}(t)$ can be obtained from Equation (5.3) with the moving load placed at different locations. It should be noted that the formulation of Equation (5.4) is different from that of Equation (3.40) since the impulse response function with the moving loads at different locations will be used in Equation (5.4) rather than the same impulse response function with the input force at a specific location used in Equation (3.40). The vectors $\ddot{h}_{s,R_\tau}(t-\tau)$ and $P_{\text{int}}(\tau)$ can be expanded in terms of the discrete wavelet transform (DWT) as (Newland 1993),

$$\ddot{h}_{s,R_\tau}(t-\tau) = h_{s,0}^{DWT} + \sum_j \sum_k h_{s,2^j+k}^{DWT} \psi\left(2^j \tau - k\right) \tag{5.5}$$

$$P_{\text{int}}(\tau) = P_0^{DWT} + \sum_j \sum_k P_{2^j+k}^{DWT} \psi\left(2^j \tau - k\right) \tag{5.6}$$

where $\psi\left(2^j \tau - k\right)$ is the wavelet basis function, $h_{s,2^j+k}^{DWT}$ and $P_{2^j+k}^{DWT}$ are the expansion coefficients for the impulse response function and moving force vectors respectively. Substituting Equations (5.5) and (5.6) into the convolution integral in Equation (5.4), and using the orthogonal conditions of the wavelet basis functions (Daubechies 1992) as follows,

$$\int_0^t \psi\left(2^j \tau - k\right) d\tau = 0 \tag{5.7}$$

$$\int_0^t \psi\left(2^j \tau - k\right) \psi\left(2^r \tau - s\right) d\tau = \begin{cases} 1/2^j & \text{when } r = j \text{ and } s = k \\ 0 & \text{otherwise} \end{cases} \tag{5.8}$$

The following formula can then be derived as

$$\ddot{x}_s(t) = \ddot{h}_s^{DWT}(t) P_{\text{int}}^{DWT} \tag{5.9}$$

in which, $\ddot{h}_s^{DWT}(t)$ and P_{int}^{DWT} are the discrete wavelet transforms of $\ddot{h}_{s,u_\tau}(t-\tau)$ and $P_{\text{int}}(\tau)$, respectively and they are given as,

$$P_{\text{int}}^{DWT} = \begin{bmatrix} P_0^{DWT} & P_1^{DWT} & \cdots & P_{2^j+k}^{DWT} \end{bmatrix}^T \tag{5.10}$$

$$\ddot{h}_s^{DWT}(t) = [\ddot{h}_{s,0}^{DWT}(t) \quad \ddot{h}_{s,1}^{DWT}(t) \quad \cdots \quad \ddot{h}_{s,2^j+k}^{DWT}(t)/2^j] \tag{5.11}$$

For the entire time history data, for example, $\ddot{x}_s = \left[\ddot{x}_s(t_1) \quad \ddot{x}_s(t_2) \quad \cdots \quad \ddot{x}_s(t_n)\right]^T$, the system input-output relationship for the structure subject to moving loads can be expressed as,

$$\ddot{x}_{s(n\times 1)} = \ddot{h}_s^{DWT}{}_{(n\times rl)} P_{\text{int}}^{DWT}{}_{(rl\times 1)} \tag{5.12}$$

in which,

$$\ddot{h}_s^{DWT} = \begin{bmatrix} \ddot{h}_s^{DWT}(t_1) \\ \ddot{h}_s^{DWT}(t_2) \\ \vdots \\ \ddot{h}_s^{DWT}(t_n) \end{bmatrix} \tag{5.13}$$

where n, r and l are the number of sampled data in the response data, the number of input excitations and the number of wavelet coefficients in the discrete wavelet transform, respectively.

5.2.1.3 Response Reconstruction in a Substructure Subject to Moving Loads

The measured responses from the structure subject to moving loads are divided into two sets, noted as the First-set response vector $\ddot{x}_1(t)$ and the Second-set response vector $\ddot{x}_2(t)$ respectively. They are represented in the wavelet domain from Equation (5.12) as follows,

$$\begin{cases} \ddot{x}_1(t)_{(mn\times 1)} = \ddot{h}_1^{DWT}{}_{(mn\times rl)} P_{\text{int}}^{DWT}{}_{(rl\times 1)} \\ \ddot{x}_2(t)_{(qn\times 1)} = \ddot{h}_2^{DWT}{}_{(qn\times rl)} P_{\text{int}}^{DWT}{}_{(rl\times 1)} \end{cases} \tag{5.14}$$

in which, m, q, n, r and l are the number of measurements in the First-set response vector, the number of measurements in the Second-set response vector, the number of sampled data points in each measurement, the number of moving loads, and the number of wavelet coefficients in the discrete wavelet transform, respectively.

When the number of measurements in the First-set response vector is at least equal or larger than the number of moving loads on the structure, the pseudo-inverse $\left(h_1^{DWT}\right)^+$ exists and the following equation can be obtained from the first row of Equation (5.14),

$$P_{\text{int}}^{DWT} = \left(\ddot{h}_1^{DWT}\right)^+ \ddot{x}_1(t) \tag{5.15}$$

Substituting Equation (5.15) into the second row of Equation (5.14), we have,

$$\ddot{x}_{2r}(t) = T_{12}\ddot{x}_1(t) \tag{5.16}$$

where,

$$T_{12} = \ddot{h}_2^{DWT} \left(\ddot{h}_1^{DWT} \right)^+ \tag{5.17}$$

The Second-set response vector $\ddot{x}_{2r}(t)$ can be reconstructed from the First-set response vector $\ddot{x}_1(t)$ in the structure from Equation (5.16). Moreover, Equation (5.17) defines the transmissibility matrix in wavelet domain between two sets of response vectors of the structure and the presented response reconstruction technique can be applied for the structural damage identification in the next section.

5.2.1.4 Structural Damage Identification

Finite element model updating method and damage model assumption in Chapter 4 are also used here. The objective function is defined as the difference between two sets of response vectors

$$f_{obj} = \left\| \ddot{x}_{2m}(t) - \ddot{x}_{2r}(t) \right\|_2 \tag{5.18}$$

where, $\ddot{x}_{2m}(t)$ is the measured Second-set response vector from the damaged structure subject to moving loads. $\ddot{x}_{2r}(t)$ is the reconstructed Second-set response vector from Equation (5.16) with the measured First-set response vector $\ddot{x}_1(t)$ in the damaged state.

Acceleration measurements from the damaged structure under the passage of the moving loads will be used to identify structural elemental stiffness factors α_i iteratively. Initially it is assumed that each elemental stiffness factor of the analytical structural finite element model is equal to unity. It should be noted that the travelling path and velocity of the moving loads, i.e. the locations, are assumed known in the identification. An updated finite element model is assumed to be available as a reference model for the following iterative procedure of damage identification.

Step 1: Measure the dynamic acceleration responses at the First-set $\{\ddot{x}_{1m}(t)\}$ and Second-set $\{\ddot{x}_{2m}(t)\}$ measurement locations from the damaged structure subject to moving vehicular loads.

Step 2: Compute the unit impulse response function matrices $\ddot{h}_1^{DWT}$ and $\ddot{h}_2^{DWT}$ in Equation (5.13) for the First-set and Second-set measurement DOFs respectively from the analytical finite element model of the structure with Equation (5.3). Calculate the matrix T_{12} in Equation (5.17) and the reconstructed Second-set response vector $\{\ddot{x}_{2r}(t)\}$ is obtained from Equation (5.16).

Step 3: The vector of response difference $\{\Delta\ddot{x}\}$ is computed between the Second-set measured response vector $\{\ddot{x}_{2m}(t)\}$ in Step 1 and the reconstructed Second-set response vector $\{\ddot{x}_{2r}(t)\}$ in Step 2. The sensitivity matrix $[S]$ of the response $\ddot{x}_{2r}(t)$ with respect to structural elemental stiffness factors is obtained using the numerical finite difference method (Zivanovic *et al.* 2007).

Step 4: Obtain the perturbation vector of structural elemental stiffness factors $\{\Delta\alpha\}$ with the adaptive Tikhonov regularization technique.

Step 5: The vector of structural elemental stiffness factors is iteratively updated with $\alpha_{i+1} = \alpha_i + \Delta\alpha$ for the next iteration. Repeat Steps 2 to 4 until the following convergence criterion is satisfied.

$$\frac{\|\alpha_{i+1} - \alpha_i\|_2}{\|\alpha_i\|_2} \leq Tolerance \tag{5.19}$$

where i denotes the ith iteration. The *tolerance* value is taken as 1.0×10^{-4} in this study.

In the above-mentioned iterative scheme for damage identification, it should be noticed that: (a) the properties of the moving vehicle and the time-histories of the moving loads on the bridge structure are not required to be identified; (b) the locations of the moving loads are assumed to be known.

5.2.2 Numerical Simulation

The same bridge girder in Section 4.3.2 in Chapter 4 is used here and numerical studies on the bridge deck subject to moving vehicular loads are conducted to demonstrate the accuracy and effectiveness of the proposed damage identification approach.

In engineering applications, moving loads induced by the passage of a vehicle are often considered as excitations to the bridge structures for the condition assessment. The moving load has been represented very often as a multi-sine wave moving force in many studies (Zhu and Law 2007, Law *et al*. 2007a) for an easier and simpler structural analysis of the bridge-vehicle system. The first example of numerical studies has a box-section girder bridge subject to a single multi-sine wave moving force. The second example has the girder structure under the passage of a two-axle three-dimensional vehicle which represents the more realistic moving vehicle model. The road surface roughness effect will also be included in the bridge-vehicle system analysis.

5.2.2.1 Example 1: A Bridge Deck Subject to a Single Moving Force

Damage is introduced in the box-section bridge deck as a reduction of elastic modulus in several elements. In this study, 10% damage is simulated in both the 28th and 29th elements at mid-span of the deck as shown in Figure 5.1(a). The moving force is represented as,

$$P(t) = 160000\left(1 + 0.1\sin(10\pi t) + 0.05\sin(30\pi t)\right)N \qquad (5.20)$$

Damage identification is performed with the moving force crossing the bridge along the centreline of the deck as shown in Figure 5.1(a). The force vector acting at an arbitrary location on a shell element of the bridge deck is transformed into nodal loads using the Hermite interpolation function (Wu 2007). Six sensors are assumed distributed on top of the deck to measure the acceleration responses from the damaged structure subject to the moving force. The measurements are divided into two sets of responses and they are shown in Table 5.1. The number of measurements in the First-set response vector is two and it is greater than the number of moving force. The velocity of the moving force is 20 m/s and the sampling rate is 100Hz. The acceleration response data within first 3 seconds are used except otherwise stated.

Forward Response Reconstruction in Wavelet Domain

The accuracy of the proposed method for the response reconstruction in the structure subject to moving loads will be examined. The simulated local damages are introduced in the structure and the responses are obtained at the First-set and Second-set sensor locations in the damaged state. The reconstructed Second-set response vector is obtained from Equation (5.16) and is compared with the analytical Second-set response which is taken as the true response vector. In this study, Daubechies 8-coefficient wavelet is chosen as the basis functions in the DWT due to its orthogonality properties and fairly smooth interpolation nature (Robertson *et al.* 1998). It should be noticed that no noise is added to the measurements here. Results of forward response reconstruction are shown in Figure 5.2. Figures 5.2(a), 5.2(c), 5.2(e) and 5.2(g) show the true and reconstructed responses at those sensor locations in the Second-set response vector, respectively. It can be found that these two responses are overlapping indicating that the response reconstruction process is very accurate.

The difference vectors $\left(\ddot{x}_{true}(t) - \ddot{x}_{ur}(t)\right)$ between the true and reconstructed responses of the four sensors in the Second-set response vector are shown in Figures 5.2(b), 5.2(d), 5.2(f) and 5.2(h). The relative errors at these four sensors are 5.97×10^{-12}, 8.47×10^{-12}, 7.47×10^{-12} and 3.48×10^{-12}, respectively. It is indicated that the proposed method for dynamic response reconstruction in the structure under the passage of the moving force is very accurate. It may also be noted that different sensor placement configurations in the First-set and Second-set response vectors may give different accuracies in the response reconstruction process.

Damage Identification Results

The iterative procedure described in Section 5.2.1.4 is followed to obtain an updated set of elemental stiffness factors. The acceleration responses in the damaged state are obtained from Equation (5.1) and they are taken as the simulated "measured" responses. 10% noise effect is included in the acceleration measurements for this study.

Acceleration measurements without and with noise effect are used for damage identification. Table 5.2 gives the associated information on convergence of the iterative procedure. The required iterations and error of convergence calculated from Equation (5.19) are listed. It should be noticed that approximately 1.5 hours are required for one iteration with a Intel Core 2 Quad 2.4G PC with 8G memory due to the large size of the structural finite element model for the computation of responses and sensitivity matrix of the structure by the finite difference method.

The damage identification results are shown in Figure 5.3. For the noise-free case, the dynamic response data within the first 3 seconds are used for the damage identification. The locations of the simulated damage can be identified accurately. The identified extents of local damage in 28th and 29th elements without noise effect are 9.997% and 9.999% respectively. They are very close to the true values indicating that the proposed approach for damage identification in the structure under moving loads is effective and can give very accurate damage values. For the case with 10% noise, the identification results could be influenced by the noise effect. In this case, the dynamic response data within the first 0.5 second and 1.5 to 2 seconds are used for the identification since the responses in these periods are much larger and could be less sensitive to the noise effect. Figure 5.3 shows that the damage can be identified effectively with 10% noise effect with 8.32% and 11.23% stiffness reductions in 28th and 29th elements respectively, and the adopted adaptive Tikhonov regularization technique described contributes to yield identification results on the undamaged elements with very small false positives and false negatives.

5.2.2.2 Example 2: A Bridge Deck Subject to a Two-Axle Three-Dimensional Moving Vehicle

Dynamic Analysis of the Bridge-Vehicle System

The bridge-vehicle system in this study is represented as a simply supported box-section bridge deck subject to a two-axle three-dimensional vehicle model with seven DOFs. The vehicle model, as shown in Figure 5.4, is represented according to H20-44 truck in AASHTO 2007. The specific parameters of the vehicle are referred in (Zhu and Law 2002), with a mass of 17 000kg. The dynamic responses of the bridge structure are obtained by solving the coupled bridge-vehicle system equation of motion (Law *et al*. 2007b).

The three-dimensional two-axle vehicle crosses the bridge along the travelling path as shown in Figure 5.1(a). Seven sensors are assumed distributed on the deck in this case to measure the acceleration responses from the damaged bridge deck. The measurements are divided into two sets of responses and they are shown in Table 5.3. The number of measurements in the First-set response vector is equal to five and it is greater than the number of interaction forces induced by the moving vehicle which is four. The velocity of the moving force is 20 m/s and the sampling rate is 100Hz. Class *C* road surface roughness (*ISO8606,* 1995), corresponding to the average road pavement condition, is included in the bridge-vehicle system analysis. The acceleration response data within the first 3 seconds are used except otherwise stated.

Forward Response Reconstruction in Wavelet Domain

The damage scenario in the girder structure is the same as for the last example, which is, 10% damage in both the 28^{th} and 29^{th} elements in the web of the bridge structure in the form of a reduction in the elastic modulus of these elements. The simulated local damages are introduced in the structure and responses are obtained at the First- and Second-set sensor locations in the damaged state. The reconstructed

Second-set response vector is obtained from Equation (5.16) and is compared with the true Second-set response. It should be noticed that no noise is added to the measurements here. The comparisons of forward response reconstruction results are shown in Figure 5.5. Figures 5.5(a) and 5.5(c) show the true and reconstructed responses at the sensor locations in the Second-set response vector. The difference vectors $\left(\ddot{x}_{true}(t)-\ddot{x}_{ur}(t)\right)$ between the true and reconstructed responses of these two sensors in the Second-set response vector are shown in Figures 5.5(b) and 5.5(d).with the coresponding relative errors 1.74×10^{-11} and 1.39×10^{-11}, respectively. These results indicated that the proposed response reconstruction method in the structure subject to moving vehicular loads is very accurate. It may be noticed that different sensor selections in the First-set and Second-set response vectors would give different accuracies in the response reconstruction process.

Damage Identification Results

Damage identification is performed with the two-axle three-dimensional vehicle crossing the bridge along the travelling path shown in Figure 5.1(a). The acceleration responses are obtained from the damaged bridge structure subject to the moving vehicle and they are taken as the simulated "measured" responses. 10% noise effect is included in the acceleration measurements.

Acceleration measurements with and without noise effect are used for the damage identification. Table 5.4 gives the associated information on convergence of the iterative procedure. The computation of matrix T_{12} in this case becomes intensive since four interaction forces from the moving vehicle are applied on the bridge structure. It should be noticed that approximately 6 hours are required for one iteration with a Intel Core 2 Quad 2.4G PC with 8G memory due to the high computation cost in the bridge-vehicle system analysis and in the process of computing sensitivity matrix for the structure subject to moving loads.

The damage identification results are shown in Figure 5.6. For the noise-free case, the dynamic response data within the first 3 seconds are used for damage identification. The damage locations and extents are identified accurately with 9.9996% and 9.9987% stiffness reductions in 28th and 29th element respectively. This indicates that the proposed approach for damage identification in the structure under moving vehicle loads is effective and can give very good results. For the case with 10% noise, the identification results would be influenced by the noise effect. The first 0.8 second and 1.5 to 2.2 seconds of the response data are used for the identification since the responses in these periods are much larger and could be less sensitive to the noise effect. Figure 5.6 shows that the damage can be identified effectively with 10.41% and 11.84% stiffness reduction in 28th and 29th elements respectively when 10% noise effect is included in the measurements, and it is noted that the adopted adaptive Tikhonov regularization technique improves the identification results on the undamaged elements with very small false positives and false negatives similar to the observations in Figure 5.3. In addition, it should be noticed that the sensor selections in the First-set and Second-set response vectors would influence the damage identification results especially for the case with noisy measurements. However, the issue on optimal placement of sensor numbers and locations in the First-set and Second-set response vectors is not examined in this study.

5.2.2.3 Effect of Initial Model Errors on the Identification Results

The influence of initial model errors in the finite element model on the effectiveness and performance of the proposed damage identification approach will be investigated. The initial model errors in the stiffness of elements and in the support stiffness are considered in this study. Other model error sources, such as uncertainties in the mesh and element type in the finite element analysis, mass matrix and temperature effect, etc. are not included. Example 2 in Section 5.2.2.2 with the bridge deck subject to a moving vehicle is used. Three scenarios in Table 5.5 are defined. 20 % stiffness reductions are introduced in both the 28th and 29th elements of the deck. It is assumed that the initial finite element model corresponds to a normal random distribution of the elastic modulus with a mean of $2.6\times10^{4} MPa$ and a coefficient of variation equal to 5% in Scenario 1. 10% increase in the support stiffness is assumed in Scenario 2. Scenario 3 includes the above two kinds of initial model errors.

The identification results of these three scenarios are shown in Figures 5.7(a), (b) and (c), respectively. In Scenario 1, for the noise-free case, the simulated damage in 28th and 29th elements and model errors in the stiffness of other undamaged elements are identified accurately. For the case with 10% noise effect, the identified extents in 28th and 29th elements are 19.49% and 19.52%, respectively. It is found that the model errors in stiffness may not be identified accurately in all elements and there are several large false positives and false negatives in the identification results. In Scenario 2, the identification results from measurements without and with noise effect will both be influenced by the model error in the support stiffness. The identified extents in 28th and 29th elements are 14.48% and 12.41%, 21.90 and 11.26% for the case without measurement noise and with 10% noise, respectively. The adoptive Tikhonov regularization technique improves the identification results with less false negatives, but several false positives in results are observed due to the model error in the support stiffness. The identification results in Scenario 3 from measurements with and without noise effect will be affected by the initial model errors in the stiffness and in the support. The identified extents in 28th and 29th elements are 19.81% and 21.87%, 16.62% and 16.99% for the case without noise and with 10% noise, respectively. Several false positives and false negatives may exist in the identification results.

5.3 Damage Identification in a Substructure Subject to Moving Vehicular Loads

Many studies (Huang and Yang 2008, Law *et al*. 2010) explored the simultaneous identification of both the input excitations and system parameters in substructural condition assessment. However, study on substructural damage identification under moving vehicular loads is seldom reported. The above response reconstruction and damage identification for a bridge structure subject to moving loads is developed for the scenario where a target substructure is included in the damage identification algorithm.

5.3.1 Theoretical Formulation

5.3.1.1 Response Reconstruction in a Substructure Subject to Moving Loads

When a target substructure is subject to both the interaction forces induced by the moving vehicle and the interface forces from adjacent substructures, the dynamic acceleration response of the substructure can be written as,

$$\ddot{x}(t) = \ddot{h}_{\text{int}}^{DWT} P_{\text{int}}^{DWT} + \ddot{h}_I^{DWT} F_I^{DWT} \tag{5.21}$$

where, P_{int}^{DWT} and F_I^{DWT} are the discrete wavelet transforms of interaction force and interface force vectors on the substructure, respectively. $\ddot{h}_{\text{int}}^{DWT}$ and $\ddot{h}_I^{DWT}$ are the impulse response function matrices corresponding to the moving loads and interface forces, respectively. It should be noticed that the finite element model of the target substructure is used in Equation (5.3) to obtain matrices $\ddot{h}_I^{DWT}$ and $\ddot{h}_{\text{int}}^{DWT}$.

Equation (5.21) can also be represented as,

$$\ddot{x}(t) = \ddot{H}F \tag{5.22}$$

in which, $\ddot{H} = \left[\ddot{h}_{\text{int}}^{DWT}, \ddot{h}_I^{DWT}\right]$, $F = \left[P_{\text{int}}^{DWT}, F_I^{DWT}\right]^T$.

The measured acceleration responses from the substructure subject to moving loads are also divided into two sets, denoted as the First-set response vector $\ddot{x}_1(t)$ and the Second-set response vector $\ddot{x}_2(t)$ respectively. They are represented in the wavelet domain from Equation (5.22) as follows,

$$\begin{cases} \ddot{x}_1(t) = \ddot{H}_1 F \\ \ddot{x}_2(t) = \ddot{H}_2 F \end{cases} \tag{5.23}$$

When the number of measurements in the First-set response vector is at least equal or larger than the number of both the interaction forces and interface forces on the substructure, the following equation can be obtained from the first row of Equation (5.23),

$$F = \left(\ddot{H}_1\right)^{+} \ddot{x}_1(t) \tag{5.24}$$

Substituting Equation (5.24) into the second row of Equation (5.23), we have,

$$\ddot{x}_{2r}(t) = T_{12}\ddot{x}_1(t) \tag{5.25}$$

where,

$$T_{12} = \ddot{H}_2\left(\ddot{H}_1\right)^{+} \tag{5.26}$$

The reconstructed Second-set response vector $\ddot{x}_{2r}(t)$ is obtained from Equation (5.25) from the First-set response vector $\ddot{x}_1(t)$ in the substructure. Equation (5.26) defines the transmissibility matrix between two sets of time-domain response vectors from the substructure subject to moving loads and this response reconstruction technique will be applied for the substructural damage identification in the following section.

5.3.1.2 Substructural Damage Identification

Dynamic acceleration measurements from the damaged substructure under the passage of the moving loads will be used to identify the substructural elemental stiffness factors α_i iteratively. Initially, it is assumed that each substructural elemental stiffness factor of the analytical finite element model of the substructure is equal to unity. It should be noted that the travelling path and velocity of the moving loads, i.e. the locations of the moving loads, are assumed to be known in the identification. An updated finite element model is assumed to be available as a reference model for the following iterative procedure of damage identification.

Step 1: Measure the dynamic acceleration responses at the First-set $\{\ddot{x}_{1m}(t)\}$ and Second-set $\{\ddot{x}_{2m}(t)\}$ measurement locations from the damaged substructure subject to moving loads.

Step 2: Compute the unit impulse response function matrices $\ddot{H}_1$ and $\ddot{H}_2$ in Equation (5.23) which correspond to the First-set and Second-set measurements respectively from the analytical finite element model of the substructure. Calculate matrix T_{12} in Equation (5.26) and the reconstructed Second-set response vector $\{\ddot{x}_{2r}(t)\}$ is obtained from Equation (5.25).

Step 3: The vector of response difference $\{\Delta\ddot{x}\}$ is computed between the Second-set measured response vector $\{\ddot{x}_{2m}(t)\}$ in Step 1 and the reconstructed Second-set response vector $\{\ddot{x}_{2r}(t)\}$ in Step 2. The sensitivity matrix $[S]$ of the response $\ddot{x}_{2r}(t)$ with respect to substructural elemental stiffness factors is obtained using the numerical finite difference method.

Step 4: Obtain the perturbation vector of substructural elemental stiffness factors $\{\Delta\alpha\}$ with the adaptive Tikhonov regularization technique.

Step 5: The vector of substructural elemental stiffness factors is iteratively updated with $\alpha_{i+1} = \alpha_i + \Delta\alpha$ for the next iteration. Repeat Steps 2 to 4 until the following convergence criterion is satisfied.

$$\frac{\|\alpha_{i+1} - \alpha_i\|_2}{\|\alpha_i\|_2} \le Tolerance \tag{5.27}$$

where i denotes the i th iteration.

The *Tolerance* value is taken as 1.0×10^{-4} for the noise-free case and 1.0×10^{-3} for the case with noise. It may be noticed that more iterations are required when a smaller tolerance value is defined for convergence.

In the above-mentioned iterative scheme for damage identification, it should be noted that: a) only the finite element model of the target substructure and measured responses from the substructure in the damaged state are required; b) the time-histories of the interface forces and interaction forces induced by moving vehicular loads on the substructure are not required and only the locations of the moving loads are assumed to be known.

5.3.2 Numerical Simulation

Numerical studies on a simply-supported box-section bridge deck structure subject to moving loads are conducted to investigate the performance of the proposed approach for substructural damage identification. The same bridge model in Section 5.2.2 is used. The target substructure to be investigated in this study is shown in Figure 5.8 with 36 nodes and 30 elements and the six interface nodes are from Nodes 31 to 36. The numberings of nodes and elements of the finite element model of the target substructure are also shown in Figure 5.8(a) and the cross-section is shown in Figure 5.8(b).

Two examples of numerical studies are conducted. The first example has the box-section girder bridge deck subject to a single multi-sine wave moving force along the centerline of the deck. The second example has the girder structure under the passage of a two-axle three-dimensional vehicle which represents a more realistic moving vehicle model crossing the bridge. The road surface roughness effect will also be included in the bridge-vehicle system analysis.

5.3.2.1 Model Condensation of the Target Substructure

The target substructure has 36 interface DOFs at the six interface nodes of Nodes 31 to 36 as shown in Figure 5.8(a), and there are 36 interface forces acting on this substructure. When a single moving force is crossing the bridge deck, at least 37 measured accelerations are required in the First-set response vector to reconstruct the Second-set response vector as indicated in Equation (5.25). Normally it is not easy to provide such a large number of measurements in practice due to the cost of data acquisition. An attempt is made to reduce the number of required sensors using the model condensation technique, and the IIRS model condensation scheme is adopted. The slave DOFs should be those interface DOFs carrying relatively smaller interface forces such that the error of model condensation would be smaller and less affects the accuracy of subsequent substructural response reconstruction and damage identification. In this study, interface DOFs at the interface nodes, such as DOFs at Node 31(x), 31(z), 31(θ_x), 31(θ_y), 31(θ_z), Node 32(θ_z), Node 33(θ_z), Node 34(x), Node 34(θ_z), Node 35(θ_x), 35(θ_y), 35(θ_z), Node 36(θ_x), 36(θ_y) and 36(θ_z) are taken as the slave DOFs to be reduced. Most DOFs at Nodes 32 to 34 are included in the master DOFs since the bending behavior of the deck becomes significant when the moving force or moving vehicle is passing on top of the target substructure. Thus the 36 interface forces on the substructure are reduced to 21 interface forces with 15 slave DOFs at interface nodes defined in the process of model condensation.

5.3.2.2 Example 1: A Bridge Deck Subject to a Single Moving Force

Damage is introduced in the box-section bridge deck as the reduction of elastic modulus in several elements. In this study, 20% damage is simulated in both the 10th and 11th elements in the web of the substructure as shown in Figure 5.8(a). The moving force is represented as,

$$P(t) = 160000\left(1 + 0.1\sin(10\pi t) + 0.05\sin(30\pi t)\right)N \tag{5.28}$$

Damage identification is performed with the moving force along the centerline of the bridge deck of the target substructure. The force vector acting at an arbitrary location on a shell element of the bridge deck can be transformed into nodal loads using the Hermite interpolation function (Wu 2007). The velocity of the moving force is 20 m/s and the sampling rate is 100Hz.

Sensor Placement Configurations

Two sensor placement configurations are defined in Table 5.6, noted as SP1 and

SP2 respectively. The number of sensors in the First-set response vector is twenty-eight which is larger than the number of both reduced interface forces and moving force on the target substructure. Two sensors are deployed in the Second-set.

Forward Response Reconstruction in Wavelet Domain

Since model condensation to reduce the number of interface forces on the substructure will induce additional error in the response reconstruction process in Equation (5.25), the accuracy of the forward response reconstruction in the target substructure subject to moving loads will be firstly examined. The simulated local damages are introduced in the substructure and the responses are obtained at the First- and Second-set sensor locations in the damaged state when the substructure is subject to the moving force. No noise is added to the measurements here. The reconstructed Second-set response vector is obtained from Equation (5.25) and is compared with the analytical Second-set response vector which is taken as the true Second-set response. Results of forward response reconstruction with SP1 sensor placement are shown in Figure 5.9. Figures 5.9(a) and 5.9(c) show the true and reconstructed responses at the two sensor locations in the Second-set response vector, respectively.

The difference vectors $\left(\ddot{x}_{true}(t) - \ddot{x}_{ur}(t)\right)$ between the true and reconstructed responses of tho two sensors in the Second-set response vector are shown in Figures 5.9(b) and 5.9(d) with the relative errors of 1.16% and 1.78%, respectively. These relative errors are not as small as those observed in the studies of response reconstruction in a substructure using the wavelet domain method in wavelet domain, since additional error has been introduced by the model condensation.

Damage Identification Results

The iterative procedure described in Section 5.3.1.2 is followed to obtain an updated set of substructural elemental stiffness factors. The acceleration responses in the damaged state are obtained and they are taken as the simulated “measured” responses. 5% noise effect is included in the measurements.

Acceleration measurements with and without 5% noise effect are used for the damage identification. Table 5.7 gives the associated information on convergence of the iterative procedure. It should be noticed that approximately 2 hours are required for one iteration with a Intel Core 2 Quad 2.4G PC with 8G memory due to the high computation load of sensitivity matrix by the finite difference method.

Figures 5.10(a) and 5.10(b) show the substructural damage identification results with SP1 and SP2 sensor placement, respectively. The measured data during the whole duration when the force is moving on the target substructure is used for the response reconstruction and damage identification. With SP1 sensor placement, the stiffness reductions in 10^{th} and 11^{th} elements are identified as 19.35% and 18.41% respectively which are close to the true values of simulated damages. However, several small false positives exist which are believed due to the additional error introduced by the model condensation in the forward response reconstruction.

For the case with 5% noise included in the measurements, the identification results would be influenced by both the error induced by the model condensation of the substructure and the measurement noise effect. The measurement data within the first 0.5s are used for identification since the responses in this period are much larger and could be relatively less sensitive to the noise effect. The damages in the 10^{th} and 11^{th} elements are identified as 15.62% and 13.57% stiffness reduction respectively. It is noted that a few more false positives are obtained than the case without noise above.

The damage identification results with SP2 sensor placement are shown in Figure 5.10(b). It is noted that different selections in First-set and Second-set response vectors would affect the accuracy of damage identification results. The local damages can be identified effectively with SP2 sensor placement and similar observations in the results are made as in Figure 5.9(a) for SP1.

5.3.2.3 Example 2: A Bridge Deck Subject to a Two-Axle Three-Dimensional Moving Vehicle

Dynamic Analysis of the Bridge-Vehicle System

The same bridge deck is subject to a two-axle three-dimensional vehicle model with seven DOFs. The vehicle model is as same as the one used in Section 5.2.2.2, as shown in Figure 5.4. The dynamic responses of the bridge structure are obtained by solving the coupled equation of motion of the bridge-vehicle system.

The vehicle crosses the bridge along the travelling path as shown in Figure 5.8(a). Thirty-two sensors are assumed to be placed on the substructure to measure the acceleration responses from the damaged bridge deck subject to the moving vehicle. These measurements are divided into two sets of response vectors, noted as First-set and Second-set response vectors in Table 5.8. The number of sensors in the First-set response vector is equal to thirty and is greater than the sum of the four interaction forces of the moving vehicle and the reduced twenty-one interface forces on the substructure. The velocity of the moving force is 20 m/s and the sampling rate is 100Hz. Class *C* road surface roughness, corresponding to the average road pavement condition, is included in the bridge-vehicle system analysis. The acceleration response data when the vehicle is moving on the substructure are used for response reconstruction and subsequent damage identification.

Forward Response Reconstruction in Wavelet Domain

The same damage scenario in the target substructure as for Example 1 is used in this example. Responses are obtained at the First-set and Second-set sensor locations from the substructure in the damaged state when the vehicle crosses the target bridge substructure. The reconstructed Second-set response vector is obtained from Equation (5.25) and is compared with the true Second-set response. No noise effect is included in the two sets of measurement. Figures 5.11(a) and 5.11(c) show the true and reconstructed responses at the two sensor locations in the Second-set response vector. The difference vectors $(\ddot{x}_{true}(t) - \ddot{x}_{ur}(t))$ between the true and reconstructed responses of these two sensors in the Second-set response vector are shown in Figures 5.11(b) and 5.11(d) with the relative errors of 1.4% and 0.99% respectively. It is noted that different sensor selections in the First-set and Second-set response vectors would give different accuracies in the response reconstruction process. However, the issue on optimal sensor placement configuration in the First-set and Second-set response vectors is not examined in this paper.

Damage Identification Results

Damage identification is performed with the two-axle three-dimensional vehicle crossing the target substructure. The acceleration responses are obtained from the damaged substructure subject to the moving vehicle and they are taken as the simulated "measured" responses.

Acceleration measurements without and with 5% noise effect are computed for the damage identification. Table 5.9 gives the associated information on convergence of the iterative procedure. The computation load to obtain T_{12} is intensive since four interaction forces induced by the moving vehicle are involved. Approximately 5.5 hours are required for one iteration with a Intel Core 2 Quad 2.4G PC with 8G memory to calculate the transmissibility matrix T_{12} in the computation of impulse response function and to compute the sensitivity matrix $[S]$ for the substructure subject to the moving vehicle.

Figure 5.12 shows the damage identification results. For the case without noise, the identified stiffness reductions in 10^{th} and 11^{th} elements are 18.69% and 19.73% respectively. Several small false positives exist in the identification results which are believed due to the error induced by the model condensation of the substructure. These observations are similar to those in Figure 5.10. The identification results would additionally be influenced by the noise effect, and the identified stiffness reductions in 10^{th} and 11^{th} elements are 15.21% and 16.29% respectively. However, a few significant false positives are found due to the noise and smearing effect, such as the identified stiffness reductions in 12th element.

5.4 Summary

A damage identification approach in a bridge structure or in a target substructure subject moving vehicular loads based on the dynamic response reconstruction technique is proposed. The transmissibility matrix between two sets of time-domain response vectors from the structure or the substructure subject to moving loads is formulated using the unit impulse response function in the wavelet domain. Measured acceleration responses from the damaged structure or the damaged substructure are used for the identification. For the damage identification in the full structure, the properties of the moving vehicular loads are not assumed known and the time-histories of moving loads are not required to be identified. The finite element model of the bridge structure will be used to derive the unit impulse response function. For the damage identification in the target substructure, dynamic responses at the interface DOFs are not required and the time-histories of both moving loads and interface forces are not needed. The unit impulse response function from the finite element model of the substructure is used to formulate the transmissibility matrix. A dynamic response sensitivity-based method is used for the structural damage identification with the local damage modeled as a reduction in the elemental stiffness factors. The adaptive Tikhonov regularization technique is adopted to improve the identification results when noise effect is included in the measurements. Numerical studies on a three-dimensional box-section bridge deck subject to a single moving force or a two-axle three-dimensional vehicle are performed to validate the proposed approach for damage identification in a structure or in a substructure. The simulated damage can be identified effectively even with noise effect included in the measurements. The sensor selections for measurements would affect the accuracy of response reconstruction and subsequent damage identification.

Table 5.1: Sensor placement configuration of Example 1

Sensor Placement Configuration	Sensor locations
First-set	Node 14(z), 51(z)
Second-set	Node 8(z), 21(z), 45(z), 56(z)

Note: “Node 14(z)” denotes the sensor is placed along the z-direction at Node 14.

Table 5.2: Information on convergence of Example 1

	No noise	10% noise
Required iterations	5	18
Error of convergence	5.39×10^{-5}	9.56×10^{-5}

Table 5.3: Sensor placement configuration of Example 2

Sensor Placement Configuration	Sensor locations
First-set	Node 8(z), 20(z), 21(z), 45(z), 56(z)
Second-set	Node 14(z), 51(z)

Table 5.4: Information on convergence of Example 2

	No noise	10% noise
Required iterations	6	22
Error of convergence	2.01×10^{-5}	9.85×10^{-5}

Table 5.5: Damage scenarios with initial model errors

Scenario	Damage	Model errors	Noise effect
1	20% stiffness reductions in both 28th and 29th elements	5% random stiffness changes in all elements	10%
2		10% increase in the support stiffness	10%
3		Include all above model errors	10%

Table 5.6: Sensor Placement Configurations of Example 1

Sensor Placement Configuration		Sensor locations
SP1	First-set response vector	25(y, z), 26(y, z), 27(y, z), 28(y, z), 19(y, z), 20(y, z), 21(y, z), 22(y, z), 13(y, z), 14(y, z), 16(y, z), 9(y, z), 2(y, z), 15(y), 8(y)
	Second-set response vector	8(z), 15(z)
SP2	First-set response vector	25(y, z), 26(y, z), 27(y, z), 28(y, z), 19(y, z), 8(y, z), 21(y, z), 22(y, z), 13(y, z), 14(y, z), 16(y, z), 9(y, z), 2(y, z), 15(y), 20(y)
	Second-set response vector	15(z), 20(z)

Table 5.7: Information on convergence of Example 1

	SP1		SP2	
	No noise	5% noise	No noise	10% noise
Required iterations	52	7	62	5
Error of convergence	9.58×10^{-5}	9.67×10^{-4}	9.77×10^{-5}	9.69×10^{-4}

Table 5.8: Sensor placement configuration of Example 2

Sensor Placement Configuration	Sensor locations
First-set response vector	25(y, z), 26(y, z), 27(y, z), 28(y, z), 29(y, z), 30(y, z), 19(y, z), 21(y, z), 22(y, z), 23(y, z), 24(y, z), 14(y, z), 8(y, z), 9(y, z), 15(y), 20(y)
Second-set response vector	20(z), 15(z)

Table 5.9: Information on convergence of Example 2

	No noise	10% noise
Required iterations	21	4
Error of convergence	9.43×10^{-5}	8.07×10^{-4}

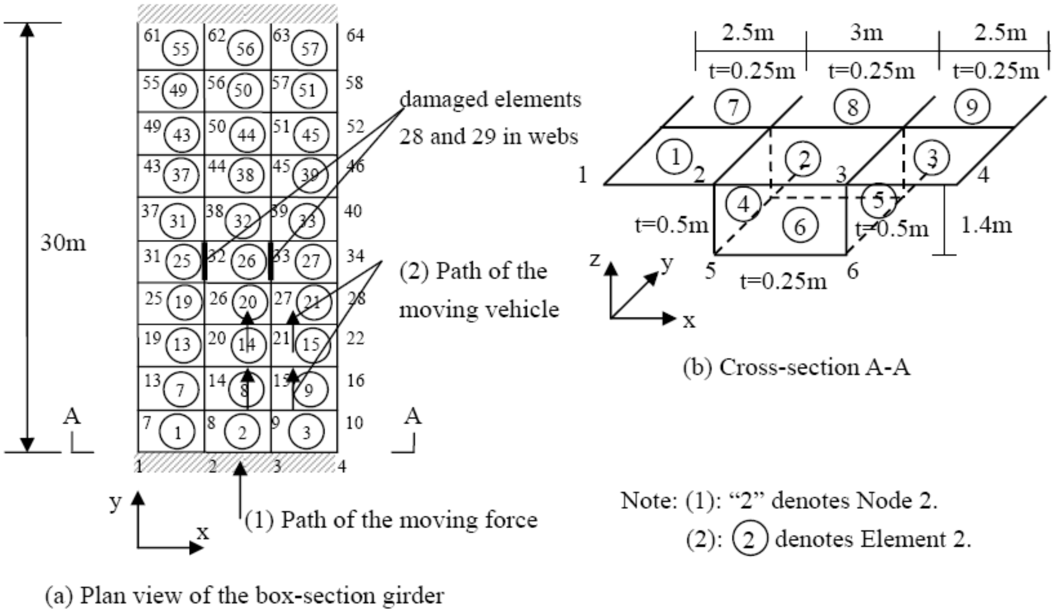

Figure 5.1: Finite element model of the box-section girder structure

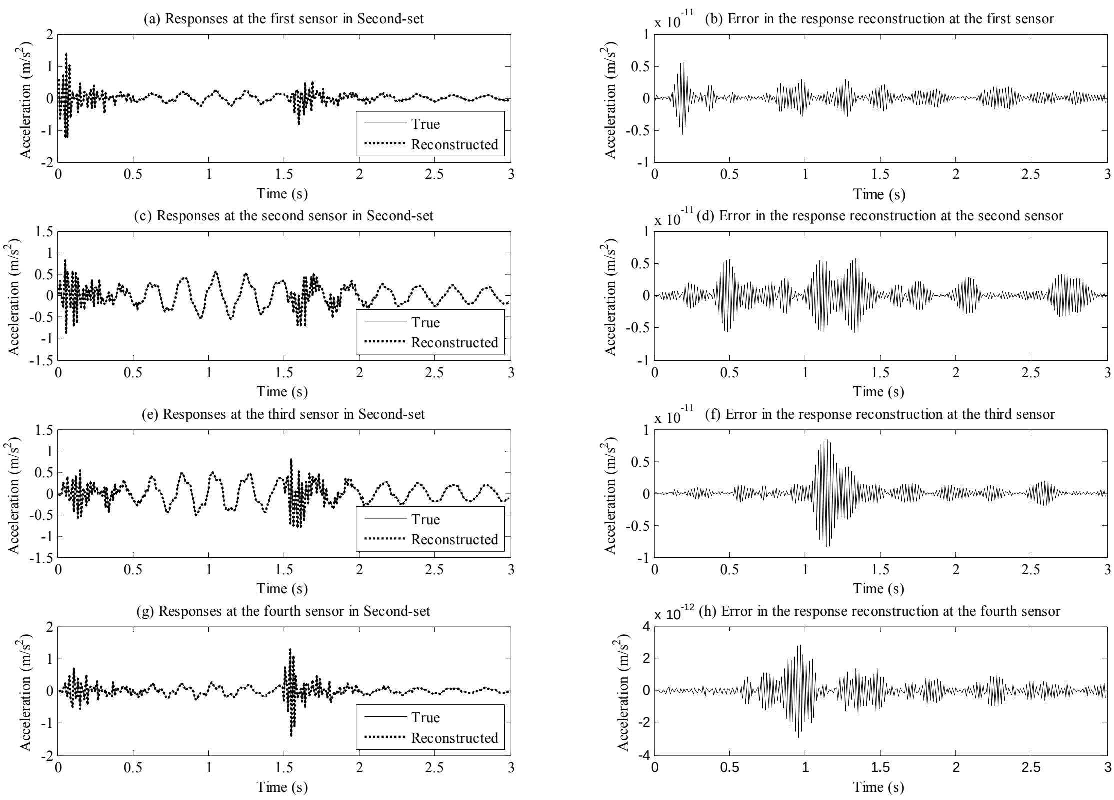

Figure 5.2: True and reconstructed responses in the Second-set response vector of Example 1

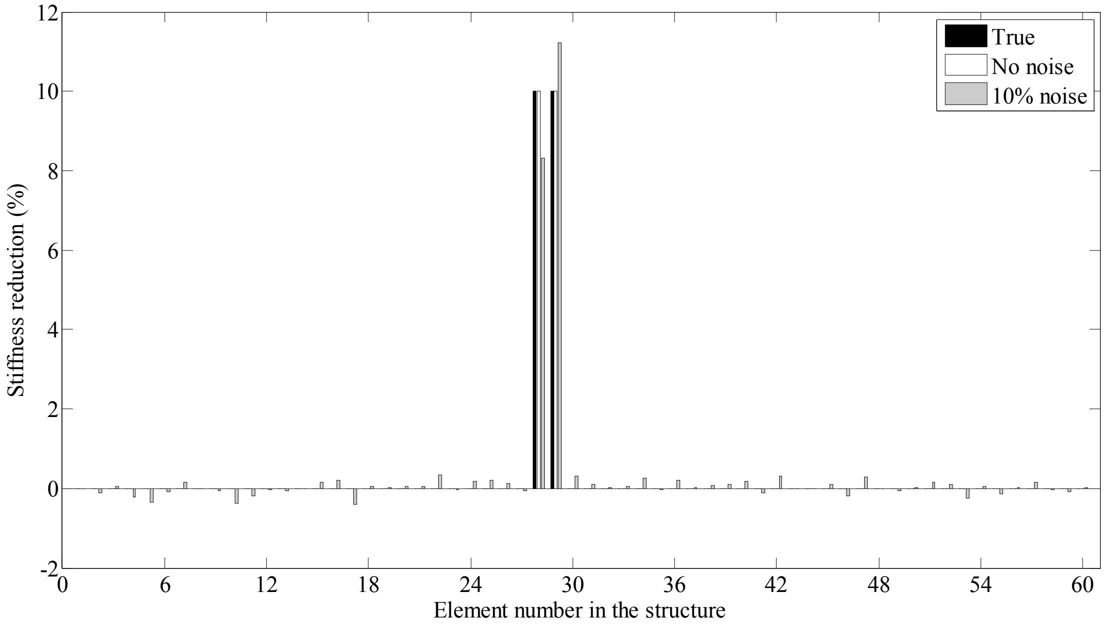

Figure 5.3: Damage identification results of Example 1

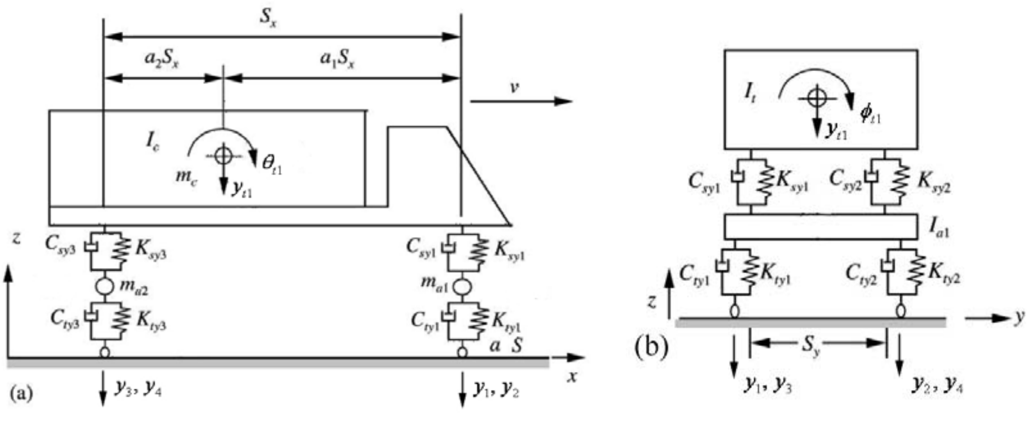

Figure 5.4: A three-dimensional two-axle vehicle with seven DOFs

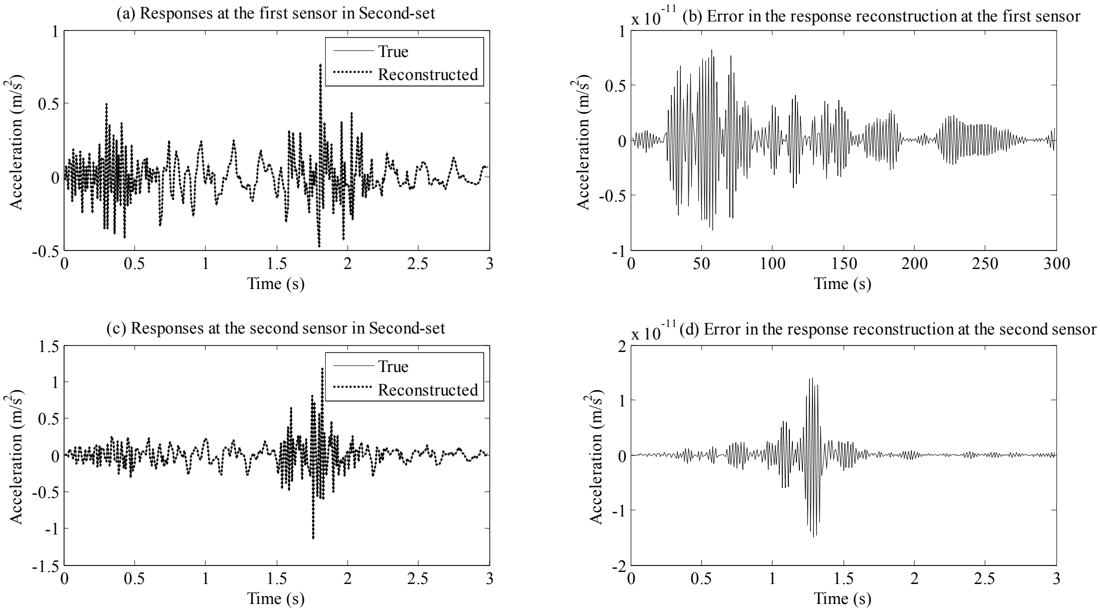

Figure 5.5: True and reconstructed responses in the Second-set response vector of Example 2

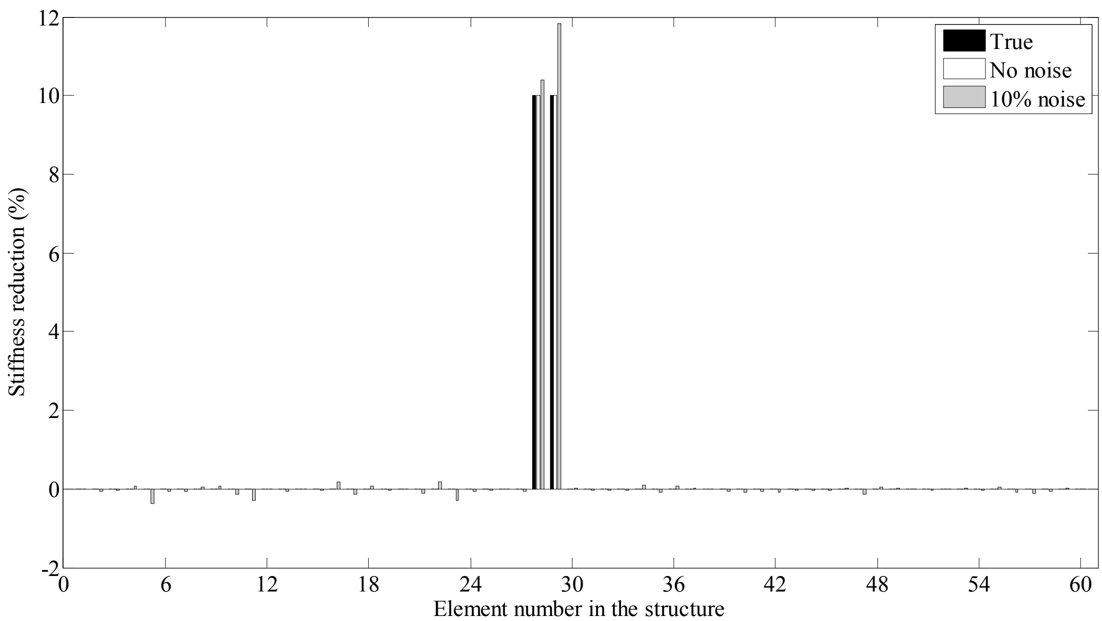

Figure 5.6: Damage identification results of Example 2

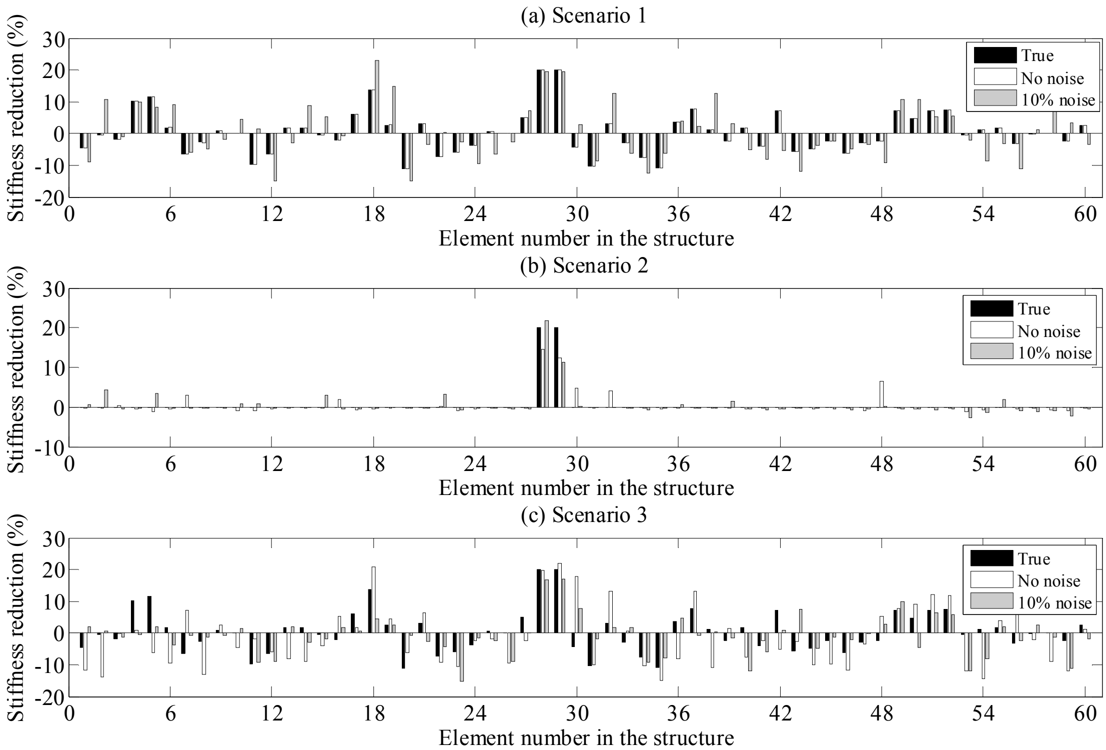

Figure 5.7: Damage identification results with initial model errors

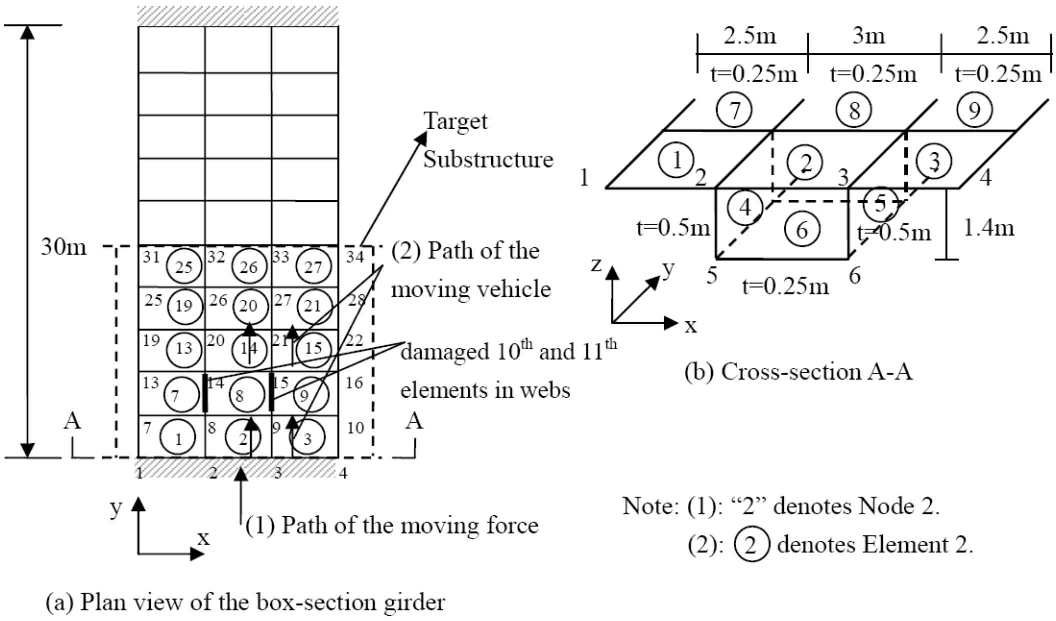

Figure 5.8: The numberings of the target substructure in the finite element model of the bridge

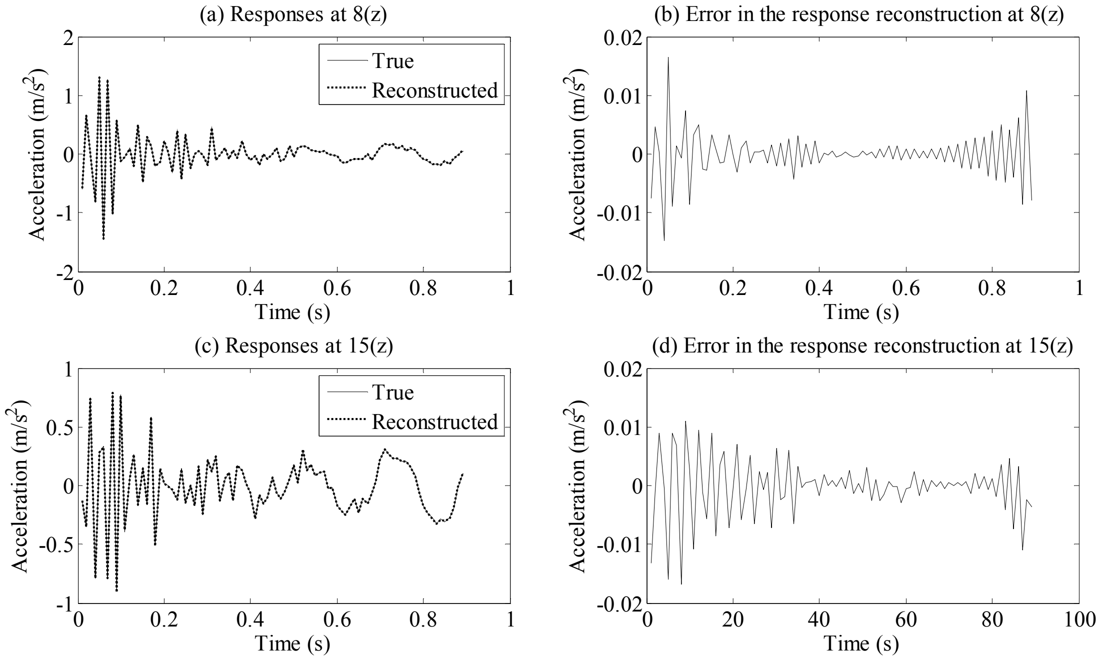

Figure 5.9: True and reconstructed responses in the Second-set response vector with SP1 sensor placement

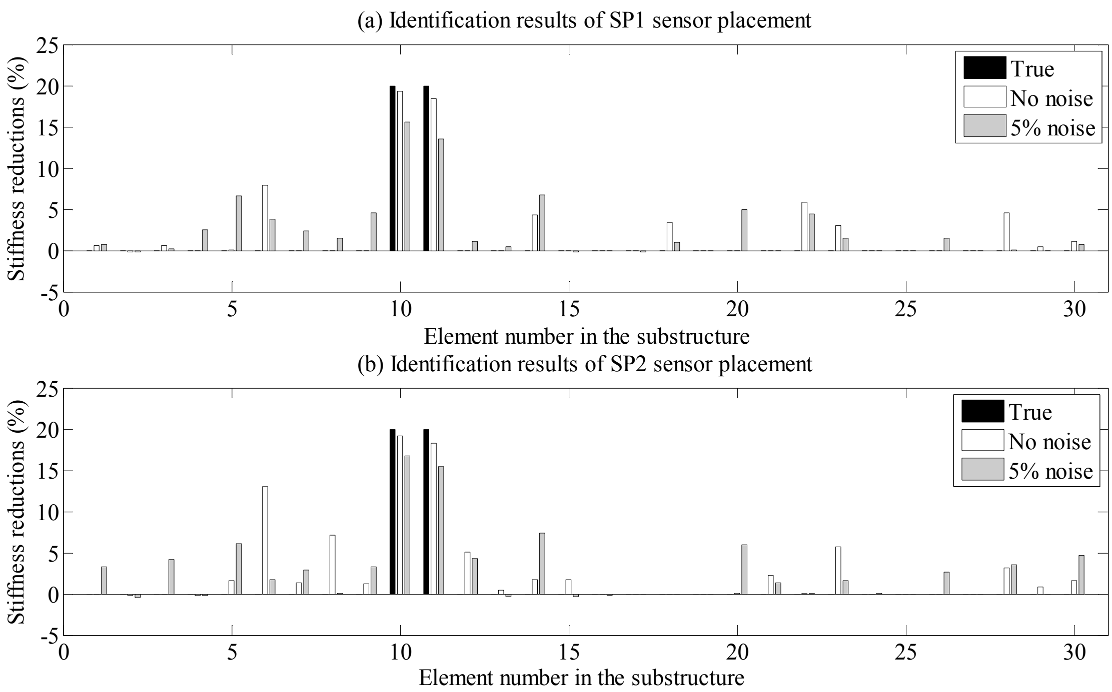

Figure 5.10: Damage identification results of Example 1

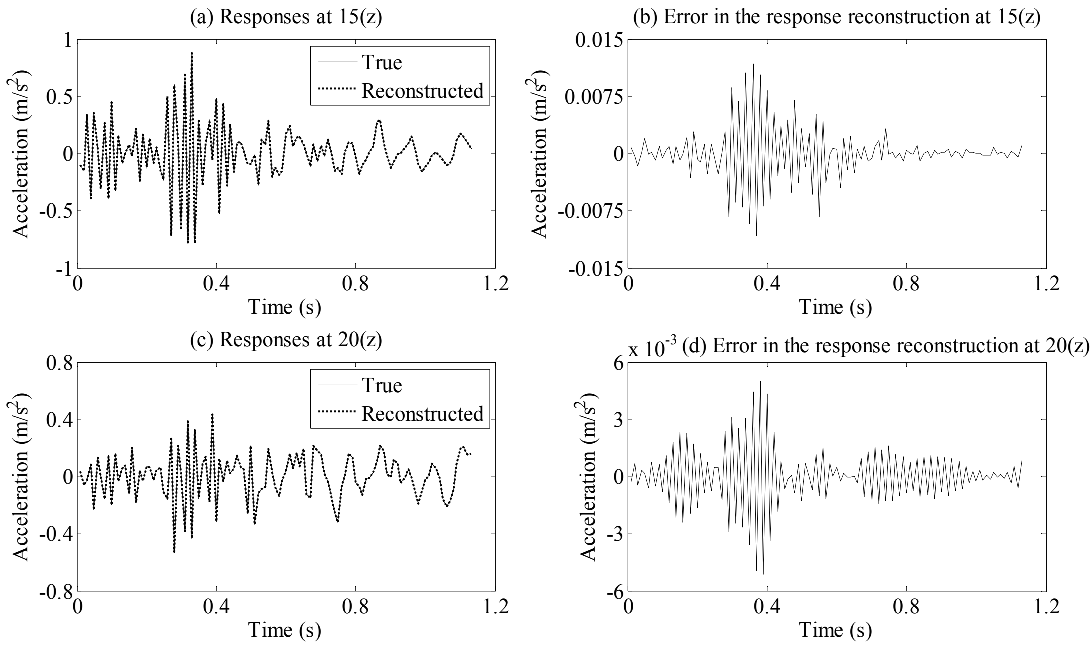

Figure 5.11: True and reconstructed responses in the Second-set response vector of Example 2

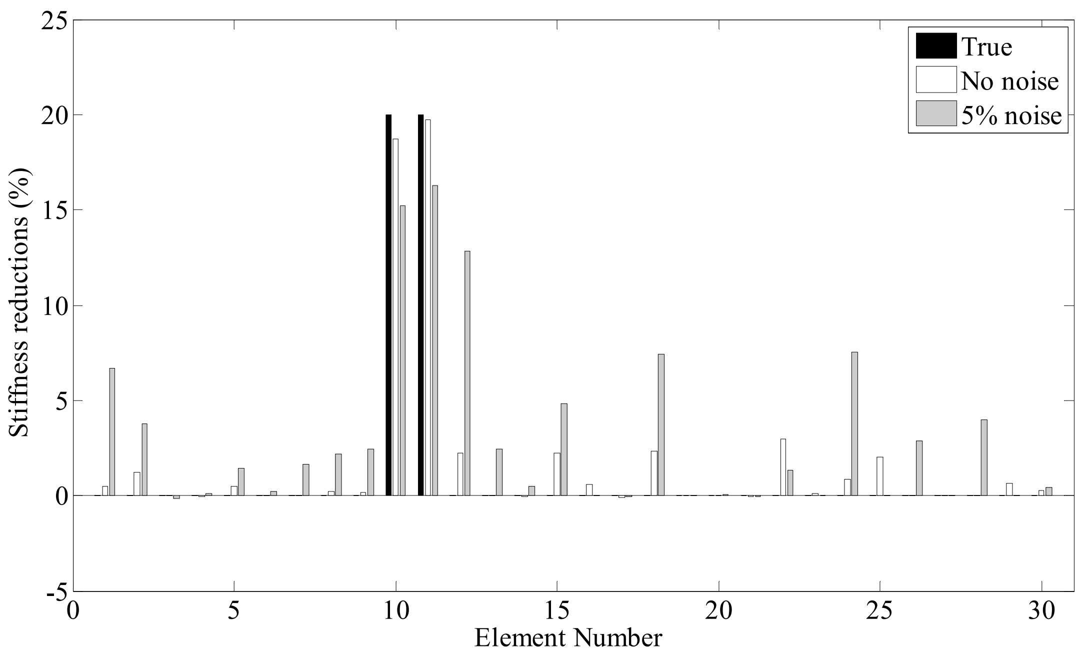

Figure 5.12: Damage identification results of Example 2

CHAPTER 6

EXPERIMENTAL VERIFICATION

6.1 Introduction and Experimental Setup

Structural dynamic response reconstruction techniques in both the frequency and wavelet domains are proposed in Chapter 3. The damage identification approach in a target substructure is formulated based on the response reconstruction in Chapter 4. Numerical studies demonstrated that the proposed substructural condition assessment approach both in the frequency and wavelet domains can identify the locations and extents of local structural damage effectively. Experimental studies will be conducted to investigate the correctness and effectiveness of the proposed response reconstruction techniques and substructural damage identification approach. A fabricated structure with model uncertainties and acceleration responses with environmental noise in the laboratory are used in this Chapter to verify the performance of response reconstruction and substructural damage identification approaches.

A seven-storey steel frame is designed and fabricated in the laboratory. The dimensions of the frame are shown in Figure 6.1. The column of the frame has a total height of 2.1m with 0.3m each storey. The length of the beam is 0.5m. The cross-sections of the column and beam elements are measured as $49.98\text{mm} \times 4.85\text{mm}$ and $49.89\text{mm} \times 8.92\text{mm}$, respectively. The measured mass densities of the column and beam elements are 7850kg/m^3 and 7734.2kg/m^3, respectively. The initial Young's modulus is taken as 210Gpa. The connections between column and beam elements are continuously welded at the bop and bottom of the beam section. Two pairs of mass blocks with each weight to 4kg approximately, are fixed at the quarter and three-quarter length of the beam in each storey to simulate the mass from the floor of a building structure. The general layout of the laboratory frame can be seen in Figure 6.2. Figure 6.3(a) shows a pair of steel blocks in more details. The two blocks are bolted to the top and bottom of the beam to have the centroid coincides with that of the beam section. They are bolted rather than welded onto the beam directly to make sure that the stiffness of beam will not be changed significantly with welding. The bottoms of two columns of the frame are welded onto a thick and solid steel plate that was fixed on the ground, as shown in Figure 6.3(b). The data recording computer and data acquisition board were grounded to reduce the disturbance of AC power effect on the measured signals.

B&K 3023 and KD 1010 accelerometers were used in the laboratory dynamic testing to measure the acceleration responses of the structure. B&K 3023 sensor is shown in Figure 6.4(a). Sensor signals are often incompatible with data acquisition hardware. To overcome this incompatibility, the sensor signal must be conditioned. Common ways to condition signals include amplification to increase the signal-noise ratio and filtering to remove the unwanted higher frequency components. B&K Type 2365 and Nexus conditioners are used in the test to amplify the raw signals, and they are shown in Figures 6.4(b) and 6.4(c). The measuring frequency range is set as 0.1 Hz ~ 1000Hz and the signal is low-pass filtered with cutoff frequency of 1000Hz. Hammer testing is usually used in the laboratory environment as it is an easy and economical way to produce the excitation to the structure. The SINOCERA LC-04A hammer with a rubber tip shown in Figure 6.4(d) was used in the test and its specifications are listed in Table 6.1. The rubber tip is used to produce a more uniform lower frequency content of the impact force than the steel and aluminum tips since civil structures normally exhibit low frequency responses. National Instruments (NI) data acquisition board and measurement system as shown in Figure 6.4(e) are used to record and save the signals. DEWESoft data acquisition software is employed to communicate with the NI acquisition board, such as debugging the set-up of sensors, displaying the recording signals, configuring the sampling rate and storing the measured data into the computer. Figure 6.5 shows the schematic layout of the data acquisition system.

Figure 6.6 shows the finite element model of the frame structure. It consists of

65 nodes and 70 planar frame elements. The weights of steel blocks are added at the corresponding nodes of the finite element model as concentrated masses. Each node has three DOFs (two translational displacements x, y and a rotational displacement θ), and the system has 195 DOFs in total. The weights and locations of each pair of steel blocks are shown in Table 6.2. The translational and rotational restraints at the supports, that are Nodes 1 and 65, are represented initially by a large stiffness of 3×10^9 N/m and 3×10^9 N·m/rad, respectively.

6.2 Initial Finite Element Model Updating

Finite element model updating in the undamaged state is conducted to minimize the discrepancies between the analytical finite element model and the experimental model in the laboratory. The model updating process in this study was conducted based on a two-stage procedure. In the first-round model updating, the elastic modulus of each element and stiffness values of restraints at the two supports are selected as parameters which are required to be updated. The dimensions and mass densities are measured in situ and they are not included as the updating parameters. Eight sensors are deployed in the hammer tests with one defined as the reference sensor and the others are placed at the joints between the columns and beams. This test is repeated to record the responses at all the beam-column joints with different layouts of sensors. Experimental modal analysis is performed to extract the natural frequencies and modal shapes of the frame structures from the measured acceleration responses. Natural frequencies are obtained by the peak-picking method and mode shapes are obtained by comparing the amplitude of Fourier spectrum of the dynamic response at a specific location with respect to that from the reference point. The first seven natural frequencies and mode shape values of the first seven modes at each joint point are obtained. The objective of the first-round model updating is to minimize the differences between the frequencies and mode shapes from the analytical finite element model and the experimental measurements. Optimization techniques, such as nonlinear least-square with Newton method based on modal sensitivities (Friswell 1995) was used here to achieve the first-round model updating. It should be noticed that 7 measured frequencies and 7×14 mode shape values are used in the updating and 70 elastic modulus values and 6 support stiffness values are required to be updated. The number of equations for updating is 105 and it is larger than the number of selected unknown parameters which is 76.

Based on the first-round updated results, the second-round model updating further refines the updated model by using the dynamic response sensitivity method (Lu and Law 2007b). The objective of the second-round model updating is to make the calculated dynamic responses from the finite element model match the measured ones as closely as possible. Measured responses from seven sensors of a hammer test with the impact at the right column of seventh floor are used in this model updating. These seven sensor locations are listed in Table 6.3. The differences between the measured time domain responses and analytical responses from the finite element model are minimized. Figure 6.7(a) shows the recorded dynamic response in time domain at Node 13(x) and Figure 6.7(b) is the Fourier spectrum with the response transformed in frequency domain. It can be seen from Figure 6.7(a) that the dynamic response costs more than 40 seconds to damp out close to zero indicating that the frame structure is very slightly damped with very low damping ratios. The Fourier spectrum shows that the frequency response after 40Hz is very small such that the raw response data is filtered using a low-pass filter with cutoff frequency at 36Hz to remove the higher frequency response and noise effect. Rayleigh damping is assumed in this study. The first two damping ratios of the intact frame structure are obtained from the half-power bandwidth method (Chopra 2007), and they are calculated as 0.0017 and 0.0012 for the first two modes, respectively. The elastic modulus of all the elements is selected in the second-round updating process. Response data in the first two seconds of these seven sensors are used in the model updating.

Table 6.4 shows the measured and analytical frequencies before and after model updating and Table 6.5 shows the MAC values before and after updating. It is found that the frequencies form the analytical finite element model after updating are very close to the measured ones and all the MAC values of the first seven modes almost equal to ones. Table 6.6 shows the updated stiffnesses of support at Nodes 1 and 65 of the frame structure. Figure 6.8 shows the first- and second-round updating results of young's modulus of all the elements in the finite element model. It is found that minor changes occurred in the second-round updating since the natural frequencies of the analytical finite element after the first-round updating are already very close to the measured frequencies and MAC values after the first-round updating are close to ones. Figure 6.9 shows the measured and calculated responses at Node 13(x) after the second-round updating. The relative error between these two responses is 2.31%. It is demonstrated that the updated model matches the experimental model well in the modal information and vibration responses. Then this updated finite element model is used as the baseline model in the following studies of dynamic response reconstruction and subsequent damage identification.

6.3 Dynamic Response Reconstruction in Intact Stage

6.3.1 Response Reconstruction in a Full Structure

Equations (3.9) and (3.52) are used to conduct the structural dynamic response reconstruction in the full structure from frequency and wavelet domain methods, respectively. Two sensor placement configurations are considered in this study and they are shown in Table 6.7. The sensor placement configuration SP1 includes 5 sensor locations in the First-set which is considered as the Known-set response vector, and 2 sensors in the Second-set which is taken as the Unknown-set response vector that is going to be predicted. The reconstructed responses of the Second-set from frequency and wavelet domain methods are then compared with their measured ones which are considered as the true responses. The excitation location of the hammer test is at the beam-column joint point in the right column of the seventh storey, and acceleration responses from the sensor locations are recorded. The sampling rate is 1000Hz and the measured responses are low-pass filtered with a cut-off frequency at 36Hz. The measured data within 16.384s are used for structural response reconstruction with the frequency domain method. Due to large sizes of matrices $\ddot{h}_k^{DWT}$ and $\ddot{h}_u^{DWT}$, only first two seconds data is considered for response reconstruction using the wavelet domain method.

It has been reported that the deconvolution technique for the reconstruction of force is very ill-posed and the results may be unstable (Jacquelin *et al*. 2003). It is also proved that those small singular values from singular value decomposition (SVD) would introduce large rounding errors in the inverse analysis and make it impossible to recover the force. The error in the deconvolution process will be amplified and propagates when the noisy measured responses and a structural system with model errors are used.

The Truncated SVD (TSVD) technique is used to stabilize the solution of pseudo-inverse (Hansen 1998). The tolerance value of the pseudo-inverse is set as 1.0×10^{-3} to eliminate the small singular values and their oscillating singular vectors in the SVD.

Figures 6.10 and 6.11 show the comparisons between the measured and reconstructed Second-set response vectors in the first two seconds from frequency and wavelet domain methods with SP1, respectively. The differences between the measured and reconstructed responses of the two sensors in the Second-set are small and the relative errors from frequency and wavelet domain methods are shown in Table 6.8. The system measurement noise, environmental noise due to ambient excitation sources and model errors in the finite element model would affect the accuracy of response reconstruction. It can be found that the errors from frequency domain method are less than 5% and are slightly larger than those from wavelet domain method.

6.3.1.1 Effect of Sampling Duration and Sampling Rate

The effect of sampling duration and sampling rate on the accuracy of response reconstruction is investigated. The sampling duration is selected to vary from 8.912s to 32.786s at a constant sampling rate of 1000Hz. In another study, the sampling rate varies from 250Hz to 1000Hz with a constant sampling duration of 16.384s. The sampling duration is however limited to 2s in the response reconstruction with the wavelet domain method. Table 6.9 lists the relative errors of the two sensors in the Second-set response of SP1 from both frequency and wavelet domain methods. It is noted that the frequency domain method gives a better accuracy when a longer sampling duration or a higher sampling rate is used. On the other hand, the accuracy of response reconstruction using the wavelet domain method is not obviously affected by the sampling rate, and it is slightly better than that from frequency domain method. These observations are consistent with results from numerical studies in Section 3.4.2.1.

6.3.1.2 Effect of Measured Responses in the First-set Response

SP2 sensor placement configuration in Table 6.7 consists of two sensors in the First-set and five sensors in the Second-set. The relative errors in the response reconstruction results from frequency and wavelet domain methods with different sampling duration and sampling rate are shown in Table 6.10. It can also be found that the longer sampling duration or higher sampling rate would contribute to a better accuracy. SP1 sensor placement with more measurements in the First-set gives slightly better response reconstruction results than SP2 sensor set.

6.3.2 Response Reconstruction in a Substructure

6.3.2.1 When the Finite Element Model of the Full structure is Available

When the finite element model of the full structure and the impact force are available, the interface forces of the substructure can be obtained by computation from the finite element analysis and Equations (3.16) and (3.57) are used to reconstruct the responses in the Second-set that are required to be predicted. Figure

6.12 shows the target substructure defined in this study. It includes the 4^{th} to 7^{th} storeys of the frame structure with 43 nodes and 46 elements. The hammer excitation location is at the same location as for last study, as shown in Figure 6.12. Eight sensors are placed in this target substructure and two sensor placement configurations are defined in this study, as shown in Table 6.11. The sensor placement configuration SP1 includes seven sensor locations in the First-set which is considered as the Known-set response vector, and one sensor in the Second-set which is taken as the Unknown-set response vector that is required to be predicted. The sampling rate is 1000Hz with a sampling duration of 16.384s for the frequency domain method. Only the response data in the first second is considered in the response reconstruction using wavelet domain method. The interface forces from the finite element analysis of the full structure model are obtained with ZOH and FOH force approximations, respectively. Figures 6.13 and 6.14 show the response reconstruction results in the Second-set response of SP1 from frequency domain method using interface forces with ZOH and FOH force approximations, respectively. The reconstructed responses with ZOH and FOH are close to those measured ones and the relative errors between the measured and reconstructed responses are 5.91% and 9.50%, respectively. Figure 6.15 shows the measured and reconstructed responses from the wavelet domain method. The reconstructed response almost overlaps with the measured one and the relative error is 8.12%.

Effect of Sampling Duration and Sampling Rate

The sampling duration is considered varying from 8.192s to 32.768s and the sampling rate varies from 250Hz to 1000Hz in this study. When the sampling duration varies, the sampling rate is kept constant at 1000Hz. When the sampling rate varies, the sampling duration is set as 16.384s. Table 6.12 lists the relative error of the reconstructed response in the Second-set response of SP1 with different sampling duration and sampling rate from frequency and wavelet domain methods. The relative errors in the response reconstruction using 16.384s and 32.768s data are very close, while the relative error using 8.192s data is larger since system damping ratios of the frame structure are very small and the structural response, as shown in Figure 6.7, needs far more than 8.192s to damp out close to zero for FFT analysis to eliminate the end effect.

In another study with different sampling rate from 250Hz to 1000Hz, the accuracies in the response reconstruction results using both the frequency and wavelet domain methods are not good and it should be noted that reconstruction with FOH force approximation with sampling rate 500Hz gives better results than that with ZOH. Figure 6.16(a), (b) and (c) show the sampled impact force at 1000Hz, 500Hz, 250Hz, respectively. The recorded impact forces at 500Hz and 250Hz may not represent accurately the original impact force, with a very short duration of the impact force within 0.006s, as shown in Figure 6.16(a), and the frequency range of the hammer force is 0~500Hz as indicated in Table 6.1. Therefore the sampling rate of hammer force with 500Hz and 250Hz is not high enough and the interface forces computed from the finite element analysis have a large error from using this inaccurate sampled hammer impact force. Therefore the response reconstruction from Equations (3.16) and (3.57) using the computed interface forces from the hammer impact forces is not good.

Effect of Number of Measured Responses

Sensor placement SP2 is used in this study. The relative errors in the response reconstruction with different sampling duration and sampling rate are listed in Table 6.13. It is found that SP1 with more measurements in the First-set gives better response reconstruction accuracies than SP2. Similar observations are made on the response results when the sampling rate is set as 250Hz and 500Hz. The accuracy in the response reconstruction results from response data with sampling rate 250Hz and 500Hz is not good since the hammer impact force is not sampled correctly. The reconstruction performs very well with the duration larger than 16.384s and sampling rate of 1000Hz for both the frequency and wavelet domain methods.

6.3.2.2 When the Finite Element Model of the Target Substructure is Available

Hammer Impact Force is Measured and Available

When only the finite element model of the substructure is available and the number of measurements in the First-set is equal or larger than the number of interface forces of the substructure, Equations (3.18) and (3.61) can be used to conduct the response reconstruction in the substructure from frequency and wavelet domain methods. It should be noticed that the external excitation on the substructure, such as the hammer impact force is available in the reconstruction from measurement. The target substructure in Figure 6.12 has six interface forces and therefore at least six measurements should be included in the First-set response vector. Recorded response data from six sensor locations at Node 10(x), 13(x), 19(x), 47(x), 50(x) and 53(x) are taken in the First-set response vector to predict the response at Node 16(x). The measured hammer impact force is used in the response reconstruction. The sampling rate is 1000Hz and sampled data within 16.384s are used and Figures 6.17(a) and (c) show the response reconstruction results from frequency and wavelet domain methods, respectively. It can be noted that the reconstructed response almost overlap with the measured one indicating the response reconstruction process is accurate. Figures 6.17(b) and (d) show the error vector between measured and reconstructed responses. Table 6.14 shows the relative errors in the response reconstruction results with different sampling duration and sampling rate. The accuracy with different sampling rate and sampling duration using frequency domain method is very similar. For the wavelet domain method, the response reconstruction with a higher sampling rate gives slightly better accuracy.

Hammer Impact Force is not Available

When only the finite element model of the target substructure is available and the hammer impact force is not measured, the response reconstruction can be conducted by taking both the external force and interface forces as unknown excitations to the substructure and the target substructure is considered as an independent structure. Then Equations (3.9) and (3.52) are used for the response reconstruction in the substructure. It should be noticed that the number of measured responses in the First-set should be larger than the sum of the external excitations and interface forces on the substructure in this case. In this study, there are one impact force and six interface forces on the substructure, and therefore at least seven sensors are required in the First-set that is considered as the Known-set response vector. A sensor placement configuration is adopted with seven measurements in the First-set at Node 10(x), 13(x), 19(x), 22(x), 47(x), 50(x) and 53(x), and one measurement in the Second-set at Node 16(x). The measured responses in the First-set response vector are used to reconstruct the response at the sensor location in the Second-set, and the reconstructed response is compared with the measured one. The sampling duration is 16.384s with the sampling rate 1000Hz. Measured and reconstructed responses in the Second-set by using the frequency and wavelet domain methods are shown in Figures 6.18(a) and (c), respectively. The error vectors in the response reconstruction results are shown in Figures 6.18(b) and (d). The effect of sampling rate and sampling duration is investigated and the relative errors between measured and reconstructed responses are shown in Table 6.15. Both frequency and wavelet domain methods give good response reconstruction accuracies at different sampling duration and rate. Frequency domain method gives very similar accuracy with different sampling rate and sampling duration, while wavelet domain methods provides better reconstruction with a higher sampling rate.

Use of IIRS to Reduce the Number of Interface Forces

The IIRS method is explored to be used for the model condensation of the substructure to reduce the number of interface forces and the required sensor number in the First-set response vector to conduct the response reconstruction. In this study, the rotational DOFs of the two interface nodes are taken as the slave DOFs which are going to be eliminated in the model condensation of the substructure and other remaining DOFs of the substructure are kept as the main DOFs. Then the number of interface forces is reduced to four. The hammer impact force is taken as the unknown force on the substructure in the response reconstruction since studies show that a sampling rate less than 500Hz would give inaccurate response reconstruction results. Therefore five measurements at Nodes 10(x), 13(x), 16(x), 19(x) and 22(x) are included in the First-set and other three measured responses at Nodes 47(x), 50(x) and 53(x) are considered as the unknown Second-set response vector that is required to be predicted. The reconstructed response is compared with the measured one which is taken as the true response. Equations (3.9) and (3.52) are used for the response reconstruction in the substructure. The same setting for frequency domain method with response data for a duration of 16.384s with 1000Hz sampling rate is used. The response data in the first second is considered for the wavelet domain method. Figures 6.19 and 6.20 show measured and reconstructed responses in the first second by using the frequency and wavelet domain methods, respectively. Both methods give good response reconstruction results. Table 6.16 lists the relative errors in the response reconstruction results in the first second with different sampling duration and sampling rate. Good response reconstruction accuracies are obtained with different sampling rate and sampling duration from the frequency domain method. The higher sampling rate gives better response reconstruction results from the wavelet domain method.

6.4 Damage Identification in Frequency Domain

The target substructure adopted in this section for damage identification and the numberings of element are shown in Figure 6.21. The length of each finite element in the frame structure is 100mm and the damage was introduced in the element as two cuts with width $b = 30mm$ and depth $d = 10mm$, as shown in Figure 6.22. Two damage scenarios, namely Scenario A with single damage and Scenario B with multi-damage, were considered and their locations are listed in Table 6.17. Figure 6.23 shows these two damage scenarios in the frame structure. The equivalent stiffness reduction in the damaged element can be approximately obtained from the displacement method in the finite element analysis (Zhu and Xu 2005; Bucciarelli 2009). The required force to produce a unit displacement at a specific DOF can be represented as the stiffness value. Then the analytical stiffness reduction in the damaged element is derived as 12.5% and it is considered as the theoretical damage extent in this study, which is taken as the true value. The excitation of the hammer force is applied at Node 44(x) of the frame structure, as shown in Figure 6.21. Hammer tests were conducted in these two damaged states and acceleration response data from the structure were recorded for substructural damage identification. The updated finite element model in the intact stage in Section 3.2 is defined as the baseline model and the stiffness reduction in a specific element can be identified as the change in the elemental stiffness factors with respect to the baseline model.

6.4.1 Damage Scenario A

The hammer impact force is in a very short duration with high frequency response range even up to 500Hz, thus it is very difficult to measure the impact force accurately especially with lower sampling rates as indicated from Figure 6.16. The accuracy in the response reconstruction results will be affected with the incorrectly sampled hammer force if the measured impact force will be used in the response reconstruction process. The comparison of Tables 6.14 and 6.15 shows that the response reconstruction with a lower sampling rate also gives good accuracy when the hammer impact force is also taken as the unknown force on the substructure. Thus the hammer impact force and the interface forces are treated as unknown excitations to the substructure in the response reconstruction and subsequent damage identification. Computation procedures in Sections 4.2.1.2 and 4.3.1.3 are used for conducting the damage identification with the frequency and wavelet domain methods, respectively, and Equations (3.9) and (3.52) are used for the response reconstruction in the substructure. Two sensor placement configurations listed in Table 6.18, denoted as SP1 and SP2, are defined in this study. The number of measurement in the First-set response vector of SP1 and SP2 is eight which is larger than the sum of the number of interface force and the number of hammer impact force. One sensor in the Second-set of SP1 is placed close to the damage location and two sensors in the Second-set of SP2 are deployed far away from the damaged element. This two sensor placement configurations are defined to investigate the performance of the proposed damage identification approach and how the sensor placement in the Second-set affect the identification results. The sampling duration is taken as 32.768s with the sampling rate 1000Hz. The first two natural frequencies of the frame structure are extracted from the Fourier spectrum of the measured responses as 2.537Hz and 7.656Hz, and the first two damping ratios are computed as 0.0019 and 0.0013 for the first two modes, respectively. Rayleigh damping is assumed in this study and the Rayleigh damping coefficients can be computed from the extracted first two natural frequencies and damping ratios from measurements. The measured responses in the both First- and Second-set are low-pass filtered with a cutoff frequency of 36Hz. The first second response data of the sensors in the Second-set are used for damage identification. The convergence tolerance is set as 1.0×10^{-3} which is larger that that for simulation since the measurement noise, environmental noise and model errors in the finite element model exist in the damage identification procedure.

Figure 6.24 shows the damage identification results for Scenario A with SP1 and SP2 sensor placement configurations. Table 6.19 lists the required iteration and error of convergence on the identification results. The identified stiffness reductions in the preset damaged 11th element of the substructure, are 11.42% and 13.37% with SP1 and SP2, respectively and these identified damage extents are close to the true value which is 12.5% indicating that the damage location and extent in the substructure can be identified effectively and accurately. It is found that SP1 gives better identification results with less false positives in the undamaged elements than SP2. Two large false positives appeared in the 58th and 60th elements in results from SP2 sensor set. It should be noticed that the damaged 11th element is in the left column of the 4th storey and 58th and 60th elements are in the right column of the 4th storey. Since the measurements in the Second-set of SP2 used for damage identification are far away from the damaged element and may not be sensitive to the damage, stiffness in the elements at the same level are wrongly identified as damaged and elements in both columns contribute to the storey stiffness of the frame structure. The identified values in the undamaged elements are converged to zeros as the reference value in the adaptive Tikhonov regularization technique is defined as zero. It should be noticed that around 30 minutes are required in an iteration of the identification procedure.

6.4.2 Damage Scenario B

Scenario B includes two identical local damages in the 5th and 11th elements of the frame structure. The sampling duration is 32.768s with the sampling rate 1000Hz. The first two natural frequencies of the damaged frame structure are extracted from the measured responses as 2.508Hz and 7.628Hz, and the first two damping ratios are obtained as 0.0024 and 0.0013 for the first two modes, respectively. Table 6.20 shows the sensor placement configuration for the damage identification of Scenario B. Eight sensors are included in the First-set response and two in the Second-set. The sensor locations of the Second-set response are not near the damage area. Response data in the first second are used for the damage identification. The number of identification equations is $2 \times 1000 = 2000$ and it is far larger than the number of unknown substructural stiffness parameters. Table 6.21 lists the information on convergence of Scenario B. Figure 6.25 shows the damage identification results of Scenario B and the identified values of stiffness reduction in the 5th and 11th elements are 8.08% and 14.18%, respectively. Few false positives exist in the identification results. It is demonstrated that the proposed substructural damage identification approach based on the response reconstruction from frequency domain method can identify the locations and extents of local damage in a target substructure efficiently.

6.4.3 Effect of Use of IIRS

The IIRS method is used for the model condensation of the substructure in order to reduce the number of interface forces as well as the required number of measurements in the First-set response vector. The computation time in the identification process would be reduced. The rotational DOFs of interface nodes 2 and 64 are defined as the slave DOFs of the substructure, and they are eliminated in the IIRS model condensation process. The number of interface forces of the substructure is reduced to four. Same measured response data from the two damage states as for last study are used for damage identification to validate the possible use of IIRS in the substructural damage identification. Sensor placement configurations for Scenarios A and B are shown in Table 6.22. Six and two sensors are defined in the First- and Second-set of Scenario A, respectively. Figure 6.26 shows the damage identification results of Scenario A when IIRS is used. It is demonstrated that the location of the damage is identified correctly and the identified extent is 6.83% in the 11th element while the true value is 12.5%. A comparison between the damage identification results with SP2 in Figure 6.24 and Figure 6.26 shows that the identified extent in the damaged element in Figure 6.24 is closer to the true value than the identified value in Figure 6.26. Since the sensors in the Second-set of SP2 are far away from the damaged element, some false positives are wrongly identified in the same storey. When the IIRS is used to eliminate the rotational interface DOFs, the required sensor in the First-set can be reduced. On the other hand, the adaptive Tikhonov regularization technique could make those small false positives converge to zero, as shown in Figure 6.26.

For the Scenario B, seven and two sensors are used in the First- and Second-set, respectively. The identification results are shown in Figure 6.27 and the identified damage extents in the 5th and 11th elements are 15.78% and 6.81%. A comparison of Figure 6.27 and Figure 6.25 indicates that large false identification results exist in the 8th and 29th elements due to the error introduced with the use of IIRS. Therefore it may be concluded that it is possible to use the IIRS scheme to reduce the number of the interface DOFs and the required sensor measurements in the First-set response vector. However, the damage identification would be affected by the additional error due to the use of IIRS.

6.5 Damage Identification in Wavelet Domain

The same target substructure, damage scenarios (Scenario A and Scenario B), measured response data and sensor placement settings in Tables 6.18 and 6.20 are used to validate the effectiveness of the wavelet domain method. The updated finite element model in the intact stage is used as the baseline model and the local damage in a specific element is identified as the stiffness changes with respect to the baseline model. The sampling rate is 1000Hz and the number of response data within the first 0.4s equals to 400. The response data in the first 0.4s of the sensors in the Second-set are used for damage identification to avoid large matrix of $\ddot{h}_k^{DWT}$ in the computation of pseudo-inverse. The convergence tolerance in the damage identification algorithm is set as 1.0×10^{-3}.

6.5.1 Damage Scenario A

Figure 6.28 shows the identification results with SP1 and SP2 sensor placement configurations using wavelet domain method. The location of the damaged element can be detected clearly in the 11th element from both two sensor placements and the identified extents are 10.67% and 5.99% from SP1 and SP2, respectively. SP1 gives better and more accurate identification results and it is observed that more false positives exist in the results with SP2 because the sensors in the Second-set of SP2 are further away from the damaged element. Table 6.23 shows the convergence information of Scenario A. It is found that less number of iterations is required with SP1 for convergence as the sensor locations in the Second-set of SP1 are much closer to the damaged element.

6.5.2 Damage Scenario B

The same sensor placement in Table 6.20 is used for damage identification. Figure 6.29 shows the identification results and Table 6.24 lists the information of convergence. The identified extents of local damages in the 5^{th} and 11^{th} element are 6.97% and 7.74% respectively and several large false positives in the identification results are located in the 60^{th} and 63^{rd} elements. It should be noticed that the 63^{rd} element is in the 2^{nd} storey of the right column. A comparison of Figures 6.25 and 6.29 shows that the frequency domain method gives better identified local damage with less false positives.

6.5.3 Effect of Use of IIRS

The same measured response data from these two damaged states and sensor placement configurations in Table 6.22 are used for the damage identification. Figure 6.30 shows the identification results for Scenario A from wavelet domain method. The identified damage extent in the 11^{th} element is 6.48% and it is smaller than the true value 12.5%. The identification results of Scenario B are shown in Figure 6.31 and the damage extent in the 11^{th} element is 8% while the damage extent in the 5^{th} is 1%, which is quite different from the true damage extents of 12.5%. This indicates that the use of IIRS affects the identification accuracy from using wavelet domain method obviously for the Scenario B with multi-damages.

6.6 Summary

Experimental studies are conducted to verify the proposed dynamic response reconstruction techniques in both frequency and wavelet domains in Chapter 3 and the substructural damage identification approach in Chapter 4. A seven-storey steel frame is fabricated in the laboratory and measured acceleration response data from hammer tests are used for the initial finite element model updating. The updated finite element model is considered as the baseline model and measured response data from hammer tests with the damaged frame structure are used for the damage identification. Very good accuracy of response reconstruction in the full structure and in a substructure can be achieved.

Studies on the damage identification validate the proposed dynamic substructural damage identification approach, and the local damages in the substructure are identified effectively. The locations of the damage are detected accurately and the stiffness reductions in the damaged elements of the target substructure are identified close to the theoretical values in most of the sudies. The IIRS model condensation may not be required if a sufficient number of sensors is provided for damage identification of the frame structure as the number of interface DOFs is not large. It is further validated that it is possible to use the IIRS for the model condensation of the target substructure and to reduce the required sensor number in the First-set response vector for substructural damage identification. However, the identification results may be affected by the use of IIRS as additional error is introduced in the response reconstruction and the subsequent identification algorithm.

Table 6.1: Specifications of the force hammer

Sensitivity (pC/N)	4.19
Maximum shock force (KN)	60
Frequency range	0 ~ 500Hz

Table 6.2: Weights of each pair of steel blocks

Storey	Node number	Weight (Kg)	Node number	Weight (Kg)
1	23	3.9456	25	3.9631
2	26	3.9231	28	3.9199
3	29	3.9568	31	3.9350
4	32	3.9247	34	3.9372
5	35	3.9476	37	3.9772
6	38	3.9682	40	3.9687
7	41	3.9571	43	3.9321

Table 6.3: Sensor locations of a hammer test in the model updating

Sensor number	Sensor location
1	Node 19(x)
2	Node 16(x)
3	Node 13(x)
4	Node 10(x)
5	Node 7(x)
6	Node 4(x)
7	Node 59(x)

Table 6.4: Measured and updated frequencies

Modes	measured	before updating		after first-round updating		after second-round updating	
		Analytical	error (%)	Analytical	error (%)	Analytical	error (%)
1	2.5406	2.5198	0.82	2.5433	0.11	2.5438	0.13
2	7.6599	7.5829	1.01	7.6651	0.07	7.6546	0.07
3	12.8632	12.6614	1.57	12.8987	0.28	12.8714	0.06
4	18.0283	17.6255	2.23	18.0290	0.004	18.0349	0.03
5	22.9645	22.2655	3.04	22.9141	0.22	22.9835	0.08
6	26.9852	26.1468	3.11	26.9849	0.001	27.0449	0.22
7	29.9072	28.7959	3.72	29.9192	0.04	30.0000	0.31

Table 6.5: MAC Values before and after updating

Modes	before updating	after first round updating	after second round updating
1	0.9998	0.9999	0.9999
2	0.9998	0.9997	0.9997
3	0.9997	0.9998	0.9998
4	0.9991	0.9988	0.9991
5	0.9998	0.9999	0.9998
6	0.9995	0.9998	0.9996
7	0.9995	0.9998	0.9996

Table 6.6: Updated stiffness at the supports

	Degree-of-Freedom	Support stiffness (unit)
Node 1	x	3.1753e9 N/m
	y	3.1766e9 N/m
	θ	3.1570e9 N·m/rad
Node 65	x	2.8843e9 N/m
	y	2.8670e9 N/m
	θ	2.2410e9 N·m/rad

Table 6.7: Sensor placement configurations

Sensor Placement Configuration		Sensor locations
SP1	First-set	Node 4(x), 7(x), 16(x), 19(x), 59(x)
	Second-set	Node 10(x) 13(x)
SP2	First-set	Node 10(x) 13(x)
	Second-set	Node 4(x), 7(x), 16(x), 19(x), 59(x)

Table 6.8: Relative errors in the response reconstruction from SP1

Sensor location	Relative error (%)	
	Frequency domain method	Wavelet domain method
Node 10(x)	3.46	2.22
Node 13(x)	4.81	2.59

Table 6.9: Relative errors (%) in the response reconstruction with different sampling duration and sampling rate from SP1

	Second-set Sensor Location	Sampling Duration (s) (Sampling Rate = 1000 Hz)			Sampling Rate (Hz) (Sampling Duration = 16.384s)		
Frequency domain method		8.192	16.384	32.768	250	500	1000
	10(x)	5.86	3.46	2.78	3.45	3.46	3.46
	13(x)	5.80	4.81	3.19	4.88	4.83	4.81
		Sampling Duration = 2.0 s			Sampling Rate (Hz) (Sampling Duration = 2.0 s)		
Wavelet domain method		1000Hz			250	500	1000
	10(x)	2.22			2.67	2.22	2.22
	13(x)	2.59			3.15	2.59	2.59

Table 6.10: Relative errors (%) in the response reconstruction with different sampling duration and sampling rate from SP2

	Second-set Sensor Location	Sampling Duration (s) (Sampling Rate = 1000 Hz)			Sampling Rate (Hz) (Sampling Duration = 16.384s)		
Frequency domain method		8.192	16.384	32.768	250	500	1000
	4(x)	6.43	2.46	1.33	2.47	2.46	2.46
	7(x)	8.66	5.44	5.05	5.48	5.45	5.44
	16(x)	8.96	5.78	4.37	5.94	5.83	5.78
	19(x)	11.45	9.21	6.26	9.26	9.22	9.21
	59(x)	7.43	3.21	2.58	3.28	3.23	3.21
		Sampling Duration = 2.0 s			Sampling Rate (Hz) (Sampling Duration = 2.0 s)		
Wavelet domain method		1000Hz			250	500	1000
	4(x)	1.05			1.81	1.05	1.05
	7(x)	4.93			5.16	4.92	4.93
	16(x)	3.36			4.47	3.32	3.36
	19(x)	5.60			7.17	5.20	5.60
	59(x)	2.34			2.98	2.33	2.34

Table 6.11: Sensor placement configurations

Sensor placement configuration		Sensor locations
SP1	First-set	Node 10(x), 13(x), 16(x), 19(x), 22(x), 47(x), 50(x)
	Second-set	Node 53(x)
SP2	First-set	Node 10(x), 16(x), 22(x), 47(x)
	Second-set	Node 53(x), 13(x), 19(x), 50(x)

Table 6.12: Relative errors (%) in the response reconstruction in the first second with SP1

	Second-set Sensor Location		Sampling Duration (s) (Sampling Rate = 1000 Hz)			Sampling Rate (Hz) (Sampling Duration =16.384s)		
Frequency domain method			8.192	16.384	32.768	250	500	1000
	ZOH	53(x)	17.93	5.91	5.64	68.14	22.53	5.91
	FOH	53(x)	20.24	9.50	9.28	42.57	9.88	9.50
			Sampling Duration = 1.0 s			Sampling Rate (Hz) (Sampling Duration = 1.0 s)		
Wavelet domain method			1000Hz			250	500	1000
	53(x)		8.12			69.31	27.68	8.12

Table 6.13: Relative errors (%) in the response reconstruction in the first second with SP2

		Second-set Sensor Location	Sampling Duration (s) (Sampling Rate = 1000 Hz)			Sampling Rate (Hz) (Sampling Duration =16.384s)		
			8.192	16.384	32.768	250	500	1000
Frequency domain method	ZOH	53(x)	21.95	7.43	6.66	77.08	27.03	7.43
		13(x)	21.65	8.66	8.12	77.30	27.84	8.66
		19(x)	22.23	9.33	8.98	81.53	36.55	9.33
		50(x)	14.42	8.74	8.14	63.27	33.78	8.74
	FOH	53(x)	24.34	10.57	10.02	46.94	11.05	10.57
		13(x)	23.77	11.00	10.58	47.90	11.56	11.00
		19(x)	23.95	11.69	11.89	45.59	12.37	11.69
		50(x)	16.44	10.41	10.21	34.77	10.96	10.41
			Sampling Duration = 1.0 s			Sampling Rate (Hz) (Sampling Duration = 1.0 s)		
			1000Hz			250	500	1000
Wavelet domain method		53(x)	10.14			76.34	32.15	10.14
		13(x)	11.41			76.28	32.81	11.41
		19(x)	12.09			70.49	33.41	12.09
		50(x)	11.40			42.78	32.90	11.40

Table 6.14: Relative errors (%) in the response reconstruction in the first second

	Second-set Sensor Location	Sampling Duration (s) (Sampling Rate = 1000 Hz)			Sampling Rate (Hz) (Sampling Duration = 16.384s)		
Frequency domain method		8.192	16.384	32.768	250	500	1000
	16(x)	2.69	2.56	2.56	2.57	2.56	2.56
		Sampling Duration = 1.0 s			Sampling Rate (Hz) (Sampling Duration = 1.0 s)		
Wavelet domain method		1000Hz			250	500	1000
	16(x)	3.53			9.30	4.57	3.53

Table 6.15: Relative errors (%) in the response reconstruction in the first second

	Second-set Sensor Location	Sampling Duration (s) (Sampling Rate = 1000 Hz)			Sampling Rate (Hz) (Sampling Duration = 16.384s)		
Frequency domain method		8.192	16.384	32.768	250	500	1000
	16(x)	2.67	2.56	2.54	2.55	2.55	2.56
		Sampling Duration = 1.0 s			Sampling Rate (Hz) (Sampling Duration = 1.0 s)		
Wavelet domain method		1000Hz			250	500	1000
	16(x)	2.58			3.88	2.95	2.58

Table 6.16: Relative errors (%) in the response reconstruction in the first second

	Second-set Sensor Location	Sampling Duration (s) (Sampling Rate = 1000 Hz)			Sampling Rate (Hz) (Sampling Duration = 16.384s)		
Frequency domain method		8.192	16.384	32.768	250	500	1000
	47(x)	4.29	4.64	3.93	4.68	4.66	4.64
	50(x)	1.66	1.32	1.42	1.32	1.32	1.32
	53(x)	3.89	4.00	3.78	3.94	3.99	4.00
		Sampling Duration = 1.0 s			Sampling Rate (Hz) (Sampling Duration = 1.0 s)		
Wavelet domain method		1000Hz			250	500	1000
	47(x)	8.65			11.72	9.20	8.65
	50(x)	5.87			10.13	6.70	5.87
	53(x)	7.89			12.44	7.95	7.89

Table 6.17: Damage scenarios in the experimental testing

Damage scenario	Damaged element in the substructure
Scenario A: Single damage	11^{th} element
Scenario B: Multi-damage	5^{th} and 11^{th} element

Table 6.18: Sensor placement configurations of Scenario A

Sensor placement configuration		Sensor locations
SP1	First-set	Node 4(x), 7(x), 9(x), 17(x), 47(x), 50(x), 53(x), 56(x)
	Second-set	Node 11(x)
SP2	First-set	Node 4(x), 7(x), 9(x), 11(x), 17(x), 47(x), 53(x), 56(x)
	Second-set	Node 15(x), 50(x)

Table 6.19: Information on convergence of Scenario A

	SP1	SP2
Required iterations	5	5
Error of convergence	9.2×10^{-4}	8.7×10^{-4}

Table 6.20: Sensor placement configurations of Scenario B

Sensor placement configuration	Sensor locations
First-set	Node 4(x), 5(x), 11(x), 14(x), 19(x), 53(x), 56(x), 59(x)
Second-set	Node 9(x), 50(x)

Table 6.21: Information on convergence of Scenario B

Required iterations	7
Error of convergence	7.9×10^{-4}

Table 6.22: Sensor placement configurations when the IIRS is used

Sensor placement configuration		Sensor locations
Scenario A	First-set	Node 4(x), 7(x), 9(x), 11(x), 53(x), 56(x)
	Second-set	Node 15(x), 50(x)
Scenario B	First-set	Node 5(x), 14(x), 19(x), 50(x), 53(x), 56(x), 59(x)
	Second-set	Node 9(x), 11(x)

Table 6.23: Information on convergence of Scenario A

	SP1	SP2
Required iterations	6	8
Error of convergence	7.3×10^{-4}	8.5×10^{-4}

Table 6.24: Information on convergence of Scenario B

Required iterations	7
Error of convergence	9.5×10^{-4}

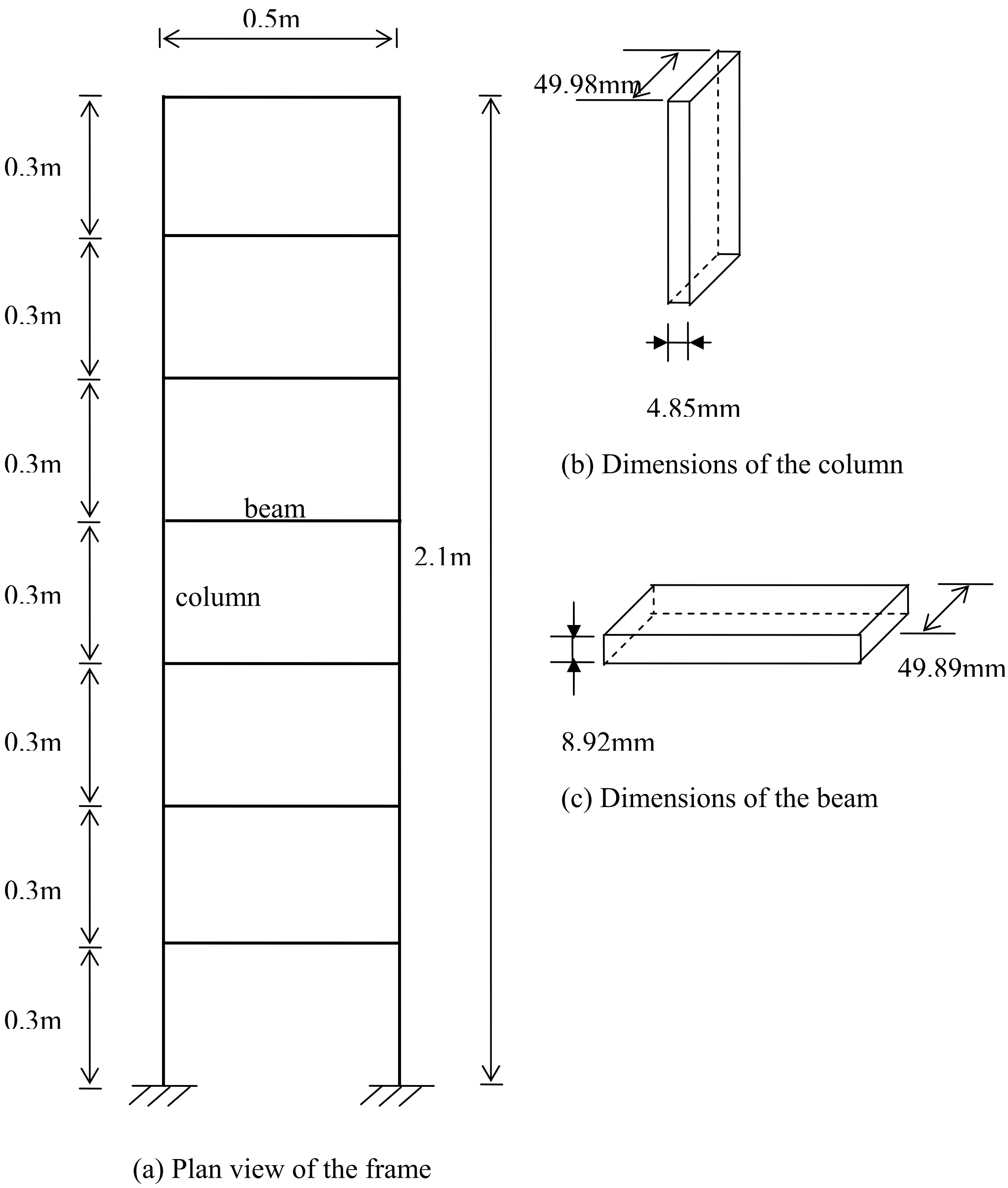

Figure 6.1: Dimensions of the steel frame

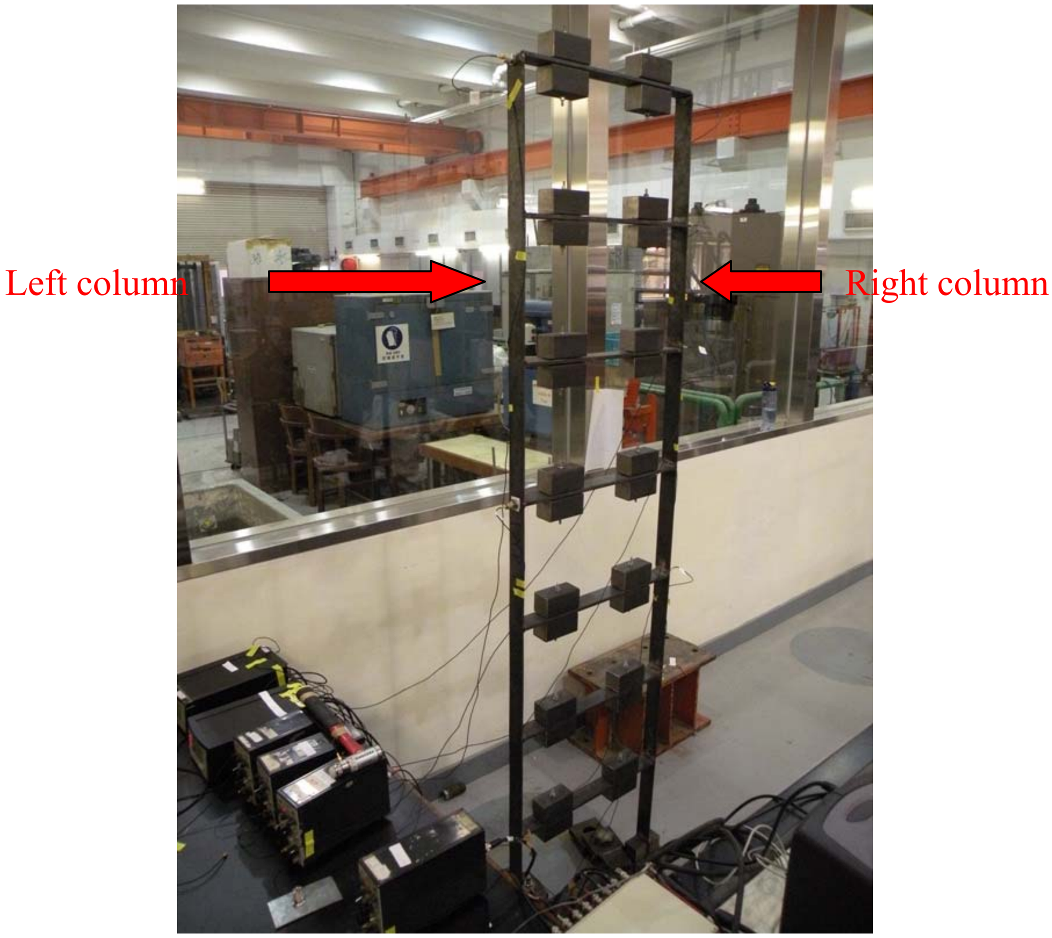

Figure 6.2: The laboratory steel frame model

(a) A pair of mass blocks

(b) Support of the frame structure

Figure 6.3: Steel mass blocks and support of the frame

(a) B&K 3023 accelerometer

(b) B&K 2365 conditioner

(c) B&K Nexus conditioner

(d) hammer

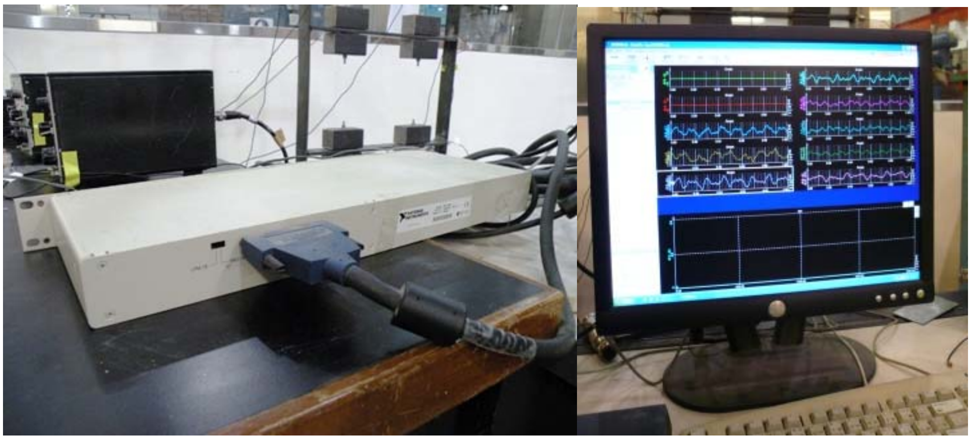

(e) NI data acquisition board and recording computer

Figure 6.4: Experimental instruments

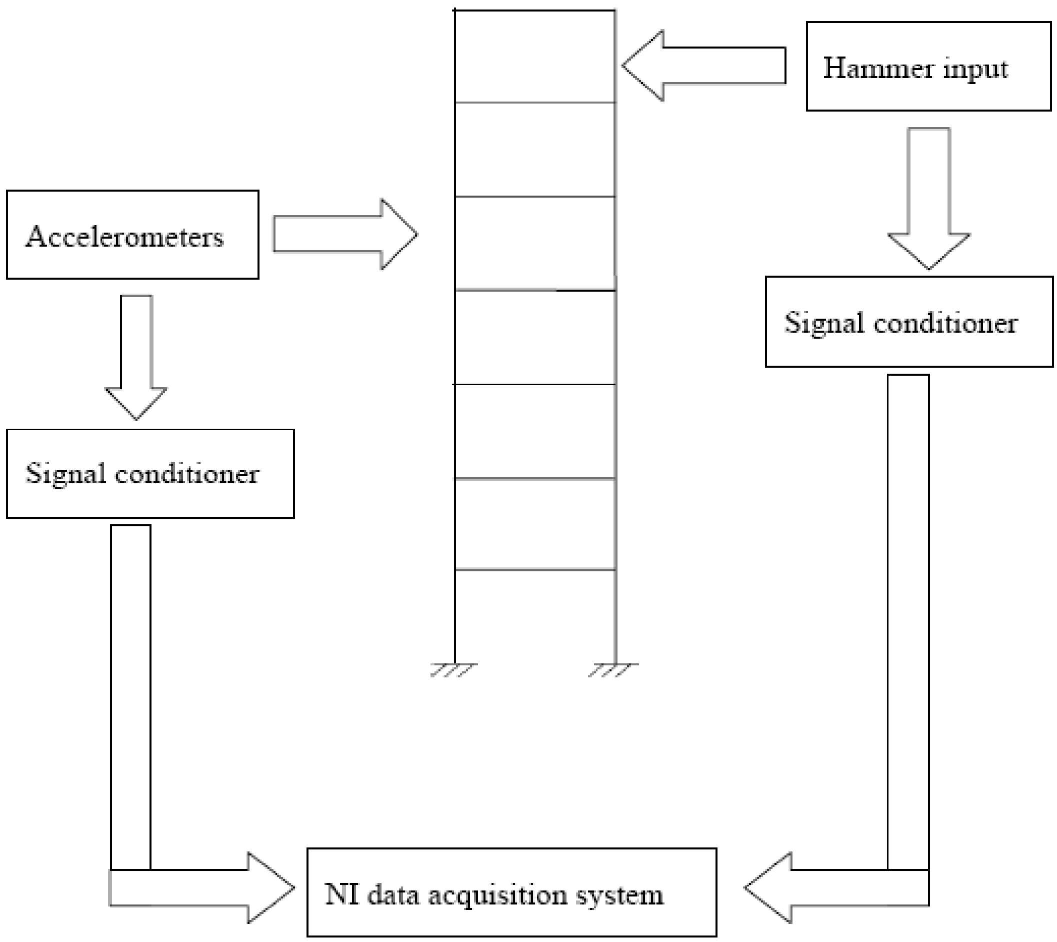

Figure 6.5: Layout of data acquisition system

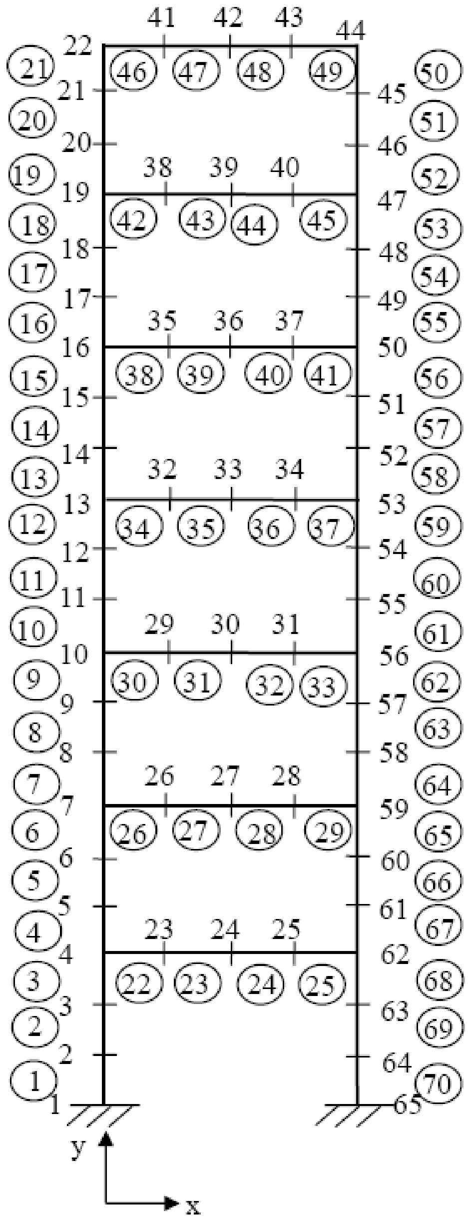

Note: (1): 1 denotes the node number

(2): (1) denotes the element number in the structure

Figure 6.6: Finite element model of the planar frame structure

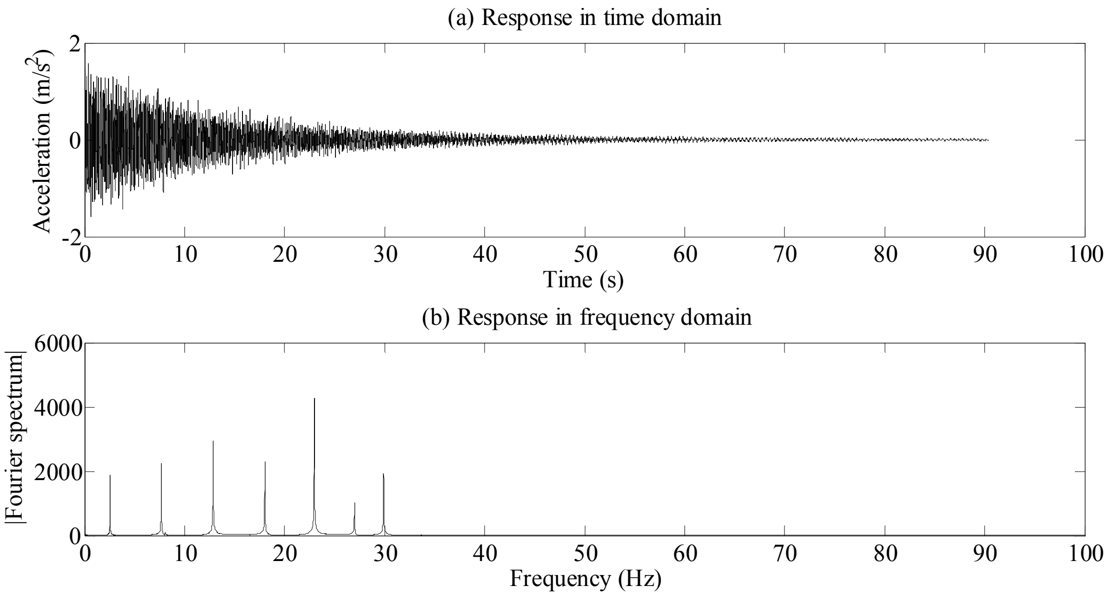

Figure 6.7: Dynamic responses at the Node 13(x)

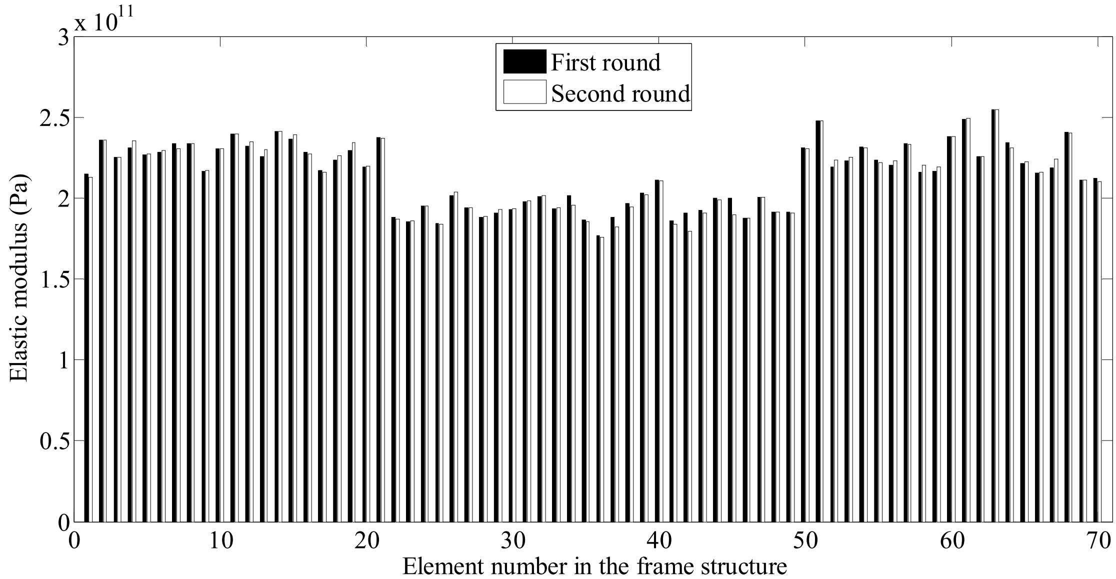

Figure 6.8: Model updating results of the first and second round

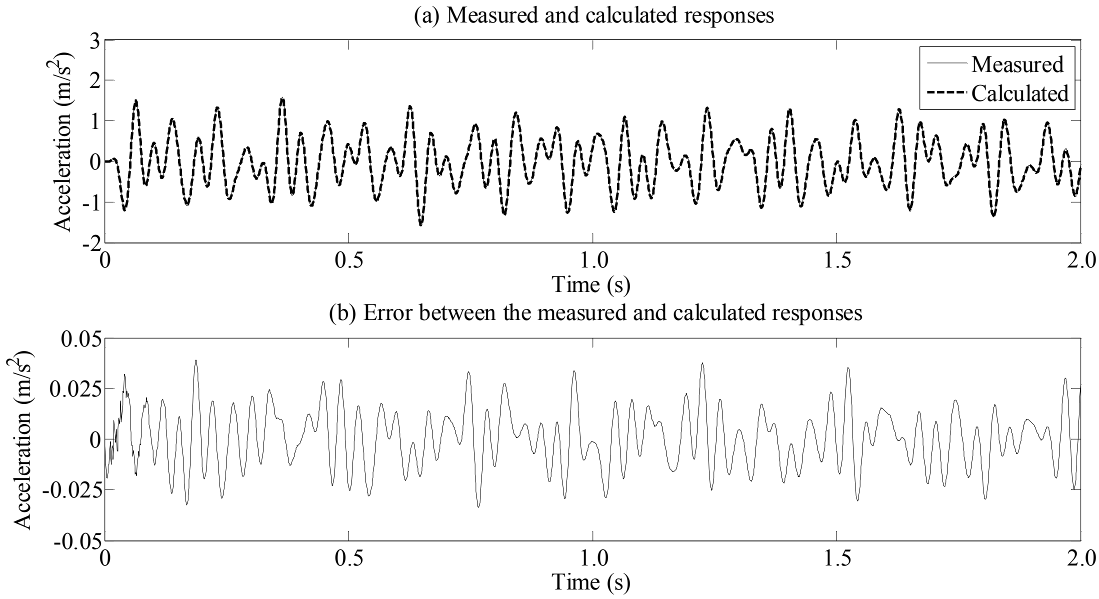

Figure 6.9: Measured response and calculated response after updating at Node 13(x)

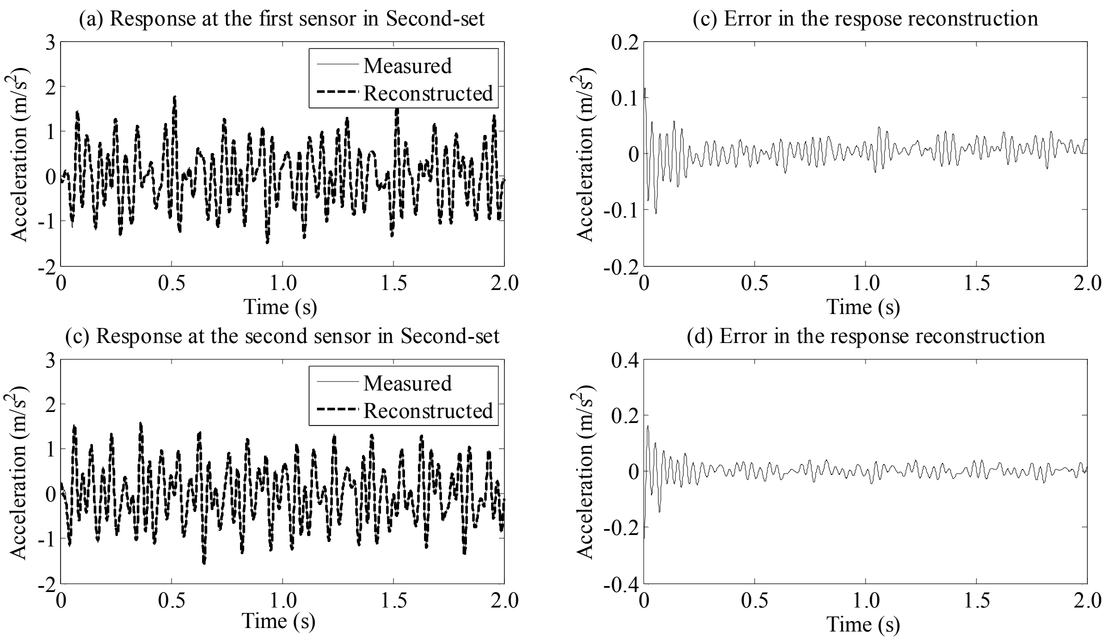

Figure 6.10: Measured and reconstructed responses in the Second-set response vector of SP1 from frequency domain method

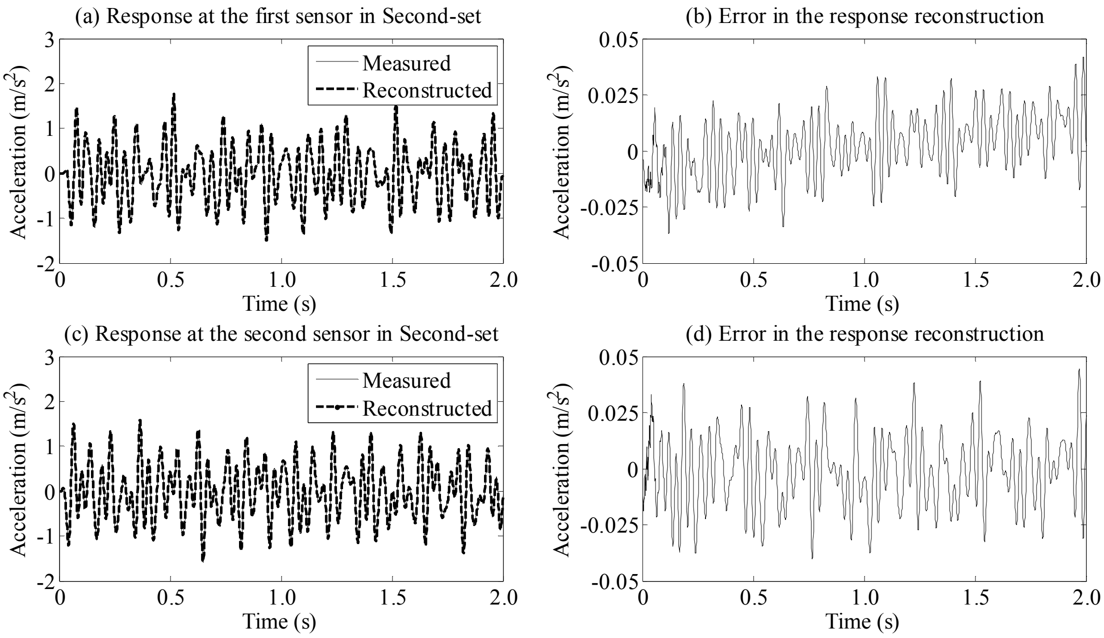

Figure 6.11: Measured and reconstructed responses in the Second-set response vector of SP1 from wavelet domain method

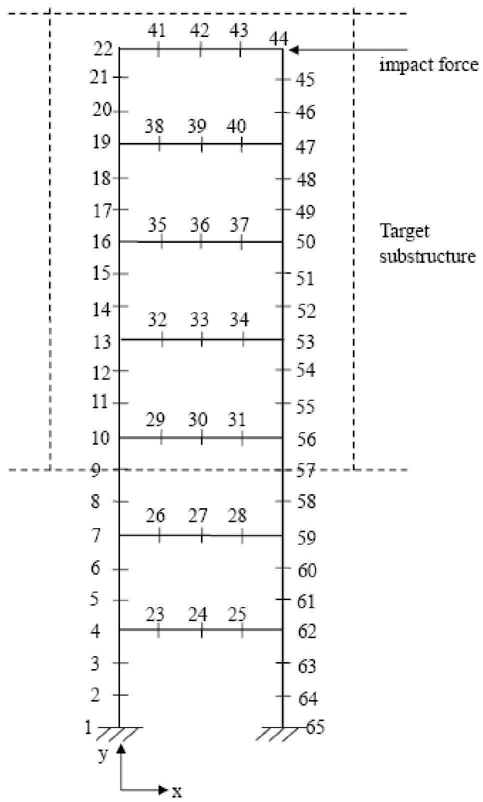

Figure 6.12: The target substructure

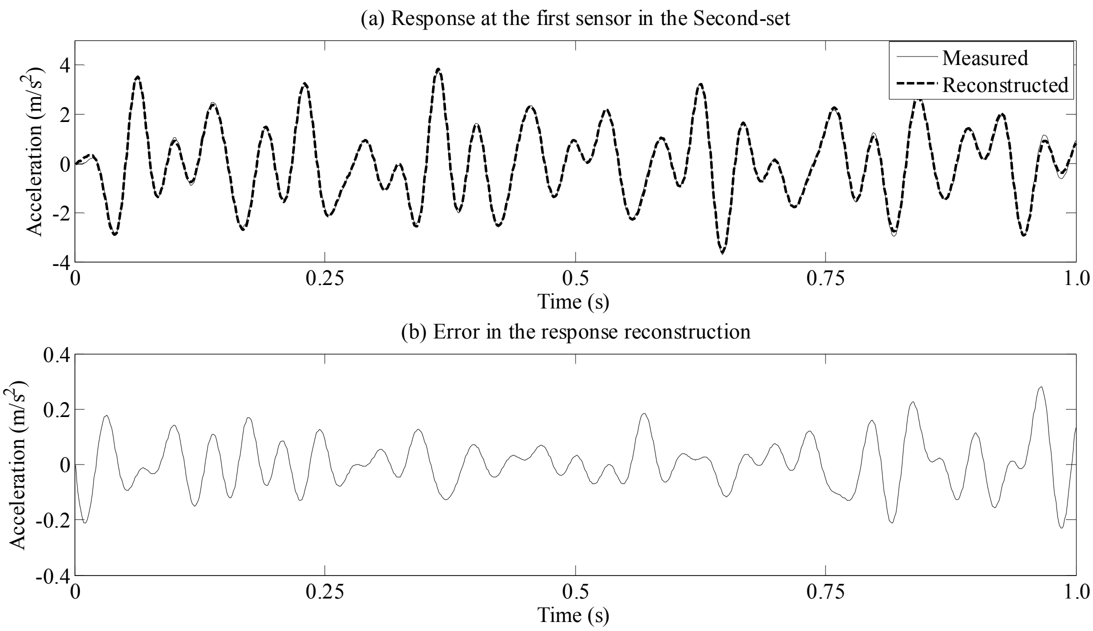

Figure 6.13: Measured and reconstructed responses in the Second-set response from frequency domain method with ZOH

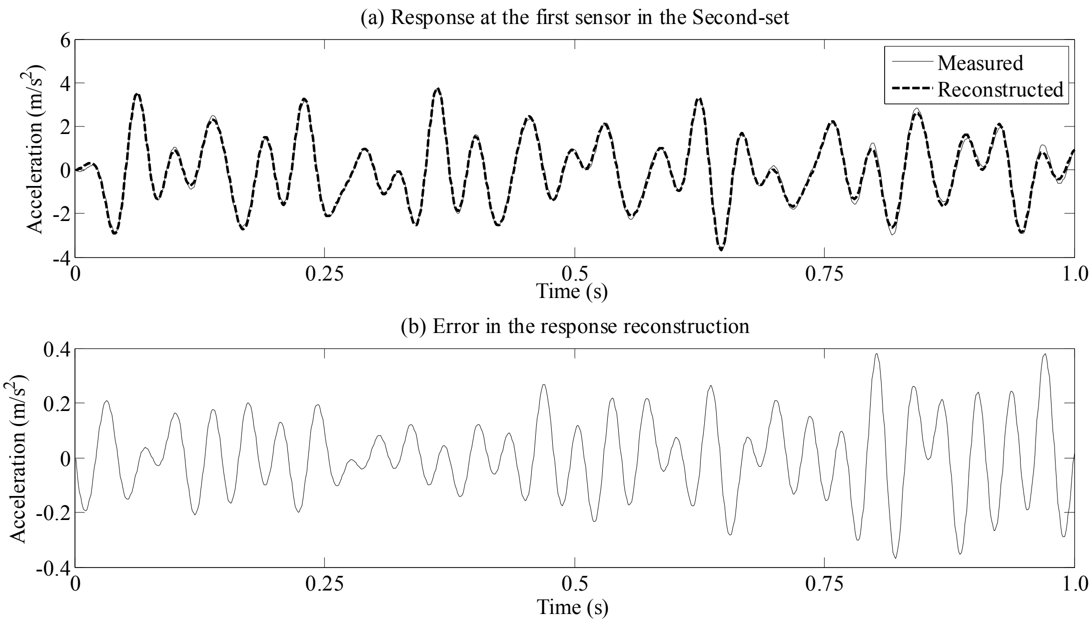

Figure 6.14: Measured and reconstructed responses in the Second-set response from frequency domain method with FOH

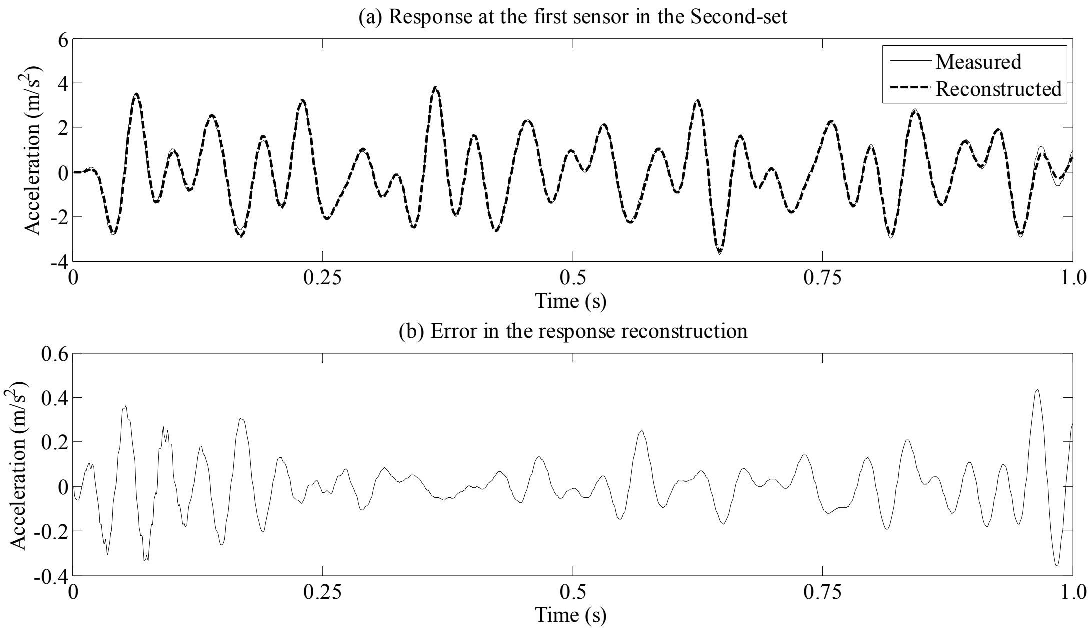

Figure 6.15: Measured and reconstructed responses in the Second-set response from wavelet domain method

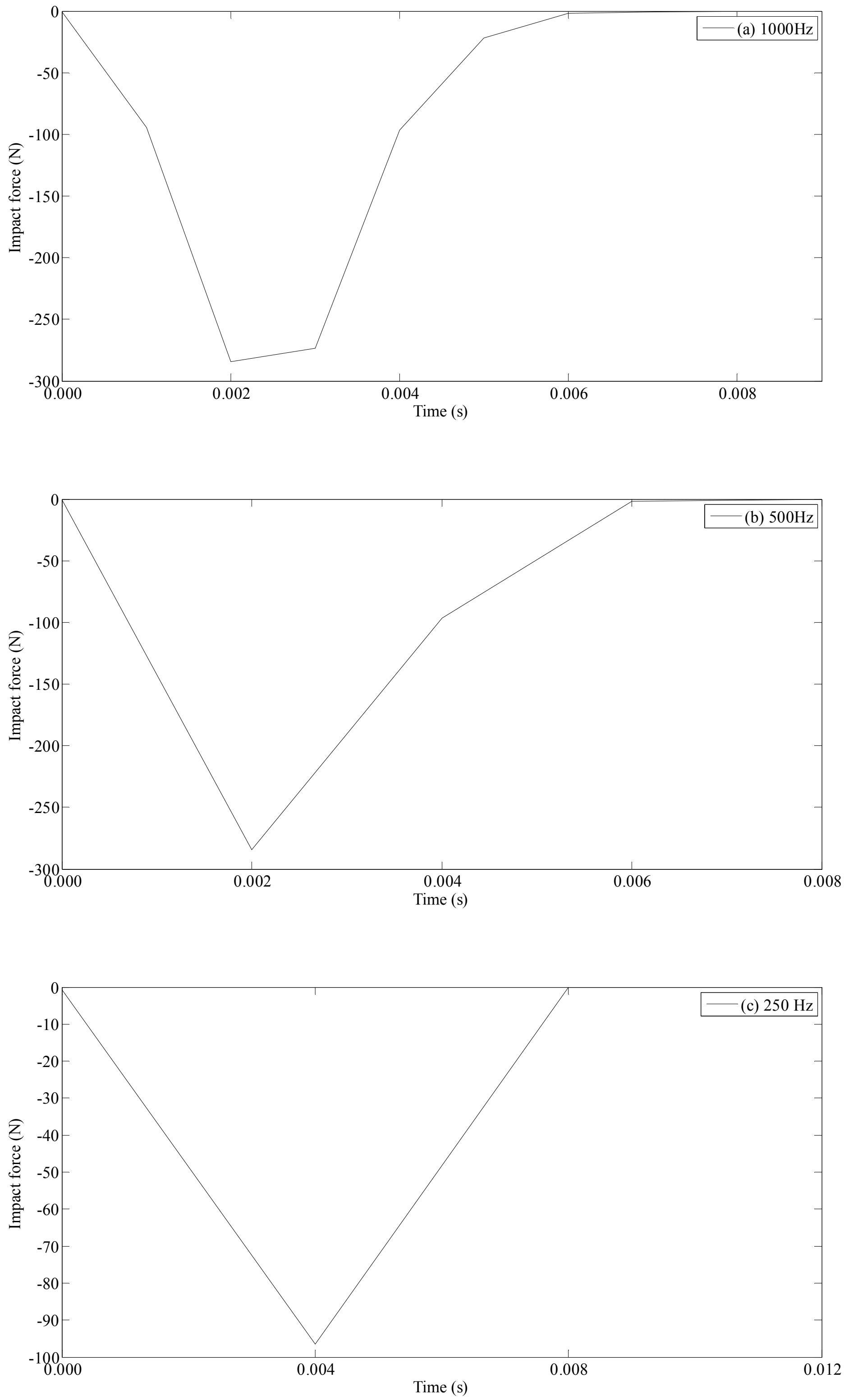

Figure 6.16: Recorded force with different sampling rate

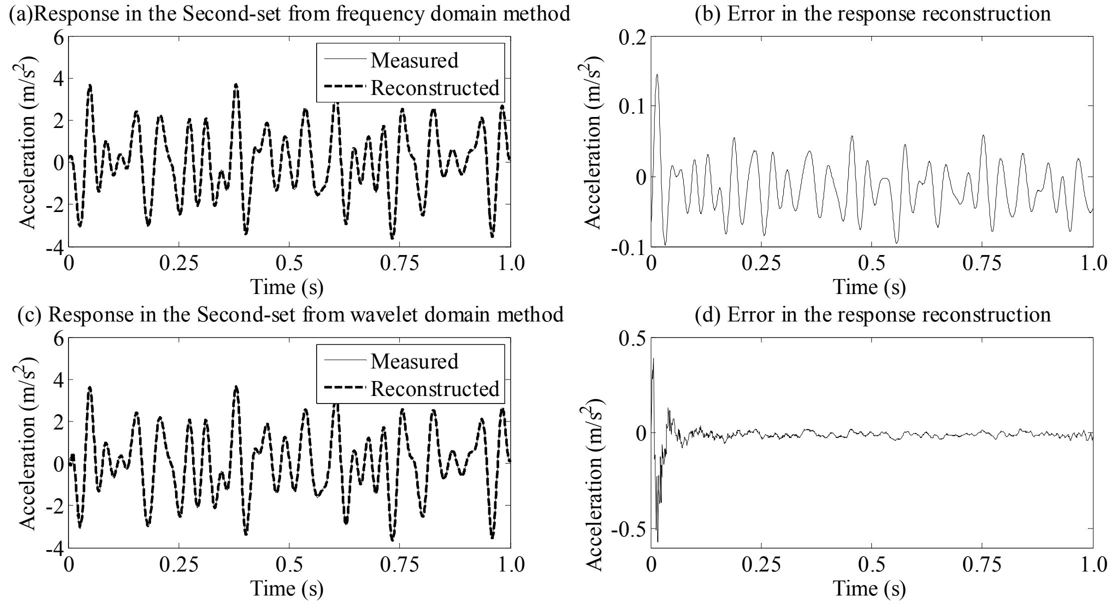

Figure 6.17: Measured and reconstructed responses in the Second-set response from frequency and wavelet domain methods

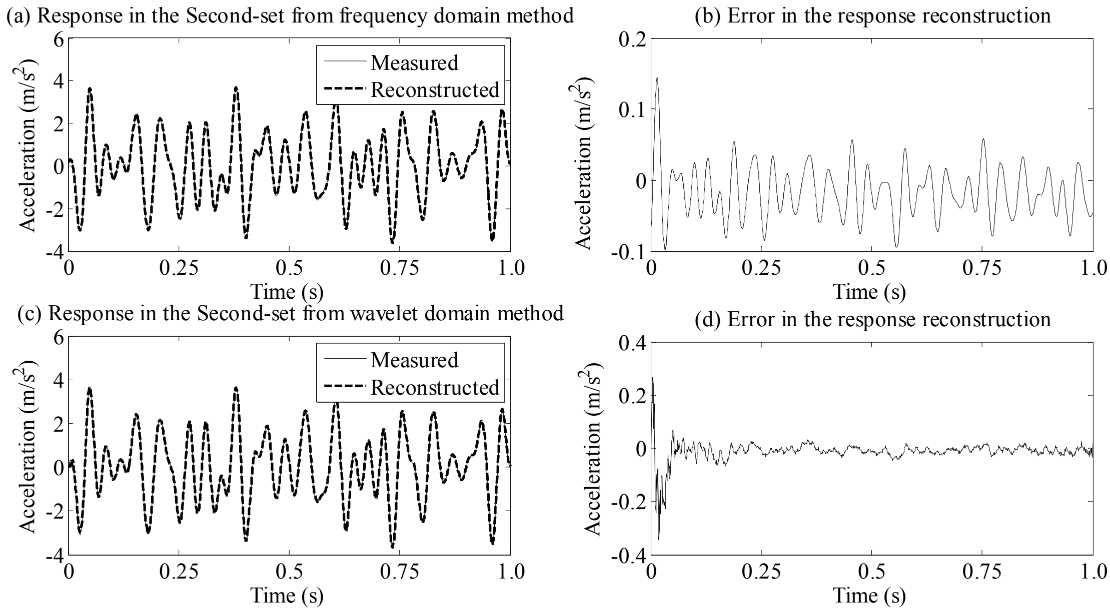

Figure 6.18: Measured and reconstructed responses in the Second-set response from frequency and wavelet domain methods

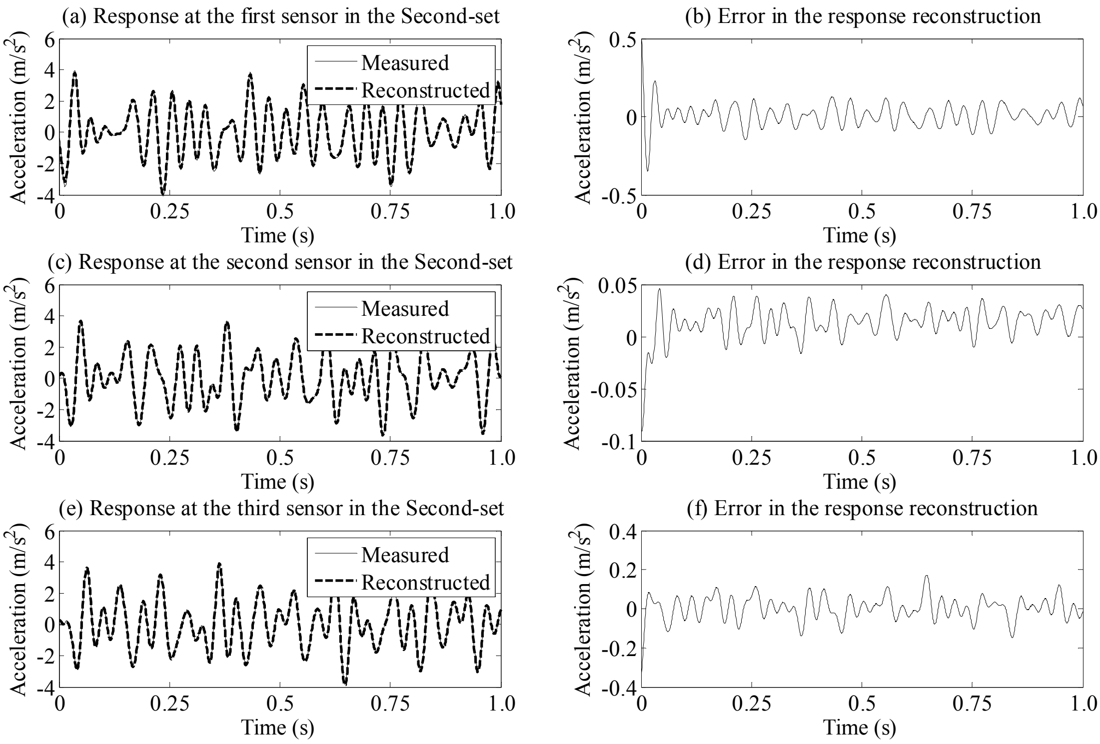

Figure 6.19: Measured and reconstructed responses in the Second-set response from frequency domain method with IIRS

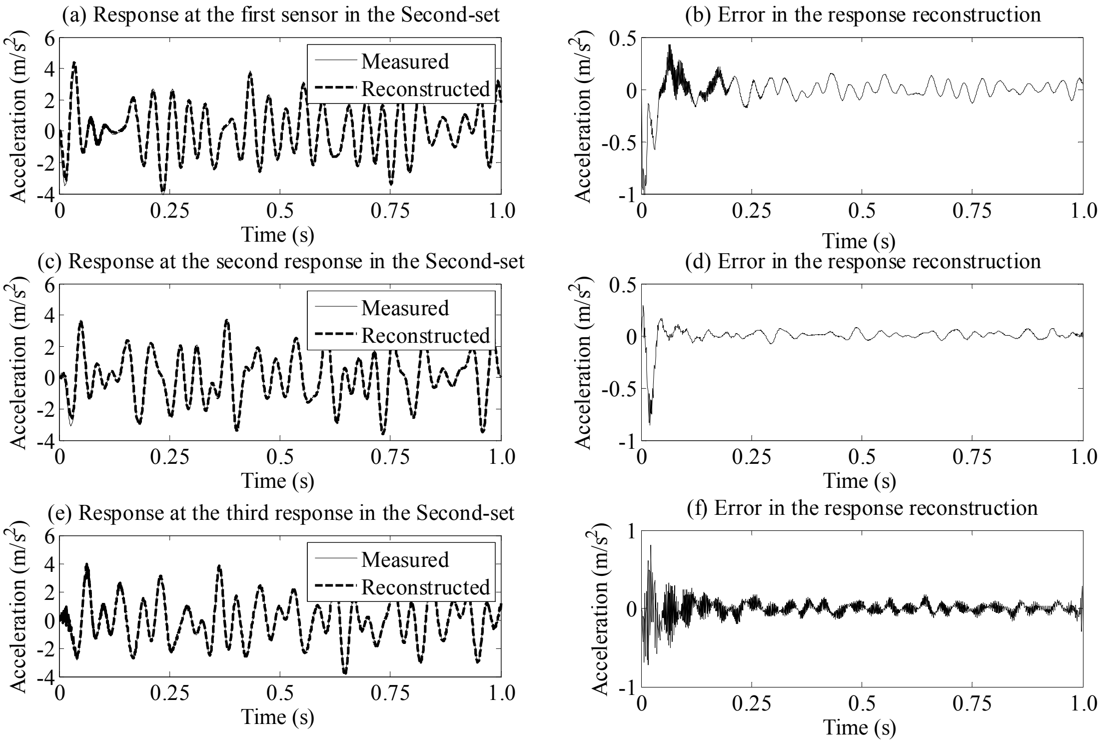

Figure 6.20: Measured and reconstructed responses in the Second-set response from wavelet domain method with IIRS

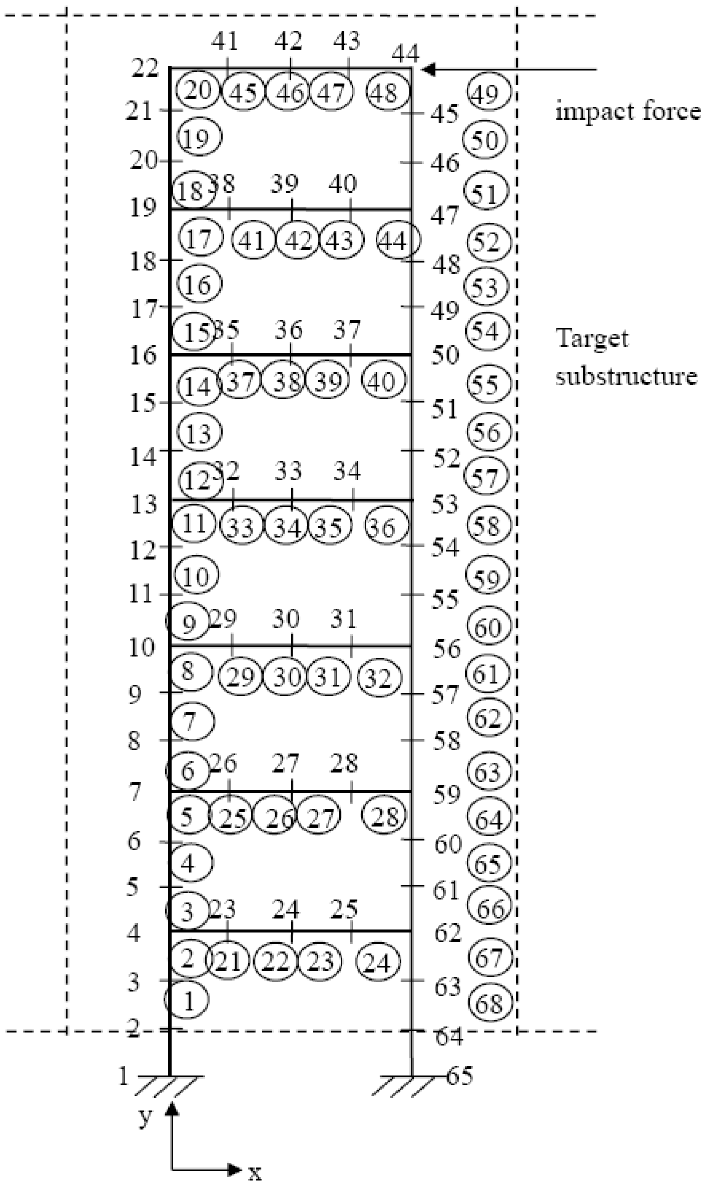

Note: (1): 1 denotes the node number
(2): (1) denotes the element number in the substructure

Figure 6.21: Finite element model of the target substructure in the damage identification

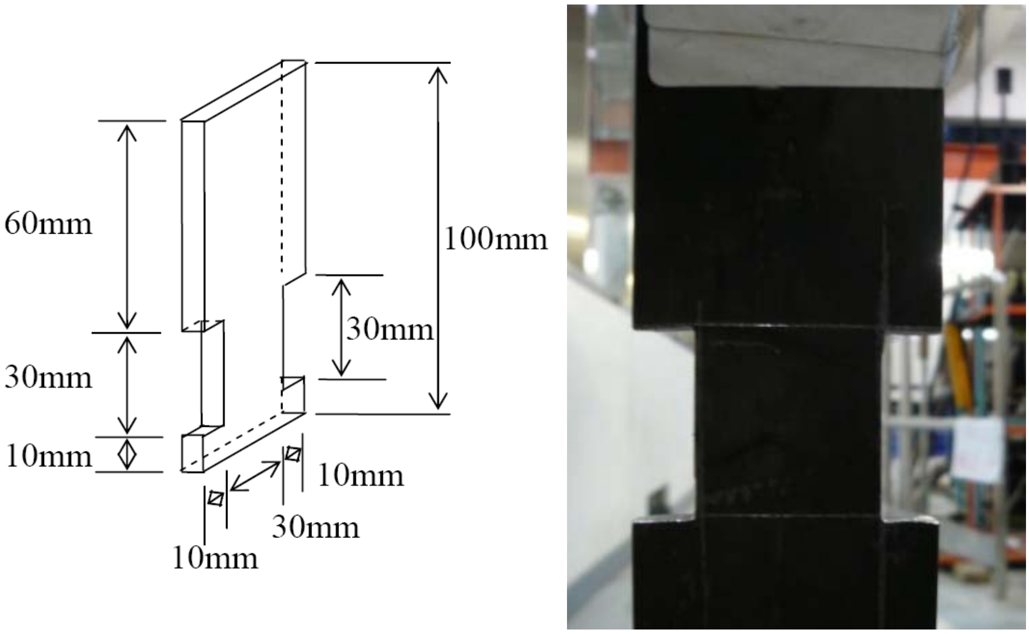

Figure 6.22: Width and depth of the cut in the damaged element

(a) Damage scenario A

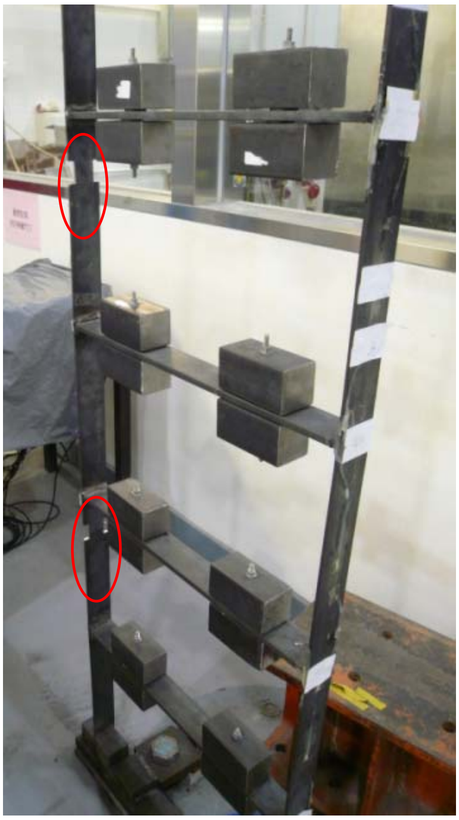

(b) Damage scenario B

Figure 6.23: Introduced damage in the frame structure

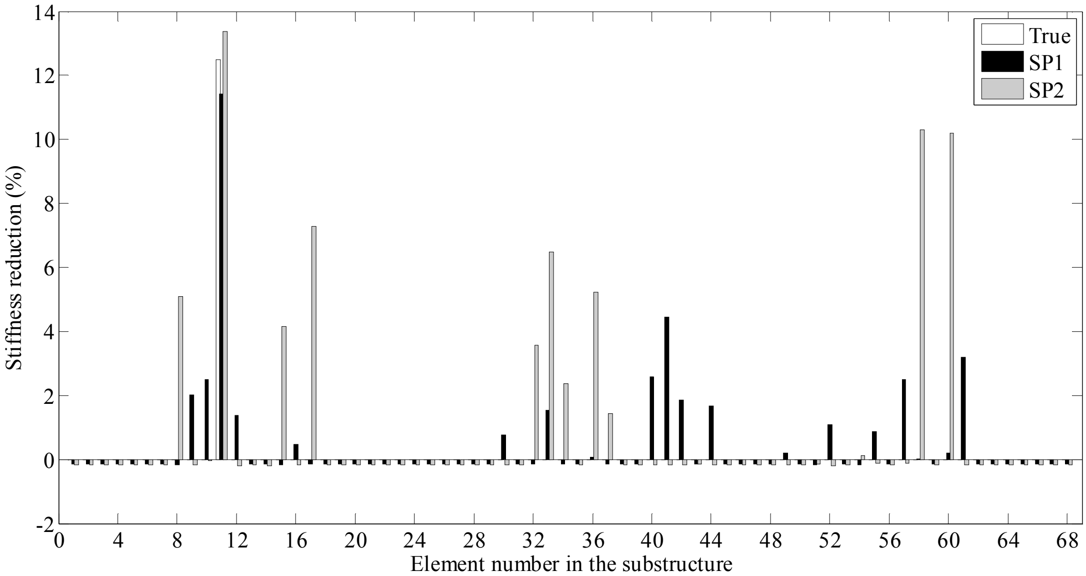

Figure 6.24: Damage identification results for Scenario A from frequency domain method

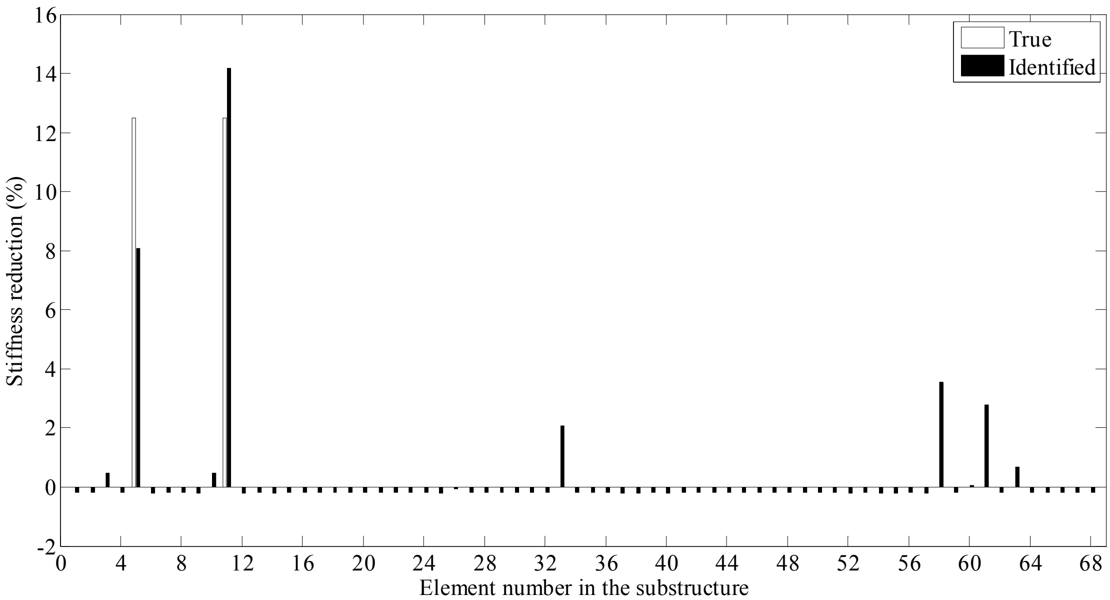

Figure 6.25: Damage identification results for Scenario B from frequency domain method

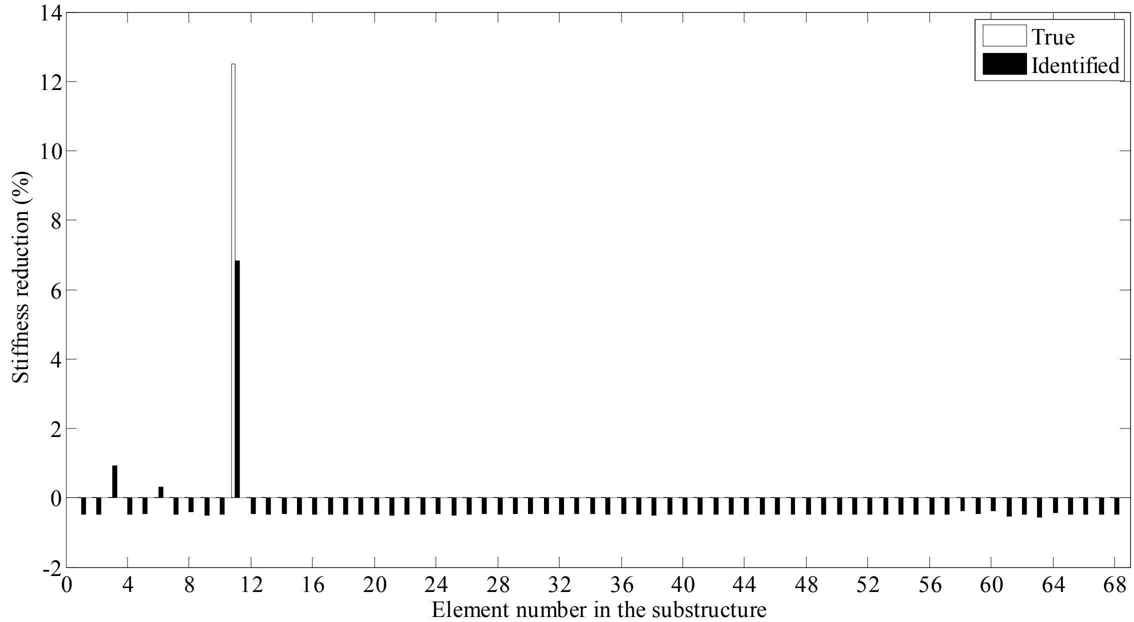

Figure 6.26: Damage identification results for Scenario A from frequency domain method with IIRS

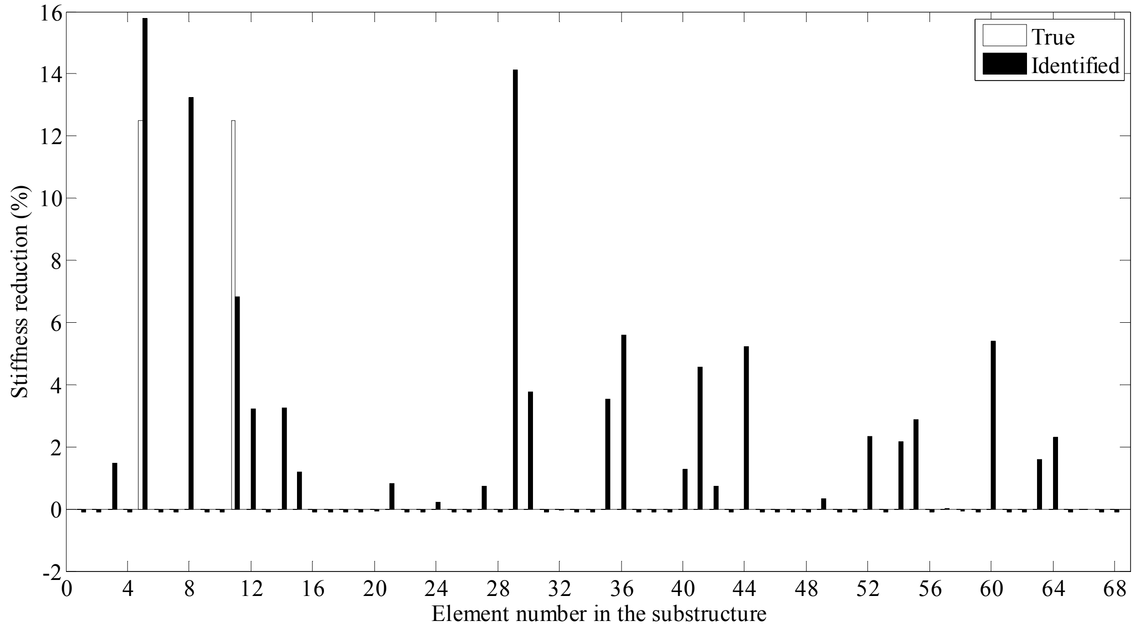

Figure 6.27: Damage identification results for Scenario B from frequency domain method with IIRS

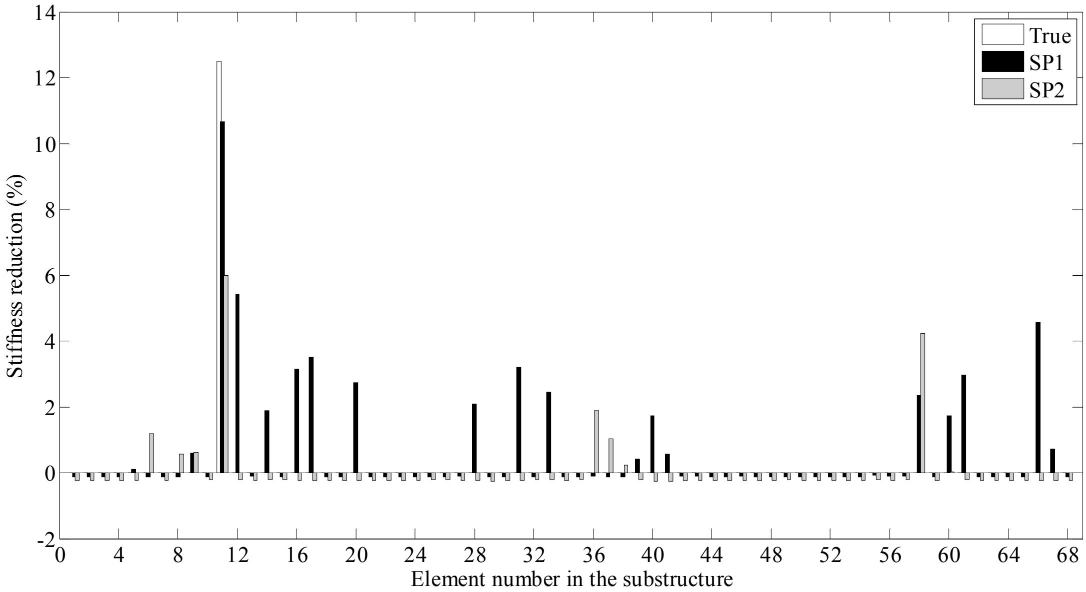

Figure 6.28: Damage identification results for Scenario A from wavelet domain method

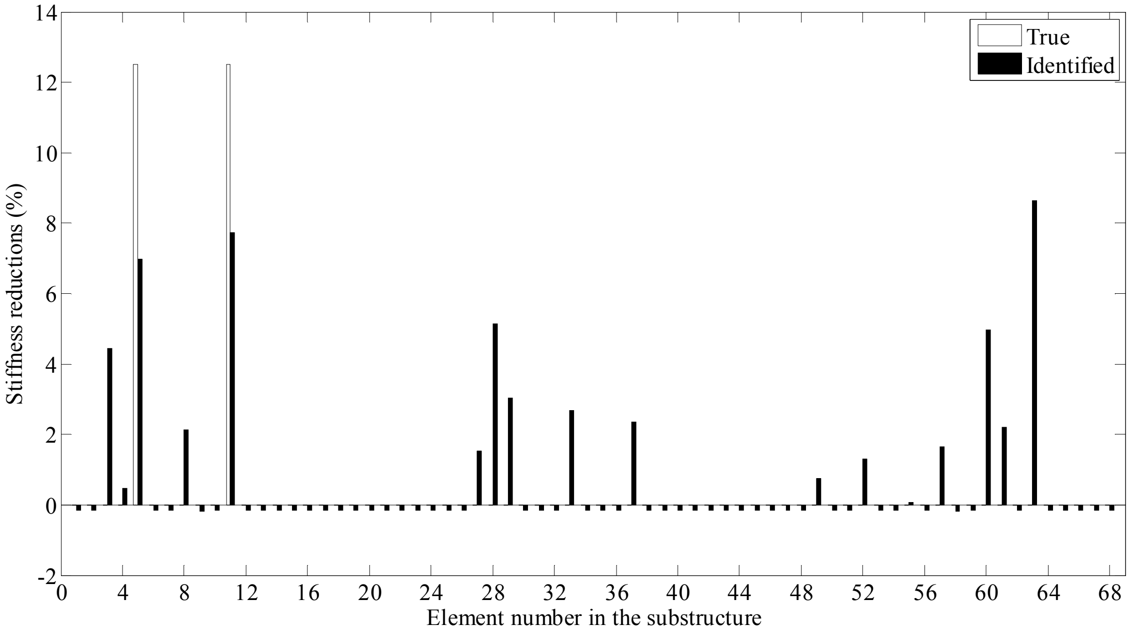

Figure 6.29: Damage identification results for Scenario B from wavelet domain method

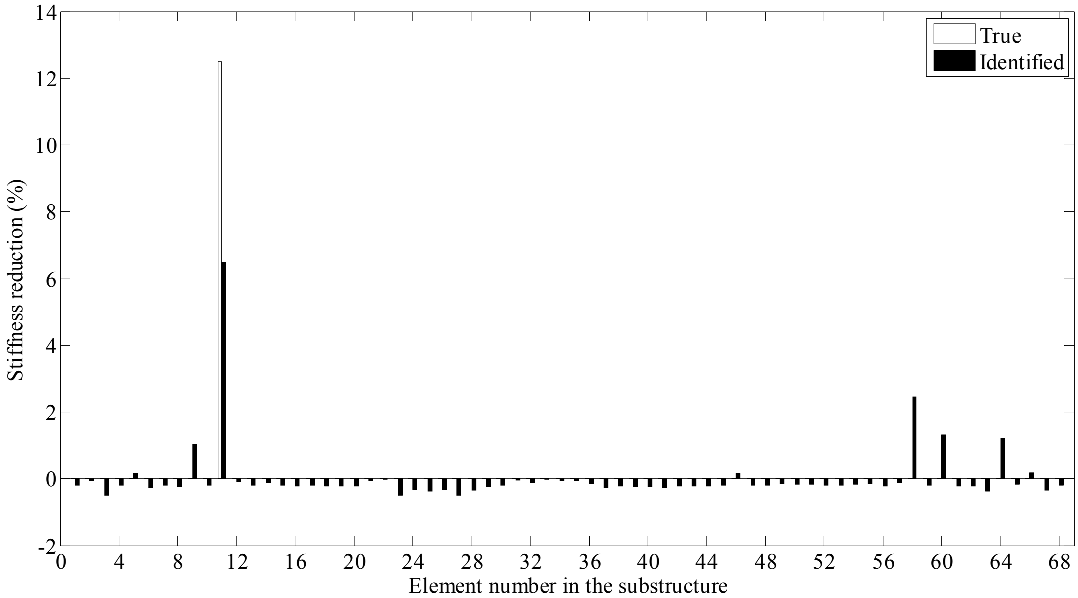

Figure 6.30: Damage identification results for Scenario A from wavelet domain method with IIRS

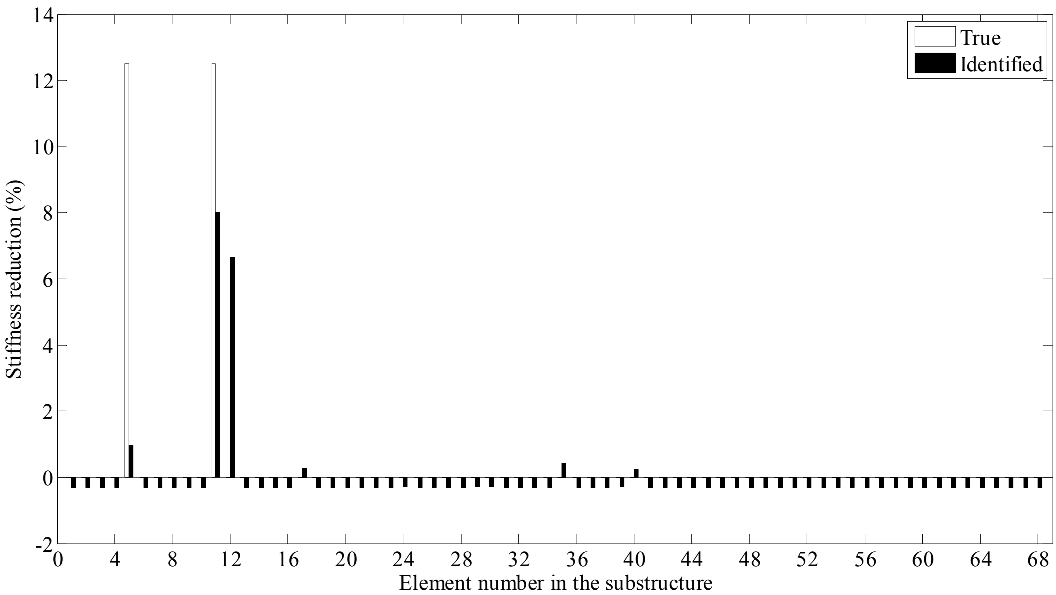

Figure 6.31: Damage identification results for Scenario B from wavelet domain method with IIRS

CHAPTER 7

CONCLUSIONS AND RECOMMENDATIONS

7.1 Conclusions

Vibration measurements, such as dynamic acceleration response data from civil infrastructures, are usually used for structural condition assessment with system identification techniques. Substructural condition assessment approaches are receiving increasing attentions in recent years since they have the advantages of reducing the number of unknown system parameters to be identified and system DOFs involved in the computation. Measurements at the interface DOFs are normally required and treated as input excitations to the target substructure in many existing substructural identification approaches. However, it may not be possible to measure all the responses at the interface DOFs. This dissertation proposes a dynamic substructural condition assessment approach without the information of responses and forces at the interface DOFs. Dynamic response reconstruction techniques in both the frequency and wavelet domains are proposed. The relationship between two sets of time-domain response vectors is formulated. Only the finite element model of the intact target substructure and measured acceleration data from the substructure in the damaged state are required in the identification. A dynamic response sensitivity-based method is used to formulate the damage identification algorithm and the adaptive Tikhonov regularization technique is adopted to improve the identification results when large noise effect is included in the measurements. Local damage is identified as the change in the elemental stiffness factors. Numerical and experimental studies are conducted to validate the effectiveness and accuracy of the proposed substructural damage identification approach.

Another development in the condition assessment is to detect the local damage using measured acceleration responses from the substructure subject to moving vehicular loads which serve as excitations to the substructure. The dynamic response reconstruction in wavelet domain is developed for the scenario when a structure or a target substructure is subject to moving vehicular loads. The transmissibility matrix between two sets of time-domain response vectors is formulated using the unit impulse response functions when the moving loads are at different locations. Measured acceleration responses from the structure or the substructure in the damaged state are used for the damage identification. A three-dimensional box-section girder subject to a two-axle three-dimensional moving vehicle is taken as an example to validate the proposed approach for damage identification. The simulated damage can be effectively identified with noise effect included in the measurements.

The main contributions of this dissertation and conclusions achieved are summarized as follows:

1. **New dynamic response reconstruction techniques in both the frequency and wavelet domains**

New structural dynamic response reconstruction techniques in both the frequency and wavelet domains are developed. Numerical and experimental studies are conducted to investigate the accuracy and efficiency of the proposed methods for response reconstruction. It is demonstrated that these two techniques were successfully used for response reconstruction in a full structure and in a substructure.

(1) Response reconstruction in a full structure treats the applied external excitations as unknown force vectors on the structure and the transmissibility matrix is formulated with frequency response function in the frequency domain or the unit impulse response function in the wavelet domain. The relationship between two sets of time-domain response vectors is formed. The locations of these excitations should be assumed available, while the time-histories of applied excitations are not required. The FOH discrete force approximation is used in the forward response computation to improve the accuracy of the dynamic

response analysis in the simulation studies. It shows that response reconstruction using the frequency domain method with FOH discrete gives better response reconstruction results than that with ZOH.

(2) Two cases for response reconstruction in a substructure are considered. The first case is that the interface forces are available either from measurements or from computation with the full structure model is available. The external excitations on the structure are used in the dynamic response analysis and then the interface forces are obtained from the finite element analysis of the full structure. The second case eliminates this restraint with only the finite element model of the substructure available in the response reconstruction process. The interface forces are treated as the unknown input excitations to the substructure. The transmissibility matrix is formulated based on the frequency response function or unit impulse response function computed from the finite element model of the substructure.

It is found that more accurate response reconstruction results can be obtained from frequency domain method when a longer sampling duration or a higher sampling rate is used, while the accuracy of response reconstruction from wavelet domain method is not subject to the sampling duration and sampling rate. More measurements in the Known-set response vector would contribute to a higher accuracy of reconstruction. For the noise-free case, the relative errors in the response reconstruction results from wavelet domain method are far less than those from frequency domain method. For the case with the measurements included some noise effects, similar accuracies of response reconstruction are obtained from the frequency and wavelet domain methods. It is observed that good response reconstruction results are obtained when there is significant vibration component in the response close to the beginning of excitation.

2. New substructural condition assessment method in both the frequency and wavelet domains

A substructural condition assessment approach is developed based on the dynamic response reconstruction techniques in both the frequency and wavelet domains. The information of responses and forces at the interface DOFs is not required. The relationship between two-sets of time-domain response vectors is formulated based on the transmissibility matrix with the frequency response function in the frequency domain or the unit impulse response function in the wavelet domain. The finite element model of the intact target substructure and acceleration measurements from the damaged substructure are required in the damage identification. A dynamic response sensitivity-based method is used to formulate the substructural damage identification algorithm and the adaptive Tikhonov regularization technique is adopted to improve the identification results especially for the case with measurement noise effect. Numerical studies are conducted to illustrate the performance of the proposed substructural damage identification approach. Under the circumstance when a target substructure has a large number of interface DOFs, the IIRS model condensation may be used to reduce the number of interface forces as well as the required sensor measurements in the First-set response vector. The influence of model errors on the performance of the proposed approach is also investigated. The accuracy and effectiveness of the proposed approach is numerically verified and the simulated damage in the substructure can be identified effectively with 10% noise effect in the measurements and initial model errors.

3. Extending the damage identification method to a bridge structure or a target substructure subject to moving vehicular loads

The damage identification in a bridge structure or in a target substructure subject to moving vehicular loads is conducted based on the proposed dynamic response reconstruction technique in the wavelet domain. The transmissibility matrix between two sets of time-domain response vectors from the structure or the substructure subject to moving loads is formulated using the unit impulse response function in the wavelet domain with the moving loads at different locations. Measured acceleration responses from the damaged structure or the damaged substructure are used for the identification. For the damage identification in a full structure, the time-histories of moving loads and the properties of moving vehicle are not required. For the damage identification in a target substructure, dynamic responses at the interface DOFs, the time-histories of both the moving loads and interface forces are not needed. The finite element model of the intact substructure is used as the baseline model and to derive the unit impulse response function. Numerical studies on a three-dimensional box-section bridge deck subject to a single moving force or a two-axle three-dimensional vehicle are separately investigated to validate the proposed approach for damage identification. The simulated damage can be identified effectively even with noise effect included in the measurements and initial model errors in the finite element model.

4. Experimental studies on the performance of the proposed substructural condition assessment approach

Experimental studies are conducted to verify the proposed dynamic response reconstruction techniques in both the frequency and wavelet domains and the substructural damage identification approach. A seven-storey steel frame is fabricated in the laboratory and measured acceleration response data from hammer tests are used for the initial finite element model updating. The updated finite element model is considered as the baseline model and measured response data from hammer tests from the damaged frame structure are used for the response reconstruction and damage identification. It is demonstrated that excellent accuracy of response reconstruction in the full structure and in a substructure is achieved. Two damage scenarios with single- and multi-damage cases are then introduced in the frame structure. Measured response data from hammer tests are used for identification, and the local damages in the substructure are identified effectively. The locations of the damage are detected accurately and the stiffness reductions in the damaged elements of the target substructure are identified close to the true values. Several false positives may exist in the damage identification results due to the measurement noise and model uncertainties in the finite element model. The IIRS model condensation may not be required if a sufficient number of sensors is provided for damage identification in a target substructure of the frame structure when the number of the interface DOFs is not large. It is possible to use the IIRS for the model condensation of the target substructure and to reduce the required sensor number in the First-set response vector. However, the damage identification results may be affected by the use of IIRS as additional error is introduced in the response reconstruction and the subsequent substructural damage identification algorithm.

7.2 Recommendations on Future Studies

It has been investigated numerically and experimentally that the proposed dynamic substructural condition assessment approach based on the response reconstruction techniques in both the frequency and wavelet domains can be used to identify the local damage in structures successfully and efficiently. The proposed substructural damage identification approach can generally be applied to other types of civil structures. The following recommendations are provided for further research and exploration:

(1) The wavelet domain method for response reconstruction is developed for the bridge structure subject to moving vehicle excitations. The damage identification in the bridge structure or in a target substructure is numerically verified. Further studies are required to demonstrate the performance of the proposed damage identification approach with in-field testing data.

(2) Measured acceleration response data from hammer tests are used to validate the proposed substructural damage identification algorithm in the frequency and wavelet domains. Studies on the performance of the proposed substructural damage identification approach using response data from shaking-table tests may be conducted.

(3) The excitations applied on the structures in the above works are general forces at some specific locations or moving load excitations. The response reconstruction is also explored with a scenario where the structure is under seismic excitations. The response reconstruction techniques may be further developed for the case when the structure is subject to ambient excitation using a statistical approach. The propagation of system uncertainties on the damage identification may be analyzed.

(4) It is noted that the sensor number and locations in the First- and Second-set response vectors may affect the accuracy of forward response reconstruction in the full structure or in a target substructure and subsequent damage detection. The issue of optimal sensor placement may be further examined.

(5) Further research work may be explored to apply the proposed substructrual approach for condition assessment of large-scale engineering structures, such as, long-span bridges.

APPENDIX A

The impulse response of the extrapolation filter for the triangle hold and block diagram of the triangle hold are shown in the following figures.

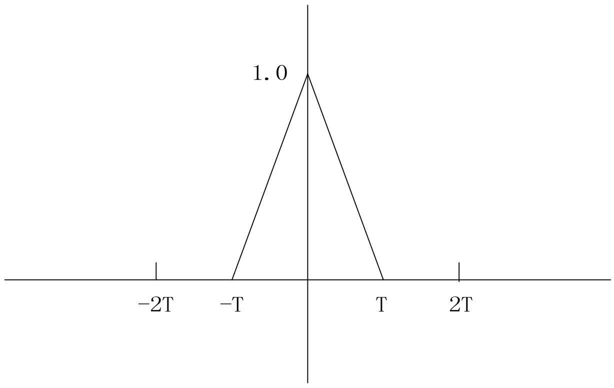

Figure A-1: Impulse response of the extrapolation filter for the triangle hold

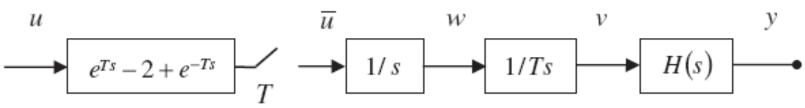

Figure A-2: Block diagram of the triangle-hold equivalent

REFERENCES

AASHTO LRFD bridge design specifications. American Association of State Highway and Transportation Officials. Washington, DC. 2007.

Ahmadian, H., Mottershead, J. E., and Friswell, M. I., 1998, "Regularization methods for finite element model updating", *Mechanical Systems and Signal Processing*, 12(1): 47-64.

Alvin, K. F., Robertson, A. N., Reich, G. W., and Park, K. C., 2003, "Structural system identification: from reality to models," *Computers and Structures*, 81(12): 1149-1176.

Au, F. T. K., Jiang, R. J., and Cheung, Y. K., 2004, "Parameter identification of vehicles moving on continuous bridges", *Journal of Sound and Vibration*, 269(1-2): 91-111.

Bakir, P. G., Reynders, E., and Roeck, G. D., 2008, "Sensitivity-based finite element model updating using constrained optimization with a trust region algorithm", *Journal of Sound and Vibration*, 305(1-2): 211-225.

Bakir, P. G., Reynders, E., and Roeck, G. D., 2008, "An improved finite element model updating method by the global optimization technique 'Coupled Local Minimizers'", *Computers and Structures*, 86(11-12): 1339-1352.

Banan, M. R., Banan, M. R., and Hjelmstad, K. D., 1995, "Time-domain parameter estimation algorithm for structures II: numerical simulation studies," *Journal of Engineering Mechanics ASCE,* 121(3): 435–447.

Brownjohn, J. M. W., Xia, P. Q., Hao, H., and Xia, Y., 2001, "Civil structure condition assessment by FE model updating: methodology and case studies", *Finite Elements in Analysis and Design*, 37(10): 761-775.

Bucciarelli, L. L., *Engineering Mechanics for Structures*, Dover publications, 2009.

Carden, E. P., and Fanning, P., 2004, "Vibration based condition monitoring: a review," *Structural Health Monitoring*, 3(4): 355-377.

Cattarius, J., and Inman, D. J., 1997, "Time domain analysis for damage detection in smart structures," *Mechanical Systems and Signal Processing*, 11(3): 409-423.

Cawley, P., and Adams, R. D., 1979, "The locations of defects in structures from measurements of natural frequencies," *Journal of Strain Analysis*, 14(2): 49-57.

Choi, S., and Stubbs, N., 2004, "Damage identification in structures using the time-domain response," *Journal of Sound and Vibration*, 275(3-5): 577-590.

Chopra, A. K., *Dynamics of Structures: Theory and Applications to Earthquake Engineering*, Upper Saddle River, NJ : Prentice Hall, 2007.

Darby, A. P., Blakeborough, A., and Williams, M. S., 2001, "Improved control algorithm for real-time substructure testing", *Earthquake Engineering and Structural Dynamics*, 30(3): 431-448.

Daubechies, I., *Ten Lectures on Wavelets*, SIAM, Philadelphia, PA, 1992.

Deng, L., and Cai, C. S., 2009, "Identification of parameters of vehicles moving on bridges", *Engineering Structures*, 31(10): 2474-2485.

Deng, L., and Cai, C. S., 2010, "Identification of dynamic vehicular axle loads: theory and simulations", *Journal of Vibration and Control*, 16(14): 2167-2194.

Devriendt, C., and Guillaume, P., 2007, "The use of transmissibility measurements in output-only modal analysis", *Mechanical Systems and Signal Processing*, 21(7): 2689-2696.

Devriendt, C., and Guillaume, P., 2008, "Identification of modal parameters from transmissibility measurements", *Journal of Sound and Vibration*, 314(1-2): 343-356.

Doebling, S. W., 1996, "Minimum-Rank Optimal Update of Elemental Stiffness Parameters for Structural Damage Identification", *AIAA Journal*, 34(12): 2615-2621.

Doebling, S. W., Farrar, C. R., and Prime, M. B., 1998, "A summary review of vibration-based damage identification methods", *The Shock and Vibration Digest*, 30(2): 91-105.

Doherty, J. E., 1993, "Nondestructive evaluation", in Handbook on Experimental Mechanics, 2nd ed., New York: VCH; Bethel: Society for Experimental Mechanics, 527-556.

Dong, Y. F., Li, Y. M., Lai, M., and Xiao, M. K., 2008, "Nonlinear structural response prediction based on support vector machines," *Journal of Sound and Vibration*, 311(3-5): 886-897.

Farrar, C. R., Doebling, S. W., and Nix, D. A., 2001, "Vibration-based structural damage identification", *Philosophical Transactions of the Royal Society of London Series A- Mathematical Physical and Engineering Sciences*, 359(1778): 131-149.

Farrar, C. R., and James, G. H., 1999, "System identification from ambient vibration measurements on a bridge", *Journal of Sound and Vibration*, 205(1): 1-18.

Farrar, C. R., and Jauregui, D. A., 1998a, "Comparative study of damage identification algorithms applied to a bridge: I. Experiment," *Smart Materials and Structures*, 7(5): 704-719.

Farrar, C. R., and Jauregui, D. A., 1998b, "Comparative study of damage identification algorithms applied to a bridge: II. Numerical study," *Smart Materials and Structures*, 7(5): 720-731.

Fox, C. H. J., 1992, "The location of defects in structures: a comparison of the use of natural frequency and mode shape data," *Proceedings of the 10th International Modal Analysis Conference*, 522-528.

Frahat, C., and Hemez, F. M., 1993, "Updating of FE dynamic models using an element by element sensitivity methodology", *AIAA Journal*, 31(9): 1702-1711.

Franklin, G. F., Powell, J. D., and Workman, M. L., *Digital Control of Dynamic Systems*, third ed., Menlo Park, Calif, Addison-Wesley, 1998.

Friswell, M. I., Garvey, S. D., and Penny, J. E. T., 1995, "Model reduction using dynamic and iterated IRS technique", *Journal of Sound and Vibration*, 186(2): 311-323.

Friswell, M. I., and Mottershead, J. E., *Finite Element Model Updating in Structural Dynamics*, Kluwer Academic Publishers, Dordrecht, 1995.

Furukawa, A., Otsuka, H., and Kiyono, J., 2006, "Structural damage detection method using uncertain frequency response functions," *Computer-Aided Civil and Infrastructure Engineering*, 21(4): 292-305.

Ghanem, R., and Shinozuka, M., 1995, “Structural system identification I: theory,” *Journal of Engineering Mechanics ASCE*, 121(2): 255-264.

González, A., Rowley, C., and O’Brien, E. J., 2008, “A general solution to the identification of moving vehicle forces on a bridge”, *International Journal for Numerical Methods in Engineering*, 75(3), 335-354.

Gorl, E., Link, M., 2003, “Damage identification using changes of eigenfrequencies and mode shapes”, *Mechanical systems and Signal Processing*, 17(1): 103-110.

Gupta, A. K., Hassan, T., and Gupta, A., 1996, “Time and frequency domain analyses of single-degree-of-freedom systems”, *Nuclear Engineering Design*, 167(1): 1-5.

Hassiotis, S., and Jeong, G. D., 1995, “Identification of stiffness reductions using natural frequencies”, *Journal of Engineering Mechanics ASCE*, 121(10): 1106-1113.

Hjelmstad, K. D., Banan, M. R., and Banan, M. R., 1995, “Time-domain parameter estimation algorithm for structures I: computational aspects,” *Journal of Engineering Mechanics ASCE,* 121(3): 424–434.

Huang, H. W., Yang, J. N., 2008, “Damage identification of substructure for local health Monitoring”, *Smart Structures and Systems*, 4 (6): 795-807.

Huth, O., Feltrin, G., Maeck, J., Kilic, N. and Motavalli, M., 2005, “Damage identification using modal data: experiences on a prestressed concrete bridge,” *Journal of Structural Engineering ASCE*, 131(12): 1898-1910.

ISO 8606: 1995(E). Mechanical vibration – road surface profiles – reporting of measured data.

Jaishi, B., and Ren, W. X., 2006, “Damage detection by finite element model updating using modal flexibility residual”, *Journal of Sound and Vibration*, 290(1-2): 369-387.

Jaishi, B., and Ren, W. X., 2008, “Finite element model updating based on eigenvalue and strain energy residuals using multiobjective optimisation technique”, *Mechanical Systems and Signal Processing*, 21(5): 2295-2317.

Jiang, R. J., Au, F. T. K., Cheung, Y. K., 2003, “Identification of masses moving on multi-span beams based on a genetic algorithm", *Computers and Structures*, 81(22-23): 2137-2148.

Jiang, R. J., Au, F. T. K., Cheung, Y. K., 2004, "Identification of vehicles moving on continuous bridges with rough surface", *Journal of Sound and Vibration*, 274(3-5): 1045-1063.

Johnson, T. J., and Adams, D. E., 2002, "Transmissibility as a differential indicator of structural damage", *Journal of Vibration and Acoustics ASME*, 124(4): 634-641.

Juang, J. N., and Pappa, R. S., 1985, "An Eigensystem Eealization Algorithm for Modal Parameter Identification and Model Reduction", *Journal of Guidance, Control, and Dynamics*, 8(5): 583-592.

Kammer, D. C., 1997, "Estimation of structural response using remote sensor locations", *Journal of Guidance, Control and Dynamics*, 20(3): 501-508.

Kang, J. S., Park, S. K., Shin, S., and Lee, H. S., 2005, "Structural system identification in time domain using measured acceleration," *Journal of Sound and Vibration*, 288(1-2): 215-234.

Kaouk, M., and Zimmerman, D. C., 1994, "Structural damage assessment using a generalized minimum rank perturbation theory", *AIAA Journal*, 32(4): 836-842.

Kim, H. M., and Bartkowicz, T. J., 1993, "Damage detection and health monitoring of large space structures", *Sound and Vibration*, 27(6): 12–17.

Kim, C. Y., Jung, D. S., Kim, N. S., Kwon, S. D., and Feng, M. Q., 2003, "Effect of vehicle weight on natural frequencies of bridge measured from traffic-induced vibration", *Earthquake Engineering and Engineering Vibration*, 2(1): 109-115.

Koh, C. G., See, L. M., and Balendra, T., 1995, "Damage detection of buildings: numerical and experimental studies," *Journal of Structural Engineering ASCE*, 121(8): 1150-1160.

Koh, C. G., Hong, B., and Liaw, C. Y., 2003, "Substructural and Progressive Structural Identification Methods", *Engineering Structures*, 25(12): 1551-1563.

Koh, C. G., See, L. M., and Balendra, T., 1991, "Estimation of Structural Parameters in Time Domain: a Substructure Approach", *Earthquake Engineering and*

Structural Dynamics, 20(8): 787-801.

Koh, C. G., and Shankar, K., 2003, "Substructural Identification Method without Interface Measurement", *Journal of Engineering Mechanics ASCE*, 129(7): 769-776.

Kosmatka, J. B., and Ricles, J. M., 1999, "Damage detection in structures by modal vibration characterization", *Journal of Structural Engineering ASCE*, 125(12): 1384-1392.

Kwon, Y. W., and Bang, H. C., *The Finite Element Method using MATLAB*, 2^{nd}-ed. USA: CRC Press LLC; 2000.

Law, S. S., Bu, J. Q., Zhu, X. Q., and Chan, S. L., 2004, "Vehicle axle loads identification using finite element method", *Engineering Structures*, 26(8): 1143-1153.

Law, S. S., Bu, J. Q., Zhu, X. Q., and Chan, S. L., 2007a, "Moving load identification on a simply supported orthotropic plate", *International Journal of Mechanical Sciences*, 49(11), 1262-1275.

Law, S. S., Chan, T. H. T., Zhu, X. Q. and Zeng, Q. H., 2001, "Regularization in moving force identification", *Journal of Engineering Mechanics ASCE*, 127(2), 136-148.

Law, S. S., Li, J., and Wu, S. Q., 2007b, "Prestress identification in box-girder bridge deck under traffic load", *Proceedings of the 3^{rd} International Symposium on Environment Vibrations: Prediction, Monitoring, Mitigation and Evaluation*, Taipei, TAIWAN, 631-638.

Law, S. S., and Li, J., 2010, "Updating the reliability of a concrete bridge structure based on condition assessment with uncertainties", *Engineering Structures*, 32(1): 286-296.

Law, S. S., and Li, X. Y., 2007, "Wavelet-based Sensitivity Analysis of the Impulse Response Function for Damage Detection", *Journal of Applied Mechanics ASME*, 74(2): 375-377.

Law, S. S., Li, X. Y., and Lu, Z. R., 2006, "Structural damage detection from wavelet coefficient sensitivity with model errors", *Journal of Engineering*

Mechanics ASCE, 132(10): 1077-1087.

Law, S. S., and Yong, D., 2011, "Substructure methods for structural condition assessment," *Journal of Sound and Vibration*, 330(15): 3606-3619.

Law, S. S., Zhang, K., and Duan, Z. D., 2010, "Structural damage detection from coupling forces between substructures under support excitation", *Engineering Structures*, 32 (8): 2221-2228.

Lee, J. W., Kim, J. D., Yun, C. B., Yi, J. H., and Shim, J. M., 2002, "Health-monitoring method for bridges under ordinary traffic loadings", *Journal of Sound and Vibration*, 257(2): 247-264.

Lei, Y., Xu, Z. Q., Ni, P. H., and Mao, Y. K., 2010, "A substructural appraoch for damage detection of large size structures under limited input and output measurements," *Proceedings of Earth and Space 2010: Engineering, Science, Construction and Operations in Challenging Environments ASCE*, 2395-2604.

Li, X. Y., and Law, S. S., 2008a, "Damage identification of structures including system uncertainties and measurement noise", *AIAA Journal*, 46(1): 263-276.

Li, X. Y., and Law, S. S., 2008b, "Structural damage detection with statistical analysis from support excitation," *Mechanical Systems and Signal Processing*, 22(8): 1793-1808.

Li, X. Y., and Law, S. S., 2010, "Adaptive Tikhonov regularization for damage detection based on nonlinear model updating," *Mechanical Systems and Signal Processing*, 24(6): 1646-1664.

Li, Y., Mau, S. T., 1991, "A case study of MIMO system identification applied to building seismic records," *Earthquake Engineering and Structural Dynamics*, 20(11): 1045-1064.

Limongelli, M. P., 2003, "Optimal location of sensors for reconstruction of seismic responses through spline function interpolation," *Earthquake Engineering and Structural Dynamics*, 32(7): 1055-1074.

Lin, C. W., and Yang, Y. B., 2005, "Use of a passing vehicle to scan the fundamental bridge frequencies: An experimental verification", *Engineering Structures*, 27(13): 1865-1878.

Link, M., and Weiland, M., 2009, “Damage identification by multi-model updating in the modal and in the time domain”, *Mechanical Systems and Signal Processing*, 23(6): 1734-1746.

Liu, P. L., 1995, “Identification and damage detection of trusses using modal data,” *Journal of Structural Engineering ASCE*, 121(4): 599–608.

Lu, Z. R., and Law, S. S., 2006a, “Identification of prestress force from measured structural responses”, *Mechanical Systems and Signal Processing*, 20(8): 2186-2199.

Lu, Z. R., and Law, S. S., 2006b, “Force identification based on sensitivity in time domain”, *Journal of Engineering Mechanics ASCE*, 132(10): 1050-1056.

Lu, Z. R., and Law, S. S., 2007a, “Features of dynamic response sensitivity and its application in damage detection,” *Journal of Sound and Vibration*, 303(1-2): 305-329.

Lu, Z. R., and Law, S. S., 2007b, “Identification of system parameters and input force from output only”, *Mechanical Systems and Signal Processing*, 21(5): 2099-2111.

Lu, Z. R., and Liu, J. K., in press, “Identification of both structural changes in bridge deck and vehicular parameters using measured dynamic responses”, *Computers and Structures*.

Ma, X., Vakakis, A. F., and Bergman, L. A., (2001) “Karhunen-Loeve modes of a truss: transient response reconstruction and experimental verification,” *AIAA Journal*, 39(4): 687-697.

Mace, B. R., and Halkyard, C. R., 2000, “Time domain estimation of response and intensity in beams using wave decomposition and reconstruction,” *Journal of Sound and Vibration*, 230(3): 561-589.

Maeck, J., Wahab, M. A., Peeters, B., Roeck, G. D., Visscher, J. D., Wilde, W. P. D, Ndambi, J. M and Vantomme, J., 2000, “Damage identification in reinforce concrete structures by dynamic stiffness determination”, *Engineering Structures*, 22(10): 1339-1349.

Majumder, L., and Manohar, C. S., 2003, “A time-domain approach for damage detection in beam structures using vibration data with a moving oscillator as an excitation source", *Journal of Sound and Vibration*, 268(4): 699-716.

Majumder, L., and Manohar C. S., 2004, "Nonlinear reduced models for beam damage detection using data on moving oscillator-beam interactions", *Computers and Structures*, 82(2-3): 301-314.

Mazurek, D. F., and Dewolf, J. T., 1990, "Experimental study of bridge monitoring techniques", *Journal of Structural Engineering ASCE*, 115(9): 2532 - 2549.

McGowan, P. E., Smith, S. W., and Javeed, M., 1990, "Experiments for locating damage members in a truss structure", *Proceedings of 2nd USAF/NASA Workshop on System Identification and Health Monitoring of Precision Space Structures*, 571-615.

Moaveni, B., Conte, J. P., and Hemez, F. M., 2009, "Uncertainty and sensitivity analysis of damage identification results obtained using finite element model updating", *Computer-Aided Civil and Infrastructure Engineering*, 24(5): 320-334.

Morton, K. W., and Mayers, D. F., 2005, *Numerical solution of partial differential equations, an introduction*, Cambridge University Press.

Mottershead, J. E., and Friswell, M. I., 1993, "Model updating in structural dynamics: a survey", *Journal of Sound and Vibration*, 167(2): 347-375.

Mottershead, J. E., Friswell, M. I., and Ng, G. H. T., 1996, "Geometric parameters for finite element model updating of joints and constraints", *Mechanical Systems and Signal Processing*, 10(2): 171-182.

Nasrellah, H. A., and Manohar, C. S., 2010, "A particle filtering approach for structural system identification in vehicle-structure interaction problems", *Journal of Sound and Vibration*, 329(9): 1289-1309.

Ndambi, J. M., Vantomme, J. and Harri, K., 2002, "Damage assessment in reinforced concrete beams using eigenfrequencies and mode shape derivatives," *Engineering Structures*, 24(4): 501-515.

Newland, D. E., 1993, *An Introduction to Random Vibrations, Spectral and Wavelet Analysis*, Third edition, Longman Group Limited, England.

Newmark, N. W., 1959, “A method of Computation for Structural Dynamics”, *Journal of Engineering Mechanics Division ASCE*, 85(3): 67-94.

Park, T., Noh, M., Lee, S., and Voyiadjis G. Z., 2009, “Identification of a distribution of stiffness reduction in reinforced concrete slab bridges subjected to moving loads”, *Journal of Bridge Engineering ASCE*, 14(5): 355-365.

PEER Strong Motion Database, http://peer.berkeley.edu/smcat/index.html, Regents of the University of California.

Pandey, A. K., Biswas, M., and Samman, M. M., 1991, “Damage detection from changes in curvature mode shapes,” *Journal of Sound and Vibration*, 145(2): 321-332.

Pandey, A. K., and Biswas, M., 1994, “Damage detection in structures using changes in flexibility,” *Journal of Sound and Vibration*, 169(1): 3-17.

Penrose, R., 1955, “A Generalized Inverse for Matrices”, *Mathematical Proceedings of the Cambridge Philosophical Society*, 51(3): 406-413.

Perera, R., and Ruiz, A., 2008, “A multistage FE updating procedure for damage identification in large-scale structures based on multiobjective evolutionary optimization”, *Mechanical Systems and Signal Processing*, 22(4): 970-991.

Perry, M., and Koh, C. G., 2008, “Output-only structural identification in time domain: Numerical and experimental studies,” *Earthquake Engineering and Structural Dynamics*, 37(4): 517-533.

Peterson, L. D., Doebling, S. W., and Alvin, K. F., 1995, “Experimental determination of local structural stiffness by disassembly of measured flexibility matrices,” *Proceedings of 36th AIAA/ASME/ASCE/AHS/ASC/ Structures, Structural Dynamics, and Materials Conference*, AIAA-95-1090-CP, 2756-2766.

Pinkaew, T., 2006, “Identification of vehicle axle loads from bridge responses using updated static component technique”, *Engineering Structures,* 28(11), 1599-1608.

Piombo, B. A. D., Fasana, A., Marchesiello, S., and Ruzzene, M., 2000, “Modelling and identification of the dynamic responses of a supported bridge”, *Mechanical*

Systems and Signal Processing, 14(1): 75-89.

Ratcliffe, C. P., 1997, "Damage detection using a modified laplacian operator on mode shape data," *Journal of Sound and Vibration*, 204(3): 505-517.

Reynders, E., Roeck, G. D., Bakir, P. G., and Sauvage, C., 2007, "Damage identification on the Tilff bridge by vibration monitoring using optical fiber strain sensors", *Journal of Engineering Mechanics ASCE*, 133(2): 185-193.

Ribeiro, A. M. R., Silva, J. M. M., and Maia, N. M. M., 2000, "On the generalisation of the transmissibility concept", *Mechanical Systems and Signal Processing*, 14(1): 29-35.

Ricles, J. M., 1991, "Nondestructive Structural Damage Detection in Flexible Space Structures Using Vibration Characterization", NASA report CR-185670.

Robertson, A. N., Park, K. C., and Alvin, K. F., 1998, "Extraction of Impulse Response Data via Wavelet Transform for Structural System Identification", *Journal of Vibration and Acoustics ASME*, 120(1): 252-260.

Salawu, O. S., 1997, "Detection of structural damage through changes in frequency: a review," *Engineering Structures*, 19(9): 718-723.

Shi, Z. Y., Law, S. S., and Zhang, L. M., 2000a, "Damage localization by directly using incomplete mode shapes," *Journal of Engineering Mechanics ASCE*, 126(6): 656-660.

Shi, Z. Y., Law, S. S., and Zhang, L. M., 2000b, "Structural damage detection from modal strain energy change," *Journal of Engineering Mechanics ASCE*, 126(12): 1216-1223.

Smith, S. W., 1992, "Iterative use of direct matrix updates: connectivity and convergence," *Proceedings of 33rd AIAA Structures, Structural Dynamics and Materials Conference*, 1797–1806.

Steenackers, G., Devriendt, C., and Guillaume, P., 2007, "On the use of transmissibility measurements for finite element model updating", *Journal of Sound and Vibration*, 303(3-5): 707-722.

Steola, R., 1998, "A spline-based state reconstructor for active vibration control of a flexible beam," *Journal of Sound and Vibration*, 213(5): 777-790.

Stubbs, N., and Osegueda, R., 1990, “Global non-destructive damage evaluation in solids,” *Modal Analysis: The International Journal of Analytical and Experimental Modal Analysis*, 5(2): 67-79.

Tee, K. F., Koh, C. G., and Quek, S. T., 2005, “Substructural first- and second-order model identification for structural damage assessment”, *Earthquake Engineering and Structural Dynamics*, 34(15): 1755-1775.

Tee, K. F., Koh, C. G., and Quek, S. T., 2009, “Numerical and experimental Studies of a substructural identification strategy”, *Structural Health Monitoring*, 8(5): 397-410.

Teughels, A., Maeck, J., and Roeck, G. D., 2002, “Damage assessment by FE model updating using damage functions”, *Computers and Structures*, 80(25): 1869-1879.

Teughels, and A. Roeck, G. D., 2004, “Structural damage identification of the highway bridge Z24 by FE model updating”, *Journal of Sound and Vibration*, 278(3): 589-610.

Teughels, A. Roeck, G. D., and Suykens, J. A. K., 2003, “Global optimization by coupled local minimizers and its application to FE model updating”, *Computers and Structures*, 81(24-25): 2337-2351.

Tikhonov, A. N., *Numerical methods for the solution of ill-posed problems*, Kluwer Academic Publisher, Boston, 1995.

Urgueira, A. P. V., Almeida, R. A. B., and Maia, N. M. M., 2011, “On the use of the transmissibility concept for the evaluation of frequency response functions”, *Mechanical Systems and Signal Processing*, 25(3): 940-951.

Verboven, P., Guillanume, P., Cauberghe, S., Vanlanduit, S., and Parloo, E., 2004, “Modal parameter estimation from input-output Fourier data using frequency-domain maximum likelihood identification”, *Journal of Sound and Vibration*, 276(3-5): 957-979.

Wahab, M. M. A., and De Roeck, G., 1999, “Damage detection in bridges using modal curvatures: applications to a real damage scenario”, *Journal of Sound and Vibration*, 226(2): 217-235.

Wahab, M. M. A., Roeck, G. D., and Peeters, B., 1999, “Parameterization of damage in reinforced concrete structures using model updating”, *Journal of Sound and Vibration*, 228(4): 717-730.

Weber, B., Paultre, P., and Proulx, J., 2009, “Consistent regularization of nonlinear model updating for damage identification”, *Mechanical Systems and Signal Processing*, 23(6): 1965-1985.

Wu, J. J., 2007, “Use of moving distributed mass element for the dynamic analysis of a flat plate undergoing a moving distributed load”, *International Journal for Numerical Methods in Engineering*, 71(3): 347-362.

Yan, Y. J., Cheng, L., Wu, Z. Y., and Yam, L. H., 2007, “Development in vibration-based structural damage detection technique,” *Mechanical Systems and Signal Processing*, 21(5): 2198-2211.

Yang, Y. B., Lin, C. W., and Yau, J. D., 2004, “Extracting bridge frequencies from the dynamic response of a passing vehicle”, *Journal of Sound and Vibration*, 272(3-5): 471-493.

Yang, J. N., Huang, H. W., and Lin, S., 2006a, “Sequential non-linear least-square estimation for damage identification of structures,” *International Journal of Non-linear Mechanics*, 41(1): 124-140.

Yang, J. N., Lin, S., Huang, H., Zhou, L., 2006b, “An adaptive extended Kalman filter for structural damage identification,” *Structural Control and Health Monitoring*, 13(4): 849-967.

Yang, J. N., Pan, S. and Lin, S., 2007a, “Least-squares estimation with unknown excitations for damage identification of structures,” *Journal of Engineering Mechanics ASCE*, 133(1): 12-21.

Yang, J. N., Pan, S., and Huang, H., 2007b, “An adaptive extended Kalman filter for structural damage identifications II: unknown inputs,” *Structural Control and Health monitoring*, 14(3): 497-521.

Yun, C. B., and Bahng, E. Y., 2000, “Substructural identification using neural networks”, *Computers and Structures*, 77(1): 41-52.

Yun, C. B., and Lee, H. J., 1997, “Substructural identification for damage Estimation of structures", *Structural Safety*, 120(7): 1961-1976.

Zhang, Q., Jankowski, Ł., and Duan, Z. D., 2010, "Simultaneous identification of moving masses and structural damage", *Structural and Multidisciplinary Optimization*, 42(6): 907-922.

Zhang, Q. W., Chang, C. C., and Chang, T. Y. P., 2000, "Finite element model updating for structures with parametric constraints", *Earthquake Engineering and Structural Dynamics*, 29(7): 927-944.

Zhao, J., and Dewolf, J. T., 1999, "Sensitivity study for vibrational parameters used in damage detection", *Journal of Structural Engineering ASCE*, 125(4): 410-416.

Zhu, H. P., and Xu, Y. L., 2005, "Damage detection of mono-coupled periodic structures based on sensitivity analysis of modal parameters", *Journal of Sound and Vibration*, 285(1-2): 365-390.

Zhu, X. Q., and Law, S. S., 2000, "Identification of vehicle axle loads from bridge dynamic responses", *Journal of Sound and Vibration*, 236(4): 705-724.

Zhu, X. Q., and Law, S. S., 2006, "Moving load identification on multi-span continuous bridges with elastic bearings", *Mechanical Systems and Signal Processing,* 20(7): 1758-1782.

Zhu, X. Q., and Law, S. S., 2007, "Damage detection in simply supported concrete bridge structure under moving vehicular loads", *Journal of Vibration and Acoustics ASME*, 129(1): 58-65.

Zimmerman, D. C., and Kaouk, M., 1994, "Structural damage detection using a minimum rank update theory", *Journal of Vibration and Acoustics ASME*, 116(2): 222-230.

Zimmerman, D. C., 2006, "Statistical confidence using minimum rank perturbation theory", *Mechanical Systems and Signal Processing*, 20(5): 1155-1172.

Zivanovic, S., Pavic, A., and Reynolds, P., 2007, "Finite element modeling and updating of a lively footbridge: The complete process", *Journal of Sound and Vibration*, 301(1-2): 126-145.